Universiteit
Leiden
The Netherlands

Discovery of novel inhibitors to investigate diacylglycerol lipases and α/β hydrolase domain 16A

Janssen, F.J.

Citation

Janssen, F. J. (2016, December 1). *Discovery of novel inhibitors to investigate diacylglycerol lipases and α/β hydrolase domain 16A*. Retrieved from https://hdl.handle.net/1887/44705

Version:	Not Applicable (or Unknown)
License:	Licence agreement concerning inclusion of doctoral thesis in the Institutional Repository of the University of Leiden
Downloaded from:	https://hdl.handle.net/1887/44705

Note: To cite this publication please use the final published version (if applicable).

Cover Page

Universiteit Leiden

The handle http://hdl.handle.net/1887/44705 holds various files of this Leiden University dissertation

Author: Janssen, Freek J.
Title: Discovery of novel inhibitors to investigate diacylglycerol lipases and α/β hydrolase domain 16A
Issue Date: 2016-12-01

Discovery of novel inhibitors to investigate diacylglycerol lipases and α/β hydrolase domain 16A

PROEFSCHRIFT

ter verkrijging van

de graad van Doctor aan de Universiteit van Leiden,

op gezag van Rector Magnificus prof. mr. C.J.J.M. Stolker,

volgens het besluit van het College voor Promoties

te verdedigen op donderdag 1 december 2016

klokke 12:30 uur

door

Freek J. Janssen

geboren te Geldrop in 1988

Promotiecommissie

Promotor	Prof. dr. H.S. Overkleeft
Co-promotor	Dr. M. van der Stelt
Overige leden	Prof. dr. M. Maccarrone
	Prof. dr. C. A. A. van Boeckel
	Prof. dr. A. K. H. Hirsch
	Prof. dr. J. Brouwer
	Dr. S. van Kasteren

Printed by: Gildeprint

Cover design: DE-SIGN-NIS

“Remember that wherever your heart is, there you will find your treasure.”

Paulo Coelho, The Alchemist

Table of contents

CHAPTER 1

General introduction

Drug discovery in industry and academia

Drug discovery is essential to improve human health and lifespan and has delivered many life-saving molecules. Yet, drug discovery is expensive, time consuming and a high risk endeavor.[1,2] Medical needs are changing due to modern way of life and a growing elderly population. As a result, society faces many disease related challenges, including, many forms of cancer, increased antimicrobial resistance and metabolic and neurodegenerative disorders (*e.g.* obesity, type-2 diabetes, Parkinson's and Alzheimer's disease). Novel therapies to prevent, or to treat these diseases are urgently required. Current market introduction rate of new drugs is low, while costs of drug development have risen substantially in the last decades,[3] due to late stage clinical failures.[4,5] Hence pharmaceutical Research & Development (R&D) is facing a productivity crisis.[6] Consequently, business models of the pharmaceutical industry are changing, which leads to mergers and acquisitions, followed by reorganizations, down-sizing of internal R&D budgets and outsourcing to lower-cost contract research organizations.[7] Nowadays, more emphasis is placed on public-private-partnerships to perform early drug discovery activities.[8] Fundamental academic research is therefore crucial for discovering novel target-lead combinations. Academia contributes to target discovery, validation and de-risking.[9] Moreover, the development of novel treatments for neglected and orphan diseases and identification of novel drug discovery methods are important fields of research for the academic drug discoverer.[9,10]

The majority of first-in-class drugs approved by the FDA between 1999 and 2013 were discovered by a target-based approach.[11] Target-based drug discovery strategies can be classified in structure-based drug design (SBDD) and ligand-based drug design (LBDD). In SBDD, knowledge of the three-dimensional structure of the target protein at a molecular level with atomic resolution is required to study the specific interactions of a ligand and its protein.[12] Usually, X-ray crystallography and/or NMR spectroscopy techniques are applied to generate three dimensional models of the protein structures. Alternatively, a homology

model can be build based on the reported structure of related proteins. The protein structure can be used to screen virtual libraries to identify novel hits and to guide the optimization of ligands.

LBDD is an important alternative drug discovery strategy when a three dimensional structure of the target is not available. High throughput screening (HTS) is the most often employed LBDD technique to discover novel ligands, especially when limited target and ligand knowledge are available. In HTS, large sets of diverse compounds are tested for their activity against purified protein or cell lysates overexpressing the target of interest, employing fast and economical multi-well activity assays most often using surrogate substrates. HTS is hampered by false positives, due to, for example, pan-assay interference compounds (PAINS)[13] or poor physico-chemical properties of the compounds. Therefore, thorough assay optimization, high assay quality and reproducibility, hit deselection and active confirmation procedures and orthogonal assays are necessary.

Another popular LBDD strategy is ligand-based pharmacophore modeling.[14] In a pharmacophore, chemical features of a series of known ligands that are deemed essential for the interaction with its target, are grouped together in a three dimensional model. The pharmacophore model can be used to mine virtual compound libraries to discover novel hits. Challenges of pharmacophore modeling include dealing with conformational flexibility and scoring and weighting of screening results.[15] Moreover, confirmation of the activity of the virtual hit in a biochemical or cellular assay is essential to identify true hits.

Serine hydrolases

Serine hydrolases are one of the largest enzyme families (>200 members) in the human genome and utilize an active site serine for substrate hydrolysis. They partake in a plethora of (patho) physiological functions, including neurotransmission, learning, pain, energy metabolism and cancer (see [16] for extensive review). Several drugs act as serine hydrolase inhibitors, such as Januvia,[17] Rivastigmine[18] and Orlistat (Tetrahydrolipstatin, marketed as Xenical and Alli).[19,20] The exact function of many serine hydrolases remains, however, unknown to date. Hence, small molecule inhibitors may help to elucidate their function in health and disease and could have tremendous untapped medical potential across this large family of proteins.

Activity-based protein profiling (ABPP) has been developed as a strategy to identify and evaluate novel inhibitors for the serine hydrolase family without having the need of knowing the endogenous substrate or developing dedicated enzymatic assays of each individual enzyme.[21] In brief, ABPP uses activity-based probes (*i.e.* inhibitors with a reporter tag, such as a fluorophore or biotin) to label endogenous activity of enzymes by mechanism-based inhibition (Figure 1A). In this manner, serine hydrolases can be investigated in complex proteomes, such as cell or tissue lysates, using for example fluorophosphonates.[21] ABPP can also be used in a competitive setting in which proteomes are pretreated with an inhibitor,

which is followed by labeling of residual enzyme activity using the activity-based probe (Figure 1B). ABPP is complementary to multi-well substrate activity assays, because it is a very powerful tool to rapidly assess inhibitor potency on target and selectivity over related enzymes.

In this Thesis, ABPP is used throughout the drug discovery process to identify and optimize inhibitors of the serine hydrolases diacylgycerol lipases (DAGLs) and α/β hydrolase domain type 16A (ABHD16A).

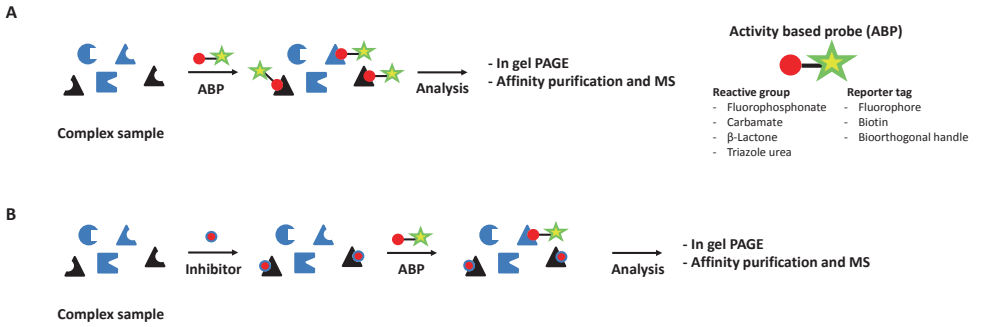

Figure 1. The concept of activity-based protein profiling (ABPP). **A)** Complex samples are incubated with an activity-based probe (ABP), which labels several proteins by mechanism-based inhibition. In case of the serine hydrolases, the active site serine is targeted with an electrophilic trap (*e.g.* fluorophosphonate, carbamate, β-lactone). In an ABP, the reactive moiety is attached to a reported tag (fluorophore or biotin). Analysis of the sample can then be performed by SDS-PAGE and standard in-gel fluorescence scanning (in case the tag is a fluorophore) or by affinity purification and mass spectrometry (MS) analysis (in case the tag is a biotin) or by Western Blot. Two-step ABPP can be performed using a biorthogonal handle as tag. **B)** In competitive ABPP, samples are pre-incubated with an inhibitor that can compete for ABP labeling. The sample is analyzed and corrected for control (vehicle).

Diacylglycerol lipases

In 1995, 2-arachidonoylglycerol (2-AG) was isolated from intestinal tissue and was characterized as the second endogenous ligand for the cannabinoid type 1 and 2 receptors (CB1R and CB2R).[22–24] The CBRs are important G-protein coupled receptors involved in a broad range of (patho)physiological functions, including addiction,[25] appetite[26–28] and memory formation.[29–31] 2-AG is considered to be an important signaling lipid. After its discovery, Stella *et al.* showed that 2-AG is highly abundant in brain and controls long term potentiation.[32] 2-AG accumulated in neurons in a Ca^{2+}-dependent manner. Combined phospholipase C (PLC) and diacylglycerol lipase (DAGL) activity were suggested as contributors to 2-AG formation (Figure 2).[32–34] In 2003, Bisogno *et al.* discovered two Ca^{2+} dependent lipases that produce 2-AG in the brain and designated them DAGLα and DAGLβ.[35] DAGLs are serine hydrolases that specifically cleave *sn*-1 fatty acyl chains of arachidonate-containing 1,2-diacylglycerols. DAGLα, a 120 kDa protein with 1042 amino acids, contains a short N-terminal sequence, followed by four transmembrane helices, an intracellular catalytic domain with a cysteine rich insert and a large C-terminal tail.[35] This tail is absent in

DAGLβ, making it a shorter homolog (672 amino acids and 70 kDa). Interestingly, DAGLα contains a PPXXF motif (Pro972-Phe976) in the C-terminus that interacts with CC-Homer proteins.[36] This interaction is required for DAGLα recruitment to the metabotropic glutamate receptor signaling complex in the plasmamembrane, but not for its enzymatic activity.[36] Both isoforms have a typical α/β hydrolase fold and a Ser-His-Asp catalytic triad typical for serine hydrolases (DAGLα: Ser472, His650, Asp524; DAGLβ: Ser443, Asp495, His: unknown). Reisenberg *et al.* postulated that both DAGLs contain a large insert of unknown structure between the 7th and 8th canonical β-sheet that may function as a regulatory loop, controlling substrate access to the catalytic site.[37]

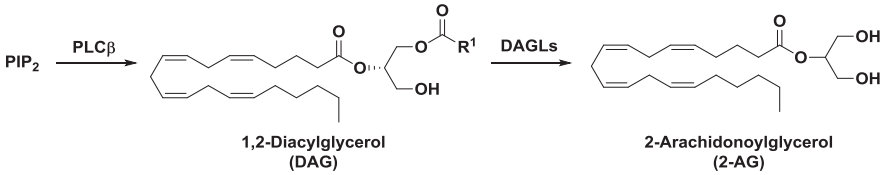

Figure 2. Phospholipase C β (PLCβ) catalyzes the formation of 1,2-diacylglycerols (DAG) from phosphatidylinositol-4,5-bisphosphate (PIP_2). *Sn*-1 specific diacylglycerol lipases (DAGLs) subsequently catalyze the formation of 2-arachidonylglycerol (2-AG) from its DAG precursor.

DAGLα and β show a marked difference in tissue expression. DAGLα is highly expressed in the central nervous system, whereas DAGLβ is predominantly located in the periphery. In line, DAGLα knockout mice show ~80% reduction in 2-AG levels in the brain and spinal cord, whereas DAGLβ knockout mice show ~50% reduction in brain.[38] In the liver of DAGLβ knockout mice 2-AG levels are reduced with ~90% , whereas for DAGLα knockout mice 2-AG levels are reduced by ~60%. A large difference was also observed in adipose tissue, where ~50% 2-AG reduction for DAGLα knockout mice was observed, while deletion of DAGLβ had no significant effect on basal 2-AG levels.[38] This indicates that specific DAGL isoforms contribute to 2-AG pools in a highly tissue dependent manner. Of note, the levels of arachidonic acid (AA), a metabolite of 2-AG, were also decreased in brain, spinal cord and liver of DAGLα knockout mice.[39] The subcellular localization of DAGLs indicate that 2-AG is produced at postsynaptic sites that are close to the presynaptically located CB receptors.[40] Gao *et al.* showed that mice lacking DAGLα have significantly reduced retrograde signaling (depolarization-induced suppression of inhibition, DSI) in brain through CB1R-dependent signaling. Moreover, both DAGLα and DAGLβ knockout mice show reduced adult neurogenesis in the hippocampus and subventricular zone. Another study performed by Tanimura *et al.* showed similar results, as both depolarization-induced suppression of excitation (DSE) and DSI were absent in DAGLα knockout mice in brain cerebellum, hippocampus, and striatum.[41] Importantly, congenital deletion of DAGLβ had no effect on retrograde suppression of synaptic transmission. This indicates that DAGLα is the main isoform responsible for the neuronal signaling pool of 2-AG.

Selective inhibitors of DAGLα may contribute to a more fundamental understanding of the physiological role of 2-AG and may serve as potential drug candidates for the treatment of obesity and neurodegenerative diseases. Currently, there are no selective inhibitors available for the study of DAGLα. The identification of selective DAGLα inhibitors is hampered by a lack of structural knowledge of the target, and lack of assays that make use of endogenous DAGLα activity in proteomes or in a multi-well format. No crystal structures are available and no homology models have been reported to aid hit identification and perform SBDD. To date, only a few DAGL inhibitors have been described, however, most of them lack selectivity, *in vivo* activity and/or pharmacokinetic properties to study the role of 2-AG in *in vivo* models of disease. Thus, there is an unmet need to identify novel chemotypes to modulate DAGL activity.

α/β Hydrolase domain type 16A

α/β Hydrolase domain type 16A (ABHD16A), has recently been identified as a key contributor to *lyso*-phosphatydylserine (*lyso*-PS) formation in mice (Figure 3).[42] *Lyso*-PS is an important signaling phospholipid involved in immune response through its interaction with Toll-like receptor 2 (TLR2).[43] In addition, *lyso*-PS has been associated with T-cell growth,[44] mast cell activation[45,46] and neurite outgrowth.[47] *Lyso*-PS is metabolized by α/β hydrolase domain type 12 (ABHD12).[48] Interestingly, absence of ABHD12 activity in humans caused by specific mutations, has been linked to the onset of multiple symptoms of the rare genetic disease polyneuropathy-hearing loss-ataxia-retinitis pigmentosa and cataract (PHARC).[49,50] As such, PHARC can be seen as a ABHD12 null model and accumulation of *lyso*-PS may be the cause rather than an effect of the disease. If this hypothesis holds true, then diminishing *lyso*-PS levels would be expected to reduce neuroinflammation, and thereby, lead to amelioration of the symptoms. To test these assumptions, *in vivo* active inhibitors of ABHD16A, which can be used in a substrate reduction therapy, are required. However, no *in vivo* active ABHD16 inhibitors have been described as of yet and their discovery is hindered by limited structural knowledge of the target, lack of multi-well activity assays and a dearth of available starting points for a hit optimization program.

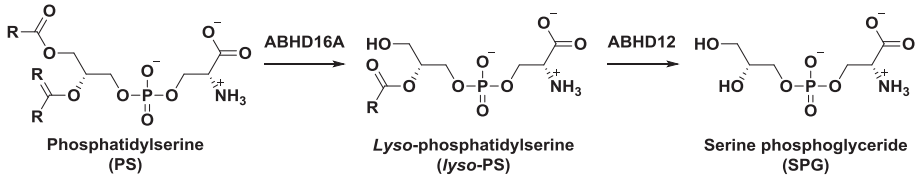

Figure 3. α/β Hydrolase domain type 16A (ABHD16A, BAT5) catalyzes the formation of *lyso*-phosphatidylserine (lyso-PS). α/β Hydrolase domain type 12 (ABDH12) subsequently hydrolases *lyso*-PS to serine phosphoglyceride (SPG).

Aim and outline of this thesis

This thesis describes the discovery and optimization of potent inhibitors for DAGLs and ABHD16A, employing several LBDD and SBDD strategies integrated with ABPP. These inhibitors can be used as tool compounds to report on the function of both targets in mammalian physiology, and may serve as leads for the development of potential drug candidates.

Chapter 2 describes the discovery of a novel reversible DAGL chemotype by *in silico* screening. The development of a ligand-based pharmacophore model, derived from a known DAGL inhibitor (Tetrahydrolipstatin), was used to screen a subset of commercially available endocannabinoid metabolism targeting inhibitors. The α-keto heterocycle LEI104 was identified as the first reversible DAGLα inhibitor.[51] To explain its molecular interactions with DAGLα, a homology model was constructed and the binding mode of LEI104 was investigated. Subsequently, the structural requirements for specific DAGLα inhibition by LEI104 were further investigated by screening a focused library of 1040 compounds in **Chapter 3**.[52] This showed that α-keto oxazolo-4*N*-pyridine was the optimal scaffold for this class of DAGL inhibitors. The comprehensive structure-activity relationships were used to validate the DAGLα homology model generated in Chapter 2, which proved to be indispensible to the discovery of LEI105, a highly potent and selective dual DAGLα/β inhibitor.[53] **Chapter 4** describes the lead optimization of LEI105 leading to LEI107, an exquisitely selective DAGL inhibitor with drug-like properties. **Chapter 5** describes the first structure-activity relationship analysis of a novel class of reversible DAGL inhibitors, the glycine sulfonamides. This class was previously identified by a HTS campaign.[54] This chapter describes the discovery and optimization of LEI106, which is the first reported reversible potent dual DAGLα/ ABHD6 inhibitor.[55] Finally, potential binding modes for the glycine sulfonamides are explored using structure-guided homology modeling. **Chapter 6** describes the discovery of several new DAGLα chemotypes by HTS and ABPP. A 300.000+ compound collection was screened for activity against DAGLα using fully automated HTS, within the European Lead Factory (ELF). The colorimetric primary assay results were followed by an orthogonal ABPP assay to assess potency and selectivity of the compounds in complex mouse brain proteome. This resulted in the discovery of sulfonyl 1,2,4-triazole ureas as a novel scaffold for serine hydrolases. Moreover eight other compound classes were discovered, including α- and β-keto amides and the previously reported glycine sulfonamides. **Chapter 7** describes the development of inhibitors for ABHD16A (BAT5) by application of ABPP in LBDD. The 1,2,4-triazole sulfonamide ureas, described in Chapter 6, were found to inhibit ABHD16A by orthogonal ABPP. Subsequent optimization and characterization led to two compounds that exhibited *in vivo* activity on brain ABHD16A in mice. **Chapter 8** provides an extensive overview of all the current DAGL inhibitors and their effect in preclinical models of neurodegenerative and metabolic disorders.[56] **Chapter 9** provides a summary of this Thesis and states future directions for additional research.

References

1. Mignani, S., Huber, S., Tomás, H., Rodrigues, J. & Majoral, J. P. Why and how have drug discovery strategies in pharma changed? What are the new mindsets? *Drug Discov. Today* **21,** 239–249 (2015).
2. Hughes, J. P., Rees, S. S., Kalindjian, S. B. & Philpott, K. L. Principles of early drug discovery. *Br. J. Pharmacol.* **162,** 1239–1249 (2011).
3. DiMasi, J. A., Hansen, R. W. & Grabowski, H. G. The price of innovation: New estimates of drug development costs. *J. Health Econ.* **22,** 151–185 (2003).
4. David, E., Tramontin, T. & Zemmel, R. Pharmaceutical R&D: the road to positive returns. *Nat. Publ. Gr.* **8,** 609–610 (2009).
5. Mervis, J. Productivity Counts — But the Definition Is Key. *Science* **309,** 726–727 (2005).
6. Pammolli, F., Magazzini, L. & Riccaboni, M. The productivity crisis in pharmaceutical R&D. *Nat. Rev. Drug Discov.* **10,** 428–438 (2011).
7. Clark, D. E. & Newton, C. G. Outsourcing lead optimisation--the quiet revolution. *Drug Discov. Today* **9,** 492–500 (2004).
8. Crommelin, D. *et al.* Pharmaceutical sciences in 2020. *Nat. Rev. Drug Discov.* **9,** 99–100 (2010).
9. Wyatt, P. G. The emerging academic drug-discovery sector. *Future Med. Chem.* **1,** 1013–1017 (2009).
10. Frye, S., Crosby, M., Edwards, T. & Juliano, R. US academic drug discovery. *Nat. Rev. Drug Discov.* **10,** 409–410 (2011).
11. Eder, J., Sedrani, R. & Wiesmann, C. The discovery of first-in-class drugs: origins and evolution. *Nat. Rev. Drug Discov.* **13,** 577–87 (2014).
12. Aparoy, P., Reddy, K. K. & Reddanna, P. Structure and ligand-based drug design strategies in the development of novel 5-LOX inhibitors. *Curr. Med. Chem.* **19,** 3763–3778 (2012).
13. Baell, J. & Walters, M. A. Chemical con artists foil drug discovery. *Nature* **513,** 481–483 (2014).
14. Acharya, C., Coop, A., Polli, J. E. & Mackerell, A. D. Recent advances in ligand-based drug design: relevance and utility of the conformationally sampled pharmacophore approach. *Curr. Comput. Aided. Drug Des.* **7,** 10–22 (2011).
15. Yang, S.-Y. Pharmacophore modeling and applications in drug discovery: challenges and recent advances. *Drug Discov. Today* **15,** 444–450 (2010).
16. Long, J. & Cravatt, B. The Metabolic Serine Hydrolases and Their Functions in Mammalian Physiology and Disease. *Chem Rev* **111,** 6022–6063 (2012).
17. Kim, D. *et al.* (2R)-4-oxo-4-[3-(trifluoromethyl)-5,6-dihydro[1,2,4]triazolo[4,3-a]pyrazin-7(8H)-yl]-1-(2,4,5-trifluorophenyl)butan-2-amine: a potent, orally active dipeptidyl peptidase IV inhibitor for the treatment of type 2 diabetes. *J. Med. Chem.* **48,** 141–151 (2005).
18. Rösler, M. *et al.* Efficacy and safety of rivastigmine in patients with Alzheimer's disease: international randomised controlled trial. *BMJ* **318,** 633–8 (1999).
19. Borgstriim, B. Mode of action of tetrahydrolipstatin: a derivative of the naturally occurring lipase inhibitor lipstatin. *Enzyme* 308–316 (1988).
20. Hadváry, P., Lengsfeld, H. & Wolfer, H. Inhibition of pancreatic lipase in vitro by the covalent inhibitor tetrahydrolipstatin. *Biochem. J.* **256,** 357–361 (1988).
21. Liu, Y., Patricelli, M. P. & Cravatt, B. F. Activity-based protein profiling: the serine hydrolases. *Proc. Natl. Acad. Sci. U.S.A.* **96,** 14694–14699 (1999).
22. Sugiura, T. *et al.* 2-Arachidonoylglycerol: a possible endogenous cannabinoid receptor ligand in brain. *Biochem. Biophys. Res. Commun.* **215,** 89–97 (1995).
23. Mechoulam, R. *et al.* Identification of an endogenous 2-monoglyceride, present in canine gut, that binds to cannabinoid receptors. *Biochem. Pharmacol.* **50,** 83–90 (1995).
24. Devane, W. A. *et al.* Isolation and Structure of a Brain Constituent That binds to the Cannabinoid Receptor. *Science* **258,** 1946–1949 (1992).
25. Ledent, C. *et al.* Unresponsiveness to Cannabinoids and Reduced Addictive Effects of Opiates in CB1 receptor Knockout Mice. *Science* **283,** 401–404 (1999).
26. Colombo, G. *et al.* Appetite supression and weight loss after the cannabinoid antagonist SR 141716. *Life Sci.* **63,** 113–117 (1998).
27. Di Marzo, V. *et al.* Leptin-regulated endocannabinoids are involved in maintaining food intake. *Nature* **410,** 822–825 (2001).
28. Koch, M. *et al.* Hypothalamic POMC neurons promote cannabinoid-induced feeding. *Nature* **519,** 45–50 (2015).

29. Hampson, R. E. & Deadwyler, S. A. Role of cannabinoid receptors in memory storage. *Neurobiol. Dis.* **5,** 474–482 (1998).
30. Reibaud, M. *et al.* Enhancement of memory in cannabinoid CB1 receptor knock-out mice. *Eur. J. Pharmacol.* **379,** R1–R2 (1999).
31. Marsicano, G. *et al.* The endogenous cannabinoid system controls extinction of aversive memories. *Nature* **418,** 530–534 (2002).
32. Stella, N., Schweitzer, P. & Piomelli, D. A second endogenous cannabinoid that modulates long-term potentiation. *Nature* **388,** 773–778 (1997).
33. Prescott, S. M. & Majerus, P. W. Characterization of 1,2-diacylglycerol hydrolysis in human platelets. Demonstration of an arachidonoyl-monoacylglycerol intermediate. *J. Biol. Chem.* **258,** 764–769 (1983).
34. Farooqui, A. A., Taylor, W. A. & Horrocks, L. A. Characterizaiton and solubilization of membrane bound diacylglycerol lipases from bovine brain. **18,** 991–997 (1986).
35. Bisogno, T. *et al.* Cloning of the first sn1-DAG lipases points to the spatial and temporal regulation of endocannabinoid signaling in the brain. *J. Cell Biol.* **163,** 463–468 (2003).
36. Jung, K.-M. *et al.* A key role for diacylglycerol lipase-a in metabotropic glutamate receptor-dependent endocannabinoid mobilization. *Mol. Pharmacol.* **72,** 612–621 (2007).
37. Reisenberg, M., Singh, P. K., Williams, G. & Doherty, P. The diacylglycerol lipases: structure, regulation and roles in and beyond endocannabinoid signaling. *Philos. Trans. R. Soc. B Biol. Sci.* **367,** 3264–3275 (2012).
38. Gao, Y. *et al.* Loss of Retrograde Endocannabinoid Signaling and Reduced Adult Neurogenesis in Diacylglycerol Lipase Knock-out Mice. *J. Neurosci.* **30,** 2017–2024 (2010).
39. Nomura, D. K. *et al.* Endocannabinoid hydrolysis generates brain prostaglandins that promote neuroinflammation. *Science* **334,** 809–813 (2011).
40. Yoshida, T. Localization of diacylglycerol lipase-a around postsynaptic spine suggests close proximity between production site of an endocannabinoid, 2-arachidonoyl-glycerol, and presynaptic cannabinoid CB1 receptor. *J. Neurosci.* **26,** 4740–4751 (2006).
41. Tanimura, A. *et al.* The endocannabinoid 2-arachidonoylglycerol produced by diacylglycerol lipase a mediates retrograde suppression of synaptic transmission. *Neuron* **65,** 320–327 (2010).
42. Kamat, S. S. *et al.* Immunomodulatory lysophosphatidylserines are regulated by ABHD16A and ABHD12 interplay. *Nat. Chem. Biol.* **11,** 164–71 (2015).
43. van der Kleij, D. *et al.* A novel host-parasite lipid cross-talk. Schistosomal lyso-phosphatidylserine activates toll-like receptor 2 and affects immune polarization. *J. Biol. Chem.* **277,** 48122–48129 (2002).
44. Bellini, F. & Brunib, A. Role of a serum phospholipase A1 in the phosphatidylserine-induced T cell inhibition. *FEBS Lett.* **316,** 4–7 (1993).
45. Martin, T. W. & Lagunoff, D. Interactions of lysophospholipids and mast cells. (1979).
46. Smith, G. A., Hesketh, T. R., Plumb, R. W. & Metcalfe, J. C. The exogenous lipid requirement for histamine release from rat peritoneal mast cells stimulated by concanavalin A. *FEBS Lett.* **105,** (1979).
47. Lourenssen, S. & Blennerhassett, M. G. Lysophosphatidylserine potentiates nerve growth factor-induced differentiation of PC12 cells. *Neurosci. Lett.* **248,** 77–80 (1998).
48. Blankman, J. L., Long, J. Z., Trauger, S. a, Siuzdak, G. & Cravatt, B. F. ABHD12 controls brain lysophosphatidylserine pathways that are deregulated in a murine model of the neurodegenerative disease PHARC. *Proc. Natl. Acad. Sci. USA* **110,** 1500–1505 (2013).
49. Fiskerstrand, T. *et al.* A novel Refsum-like disorder that maps to chromosome 20. *Neurology* **72,** 20–27 (2009).
50. Fiskerstrand, T. *et al.* Mutations in ABHD12 cause the neurodegenerative disease PHARC: An inborn error of endocannabinoid metabolism. *Am. J. Hum. Genet.* **87,** 410–417 (2010).
51. Baggelaar, M. P. *et al.* Development of an activity-based probe and in silico design reveal highly selective inhibitors for diacylglycerol lipase-a in brain. *Angew. Chem. Int. Ed.* **52,** 12081–12085 (2013).
52. Janssen, F. J. *et al.* Comprehensive Analysis of Structure-Activity Relationships of α-Ketoheterocycles as sn-1-Diacylglycerol Lipase α Inhibitors. *J. Med. Chem.* **58,** 9742–9753 (2015).
53. Baggelaar, M. P. *et al.* Highly Selective, Reversible Inhibitor Identified by Comparative Chemoproteomics Modulates Diacylglycerol Lipase Activity in Neurons. *J. Am. Chem. Soc.* **137,** 8851–8857 (2015).
54. Appiah, K. K. *et al.* Identification of small molecules that selectively inhibit diacylglycerol lipase-alpha activity. *J Biomol Screen* **19,** 595–605 (2014).
55. Janssen, F. J. *et al.* Discovery of glycine sulfonamides as dual inhibitors of sn-1-diacylglycerol lipase α and α/β hydrolase domain 6. *J. Med. Chem.* **57,** 6610–6622 (2014).

56. Janssen, F. J. & van der Stelt, M. Inhibitors of diacylglycerol lipases in neurodegenerative and metabolic disorders. *Bioorg. Med. Chem. Lett.* **26,** 3831–3837 (Invited BMCL Digest) (2016).

CHAPTER 2

Potent *sn*-1 diacylglycerol lipase α inhibitor discovered by *in silico* screening*

Introduction

Sn-1 specific diacylglycerol lipase α (DAGLα) is an intracellular, multidomain protein responsible for the formation of the endocannabinoid 2-arachidonoylglycerol (2-AG) in the central nervous system.[1,2] 2-AG is an endogenous signaling lipid that interacts with the cannabinoid CB1 and CB2 receptors.[3] However, little is known about the regulation of its biosynthetic pathway and it is largely unclear to what extent 2-AG is responsible for distinct CB1 receptor mediated biological processes. Selective inhibitors of DAGLα may contribute to a more fundamental understanding of the physiological role of 2-AG and may serve as potential drug candidates for the treatment of obesity and neurodegenerative diseases.[4,5] Currently there are no selective inhibitors available to study the function of DAGLα.[6–12] The identification of selective DAGLα inhibitors is hampered by a lack of structural knowledge of the target. No crystal structures are available and no homology models have been reported to aid hit identification and to guide optimization of inhibitors. Here a knowledge-based *in silico* screening approach on DAGLα is presented, followed by screening of a focused library of lipase inhibitors. This resulted in the identification of α-keto heterocycle LEI104. A potential binding mode of LEI104 is postulated, based on covalent docking and molecular dynamics optimization. The binding mode is supported by preliminary structure-activity relationships (SAR).

* Published as part of: Baggelaar, M.P., Janssen F.J., van Esbroeck, A.C.M.; den Dulk, H., Allarà, M., Hoogendoorn, S., McGuire, R., Florea, B.I., Meeuwenoord, N., van den Elst, H., van der Marel, G A., Brouwer, J., di Marzo, V., Overkleeft, H.S., van der Stelt, M. Development of an activity-based probe and *in silico* design reveal highly selective inhibitors for diacylglycerol lipase α in brain. *Angew. Chemie Int. Ed.* **2013**, *52*, 12081–12085.

Results and discussion

To identify novel DAGLα inhibitors, a pharmacophore model based on tetrahydrolipstatin (THL), a known non-selective DAGLα inhibitor, was constructed using Discovery Studio Software Suite from Accelrys. Since THL can assume many different conformations, the protein crystallographic database was examined for crystal structures with a bioactive conformation for THL. A co-crystal structure of THL with fatty acid synthase (PDB code: 2PX6) was identified (Figure 1A)[13] that contains the same Ser-His-Asp catalytic triad and typical α/β hydrolase fold motif as DAGLα. In this co-crystal structure, the nucleophilic Ser of the enzyme is covalently attached to the carbonyl moiety. Reconstitution of the ester formed the β-lactone to recover the active warhead of THL. After optimization of the geometry of the lactone, the resulting conformation was used to generate two pharmacophore models (Figure 1B,C). The essential features of both models are 1) a hydrogen bond acceptor mimicking the carbonyl from the β-lactone; 2) hydrophobic hot spots corresponding to the lipophilic tails of THL; 3) a hydrogen-bond acceptor positioned at the *sn*-2 ester functionality and 4) exclusion volumes representing the space occupied by the nucleophilic Ser and the backbone oxyanion hole residues in the active site of DAGLα. Model 2 contained an additional hydrogen-bond donor feature derived from the leucinyl formamide moiety of THL (Figure 2C). Using these two models, a set of commercially available lipase inhibitors were screened, which were mainly selected for their reactivity towards enzymes involved in endocannabinoid signaling (Table 1).

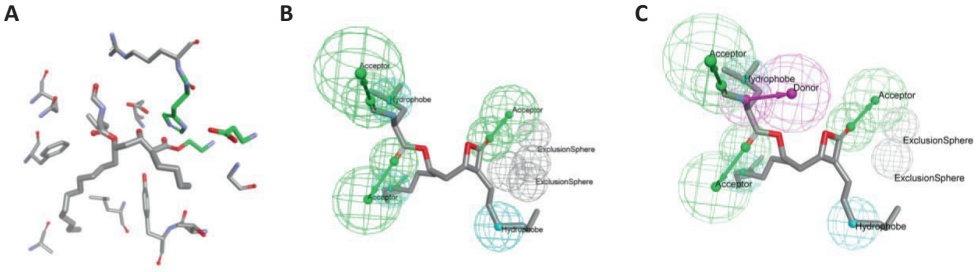

Figure 1. Development of THL based DAGLα pharmacophore models 1 and 2. **A)** Bioactive conformation of THL as retrieved from its known fatty acid synthase (FAS) co-crystal structure (PDB code 2PX6).[13] **B)** Pharmacophore model 1, consisting of 3 hydrogen bond acceptors (HBA), 1 hydrogen bond donors (HBD), 3 hydrophobic spheres and exclusion volumes as depicted. **C)** Pharmacophore model 2, consisting of 3 HBA, 3 hydrophobic spheres and exclusion volumes as depicted. Arrows represent the interaction vector.

Table 1. Structures and known targets of a set of commercially available lipase inhibitors, which were mainly selected for their reactivity towards enzymes involved in endocannabinoid signaling. Inhibitors were bought at Cayman Chemicals, Sigma Aldrich or Thermo Fisher.

Entry/Code	Structure	Target	Entry/ Code	Structure	Target
1 (LEI103) CAY10499	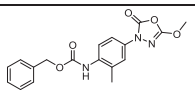	HSL	***9*** NO-1886	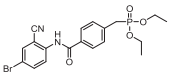	LPL
2 CAY10590	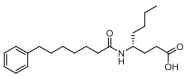	PLA_2	**10** Chlorpro-mazine	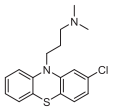	5-HT receptor
3 CAY10594	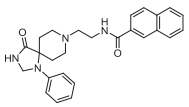	PLD_2	**11** URB597	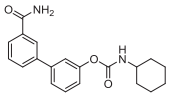	FAAH
4 CAY10566	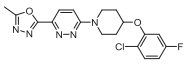	SCD	**12** JZL 184	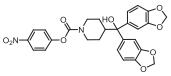	MAGL
5 (LEI104) OL-100	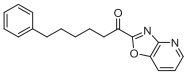	FAAH	**13** URB602	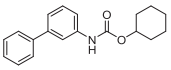	MAGL
6 JZL 195	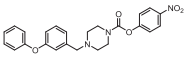	FAAH / MAGL	**14** PF-3845	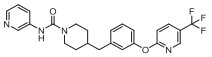	FAAH
7 WWL70	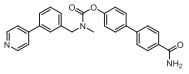	ABHD6	**15** TOFA	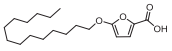	FAS
8 FIPI	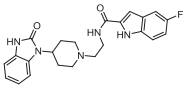	PLD	**16** RHC80267	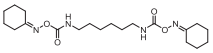	Several lipases

Analysis of the docking results revealed that two compounds ranked in the top five of both models, LEI103 (**1**) and LEI104 (**5**; Figure 2, Table 2) based on fit value. The fit value is a quantitative measure of how well the pharmacophore overlaps with the compound chemical features. Expectantly also **15**, a FAS inhibitor showed binding poses in both models. No binding mode was identified for compounds **3**, **4**, **7**–**11**, **13**, **14**, and **16** (Table 2) in either one or both models. This result demonstrates that the pharmacophore models were capable of discriminating between related structures of lipase inhibitors.

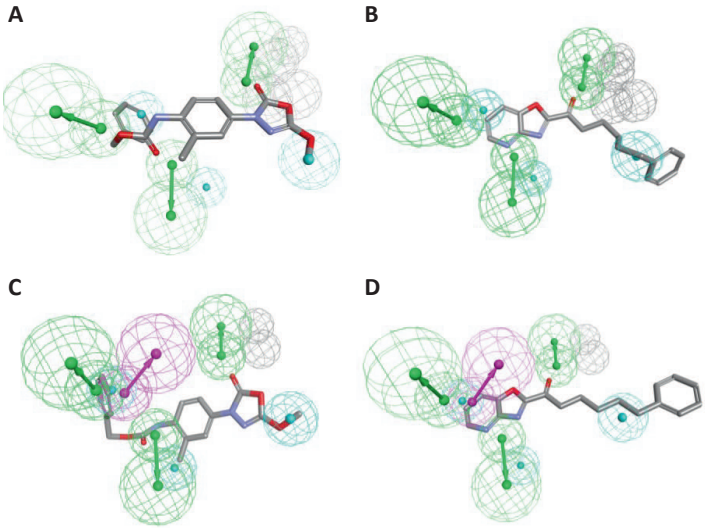

Figure 2. Docking results in pharmacophore models 1 and 2: Highest ranked binding pose of **A)** LEI103 (5 features, model 1), **B)** LEI104 (4 features, model 1), **C)** LEI103 (5 features, model 2) and **D** LEI104 (4 features, model 2).

Table 2. Ranking order of hits in both pharmacophore models, as determined by pharmacophore screening. Fit values for model 2 are lower because it is more stringent due to more features.

Rank	Model 1	Fit value	Model 2	Fit value
1	**2**	3.51	**5** (LEI104)	2.25
2	**1** (LEI103)	3.32	**12**	2.17
3	**8**	2.84	**11**	1.95
4	**5** (LEI104)	2.38	**1** (LEI103)	1.15
5	**14**	2.11	**15**	0.98
6	**12**	2.09	**6**	0.60
7	**3**	2.07	**2**	0.42
8	**6**	1.95	**3**	-
9	**15**	1.88	**8**	-
10	**11**	-	**14**	-
11	**4**	-	**4**	-
12	**7**	-	**7**	-
13	**9**	-	**9**	-
14	**10**	-	**10**	-
15	**13**	-	**13**	-
16	**16**	-	**16**	-

Compound **1**, LEI103 is an oxadiazolone known to inhibit hormone-sensitive lipase,[14] and **5**, LEI104 (OL-100) is an α-ketoheterocycle that has been reported to inhibit fatty acid amide hydrolase (FAAH).[15] LEI104 has been shown to be active in *in vivo* models of antinociception through inhibition of FAAH activity.[16–19] Both hits represent new chemotypes that have not previously been shown to display DAGLα inhibitory activity. To validate the *in silico* hits, a colorimetric biochemical DAGLα activity assay was set up, which makes use of the hydrolysis of *para*-nitrophenyl (PNP) butyrate by membrane preparations from HEK293T cells

transiently transfected with human DAGLα, as previously reported.[20] Screening of the compound library against hDAGLα (Figure 3A) confirmed LEI103 (**1**) and LEI104 (**5**) as the only compounds to inhibit hDAGLα enzymatic activity by over 50% at 10 μM. Determination of the concentration–response curves resulted in an IC_{50} of 37 nM (n = 4) for LEI104, thus making it a hundred-fold more potent than LEI103 (IC_{50} = 3.8 μM, n = 4; Figure 3B). Of note, the reported DAGLα inhibitor RHC80267 (**16**) showed no inhibitory activity at 10 μM in the biochemical assay. In addition, the activity of the hits in a radiometric assay using 1-[^{14}C]oleoyl-2-arachidonoylglycerol as natural-like substrate was investigated.[1] This assay confirmed that LEI104 is a more potent inhibitor of DAGLα (IC_{50} = 2.9 ± 0.1 μM) than LEI103 (37% inhibition at 10 μM).

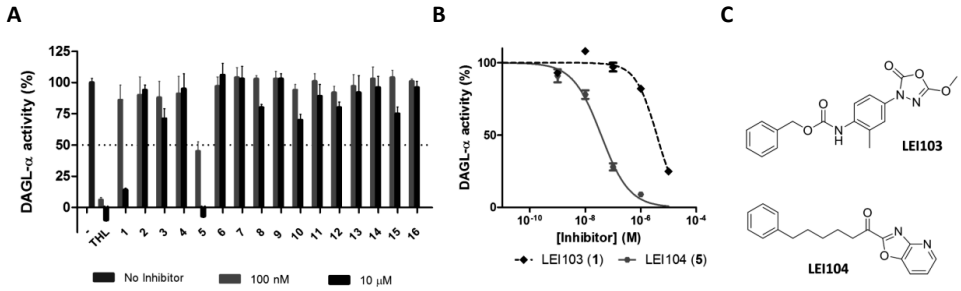

Figure 3. Characterization of novel inhibitors for DAGLα. **A)** Screen of the targeted library using the colorimetric biochemical assay. Normalized residual activity was measured against hDAGLα in HEK293T cell membranes. **B)** Dose–response curves of LEI103 (black) and LEI104 (gray) against hDAGLα as determined with the colorimetric assay. LEI103: IC_{50} = 3.8 μM; LEI104: IC_{50} = 37 nM. **C)** Structures of LEI103 and LEI104.

LEI104 was resynthesized according to Scheme 1 and retested in the colorimetric hDAGLα activity assay, displaying equipotent activity. The alcohol precursor of LEI104 (**18**) showed no activity, a result in line with the assumption that the ketone functions as a reversible electrophilic trap for the catalytic Ser472. Replacement of the oxazolopyridine heterocycle with a benzoxazole (**17**, Scheme 1) led to a 100-fold loss in activity, indicating that the pyridine nitrogen could form a potentially important interaction with the active site of the enzyme.[15] To understand the interaction of LEI104 with hDAGLα on a molecular level, a homology model was developed of DAGLα from a representative construct using the automated YASARA procedures.[21–24] The sequence used to represent DAGLα was constructed by editing the full sequence to remove the N terminal residues 1-287, the regulatory domain (residues 555- 623) and the C terminal region (residues 663-1042). These regions are not observed in crystal structures of lipases and the remaining residues form the routinely observed core α/β hydrolase fold. Deleting the regulatory domain necessitated selection of the most appropriate residues and thus optimizes alignment. This was done manually with reference to the three dimensional structure of the template. DAGLα contains a large insert compared to other lipases, the cysteine rich loop, not present in any available lipase structure. As such, residues Tyr308- Phe358 were modeled as the cysteine rich loop insert (Figure 4).

The crystal structure of the S146A mutant of Thermomyces (Humicola) Lanuginosa Lipase in complex with oleic acid (PDB code 1GT6) is the highest scoring template of an enzyme:ligand complex.[25] The alignment had 230 of 306 target residues (75.2%) aligned to template residues and 18.7% sequence identity. Given the very low sequence homology, its unmatched cysteine rich loop and the artificial construct used for the post regulatory domain, the homology model quality is good. The poor 3D-packing however, reflects the remaining uncertainties in the model (Z-score of -2.440), however the calculated overall model quality (Z-score of -1.850) together with visual analysis of the catalytic core and the residues lining the binding cavity rate the homology model acceptable. Of note, the model does not include a potential regulatory cap present in DAGLα,[2] as this sequence was not similar to other published structures.[26]

The model represents the typical α/β hydrolase fold and has the catalytic triad (Ser472, His650, and Asp524) appropriately aligned in the binding cavity (Figure 5). The tetrahedral transition state of LEI104, which is formed through the nucleophilic attack of Ser472 on the α-carbonyl, was minimized and subjected to molecular dynamics refinement. According to the model, the oxyanion intermediate is stabilized by the backbone N–H of the residue adjacent to the catalytic serine, Leu473 (71% of the snapshots taken in the molecular dynamics (MD) simulation showed this interaction). In addition, both the side chain O–H and the backbone N–H of Thr400 are observed to make hydrogen bonds with the oxyanion (93% in MD simulation). The oxazole nitrogen of LEI104 formed hydrogen-bond interactions with His650 (51% in MD simulation) and the pyridine nitrogen showed hydrogen-bond interactions with His471 (76% in MD simulation), both of which could further stabilize the transition state, while the hydrophobic pocket lined with aliphatic amino acids accommodated the flexible acyl chain of LEI104 (Figure 6). This proposed binding mode is consistent with the observed structure–activity relationships in this study.

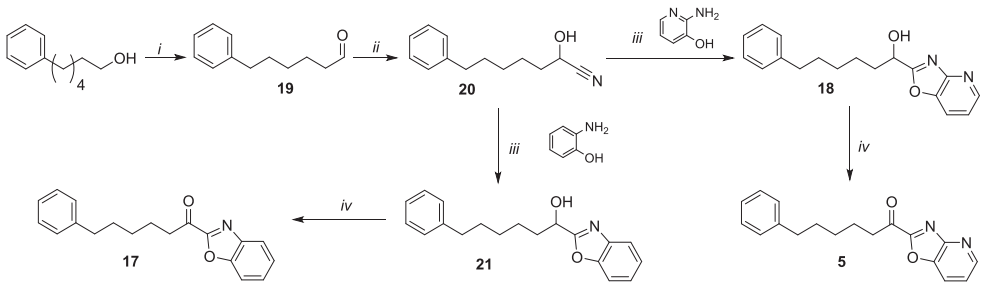

Scheme 1. Synthesis of LEI104 (**5**) and α-keto benzoxazole **17**. *i*) DMSO, oxalyl chloride, DCM, Et_3N, -78 °C, 99% *ii*) KCN, THF:H_2O (1:1), 64% *iii*) Acetyl chloride, $CHCl_3$, EtOH; 2-amino-3-hydroxy-pyridine/2-aminophenol, EtOH, reflux, 3.5% (**18**), 57% (**21**). iv) Dess-Martin periodinane, CH_2Cl_2, 44% (**5**), 98% (**17**).

```
>DAGLalpha
-----RYKEVCYYMLFALAAYGWPM----------------YLMRKPACGLCQLARSCSCCLCPARPRFA
PGVTIEEDNCCGCNAIAIRRHFLDENMTAVDIVYTSC-----HDAVYETPFYVAVDHDKKKVVISIRGTL
SPKDALTDLTGDAERLPVEGHHGTWLGHKGMVLSAEYIKKKLEQEMVLSQAFG-RDLGRGTKHYGLIVVG
HSLGAGTAAILSFLLRPQYPTLKCFAYSPPGGLLSEDAMEYSK---EFVTAVVLGKDLVPRIGLSQLEGF
RRQLLDVLQRSTKPKWREPTYFAIWGDNKAFNEVIISPAMLHEHLPYVVMEGLNKV

>1GT6-A:
EVSQDLFNQFNLFAQYSAAAYCGKNNDAPAGTNITCTGNAC----------------------------
----------------------PEVEKADATFLYSFEDSGVG-----DVTGFLALDNTNKLIVLSFRGSR
SIENWIGNLNFDLKEINDIC--SGCRGHDGFTSSWRSVADTLRQKVEDAVREHP--------DYRVVFTG
HALGGALATVAGADLRGNGYDIDVFSYGAPRVGNRAFAEFLTVQTGGTLYRITHTNDIVPRLPPREFGYS
HSSPEYWIKSGTLVPVTRNDIVKIEGIDATGGNNQPNIPDIPAHLWYFGLIGTCL-
```

Figure 4. Manually adjusted alignment of DAGLα construct and 1GT6 Cysteine-Rich Loop highlighted in yellow, post-regulatory domain region in green, catalytic residues in bold.

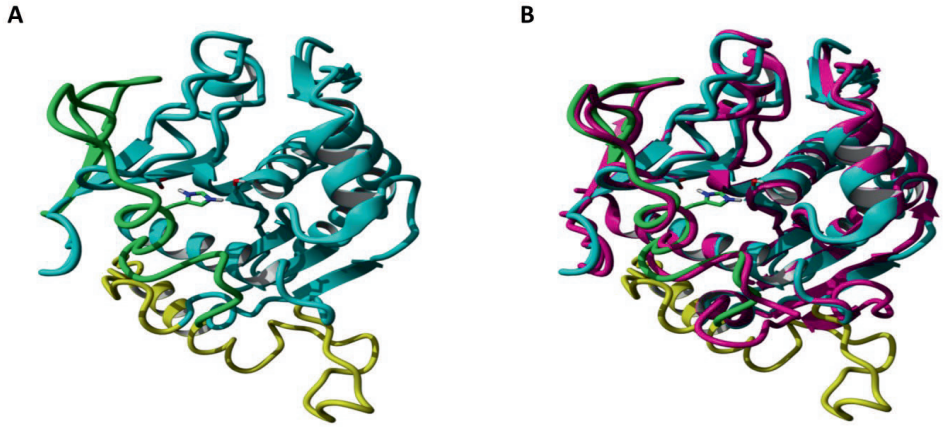

Figure 5. A) Homology model of the DAGLα construct. The sequence used to represent DAGLα was constructed by editing the full sequence to remove the N terminal residues 1-287, the regulatory domain (residues 555-623) and the C terminal region (residues 663-1042). Cysteine-rich loop highlighted in yellow, post-regulatory domain region highlighted in green. **B)** The homology model overlaid with the original template crystal structure PDB code 1GT6 (magenta).[25] Graphical representation produced using PyMol (The PyMOL Molecular Graphics System, Version 1.4.1 Schrödinger, LLC).

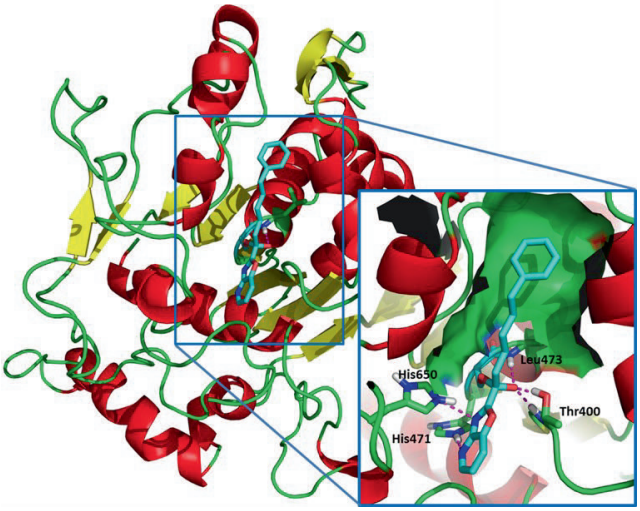

Figure 6. Binding pose of LEI104 in a homology model of hDAGLα. Docking was performed using Yasara docking procedures which implements AutoDock Vina.[27] Molecular dynamics were performed using the AMBER03 forcefield.[28] The MD trajectories were studied using Yasara analysis tools and showed that in 71% of the snapshots a hydrogen bond was observed between the oxyanion intermediate and the backbone NH of Leu473. The Thr400 residue was observed to continually interact with the oxyanion intermediate throughout the simulation with 93% of the snapshots via both the backbone NH and sidechain OH. A total of 76% of the snapshots exhibited hydrogen bonds between His471 and the pyridine nitrogen of LEI104, while H-bond formation between the catalytic His650 and the oxazole nitrogen of LEI104 was also observed in 51% of the snapshots.

Conclusions

The development of a THL based pharmacophore model and screening of a focused library rapidly identified the α-ketoheterocycle LEI104 as a DAGLα inhibitor. The development of a homology model of DAGLα was used to investigate the binding mode of LEI104, indicating a crucial role for the *4N*-oxazolopyridine nitrogen. As LEI104 was originally reported as a potent FAAH inhibitor,[15] optimization of selectivity over this target is required. The homology model provides a clear view of the opportunities to improve the potency and selectivity over FAAH. As such, it is anticipated that the α-ketoheterocycle class will provide an excellent lead series to investigate 2-AG mediated cannabinoid CB1R signaling and for the development of *in vivo* active and selective DAGLα inhibitors, because these compounds 1) have a clearly defined scaffold with good physicochemical properties; 2) are not based on the natural substrate and do not contain known toxicophores (for example fluorophosphonate);[6] 3) are plasma membrane permeable; 4) are highly selective; 5) do not form irreversible covalent bonds,[16–19] which could lead to problems with immunogenicity; and 6) have been shown to be bioavailable and active in animal models.[16–19] The structural insights provided by the DAGLα homology model, may serve as a basis for the development of new therapeutics that can be used to study and treat diseases such as obesity and neurodegeneration.

Experimental

Experimental procedures *in silico*

Development of the DAGLα pharmacophore models

The pharmacophore models are based on the bioactive conformation of THL co-crystalized in fatty acid synthase (FAS, pdb code 2PX6).[13] The β-lactone of the bioactive conformation was closed and the geometry of the reconstituted β-lactone was optimized using Discovery Software Suite 3.5 from Accelrys. The bioactive conformation was separated from the crystal structure, and pharmacophore features were assigned using the manual pharmacophore construction protocol. The essential features that were assigned to pharmacophore model 1 were: *i*) an H-bond acceptor mimicking the carbonyl from the β-lactone warhead, *ii*) hydrophobic hot spots corresponding to the lipophilic tails of THL, *iii*) an H-bond acceptor positioned at the *sn*-2 ester functionality and *iv*) exclusion volumes representing the space occupied by the nucleophilic serine and the backbone oxyanion hole residues in the active site of DAGLα. An additional donor feature derived from the leucinyl formamide moiety of THL was assigned to Model 2. The automated Screen Library protocol (Catalyst/FAST, Accelrys) available from Discovery Studio 3.5 Software was used for docking and conformation generation. This protocol uses the CHARMm force field for energy calculations and a poling mechanism.[29,30] The pharmacophore model was considered rigid, and the inhibitors flexible (255 conformations for each compound). Slight flexibility of the bioactive conformation is accounted for by the sphere radii. The remaining parameters were left on default settings. Each template was visually judged on plausible positioning towards the active site serine. Conformations that did not fit were discarded, while well positioned conformations were documented. This resulted in 36 verified conformations for Model 1 and 21 for Model 2. All conformations were ranked according to feature hits and fit value (Catalyst/FAST, Accelrys fit value calculation procedure).

Development of the DAGLα homology model

The sequence used to represent DAGLα was constructed by editing the full sequence to remove the N terminal residues 1-287, the regulatory domain (residues 555-623) and the C terminal region (residues 663-1042). The alignment) has 230 of 306 target residues (75.2%) aligned to template residues, sequence identity is 18.7% and similarity 37.4% ('similar' means blocks substitution matrix score, BLOSUM62 (> 0). Homology modeling was performed using the automated YASARA procedures.[21–24] These use PSI-Blast[31] to build a position specific scoring matrix (PSSM) from related UniProt sequences which is used to search the PDB for potential templates. Templates are ranked by alignment score and structural quality.[32] Alignments are generated using sequence-based profiles of target and template from UniProt sequences, optionally augmented with structure-based profiles from related template structures. The alignment also considers structural information contained in the template (avoiding gaps in secondary structure elements, keeping polar residues exposed etc.), as well as the predicted target secondary structure.[33] This structure based alignment correction is partly based on SSALN scoring matrices.[34] Loops arising from insertions and deletions are modeled using an indexed version of the PDB to determine optimal loop anchoring points and potential loop conformations. Prefered side chain rotamers are detected, the hydrogen bonding network is optimized and the entire system is subjected to an unrestrained high-resolution refinement with explicit solvent molecules, using a knowledge based forcefield.[24] The homology model of DAGLα was built using the crystal structure of the S146A Mutant Of Thermomyces (Humicola) Lanuginosa Lipase in Complex With Oleic Acid, PDB code 1GT6, the highest scoring template of an enzyme:ligand complex.[25] Blast E-value 3-e38, Align score 47.0, 76% coverage, Total score 19.93. The resulting homology model is shown in Figure 4, overlaid on the template 1GT6.[25] Yasara Model Quality checks compare model features with those observed in high quality X-ray structures. These checks show good quality dihedrals (Z-score 0.027) and satisfactory 1D packing (Z-score -1.844). The poor 3D-packing z-score of -2.440 reflects the remaining uncertainties in the model, however the calculated overall model quality Z-score of -1.850 (rated as

satisfactory) together with visual analysis of the catalytic core and the residues lining the binding cavity suggest the homology model is acceptable.

Docking of LEI104 in the DAGLα homology model

Docking was performed using Yasara docking procedures which implement AutoDock Vina.[27] The protein model was kept rigid while the ligand was treated flexibly. The top 12 scoring poses were retained and examined visually. Figure 5 shows the top scoring pose for LEI104. Energy minimization followed by short Molecular Dynamics simulations were run in order to refine the structure of the docked pose shown in Figure 5. This pose was modified in Yasara to covalently bind the LEI104 structure to the catalytic serine (Ser185 in the model). The geometry around the tetrahydral intermediate was updated and the structure was minimized in Yasara then subjected to a brief Molecular Dynamics procedure. The MD comprised solvating the structure in water in a simulation cell extending 10 Å around all atoms, and subsequent use of default Yasara parameters, including automatic placement of counter ions (Na^+ and Cl^-) to neutralize the simulation cell at pH 7.4, performing an initial energy minimization before reassigning velocities according to a Boltzmann distribution and then running molecular dynamics using the AMBER03 forcefield,[28] at 298 K, with periodic boundary conditions, Van der Waals interaction cut-off 7.86 Å, Long-range (particle-mesh-Ewald)[35] electrostatic interactions, timestep 2.5 fs. Simulation snapshots were saved every 25 ps over the course of the 8 ns simulation. Analysis was performed after discarding the initial 80 snapshots i.e. allowing a short 2 ns equilibration. Structural alignment of initial homology model and the minimized structure resulting from the MD-run showed an RMSD of 1.77 Å. The MD trajectories were studied using Yasara analysis tools and showed that in 71% of the snapshots a hydrogen bond was observed between the oxyanion intermediate and the backbone NH of Leu473. The Thr400 residue was observed to continually interact with the oxyanion intermediate throughout the simulation, in 93% of the snapshots via both the backbone NH and sidechain OH. 76% of the snapshots exhibited hydrogen bonds between His471 and the pyridine nitrogen of LEI104 while H-bond formation between His650 and the oxazole nitrogen of LEI104 was also observed in 51% of the snapshots. Histidine H-bonds were typically observed with suboptimal geometries but were only counted when calculated to be above the Yasara default energy cut-off of 1.5 kcal mol^{-1}.

Experimental procedures biochemistry

DAGLα plasmids

For the preparation of the hDAGLα construct, full length human cDNA was purchased from Biosource and cloned into mammalian expression vector pcDNA3.1, containing genes for ampicillin and neomycin resistance. All plasmids were grown in XL-10 Z-competent cells and prepped (Maxi Prep, Qiagen). The sequences were confirmed by sequence analysis at the Leiden Genome Technology Centre.

Cell culture and membrane preparation.

HEK293T cells were grown in DMEM with stable glutamine and phenolred (PAA) with 10% New Born Calf serum, penicillin and streptomycin. Cells were passaged every 2-3 days by resuspending in medium and seeding them to appropriate confluence. Membranes were prepared from transiently transfected HEK293T cells. One day prior to transfection 10^7 cells were seeded in a 15 cm petri dish. Cells were transfected by the addition of a 3:1 mixture of polyethyleneimine (60 µg) and plasmid DNA (20 µg) in 2 mL serum free medium. The medium was refreshed after 24 h, and after 72 h the cells were harvested by suspending them in 20 mL medium. The suspension was centrifuged for 10 min at 1000 rpm, and the supernatant was removed. The cell pellet was stored at -80 ^oC until use. Cell pellets were thawed on ice and suspended in lysis buffer A (20 mM HEPES, 2 mM DTT, 0.25 M sucrose, 1 mM $MgCl_2$, 1x cocktail (Roche cOmplete EDTA free), 25 U/µL Benzonase). The suspension was homogenized by polytrone (3 × 7 sec) and incubated for 30 min on ice. The suspension was

subjected to ultracentrifugation (93.000 × g, 30 min, 4°C, Beckman Coulter, Type Ti70 rotor) to yield the cytosolic fraction in the supernatant and the membrane fraction as a pellet. The pellet was resuspended in lysis buffer B (20 mM HEPES, 2 mM DTT, 1x Cocktail (Roche cOmplete EDTA free)). The protein concentration was determined with Quick Start Bradford assay (Biorad). The protein fractions were diluted to a total protein concentration of 1 mg/mL and stored in small aliquots at -80°C until use.

Biochemical DAGLα activity assay.

The biochemical hDAGLα activity assay is based on the hydrolysis of *para*-nitrophenylbutyrate (PNP-butyrate) by membrane preparations from HEK293T cells transiently transfected with hDAGLα. 200 µL reactions were performed in flat bottom Greiner 96-wells plates in a 50 mM pH 7.2 HEPES buffer. Membrane protein fractions from HEK293T cells transiently transfected with hDAGLα (0.05 µg/µL final concentration) were used as hDAGLα source. Inhibitors were introduced in 5 µL DMSO. The mixtures were incubated for 20-30 minutes before 5.0 µL 12 mM PNP-butyrate (final concentration 0.3 mM) in DMSO was added (final DMSO concentration 5.0%). Kinetics were followed immediately after addition of PNP-butyrate on a plate reader (TECAN GENios microplate reader), by measuring the OD_{420} every 60 seconds, for 20 minutes at 37°C. The slope of the linear region from 5-15 minutes was determined, and all experiments were performed at N = 2, n = 2 for experimental measurements and N = 2, n = 4 for controls. Data analysis: Z'-factor of each plate was determined for the validation of each experiment, using the following formula Z' = 1-3(σ pc+ σ nc)/(µ pc - µ nc). The slope from 5-15 minutes of the positive control (pc: DAGLα DMSO), and the negative control (nc: mock DMSO) was used. Plates were accepted for further analysis when Z' > 0.6. Kinetic measurements were corrected for the average absorption of the negative control (mock DMSO). The slope of the linear region from 5-15 minutes was determined. The average, standard deviation (SD) and standard error of mean (SEM) were calculated and normalized to the corrected positive control. Data were exported to Graphpad Prism 5.0 for the calculation of the IC_{50} using a nonlinear dose-response analysis.

Experimental procedures chemistry

General remarks

All reactions were performed using oven or flame-dried glassware and dry solvents. Reagents were purchased from Sigma Aldrich, Acros and Merck and used without further purification unless noted otherwise. All moisture sensitive reactions were performed under an argon atmosphere. Traces of water were removed from starting compounds by co-evaporation with toluene. ^{1}H- and ^{13}C-NMR spectra were recorded on a Bruker AV 400 MHz spectrometer at 400.2 (^{1}H) and 100.6 (^{13}C) MHz or a Bruker DMX-600 spectrometer 600 (^{1}H) and 150 (^{13}C) MHz using $CDCl_3$ or CD_3OD as solvent, unless stated otherwise. Chemical shift values are reported in ppm with tetramethylsilane or solvent resonance as the internal standard ($CDCl_3$: δ 7.26 for ^{1}H, δ 77.0 for ^{13}C, CD_3OD: δ 3.31 for ^{1}H). Data are reported as follows: chemical shifts (δ), multiplicity (s = singlet, d = doublet, dd = double doublet, td = triple doublet, t = triplet, q = quartet, quintet = quint, br = broad, m = multiplet), coupling constants *J* (Hz), and integration. HPLC purification was performed on a preparative LC-MS system (Agilent 1200serie) with an Agilent 6130 Quadruple MS detector. High-resolution mass spectra (HRMS) were recorded on a Thermo Scientific LTQ Orbitrap XL. Flash chromatography was performed using SiliCycle silica gel type SiliaFlash P60 (230 – 400 mesh). TLC analysis was performed on Merck silica gel 60/Kieselguhr F254, 0.25 mm. Compounds were visualized using either Seebach's reagent (a mixture of phosphomolybdic acid (25 g), cerium (IV) sulfate (7.5 g), H_2O (500 mL) and H_2SO_4 (25 mL)) or a $KMnO_4$ stain (K_2CO_3 (40 g), $KMnO_4$ (6 g), H_2O (600 mL) and 10% NaOH (5 mL)).

6-Phenylhexanal

A solution of DMSO (0.75 g, 10 mmol) in CH_2Cl_2 was added dropwise to a solution of oxalyl chloride (0.64 g, 5 mmol) in CH_2Cl_2 (5 mL) at -78°C. The mixture was stirred for 1 h before commercially available 6-phenylhexan-1-ol (297 mg, 1.67 mmol) in CH_2Cl_2 (1 mL) was added drop-wise. After addition, the mixture was stirred overnight, and Et_3N (1.7 mL, 16 mmol) was added drop-wise. The mixture was allowed to warm to rt and washed with 1 M HCl. The aqueous layer was extracted with CH_2Cl_2, and the combined organic layers were washed with brine and subsequently dried (Na_2SO_4). Volatiles were removed under reduced pressure and the residue was purified by flash chromatography yielding 6-phenylhexanal (289 mg, 1.65 mmol, 99 %) as a colorless oil. ^{1}H NMR (400 MHz, $CDCl_3$) δ 9.62 (t, *J* = 1.6 Hz, 1H), 7.05-7.17 (m, 5H), 2.51 (t, *J* = 7.6 Hz, 2H), 2.29 (dt, *J* = 1.6, 7.6 Hz, 2H), 1.50-1.56 (m, 4H), 1.24-1.28 (m, 2H); ^{13}C NMR (101 MHz, $CDCl_3$) δ 202.66, 142.38, 128.37, 128.23, 125.60, 43.79, 35.69, 31.21, 28.73, 21.89. Spectroscopic data are in agreement with those reported.[36]

2-Hydroxy-7-phenylheptanenitrile

To a solution of 6-phenylhexanal (289 mg, 1.6 mmol) in (1:1) THF:H_2O (100 mL) was added potassium cyanide (1.2 g, 18 mmol). The reaction mixture was stirred at rt for 72 h. H_2O (10 mL) and Et_2O (10 mL) were added, and the layers were separated. The aqueous layer was extracted with Et_2O and the combined organic layers were washed with saturated $NaHCO_3$ (aq.) and brine before drying (Na_2SO_4). Volatiles were removed under reduced pressure and the residue was purified by flash chromatography yielding 2-hydroxy-7-phenylheptanenitrile (213 mg, 1.0 mmol, 64 %) as a colorless oil. ^{1}H NMR (400 MHz, $CDCl_3$) δ 7.22-7.36 (m, 5H), 4.45 (dt, *J* = 6.0, 6.0 Hz, 1H), 3.71 (d, *J* = 4.8 Hz, 1H), 2.67 (t, *J* = 7.6 Hz, 2H), 1.85 (q, *J* = 8.4 Hz, 2H), 1.70 (quint, *J* = 7.6 Hz, 2H), 1.56 (quint, *J* = 7.2 Hz, 2H), 1.43 (quint, *J* = 7.2 Hz, 2H); ^{13}C NMR (101 MHz, $CDCl_3$) δ 142.38, 128.40, 128.32, 125.74, 120.17, 61.07, 35.68, 34.90, 31.12, 28.47, 24.40.

1-(Oxazolo[4,5-*b*]pyridin-2-yl)-6-phenylhexan-1-ol

A mixture of $CHCl_3$ (2 mL) and ethanol (2 mL) was cooled to 0°C before acetyl chloride (2 mL) was added dropwise. The mixture was stirred for 30 minutes, and 2-hydroxy-7-phenylheptanenitrile (60 mg, 0.28 mmol) in $CHCl_3$ (2 mL) was added. The mixture was stirred for another 1.5 h and the solvent was removed under reduced pressure while keeping the temperature below 25 ^{o}C. The residue was taken up in ethanol (6.5 mL) ethoxyethanol (1 mL) and 2-amino-3-hydroxypyridine (26 mg, 0.24 mmol) was added and the reaction mixture was heated to reflux for 6 h. The solvent was removed under reduced pressure, and the residue was dissolved in EtOAc (30 mL) and 1 M NaOH (10 mL) was added. The layers were separated, and the aqueous layer was extracted with EtOAc. The combined organic layers were washed with brine and dried (Na_2SO_4). Volatiles were removed under reduced pressure and the residue was further purified by flash chromatography yielding 1-(oxazolo[4,5-*b*]pyridin-2-yl)-6-phenylhexan-1-ol (3.0 mg, 0.01 mmol, 3.5 %) as a yellow solid. ^{1}H NMR (400 MHz, CDCl3) δ 8.57 (d, *J* = 3.7 Hz, 2H), 7.84 (d, *J* = 8.0 Hz, 2H), 77.34 – 7.22 (m, 3H), 7.18 – 7.14 (m, 2H), 5.00 (t, *J* = 6.2 Hz, 1H), 3.03 (bs, 1H), 2.60 (t, *J* = 7.7 Hz, 2H), 2.15 – 1.90 (m, 2H), 1.70 – 1.36 (m, 6H); ^{13}C APT NMR (101 MHz, CDCl3) δ 171.10, 154.90, 146.68, 142.55, 128.41, 128.28, 125.67, 124.81, 120.34, 118.67, 68.21, 35.81, 31.27, 29.73, 28.89, 24.72; Purity > 90 % as determined by LC-MS; mass $[M+H]^+$ = 297.07 m/z.

1-(Benzo[*d*]oxazol-2-yl)-6-phenylhexan-1-ol

A mixture of $CHCl_3$ (2.5 mL) and ethanol (2.5 mL) was cooled to 0°C before acetyl chloride (2.5 mL) was added dropwise. The mixture was stirred for 30 minutes, and 2-hydroxy-7-phenylheptanenitrile (319 mg, 1.57 mmol) in $CHCl_3$ (2.5 mL) was added. The mixture was stirred for another 1.5 h and the solvent was removed under reduced pressure while keeping the temperature below 25^{o}C. The residue was taken up in ethanol (6.5 mL), and 2-aminophenol (170 mg, 1.56 mmol) was added. The mixture was refluxed for 6 h. Volatiles were removed under reduced pressure and the residue was purified by flash chromatography yielding 1-(benzo[*d*]oxazol-2-yl)-

6-phenylhexan-1-ol (263 mg, 0.89 mmol, 57 %) as a brown solid. ^{1}H NMR (400 MHz, $CDCl_3$) δ 7.71 (m, 1H), 7.28 (m, 1H), 7.34 (m, 2H), 7.29-7.23 (m, 2H), 7.19-7.13 (m, 3H), 4.96 (dd, *J* = 5.2, 2.0 Hz, 1H), 3.15 (bs, 1H), 2.59 (t, *J* = 7.6 Hz, 2H), 2.11 – 1.91 (m, 2H), 1.64 (quint, *J* = 8.0 Hz, 2H), 1.52 (quint, *J* = 7.6 Hz, 2H), 1.44 – 1.36 (m, 2H); ^{13}C APT NMR (101 MHz, $CDCl_3$) δ 167.95, 150.95, 142.70, 140.42, 128.52, 128.38, 125.77, 125.37, 124.73, 120.11 , 110.95, 68.22, 35.94, 35.64, 31.38, 29.05, 24.90. HRMS (ESI+) m/z: calculated for $C_{19}H_{21}NO_2$ (m + H) 296.165, found 296.164.

1-(Oxazolo[4,5-b]pyridin-2-yl)-6-phenylhexan-1-one

1-(Oxazolo[4,5-*b*]pyridin-2-yl)-6-phenylhexan-1-ol (3.0 mg, 0.01 mmol) was dissolved in CH_2Cl_2 (2 mL), and Dess-Martin periodinane (6.8 mg, 0.016 mmol) was added. The mixture was stirred at rt overnight. Saturated $NaHCO_3$ (aq.) was added and the mixture was stirred for an additional 15 minutes. The layers were separated and the aqueous layer was extracted with CH_2Cl_2. The combined organic layers were washed with brine, and dried (Na_2SO_4). Volatiles were removed under reduced pressure and the residue was further purified by preparative HPLC, yielding 1-(oxazolo[4,5-*b*]pyridin-2-yl)-6-phenylhexan-1-one (1.3 mg, 4.4 μmol, 44 %) as a yellow solid. ^{1}H NMR (400 MHz, $CDCl_3$) δ 8.76 (dd, *J* = 4.7, 1.1 Hz, 1H), 8.00 (dd, *J* = 8.3, 1.3 Hz, 1H), 7.50 (dd, *J* = 8.3, 4.8 Hz, 1H), 7.31 – 7.24 (m, 2H), 7.22 – 7.12 (m, 3H), 3.28 (t, *J* = 7.4 Hz, 2H), 2.64 (t, *J* = 7.7 Hz, 2H), 1.82 (quint, *J* = 7.6, 2H), 1.70 (quint, *J* = 8.0 Hz, 2H), 1.51 – 1.41 (m, 2H); ^{13}C NMR (101 MHz, $CDCl_3$) δ 190.24, 158.48, 154.14, 148.70, 143.58, 142.33, 128.35, 128.24, 125.66, 123.11, 120.20, 39.71, 35.66, 31.09, 28.65, 23.64. Purity > 95 % as determined by LC-MS; mass (M+H) = 295.07 m/z. Spectroscopic data are in agreement with those reported.[15]

1-(Benzo[*d*]oxazol-2-yl)-6-phenylhexan-1-one

1-(Benzo[*d*]oxazol-2-yl)-6-phenylhexan-1-ol (44 mg, 0.15 mmol) was dissolved in CH_2Cl_2. Dess-Martin periodinane (96 mg, 0.23 mmol) was added, and the reaction mixture was stirred for 3.5 h. Volatiles were removed under reduced pressure, and the residue was purified by flash chromatography yielding 1-(benzo[*d*]oxazol-2-yl)-6-phenylhexan-1-one (43 mg, 0.15 mmol, 98 %) as a white solid. ^{1}H NMR (400 MHz, $CDCl_3$) δ 7.89 (d, *J* = 8.0 Hz, 1H), 7.65 (d, *J* = 8.2 Hz, 1H), 7.53 (t, *J* = 7.7 Hz, 1H), 7.46 (t, *J* = 7.7 Hz, 1H), 7.31 – 7.22 (m, 3H), 7.18 (d, *J* = 6.9 Hz, 3H), 3.22 (t, *J* = 7.4 Hz, 3H), 2.68 – 2.57 (m, 2H), 1.85 (p, *J* = 7.5 Hz, 2H), 1.76 – 1.62 (m, 2H), 1.48 (h, *J* = 7.2, 6.5 Hz, 2H); ^{13}C APT NMR (101 MHz, $CDCl_3$) δ 190.37, 157.25, 150.83, 142.54, 140.62, 128.61, 128.51, 128.39, 125.86, 125.80, 122.3, 112.07, 39.58, 35.84, 31.30, 28.83, 23.81. HRMS (ESI+) m/z: calculated for $C_{19}H_{19}NO_2$ (m + H) 294.149, found 294.149.

References

1. Bisogno, T. *et al.* Cloning of the first *sn*1-DAG lipases points to the spatial and temporal regulation of endocannabinoid signaling in the brain. *J. Cell Biol.* **163,** 463–468 (2003).
2. Reisenberg, M., Singh, P. K., Williams, G. & Doherty, P. The diacylglycerol lipases: structure, regulation and roles in and beyond endocannabinoid signaling. *Philos. Trans. R. Soc. B Biol. Sci.* **367,** 3264–3275 (2012).
3. Katona, I. & Freund, T. F. Multiple functions of endocannabinoid signaling in the brain. *Annu. Rev. Neurosci.* **35,** 529–58 (2012).
4. Di Marzo, V. Endocannabinoid signaling in the brain: biosynthetic mechanisms in the limelight. *Nat. Neurosci.* **14,** 9–15 (2011).
5. Nomura, D. K. *et al.* Endocannabinoid hydrolysis generates brain prostaglandins that promote neuroinflammation. *Science* **334,** 809–813 (2011).
6. Bisogno, T. *et al.* Development of the first potent and specific inhibitors of endocannabinoid biosynthesis. *Biochim. Biophys. Acta - Mol. Cell Biol. Lipids* **1761,** 205–212 (2006).
7. Bisogno, T. *et al.* Synthesis and pharmacological activity of a potent inhibitor of the biosynthesis of the endocannabinoid 2-arachidonoylglycerol. *ChemMedChem* **4,** 946–950 (2009).
8. Johnston, M. *et al.* Assay and inhibition of diacylglycerol lipase activity. *Bioorganic Med. Chem. Lett.* **22,** 4585–4592 (2012).
9. Ortar, G. *et al.* Tetrahydrolipstatin analogues as modulators of endocannabinoid 2-arachidonoylglycerol metabolism. *J. Med. Chem.* **51,** 6970–6979 (2008).
10. Hsu, K. L. *et al.* DAGLβ inhibition perturbs a lipid network involved in macrophage inflammatory responses. *Nat. Chem. Biol.* **8,** 999–1007 (2012).
11. Marrs, W. R. *et al.* The serine hydrolase ABHD6 controls the accumulation and efficacy of 2-AG at cannabinoid receptors. *Nat. Neurosci.* **13,** 951–7 (2010).
12. Bisogno, T. *et al.* A novel fluorophosphonate inhibitor of the biosynthesis of the endocannabinoid 2-arachidonoylglycerol with potential anti-obesity effects. *Br. J. Pharmacol.* **169,** 784–793 (2013).
13. Pemble, C. W., Johnson, L. C., Kridel, S. J. & Lowther, W. T. Crystal structure of the thioesterase domain of human fatty acid synthase inhibited by Orlistat. *Nat. Struct. Mol. Biol.* **14,** 704–9 (2007).
14. Ben Ali, Y. *et al.* The molecular mechanism of human hormone-sensitive lipase inhibition by substituted 3-phenyl-5-alkoxy-1,3,4-oxadiazol-2-ones. *Biochimie* **94,** 137–145 (2012).
15. Boger, D. L. *et al.* Exceptionally potent inhibitors of fatty acid amide hydrolase: the enzyme responsible for degradation of endogenous oleamide and anandamide. *Proc. Natl. Acad. Sci. U.S.A.* **97,** 5044–5049 (2000).
16. Lichtman, A. H. Reversible Inhibitors of Fatty Acid Amide Hydrolase That Promote Analgesia: Evidence for an Unprecedented Combination of Potency and Selectivity. *J. Pharmacol. Exp. Ther.* **311,** 441–448 (2004).
17. DeMartino, J. K., Garfunkle, J., Hochstatter, D. G., Cravatt, B. F. & Boger, D. L. Exploration of a fundamental substituent effect of a-ketoheterocycle enzyme inhibitors: Potent and selective inhibitors of fatty acid amide hydrolase. *Bioorganic Med. Chem. Lett.* **18,** 5842–5846 (2008).
18. Leung, D., Hardouin, C., Boger, D. L. & Cravatt, B. F. Discovering potent and selective reversible inhibitors of enzymes in complex proteomes. *Nat. Biotechnol.* **21,** 687–691 (2003).
19. Boger, D. L., Miyauchi, H. & Hedrick, M. P. alpha-Keto heterocycle inhibitors of fatty acid amide hydrolase: carbonyl group modification and alpha-substitution. *Bioorg. Med. Chem. Lett.* **11,** 1517–20 (2001).
20. Pedicord, D. L. *et al.* Molecular characterization and identification of surrogate substrates for diacylglycerol lipase a. *Biochem. Biophys. Res. Commun.* **411,** 809–814 (2011).
21. Krieger, E., Koraimann, G. & Vriend, G. Increasing the precision of comparative models with YASARA NOVA - A self-parameterizing force field. *Proteins Struct. Funct. Genet.* **47,** 393–402 (2002).
22. Krieger, E., Darden, T., Nabuurs, S. B., Finkelstein, A. & Vriend, G. Making optimal use of empirical energy functions: Force-field parameterization in crystal space. *Proteins Struct. Funct. Genet.* **57,** 678–683 (2004).
23. Krieger, E., Nielsen, J. E., Spronk, C. A. E. M. & Vriend, G. Fast empirical pKa prediction by Ewald summation. *J. Mol. Graph. Model.* **25,** 481–486 (2006).
24. Krieger, E. *et al.* Improving physical realism, stereochemistry and side-chain accuracy in homology modeling: four approaches that performed well in CASP8. **77,** 114–122 (2009).

25. Yapoudjian, S. *et al.* Binding of Thermomyces (Humicola) lanuginosa lipase to the mixed micelles of cis-parinaric acid/NaTDC: Fluorescence resonance energy transfer and crystallographic study. *Eur. J. Biochem.* **269,** 1613–1621 (2002).
26. Baggelaar, M. P. *et al.* Development of an activity-based probe and in silico design reveal highly selective inhibitors for diacylglycerol lipase-a in brain. *Angew. Chem. Int. Ed.* **52,** 12081–12085 (2013).
27. Trott, O. & Olson, A. AutoDock Vina: improving the speed and accuracy of docking with a new scoring function, effcient optimization and multithreading. *J. Comput. Chem.* **31,** 455–461 (2010).
28. Duan, Y. *et al.* A Point-Charge Force Field for Molecular Mechanics Simulations of Proteins Based on Condensed-Phase Quantum Mechanical Calculations. *J. Comput. Chem.* **24,** 1999–2012 (2003).
29. Smellie, A., Teig, S. L. & Towbin, P. Poling: promoting conformational variation. *J. Comput. …* **16,** 171–187 (1995).
30. Brooks, B. R. *et al.* CHARMm: The Biomolecular Simulation Program *J. Comput. Chem.* **30,** 1545–1614 (2009).
31. Altschul, S. F. *et al.* Gapped BLAST and PSI-BLAST: A new generation of protein database search programs. *Nucleic Acids Res.* **25,** 3389–3402 (1997).
32. Hooft, R. W. W., Vriend, G., Sander, C. & Abola, E. E. Errors in protein structures. *Nature* **381,** 272–272 (1996).
33. King, R. D. & Sternberg, M. J. Identification and application of the concepts important for accurate and reliable protein secondary structure prediction. *Protein Sci.* **5,** 2298–2310 (1996).
34. Qiu, J. & Elber, R. SSALN: An alignment algorithm using structure-dependent substitution matrices and gap penalties learned from structurally aligned protein pairs. *Proteins Struct. Funct. Genet.* **62,** 881–891 (2006).
35. Essmann, U. *et al.* A smooth particle mesh Ewald method. *J Chem Phys* **103,** 8577–8593 (1995).
36. Murphy, J. A. *et al.* One-carbon extrusion from a tetraazafulvalene. Isolation of aldehydes and a study of their origin. *J. Am. Chem. Soc.* **131,** 6475–6479 (2009).

CHAPTER 3

Comprehensive analysis of structure-activity relationships of α-ketoheterocycles as *sn*-1-diacylglycerol lipase α inhibitors*

Introduction

Sn-1-specific diacylglycerol lipases (DAGLs), of which two isoforms exist (DAGLα and β), catalyse the formation of the signaling lipid 2-arachidonoylglycerol (2-AG) from diacylglycerols.[1] 2-AG is a full cannabinoid CB1 receptor agonist and modulates synaptic plasticity at GABAergic and glutamatergic synapses by regulating neurotransmitter release.[2, 3] In the periphery, 2-AG is mainly produced by DAGLβ, a key enzyme involved in the regulation of macrophage pro-inflammatory responses.[4] Disruption of 2-AG signaling is linked to diet-induced obesity and related metabolic disorders, as well as to addiction and (neuro)inflammation.[2, 3, 5]

2-AG is hydrolysed by monoacylglycerol lipase (MAGL), α/β hydrolase domain 6 and 12 (ABHD6, ABHD12) to give arachidonic acid. Both 2-AG and arachidonic acid can be converted by cyclooxygenase-2 into eicosanoids, including pro-inflammatory prostaglandins (and their ester derivatives) that contribute to neuroinflammation.[6-9] The many players involved in 2-AG metabolism signify that 2-AG and its metabolic products have a wide array of physiological functions, of which many are still poorly understood.[10] For a better understanding of 2-AG-mediated physiological processes, the development of inhibitors that selectively perturb DAGL activity, and hence 2-AG biosynthesis, are of great importance.[11] In addition, these inhibitors may serve as valuable probes to evaluate DAGLα as a novel target to treat human conditions like obesity, diabetes, cardiovascular and neurodegenerative diseases.[7] Recently, α-ketoheterocycles were discovered as a novel and highly potent class of DAGLα inhibitors.[12, 13] α-Ketoheterocycles have previously been applied to the discovery of potent inhibitors of diverse serine hydrolases and cysteine proteases such as fatty acid amide (FAAH),[14] elastase,[15-17] thrombin,[18, 19] factor Xa,[20]

* Janssen, F.J., Baggelaar, M.P., Hummel, J.J.A., Overkleeft, H.S., Cravatt, B.F., Boger, D.L., van der Stelt, M. Comprehensive analysis of structure-activity relationships of α-ketoheterocycles as *sn*-1-diacylglycerol lipase α inhibitors. *J. Med. Chem.* **58**, 9742-9753 (**2015**).

chymase,[21] tryptase,[22] cathepsin K and cathepsin S.[23, 24] The α-ketoheterocycle scaffold provides an electrophilic ketone group with tunable reactivity, as well as a structural template to introduce important interactions with key amino acids in the binding site to obtain potency and selectivity.[24] α-Ketoheterocycles have been shown to be orally bioavailable and have entered human clinical trials, and thus provide an interesting scaffold for probe and drug discovery purposes. 1-(Oxazolo[4,5-*b*]pyridin-2-yl)-6-phenylhexan-1-one (LEI104, OL-100)[25] was identified via pharmocophore-based screening approach, as the first covalent and reversible inhibitor for DAGLα (Chapter 2). Compound **1** (LEI104) had an IC_{50} of 37 ± 5 nM in a colorimetric surrogate DAGLα substrate assay and was highly selective over a panel of serine hydrolases as assessed by gel-based competitive activity-based protein profiling (ABPP). FAAH was identified as its only detected off-target, which was not surprising, because **1** was originally designed as a potent inhibitor of FAAH,[14] an enzyme that inactivates the other endocannabinoid anandamide.

Here, the first extensive SAR study is reported of α-ketoheterocycles as DAGLα inhibitors, by screening of a 1040-member, focused library of FAAH inhibitors, which is mainly based on the α-ketoheterocycle scaffold. Newly synthesized analogues are included in the screens, and thereby the structural requirements for interaction of α-ketoheterocycles with DAGLα were systematically investigated.

Results and Discussion

To investigate the structure-activity relationship (SAR) of **1** a focused library consisting of 1040 previously published α-ketoheterocycles and their corresponding precursors[14, 26-33] was screened using a colorimetric DAGLα activity assay (Figure 1).[12] In total, 64 active compounds were identified with more than 50% inhibitory activity at 10 μM final inhibitor concentration. These active compounds were further analysed in concentration response experiments. To complement the SAR analysis of the focused library, 19 additional α-ketoheterocycles (**3**-**16**, **106-110**) were synthesized and tested.[12] The combined structure-activity-relationships are described in a topological fashion below.

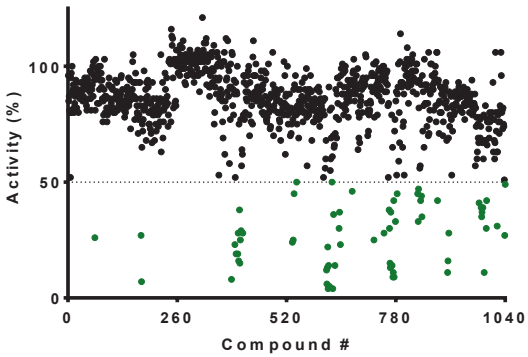

Figure 1. Screening results of the focused library of serine hydrolase inhibitors. 1040 Compounds were screened in duplicate (N = 2) at 10 μM using a colorimetric 96-well assay in which *para*-nitrophenylbutyrate

was used as a surrogate substrate on membranes of HEK293T cells overexpressing recombinant human DAGLα.[12] A total of 64 actives (indicated in green) showed >50% inhibitory activity and were selected for further concentration response analysis.

Central heterocyclic scaffold modifications

First, the influence of the central heterocyclic scaffold on DAGLα activity was explored. A diverse set of α-ketoheterocycles, including benzoxazole (**2**), benzimidazole (**3**), benzothioazole (**4**) and their 4-pyridine analogues (**1**, **5** and **6**, respectively) were analysed. *N4*-oxazolopyridine (**1**) was identified as the most potent scaffold with a pIC_{50} of 7.4 ± 0.05, whereas the other scaffolds have a pIC_{50} < 6 (Table 1) or are completely inactive (**17**-**42**). The imidazolopyridine (**5**) and thiazolopyridine (**6**) are predicted to reduce electrophilicity of the C-2 carbonyl (lower σ_i),[12, 13] thereby possibly reducing inhibitor activity.[15, 34] The basic nitrogen of the oxazolopyridine is another important feature of the scaffold, because its removal resulted in a 100-fold drop in potency (compare **1** and **2**). This observation is corroborated by the fact that other regioisomers of the oxazolopyridine scaffold (**7** and **8**) are also less potent (Table 2). Introduction of other electron withdrawing groups such as fluorine (**9**-**12**) and nitro-substituents (**13**, **14**) resulted in a 5-50 fold increased potency compared to their benzoxazole analogue (**2**), but they did not reach the same extent of inhibition as observed with the oxazolopyridine (**1**). This indicates that the nitrogen at the 4-position is not only required for its electron withdrawing properties, but may also have a specific interaction, likely an H-bond acceptor, with amino acid residues in the binding site. Interestingly, halogens at the 7-position in the heterocyclic scaffold (**12**, **16**) are not allowed.

Deconstruction of the oxazolopyridine scaffold by removal of the pyridyl moiety is not allowed, because using a simple oxazole (**43**) or oxadiazole (**44**,**61**) as scaffolds results in inactive compounds. These results align with the observation, noted above, that the pyridyl provides important interactions with amino acids in the binding pocket. Activity of the oxazole scaffold can (partly) be rescued, however, by introducing small electron withdrawing groups at the *meta*-position (X_4: **45**-**55**), but not at the *para*-position (X_5: **62**-**75**, Table 2). A clear correlation between the electron withdrawing effect of the substituents and pIC_{50} was observed. A plot of the inhibition (pIC_{50}-values) versus the Hammet σ_m constants for the substituents (Figure 2) was found to follow a well-defined correlation (r^2 = 0.78) and the substituent effect was large (ρ = 2.95). This resulted in an almost 1000-fold increase in potency per unit change in σ_m, which indicates that the electron withdrawing effect of the substituent is the dominant factor contributing to the rescue of inhibitory activity. This may be explained by the increased electrophilic character of the reacting C-2 ketone imparted by the electron withdrawing C-4 substituent that leads to an increased strength of the covalent transient state in which Ser472 of the enzyme forms a hemiketal with the inhibitor, thereby increasing its affinity. The magnitude of the effect is similar as that reported previously for the activity of the α-ketoheterocycle inhibitors on FAAH, which indicates that this is a fundamental relationship for α-ketoheterocycles as serine hydrolase inhibitors.[32]

Table 1. Structure-activity relation of compounds with a varying central heterocyclic scaffold (**1-42**)

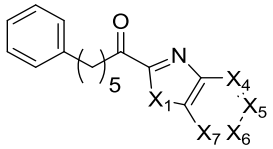

Entry	X_1	X_4	X_5	X_6	X_7	pIC_{50} ± SEM
1[12]	O	N	CH	CH	CH	7.43 ± 0.05
2[12]	O	CH	CH	CH	CH	5.44 ± 0.05
3	NH	CH	CH	CH	CH	4.92 ± 0.21
4	S	CH	CH	CH	CH	< 5
5	NH	N	CH	CH	CH	5.91 ± 0.10
6	S	N	CH	CH	CH	< 5
7	O	CH	N	CH	CH	6.69 ± 0.08
-	O	CH	CH	N	CH	Unstable
8	O	CH	CH	CH	N	5.77 ± 0.12
9	O	CF	CH	CH	CH	6.93 ± 0.17
10	O	CH	CF	CH	CH	5.85 ± 0.12
11	O	CH	CH	CF	CH	6.15 ± 0.11
12	O	CH	CH	CH	CF	< 5
13	O	CH	CNO_2	CH	CH	6.05 ± 0.08
14	O	CH	CH	CNO_2	CH	7.06 ± 0.08
15	O	CH	CH	CBr	CH	5.23 ± 0.12
16	O	CH	CH	CH	CBr	< 5

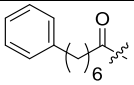

17-19	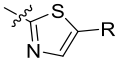	R = pyridin-2-yl, furan-2 yl, thiophen-2-yl	< 5
20-25	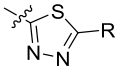	R = H, C(O)OMe, pyridine 2-yl, furan-2-yl, thiophen-2-yl, Ph	< 5
26-31	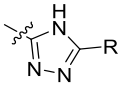	*R = H, C(O)OMe, pyridine 2-yl, furan-2-yl, thiophen-2-yl, Ph*	< 5
32-33		R = H, Me	< 5
34-38	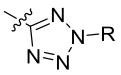	R = H, Me, pyridin-2-yl, furan-2-yl, thiophen-2-yl	< 5

39-42	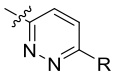	R = H, pyridin-2-yl furan-2-yl, thiophen-2-yl	< 5

The aforementioned hypothesis establishes that both the aldehyde (**52**) and trifluoromethylketone (**45**) inhibit DAGLα as carbonyl active species and not as gem-diols, as previously observed for the FAAH inhibitors.[32] This is because the σ_m values for $CH(OH)_2$ and $C(OH)_2CF_3$, (0.02 and 0.33, respectively), do not explain the observed inhibition, while the σ_m values for C(O) and $C(O)CF_3$ (0.35 and 0.63, respectively) do correlate with DAGLα perturbation. The variation in assay buffer pH (7.4 vs 9.0 for the DAGLα assay and FAAH assay, respectively) may explain the observed differences in hydration state of the activated ketones. Of note, compounds featuring a methyl ketone (**46**) or a *t*-butyl ketone (**49**) display higher than expected activity-based on their σ_m values. This would indicate that these inhibitors exhibit additional H-bond or van der Waals interactions with the enzyme. Remarkably, all *para*-substituted compounds (**62**-**75**) that are able to directly conjugate with the electrophilic carbonyl, did not show any substantial inhibitor activity, whereas the *meta*-substituted derivatives (**45**-**60**), which exert their effects only through inductive electron-withdrawing properties, do inhibit the enzyme. This might be explained by steric hindrance of the *para*-substituents, thereby generating a steric clash that precludes their interaction with DAGLα (Figure 3B). The oxazoles could however, at least theoretically, simply flip their orientation in the active site reversing the location of the nitrogen and oxygen atom of the heterocycle in a manner that places the substituent in a comparable location as the *meta*-substituents. Apparently, this does not happen, which indicates that the electron-withdrawing effect is required, but not sufficient to inhibit DAGLα with *meta*- or *para*-substituted compounds. It also suggests that an additional interaction is required with the *meta*-substituted compounds to perturb DAGLα activity (Figure 3A), which cannot be formed by their *para*-substituted analogues (Figure 3C). Indeed, the nitrogen of the oxazole-scaffold has previously been implicated in H-bonding with the histidine residue of the catalytic triad of elastase.[17] It is, therefore, reasonable to suggest that the α-ketoheterocycle oxazole nitrogen is also required for its interaction with the catalytic His650 from DAGLα. Finally, substituted oxazoles with more sterically demanding side-groups (*e.g.* phenyl/ pyridine, entries **77**-**87**, such as potent FAAH inhibitor OL-135)[26] are not active on DAGLα, which suggest that the *meta*-substituents are located in a pocket that is restricted in size.

Table 2. Structure-activity relation of isoxazoles and oxadiazoles **43-105.**[26, 27, 31-33]

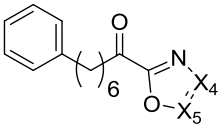

Entry	Substituent X	pIC_{50} ± SEM X_4 (X_5 = CH)	Entry	pIC_{50} ± SEM X_5 (X_4 = CH)
43	CH	< 5	-	-
44	N	5.57 ± 0.03	-	-
-	N	-	**61**	< 5
45	-CC(O)CF_3	6.91 ± 0.02	**62**	5.74 ± 0.03
46	-CC(O)CH_3	6.91 ± 0.03	**63**	< 5
47	-CCF_3	6.67 ± 0.03	**64**	< 5
48	-CSO_2Me	6.41 ± 0.03	**65**	< 5
49	-CC(O)^{t}Bu	6.32 ± 0.04	**-**	-
50	-CCN	6.24 ± 0.05	**66**	< 5
51	-CC(O)OMe	6.20 ± 0.04	**67**	< 5
52	-CCHO	5.82 ± 0.02	**68**	< 5
53	-Cl	5.63 ± 0.07	**-**	-
54	-CCl	5.62 ± 0.05	**69**	< 5
55	-$CCONMe_2$	5.47 ± 0.03	**70**	< 5
56	-COMe	< 5	**71**	< 5
57	-CBr	< 5	**72**	< 5
58	-CMe	< 5	**73**	< 5
59	-CSMe	< 5	**74**	< 5
60	-CC(O)NHMe	< 5	**75**	< 5

Entry	Substituent X	X_4	X_5	pIC_{50} ± SEM
76	-phenyl	CX	CH	5.06 ± 0.08
77	pyridin-2-yl	CX	CH	< 5
78	pyridin-4-yl	CX	CH	< 5
79	-phenyl	CH	CX	< 5
80-84	Mono substituted phenyl (*e.g.* 2, 3 or 4-F, -$COCF_3$, -OMe)	CH	CX	< 5
85-87	Mono substituted pyridine (*e.g.* 4-Me, -OMe, -CF_3)	CH	CX	< 5
88	furan-2-yl	CX	N	6.03 ± 0.03
89	6-cyanopyridin-2-yl	CX	N	5.98 ± 0.05
90	thiophen-2-yl	CX	N	5.71 ± 0.04
91	6-bromopyridin-2-yl	CX	N	5.69 ± 0.06
92	pyridin-2-yl	CX	N	5.56 ± 0.04

93-96	methyl-6-picolinate, 6-picolinic acid, 6-chloropyridin-2-yl, 6-iodopyridin-2-yl	CX	N	< 5
97-101	furan-2-yl, pyridin-2-yl, pyridin-3-yl, pyridin-4-yl, Ph	N	CX	< 5
102-105	R = C(O)OMe, thiophen-2-yl, furan-2-yl, pyridin-2-yl	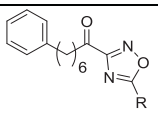		< 5

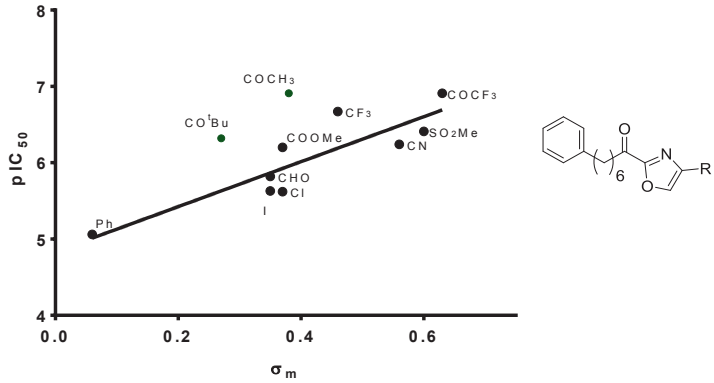

Figure 2. Effect of *meta* electron withdrawing substituent on potency of oxazoles. Electron withdrawing effect of *meta* (X_5) subsituted oxazoles, Hammet constant σ_m versus pIC_{50}. A linear correlation (R^2 = 0.78) with a slope ρ = 2.95 was found. Potency of inhibitors **46** and **49** (-CC(O)CH_3 and -CC(O)^{t}Bu) is higher than predicted solely by the electron withdrawing effect, indicating a potential additional interaction with the enzyme.

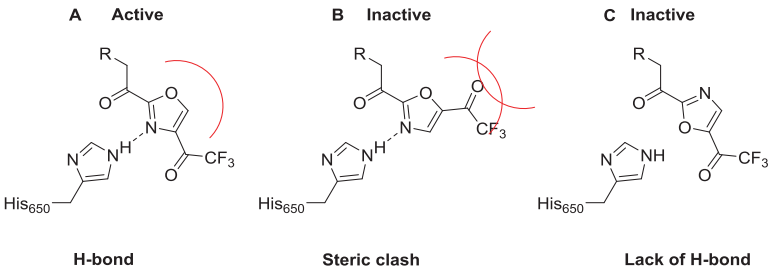

Figure 3. Proposed binding mode of substituted α-keto oxazoles. **A**. *Meta* (X_4) substituted oxazole (exemplified by **45**) forms a hydrogen bond with His650 and positions the substituent away from the highly sterically restricted pocket at X_5. **B**. *Para* (X_5) substituted oxazoles (exemplified by **62**) have a potential steric clash with the enzyme, possibly explaining their low potency on DAGLα. **C.** If the oxazole flips to avoid steric clash (*para* substituted), the oxazole nitrogen is excluded from hydrogen bond formation with His650.

Length of C2-acyl substituents

To investigate the influence of the C-2 acylphenyl spacer length the activity of analogues (**1**, **106-111**) was measured, in which the number of methylene groups was increased from 2 to 8 (Table 3). The inhibitory activity was higher with increasing number of methylene groups, and was highest at n = 8 (compound **111**), thereby making it the most potent inhibitor identified in this study with a pIC_{50} of 8.44 ± 0.04. Compound **109** (n = 6) exhibits a >10-fold drop in activity compared to compound **1** (n = 5). The reason for this reduced activity is not easily explained. When taking lipophilicity into account (i.e. lipophilic efficiency: LipE = pIC_{50} - cLogP), the most efficient linker length was n = 5 (compound **1**). A similar trend was also observed for α-ketoheterocycles in which the C-2 acyl chain consisted of either saturated or mono-unsaturated fatty acids (**112**-**123**, Table 4) Compounds bearing C_2-C_6 chains were inactive, but DAGLα inhibition increased upon further elongation of the acyl chain and was found to be optimal with an oleoyl chain ($C_{18:1}$) in compound **121**. Interestingly, compound **122** with an arachidonoyl substituent ($C_{20:4}$) displayed almost 100-fold less activity compared to its oleoyl analogue. This might indicate that the C-2 acyl chain is located in the hydrophobic channel that harbours the *sn*-1 acyl chain of the natural substrate of DAGLα.

Table 3. Structure-activity relation of C2-acyl derivatives **106-111**.[12, 14]

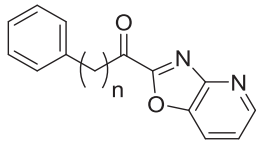

Entry	n	pIC_{50} ± SEM	cLogP	LipE
106	2	4.74 ± 0.15	2.63	2.11
107	3	5.65 ± 0.10	3.01	2.64
108	4	6.69 ± 0.07	3.54	3.15
1	5	7.43 ± 0.05	4.07	3.35
109	6	6.28 ± 0.10	4.60	1.68
110	7	7.33 ± 0.07	5.13	2.20
111	8	8.44 ± 0.04	5.66	2.78

Table 4. Structure-activity relation of of C2-acyl derivatives **112-123**.[14]

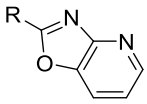

Entry	R	pIC50 ± SEM
112	$(O)C_2H_3$	< 5
113	$(O)C_5H_9$	< 5
114	$(O)C_6H_{11}$	< 5
115	$(O)C_8H_{15}$	6.20 ± 0.03
116	$(O)C_{10}H_{19}$	7.13 ± 0.02
117	$(O)C_{10:1\ \Delta 9}$	6.26 ± 0.04
118	$(O)C_{12}H_{23}$	7.51 ± 0.02
119	$(O)C_{14}H_{27}$	7.13 ± 0.06
120	$(O)C_{16}H_{31}$	7.19 ± 0.04
121	Oleoyl ($C_{18:1}$)	7.58 ± 0.03
122	Arachidonoyl ($C_{20:4}$)	5.62 ± 0.08
123	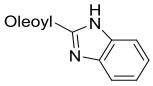	6.71 ± 0.12

FAAH off-target activity

The compounds of the focused library were originally developed as FAAH inhibitors and therefore, the DAGLα pIC_{50} data of the hits was plotted against previously reported FAAH pK_i values (Figure 4). Most of the hits are dual FAAH/DAGLα inhibitors and display high FAAH activity ($pK_i > 8$). Oleoyl-based benzimidazole (**123**, Table 4) and compound **45** were the only two inhibitors selective over FAAH, but they were only moderately potent in the DAGLα assay ($pIC_{50} < 7$).

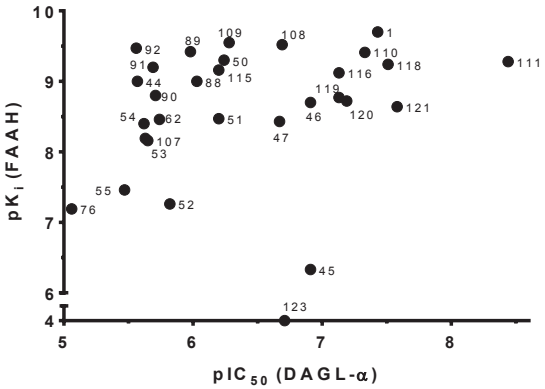

Figure 4. Graphical representation of DAGLα inhibition (pIC_{50}) versus FAAH activity (pK_i). FAAH activity is depicted as reported in literature.[14, 26-33]

Binding mode

Previously, the development of a homology model for DAGLα was reported together with a molecular dynamics simulation with **1** to understand its interaction with hDAGLα at a molecular level (Chapter 2).[12] The model represented the typical α,β-hydrolase fold and the catalytic triad, represented by Ser472, His650, and Asp524, was appropriately aligned in the binding cavity. The tetrahedral transition state of **1**, which is formed through the nucleophilic attack of Ser472 on the α-carbonyl, was minimized and subjected to a short molecular dynamics refinement. The oxyanion intermediate was stabilized by the backbone N–H of Leu473, as well as by the backbone N–H and side chain O–H of Thr400. The oxazole nitrogen of **1** formed hydrogen-bond interactions with His650 and the pyridine nitrogen showed hydrogen-bond interactions with His471 and His650, both of which could further stabilize the tetrahedral intermediate. These proposed hydrogen bonds are in line with the *4N*-oxazolopyridine being the optimal heterocycle. In addition, aliphatic amino acids like Leu427 and Val419 line the hydrophobic pocket accommodating the flexible acyl chain of **1**. This study indicates that this large pocket might normally accommodate *sn*-1 acyl chain of the natural substrate. The proposed binding mode is thus consistent with the observed structure–activity relationships reported in this study.

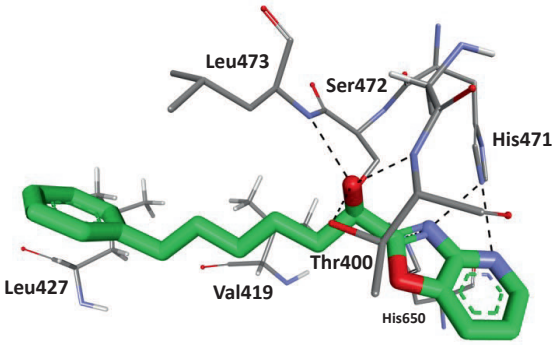

Figure 5. Proposed binding mode of **1** in DAGLα

Conclusions

Screening of an extensive focused library of α-ketoheterocyclic FAAH inhibitors, combined with the synthesis and analysis of novel α-ketoheterocycles, resulted in the rapid generation of a comprehensive and detailed set of structure-activity relationships for DAGLα inhibitors. It was shown that the binding site of DAGLα is remarkably sensitive to the type of α-ketoheterocycle with oxazolo-*4N*-pyridine as the optimal scaffold. The potency of the α-ketoheterocycle is also strongly influenced by a fundamental substituent effect. The electron-withdrawing character of the functional group on the *meta*-position of substituted oxazoles, but not on the *para*-position, increased to large extent inhibitor potency. As previously observed, the C-2 carbonyl (*i.e.* site of reversible covalent attachment) is key to inhibitor activity and its reduction to an hydroxyl group abolished DAGLα inhibition.[12,13] Increasing C-2 acyl chain length enhanced inhibitor activity and was optimal for an oleoyl ($C_{18:1}$) group, while an arachidonoyl ($C_{20:4}$) chain was less preferred. C_6-C_9 acyl chains with a distal phenyl group yielded the most potent inhibitors. These detailed SAR results provided valuable insight in the structural requirements for DAGLα inhibition by α-ketoheterocycles and was fully consistent with the proposed binding pose of **1** in the homology model. The homology mode was successfully applied to guide the design of new DAGLα inhibitors, which led to in the identification of LEI105 as a highly selective, reversible and dual DAGLα/DAGL-β inhibitor that was active in cells and reduced cannabinoid CB_1-receptor dependent synaptic plasticity.[13] Current efforts are directed towards optimizing the physicochemical properties of the α-ketoheterocycles to improve their pharmacokinetic properties. Of note, the reversible character of the α-ketoheterocycle inhibitors may have less probability to induce idiosyncratic toxic side effects, which may be associated with covalent irreversible inhibitors. Consequently, α-ketoheterocycles may provide potential leads for small molecule therapies to treat human conditions like obesity, diabetes, cardiovascular and neurodegenerative diseases where high 2-AG signaling and/or 2-AG metabolite levels play a crucial role.

Experimental

Experimental Procedures Computational Chemistry

The homology model was constructed as previously reported, based on the S146A Mutant Of Thermomyces (Humicola) Lanuginosa Lipase in Complex With Oleic Acid (PDB code 1GT6) as template (Chapter 2).[12]

Experimental Procedures Biochemistry

Cloning Procedures

Cloning procedures were performed as previously reported.[12] In brief, full-length human hDAGL-α cDNA was purchased from Biosource and cloned into mammalian expression vector pcDNA3.1, containing genes for ampicillin and neomycin resistance. The empty vector was used as a negative control (mock). All plasmids were grown in XL-10 Z-competent cells and prepped (Maxi Prep, Qiagen). The sequences were confirmed by sequence analysis at the Leiden Genome Technology Centre.

Cell Culture and Membrane Preparation

Cell culture and membrane preperations were performed as previously reported.[12] In brief, HEK293T cells were grown in DMEM with stable glutamine and phenol red (PAA) with 10% new born calf serum, penicillin, and streptomycin. Cells were passaged every 2−3 days by resuspension in medium and seeding to the appropriate confluence. Membranes were prepared from transiently transfected HEK293T cells. 24 Hours prior to transfection, 10^7 cells were seeded in a 15 cm Petri dish. Cells were transfected by the addition of a 3:1 mixture of polyethyleneimine (60 μg) and plasmid DNA (20 μg) in 2 mL of serum free medium. The medium was refreshed after 24 h, and after 72 h the cells were harvested by suspending them in 20 mL of medium. The supernatant was removed by centrifuge for 10 min at 1000 rpm. The cell pellet was flash frozen in liquid nitrogen and stored at −80 °C until use. Cell pellets were thawed on ice and suspended in lysis buffer A (20 mM HEPES, pH 7.2, 2 mM DTT, 0.25 M sucrose, 1 mM $MgCl_2$, 1× cocktail (Roche cOmplete EDTA free), 25 U/mL Benzonase). The suspension was homogenized by polytrone (3 × 7 s) and incubated for 30 min on ice. The membrane fraction was separated by ultracentrifuge (100.000g, 30 min, 4 °C, Beckman Coulter, type Ti70 rotor) and the pellet was resuspended in lysis buffer B (20 mM HEPES, pH 7.2, 2 mM DTT, 1× cocktail (Roche cOmplete EDTA free)). The protein concentration was determined with Qubit protein assay (Invitrogen). The total protein membrane was diluted to 1.0 mg/mL and the samples were flash frozen in liquid nitrogen and stored in small aliquots at −80 °C until use.

Biochemical hDAGL-α Activity Assay

The biochemical hDAGL-α activity assay was performed as previously reported.[12] In brief, the biochemical hDAGL-α activity assay is based on the hydrolysis of *para*-nitrophenylbutyrate (PNP-butyrate) by membrane preparations from HEK293T cells transiently transfected with hDAGL-α. Reactions (200 μL) were performed in a clear flat bottom Greiner 96-well plates, 50 mM HEPES pH 7.2 buffer with 0.05 μg/μL (final protein concentration) hDAGL-α transfected membrane fractions.

The focused library hit identification was performed using the 96-well plate protocol. Compound plates (13 plates, N = 2) were screened over a total of 4 days. A total of 68 actives were identified (< 50% activity at 10 μM inhibitor concentration, 6.54%).

Focused Library Dose Response Analysis

Dose response analysis was performed on the 64 hits of the hit identification screen. The hits were analysed (ten-fold serial dilution) using the above protocol[12] with minor adjustments for high throughput; 384-well plate, 50 µL total volume, OD_{405} was measured after 60 minutes incubation with PNP-butyrate (final concentration 0.3 mM) on an Envision plate reader.

Experimental Procedures Chemistry

General Remarks

All reactions were performed using oven- or flame-dried glassware and dry solvents. Reagents were purchased from Sigma-Aldrich, Acros, and Merck and used without further purification unless noted otherwise. All moisture sensitive reactions were performed under an argon atmosphere. Traces of water were removed from starting compounds by co-evaporation with toluene. ^{1}H and ^{13}C NMR spectra were recorded on a Bruker AV 400 MHz spectrometer at 400.2 (^{1}H) and 100.6 (^{13}C) MHz using the reported deuterated solvent. Chemical shift values are reported in ppm with tetramethylsilane or solvent resonance as the internal standard ($CDCl_3$: δ 7.26 for ^{1}H, δ 77.16 for ^{13}C; CD_3OD: δ 3.31 for 1H, δ 49.00 for ^{13}C). Data are reported as follows: chemical shifts (δ), multiplicity (s = singlet, d = doublet, dd = double doublet, td = triple doublet, t = triplet, q = quartet, quintet = quint, b = broad, m = multiplet), coupling constants J (*Hz*), and integration. High resolution mass spectra were recorded on a Thermo Scientific LTQ Orbitrap XL. Compound purity (>95% unless stated otherwise) was measured by liquid chromatography on a Finnigan Surveyor LC-MS system, equipped with a C18 column. Flash chromatography was performed using SiliCycle silica gel type SiliaFlash P60 (230–400 mesh). TLC analysis was performed on Merck silica gel 60/Kieselguhr F254, 0.25 mm. Compounds were visualized using either Seebach's reagent (a mixture of phosphomolybdic acid (25 g), cerium(IV) sulfate (7.5 g), H_2O (500 mL), and H_2SO_4 (25 mL)) or a $KMnO_4$ stain (K_2CO_3 (40 g), $KMnO_4$ (6 g), and H_2O (600 mL)).

2-Hydroxy-7-phenylheptanenitrile (124)

The title compound was synthesized from commercially available 6-phenylhexan-1-ol (1.70 g, 9.51 mmol) to yield 2-hydroxy-7-phenylheptanenitrile (1.67 g, 8.22 mmol, 86% over 2 steps) using previously reported procedures. Spectroscopic data are in agreement with those previously reported.[12]

1-(Oxazolo[4,5-*b*]pyridin-2-yl)-6-phenylhexan-1-ol (125)

To a dry round bottom flask containing a solution of dry EtOH (1.4 mL, 17 mmol) and dry $CHCl_3$ (1.4 mL) was added dropwise AcCl (1.4 mL, 19 mmol) at 0°C under argon. The reaction mixture was stirred for 30 minutes after which a solution of 2-hydroxy-7-phenylheptanenitrile (**124**, 117 mg, 0.58 mmol) in dried $CHCl_3$ (1.0 mL) was added dropwise at 0°C under argon. The reaction mixture was stirred for 2 h, slowly warmed up to rt and concentrated at 25°C *in vacuo*. The crude mixture was coevaporated with toluene (3x5 mL) until the white solid imidate was obtained. The solid was dissolved in dry EtOH (1.0 mL) and was added under argon to a sealed and dried microwave tube containing a prestirred solution (80˚C for 30 minutes, then to rt) of commercially available 2-amino-3-hydroxypyridine (68.8 mg, 0.63 mmol) with pyridine (50 µL, 0.63 mmol) in dry EtOH (4.0 mL). The reaction mixture was heated to reflux (80˚C) for 8 h. The reaction mixture was concentrated *in vacuo* and purified by flash chromatography to yield 1-(oxazolo[4,5-*b*]pyridin-2-yl)-6-phenylhexan-1-ol (34 mg, 0.58 mmol, 20%). Spectroscopic data are in agreement with those previously reported.[12]

1-(Oxazolo[4,5-*b*]pyridin-2-yl)-6-phenylhexan-1-one (1)

The title compound was synthesized from 1-(oxazolo[4,5-*b*]pyridin-2-yl)-6-phenylhexan-1-ol (**125**) as previously reported.[12]

1-(Benzo[*d*]oxazol-2-yl)-6-phenylhexan-1-one (2)

The title compound was synthesized from 1-(benzo[*d*]oxazol-2-yl)-6-phenylhexan-1-ol as previously reported.[12]

1-(1*H*-Benzo[*d*]imidazol-2-yl)-6-phenylhexan-1-ol (126)

The title compound was synthesized from 2-hydroxy-7-phenylheptanenitrile (**124**, 100 mg, 0.49 mmol) and commercially available benzene-1,2-diamine (55 mg, 0.51 mmol) according to the procedure described for compound **125**. This yielded 1-(1*H*-benzo[d]imidazol-2-yl)-6-phenylhexan-1-ol (136 mg, 0.46 mmol, 94%). ^{1}H NMR ($CDCl_3$, 400 MHz): δ 7.47 (dd, *J* = 7.0, 3.4 Hz, 2H), 7.25 – 7.11 (m, 3H), 7.06 (d, *J* = 7.4 Hz, 2H), 6.77 – 6.65 (m, 2H), 5.29 (bs, 2H), 4.92 (d, *J* = 6.7 Hz, 2H), 2.43 (t, *J* = 7.7 Hz, 2H), 1.94 – 1.56 (m, 4H), 1.55 – 1.04 (m, 4H). ^{13}C APT NMR ($CDCl_3$, 101 MHz): δ 157.55, 142.67, 137.57, 134.67, 128.44(2C), 128.31(2C), 125.69, 122.81, 120.49, 116.92, 115.00, 68.43, 36.90, 35.86, 31.31, 29.04, 25.23.

1-(1*H*-Benzo[*d*]imidazol-2-yl)-6-phenylhexan-1-one (3)

The title compound was synthesized from 1-(1*H*-benzo[*d*]imidazol-2-yl)-6-phenylhexan-1-ol (**126**, 65 mg, 0.22 mmol) according to the procedure described for compound **1**. This yielded 1-(1*H*-benzo[*d*]imidazol-2-yl)-6-phenylhexan-1-one (22 mg, 0.075 mmol, 34%). HRMS (ESI+) m/z: calculated for $C_{19}H_{21}N_2O$ ([M + H]), 293.1648; found, 293.1648. ^{1}H NMR ($CDCl_3$, 400 MHz): δ 10.75 (bs, 1H), 7.91 (bs, 1H), 7.55 (bs, 1H), 7.40 (bs, 2H), 7.29 – 7.23 (m, 2H), 7.21 – 7.13 (m, 3H), 3.31 (t, *J* = 7.5 Hz, 2H), 2.62 (t, *J* = 7.7 Hz, 2H), 1.85 (p, *J* = 7.5 Hz, 2H), 1.70 (p, *J* = 7.7 Hz, 2H), 1.55 – 1.41 (m, 2H). ^{13}C BBDEC NMR ($CDCl_3$, 101 MHz): δ 194.82, 147.60, 142.86 (bs), 142.52, 134.18 (bs), 128.40(2C), 128.27(2C), 125.66, 124.83 (bs, 2C), 121.42 (bs), 112.62 (bs), 38.36, 35.77, 31.30, 28.84, 23.82. Purity of >95% as determined by LC-MS.

1-(Benzo[*d*]thiazol-2-yl)-6-phenylhexan-1-ol (127)

The title compound was synthesized from 2-hydroxy-7-phenylheptanenitrile (**124**, 50 mg, 0.25 mmol) and commercially available 2-aminobenzenethiol (0.03 mL, 0.28 mmol) according to the procedure described for compound **125**. This yielded 1-(benzo[*d*]thiazol-2-yl)-6-phenylhexan-1-ol (63 mg, 0.20 mmol, 83%). ^{1}H NMR ($CDCl_3$, 400 MHz): δ 7.97 (d, *J* = 8.2 Hz, 1H), 7.87 (d, *J* = 8.2, 1H), 7.51 – 7.41 (m, 1H), 7.41 – 7.32 (m, 1H), 7.31 – 7.21 (m, 2H), 7.21 – 7.10 (m, 4H), 5.08 (t, *J* = 7.9, 1H), 2.59 (t, *J* = 7.8, 2H), 2.11 – 1.26 (m, 8H). ^{13}C APT NMR ($CDCl_3$, 101 MHz): δ 152.76, 142.61, 134.81, 130.91, 128.41(2C), 128.26(2C), 126.11, 125.64, 125.04, 122.86, 121.86, 72.29, 38.05, 35.83, 31.30, 29.01, 24.98.

1-(Benzo[*d*]thiazol-2-yl)-6-phenylhexan-1-one (4)

The title compound was synthesized from 1-(benzo[*d*]thiazol-2-yl)-6-phenylhexan-1-ol (**127**, 50 mg, 0.16 mmol) according to the procedure described for compound **1**. This yielded 1-(1*H*-imidazo[4,5-b]pyridin-2-yl)-6-phenylhexan-1-one (16 mg, 0.05 mmol, 32%). HRMS (ESI+) m/z: calculated for $C_{19}H_{20}NOS$ ([M + H]), 310.1260; found, 310.1260. ^{1}H NMR ($CDCl_3$, 400 MHz): δ 8.23 – 8.13 (m, 1H), 8.01 – 7.93 (m, 1H), 7.61 – 7.48 (m, 2H), 7.31 – 7.23 (m, 2H), 7.21 – 7.13 (m, 3H), 3.27 (t, *J* = 7.4 Hz, 2H), 2.63 (t, *J* = 7.8 Hz, 2H), 1.84 (p, *J* = 7.8 Hz, 2H), 1.70 (p, *J* = 7.8 Hz, 2H), 1.54 – 1.42 (m, 2H). ^{13}C APT NMR ($CDCl_3$, 101 MHz): δ 195.65, 166.67, 153.69, 142.65, 137.38, 128.53(2C), 128.39(2C), 127.73, 127.07, 125.78, 125.51, 122.57, 38.65, 35.88, 31.37, 28.96, 23.94. Purity of >95% as determined by LC-MS.

1-(1*H*-Imidazo[4,5-*b*]pyridin-2-yl)-6-phenylhexan-1-ol (128)

The title compound was synthesized from 2-hydroxy-7-phenylheptanenitrile (**124**, 254 mg, 1.25 mmol) and commercially available pyridine-2,3-diamine (54 mg, 0.40 mmol) according to the procedure described for compound **125**. This yielded 1-(1*H*-imidazo[4,5-*b*]pyridin-2-yl)-6-phenylhexan-1-ol (24 mg, 0.08 mmol, 16%). ^{1}H NMR (MeOD, 400 MHz): δ 8.33 (d, *J* = 4.7 Hz, 1H), 7.95 (dd, *J* = 8.1, 1.5 Hz, 1H), 7.28 (dd, J = 8.0, 4.9 Hz, 1H), 7.23 – 7.17 (m, 2H), 7.16 – 7.05 (m, 3H), 4.98 – 4.91 (m, 1H), 2.57 (t, *J* = 8.0 Hz, 2H), 2.06 – 1.82 (m, 2H), 1.61

(p, *J* = 7.4 Hz, 2H), 1.51 – 1.42 (m, 2H), 1.41 – 1.31 (m, 2H). ^{13}C APT NMR (MeOD, 101 MHz): δ 162.22, 153.23 (bs), 144.53, 143.79, 131.27 (bs), 129.36(2C), 129.22(2C), 126.60, 124.00 (bs), 119.27, 69.40, 37.70, 36.76, 32.58, 29.99, 25.97.

1-(1*H*-Imidazo[4,5-*b*]pyridin-2-yl)-6-phenylhexan-1-one (5)

The title compound was synthesized from 1-(1*H*-imidazo[4,5-*b*]pyridin-2-yl)-6-phenylhexan-1-ol (**128**, 23.7 mg, 0.08 mmol) according to the procedure described for compound **1**. This yielded 1-(1*H*-imidazo[4,5-b]pyridin-2-yl)-6-phenylhexan-1-one (10 mg, 0.034 mmol, 43%). HRMS (ESI+) m/z: calculated for $C_{18}H_{20}N_3O$ ([M + H]), 294.1601; found, 294.1600. ^{1}H NMR ($CDCl_3$, 400 MHz): δ 14.92 (bs, 1H), 8.91 (d, *J* = 4.3 Hz, 1H), 8.30 (d, *J* = 8.1 Hz, 1H), 7.43 (dd, *J* = 8.2, 4.7 Hz, 1H), 7.29 – 7.24 (m, 2H), 7.21 – 7.14 (m, 3H), 3.32 (t, *J* = 8.0, 7.0 Hz, 2H), 2.65 (t, *J* = 7.6 Hz, 2H), 1.89 (p, *J* = 7.5 Hz, 2H), 1.78 – 1.65 (m, 2H), 1.57 – 1.45 (m, 2H). ^{13}C APT NMR ($CDCl_3$, 101 MHz): δ 194.41, 149.12, 147.18, 142.52, 136.08, 136.10, 130.78, 128.42(2C), 128.27(2C), 125.67, 119.55, 38.17, 35.78, 31.28, 28.87, 23.75. Purity of >95% as determined by LC-MS.

2-Aminopyridine-3-thiol (129)

Commercially available 3-(*tert*-butylthio)pyridin-2-amine (235.4 mg, 1.291 mmol) was refluxed in 37% aq. HCl (5 mL, 60.0 mmol) for 14 h until completion. The mixture was concentrated *in vacuo* and coevaporated with toluene (3 x 20 mL). The resulting solid was taken up in sat. $NaHCO_3$ (40 mL), extracted with EtOAc (3 x 20 mL), washed with brine, dried and concentrated *in vacuo* to obtain 2-aminopyridine-3-thiol (155 mg, 1.228 mmol, 95 % yield) without further purification. ^{1}H NMR (MeOD, 400 MHz): δ 7.95 (dd, *J* = 5.0, 1.8 Hz, 1H), 7.32 (dd, *J* = 7.4, 1.8 Hz, 1H), 6.51 (dd, *J* = 7.5, 5.0 Hz, 1H). ^{13}C BBDEC NMR (MeOD, 101 MHz): 161.06, 150.74, 146.34, 114.42, 114.36.

1-(Thiazolo[4,5-*b*]pyridin-2-yl)-6-phenylhexan-1-ol (130)

The title compound was synthesized from 2-hydroxy-7-phenylheptanenitrile (**124**, 52.3 mg 0.257 mmol) and 2-aminopyridine-3-thiol (**129**, 41.9 mg, 0.332 mmol) according to the procedure described for compound **125**. This yielded 1-(thiazolo[4,5-*b*]pyridin-2-yl)-6-phenylhexan-1-ol (15.4 mg, 0.049 mmol, 19%). ^{1}H NMR ($CDCl_3$, 400 MHz): δ 8.68 (dd, *J* = 4.7, 1.6 Hz, 1H), 8.22 (dd, *J* = 8.0, 1.6 Hz, 1H), 7.30 (dd, *J* = 8.0, 4.7 Hz, 1H), 7.28 – 7.22 (m, 2H), 7.19 – 7.13 (m, 3H), 5.19 (dd, *J* = 8.0, 4.4 Hz, 1H), 3.97 (bs, 1H), 2.58 (t, *J* = 7.6 Hz, 2H), 2.12 – 1.86 (m, 2H), 1.69 – 1.48 (m, 4H), 1.46 – 1.35 (m, 2H). ^{13}C APT NMR ($CDCl_3$, 101 MHz): δ 181.08, 163.86, 148.00, 142.72, 131.12, 128.65, 128.51(2C), 128.36(2C), 125.74, 119.85, 72.49, 37.88, 35.95, 31.40, 29.12, 24.99.

1-(Thiazolo[4,5-*b*]pyridin-2-yl)-6-phenylhexan-1-one (6)

The title compound was synthesized from 1-(thiazolo[4,5-*b*]pyridin-2-yl)-6-phenylhexan-1-ol (**130**, 15.4 mg, 0.049 mmol) according to the procedure described for compound **1**. This yielded 1-(thiazolo[4,5-*b*]pyridin-2-yl)-6-phenylhexan-1-one (10.9 mg, 0.035 mmol, 71%). HRMS (ESI+) m/z: calculated for $C_{18}H_{19}N_2OS$ ([M + H]), 311.1213; found, 311.1213. ^{1}H NMR ($CDCl_3$, 400 MHz): δ 8.89 (dd, *J* = 4.5, 1.7 Hz, 1H), 8.38 (dd, *J* = 8.2, 1.7 Hz, 1H), 7.47 (dd, *J* = 8.2, 4.6 Hz, 1H), 7.31 – 7.23 (m, 2H), 7.18 (d, *J* = 7.3 Hz, 3H), 3.35 (t, *J* = 7.4 Hz, 2H), 2.63 (t, *J* = 7.8 Hz, 2H), 1.86 (p, *J* = 7.5 Hz, 2H), 1.75 – 1.64 (m, 2H), 1.54 – 1.43 (m, 2H). ^{13}C BBDEC NMR ($CDCl_3$, 101 MHz): δ 195.55, 169.14, 163.78, 149.94, 142.60, 131.94, 131.48, 128.53(2C), 128.40(2C), 125.79, 122.10, 38.89, 35.87, 31.32, 28.96, 23.96. Purity of >95% as determined by LC-MS.

3-Amino-4-hydroxypyridine (131)

To a solution of commercially available 4-hydroxy-3-nitropyridine (500 mg, 3.58 mmol) in methanol (25 mL) was added 100 mg of 10% Pd/C. The reaction mixture was stirred under hydrogen atmosphere for 10 h. Upon completion the solution was filtered and concentrated *in vacuo* to obtain 3-amino-4-hydroxypyridine (350 mg,

3.18 mmol, 89%). ^{1}H NMR (DMSO-d6, 400 MHz): δ 7.34 (dd, *J* = 6.7, 1.6 Hz, 1H), 7.12 (s, 1H), 5.99 (d, *J* = 6.6 Hz, 1H), 4.52 (s, 2H).

1-(Oxazolo[4,5-*c*]pyridin-2-yl)-6-phenylhexan-1-ol (132)

To a dry round bottom flask containing a solution of dry EtOH (1.0 mL, 17 mmol) and dry $CHCl_3$ (1.0 mL) was added dropwise AcCl (1.0 mL, 14 mmol) at 0°C under argon. The reaction mixture was stirred for 30 minutes after which a solution of 2-hydroxy-7-phenylheptanenitrile (**124**, 213 mg, 1.05 mmol) in dry $CHCl_3$ (1.0 mL) was added dropwise at 0°C under argon. The reaction mixture was stirred for 2 h, slowly warmed up to rt and concentrated at 25°C *in vacuo*. The imidate was dissolved in dry EtOH (1.0 mL) and was added under argon to a sealed microwave tube containing 3-amino-4-hydroxypyridine (**131**, 121 mg, 1.1 mmol) in dry EtOH (4.0 mL). The reaction mixture was heated to reflux (80˚C) for 8 h using microwave irradiation. The reaction mixture was concentrated *in vacuo* and purified by flash chromatography to yield 1-(oxazolo[4,5-*c*]pyridin-2-yl)-6-phenylhexan-1-ol (16 mg, 0.054 mmol, 5%). ^{1}H NMR ($CDCl_3$, 400 MHz): δ 9.03 (s, 1H), 8.56 (dd, *J* = 5.6, 1.4 Hz, 1H), 7.50 (dt, *J* = 5.6, 1.0 Hz, 1H), 7.28-7.24 (m, 2H), 7.21 – 7.10 (m, 3H), 5.00 (dd, *J* = 7.6, 5.3 Hz, 1H), 2.60 (t, *J* = 7.2 Hz, 2H), 2.13 – 1.93 (m, 2H), 1.64 (p, 2H), 1.58 – 1.47 (m, 2H), 1.46 – 1.39 (m, 2H).^{13}C APT NMR ($CDCl_3$, 101 MHz): δ 168.81, 156.07, 145.56, 142.85, 142.59, 138.46, 128.49(2C), 128.38(2C), 125.80, 106.91, 68.04, 35.91, 35.52, 31.33, 28.97, 24.92.

1-(Oxazolo[4,5-*c*]pyridin-2-yl)-6-phenylhexan-1-one (7)

To a solution of 1-(oxazolo[4,5-*c*]pyridin-2-yl)-6-phenylhexan-1-ol (**132**, 15 mg, 0.050 mmol) in dry CH_2Cl_2 (3 mL) was added Dess-Martin periodinane (43 mg, 0.1 mmol). The reaction mixture was stirred for 10 h and quenched with 5 mL sat. $NaHCO_3$ (aq.) upon completion. The organic layer was washed with sat. $NaHCO_3$ (aq.), brine, dried on $MgSO_4$, filtered, concentrated *in vacuo* and purified by flash chromatography to obtain 1-(oxazolo[4,5-*c*]pyridin-2-yl)-6-phenylhexan-1-one (9.7 mg, 0.033 mmol, 66%). HRMS (ESI+) m/z: calculated for $C_{18}H_{19}N_2O_2$ (M + H^+) 295.1441; found 295.1440. ^{1}H NMR ($CDCl_3$, 400 MHz): δ 9.26 (s, 1H), 8.77 – 8.70 (d, *J* = 3.6 Hz, 1H), 7.64 (d, *J* = 5.6 Hz, 1H), 7.29-7.25 (m, 2H), 7.19 – 7.15 (m, 3H), 3.23 (t, *J* = 7.4 Hz, 2H), 2.64 (t, *J* = 7.7 Hz, 2H), 1.87 (p, *J* = 7.5 Hz, 2H), 1.69 (p, *J* = 7.7 Hz, 2H), 1.53 – 1.42 (m, 2H). ^{13}C APT NMR ($CDCl_3$, 101 MHz): δ 189.78, 157.42, 155.66, 148.03, 145.64, 142.46, 128.51(2C), 128.42(2C), 125.85, 107.73, 39.77, 35.82, 31.26, 28.78, 23.71. Purity of 90% as determined by LC-MS.

1-(Oxazolo[5,4-*b*]pyridin-2-yl)-6-phenylhexan-1-ol (133)

The title compound was synthesized from 2-hydroxy-7-phenylheptanenitrile (**124**, 59 mg, 0.29 mmol) and commercially available 3-amino-2-hydroxypyridine (35 mg, 0.31 mmol) according to the procedure described for compound **132**. This yielded 1-(oxazolo[5,4-*b*]pyridin-2-yl)-6-phenylhexan-1-ol (5 mg, 0.018 mmol, 6%). ^{1}H NMR ($CDCl_3$, 400 MHz): δ 8.36 (dd, *J* = 5.0, 1.6 Hz, 1H), 8.03 (dd, *J* = 7.9, 1.6 Hz, 1H), 7.35 (dd, *J* = 7.8, 5.0 Hz, 1H), 7.30 – 7.27 (m, 2H), 7.20 – 7.14 (m, 3H), 5.01 – 4.95 (m, 1H), 2.60 (t, *J* = 7.6 Hz, 2H), 2.14 – 1.90 (m, 2H), 1.82 – 1.73 (m, 2H), 1.60 – 1.50 (m, 4H). ^{13}C APT NMR ($CDCl_3$, 101 MHz): δ 168.19, 159.96, 144.98, 142.65, 132.46, 128.82(2C), 128.51(2C), 128.39, 125.78, 121.16, 68.30, 35.93, 35.45, 31.37, 29.02, 24.85.

1-(Oxazolo[5,4-*b*]pyridin-2-yl)-6-phenylhexan-1-one (8)

The title compound was synthesized from 1-(oxazolo[5,4-*b*]pyridin-2-yl)-6-phenylhexan-1-ol (**133**, 5 mg, 0.018 mmol) according to the procedure described for compound **7**. This yielded 1-(oxazolo[5,4-*b*]pyridin-2-yl)-6-phenylhexan-1-one (3 mg, 0.010 mmol, 57%). HRMS (ESI+) m/z: calculated for $C_{18}H_{19}N_2O_2$ (M + H^+) 295.1441; found 295.1441. ^{1}H NMR ($CDCl_3$, 400 MHz): δ 8.58 (dd, *J* = 4.9, 1.6 Hz, 1H), 8.24 (dd, *J* = 8.0, 1.6 Hz, 1H), 7.48 (dd, *J* = 8.0, 4.9 Hz, 1H), 7.30 – 7.24 (m, 2H), 7.19 – 7.16 (m, 3H), 3.21 (t, *J* = 7.4 Hz, 2H), 2.64 (t, *J* = 7.6 Hz, 2H), 1.85 (p, *J* = 7.5 Hz, 2H), 1.75 – 1.66 (m, 2H), 1.50 – 1.44 (m, 2H). ^{13}C APT NMR ($CDCl_3$, 101 MHz): δ 189.73, 156.64, 148.66, 142.39, 132.41, 131.24, 128.40(2C), 128.30(2C), 125.72, 122.15, 39.40, 35.71, 31.15, 28.68, 23.56. Purity of >95% as determined by LC-MS.

1-(4-Fluorobenzo[*d*]oxazol-2-yl)-6-phenylhexan-1-ol (134)

The title compound was synthesized from 2-hydroxy-7-phenylheptanenitrile (**124**, 100 mg, 0.49 mmol) and commercially available 2-amino-3-fluorophenol (62 mg, 0.49 mmol) according to the procedure described for compound **125**. This yielded 1-(4-fluorobenzo[*d*]oxazol-2-yl)-6-phenylhexan-1-ol (99 mg, 0.32 mmol, 65%). ^{1}H NMR ($CDCl_3$, 400 MHz): δ 7.34 – 7.29 (m, 1H), 7.29 – 7.23 (m, 3H), 7.19 – 7.13 (m, 3H), 7.05 (ddd, *J* = 9.3, 7.8, 1.3 Hz, 1H), 4.97 (dd, *J* = 7.7, 5.2 Hz, 1H), 2.60 (t, *J* = 7.6 Hz, 2H), 2.09 – 1.91 (m, 2H), 1.68 – 1.60 (m, 2H), 1.56 – 1.46 (m, 2H), 1.44 – 1.37 (m, 2H). ^{13}C APT NMR ($CDCl_3$, 101 MHz): δ 168.28, 153.47 (d, *J* = 256.54 Hz), 153.03 (d, *J* = 7.1 Hz), 142.67, 129.23 (d, *J* = 16.2 Hz), 128.49(2C), 128.36(2C), 125.76 (d, *J* = 7.1 Hz), 125.74, 110.96 (d, *J* = 17.6 Hz), 107.07 (d, *J* = 4.5 Hz), 68.09, 35.91, 35.55, 31.36, 28.99, 24.90.

1-(4-Fluorobenzo[*d*]oxazol-2-yl)-6-phenylhexan-1-one (9)

The title compound was synthesized from 1-(4-fluorobenzo[*d*]oxazol-2-yl)-6-phenylhexan-1-ol (**134**, 63 mg, 0.20 mmol) according to the procedure described for compound **7**. This yielded 1-(4-fluorobenzo[*d*]oxazol-2-yl)-6-phenylhexan-1-one (41 mg, 0.13 mmol, 66%). HRMS (ESI+) m/z: calculated for $C_{19}H_{19}FNO_2$ ([M + H]), 312.1394; found, 312.1393. ^{1}H NMR ($CDCl_3$, 400 MHz): δ 8.23 – 8.13 (m, 1H), 8.01 – 7.93 (m, 1H), 7.61 – 7.48 (m, 2H), 7.31 – 7.23 (m, 2H), 7.21 – 7.13 (m, 3H), 3.27 (t, *J* = 7.4 Hz, 2H), 2.63 (t, *J* = 7.8 Hz, 2H), 1.84 (p, *J* = 7.8 Hz, 2H), 1.70 (p, *J* = 7.8 Hz, 2H), 1.54 – 1.42 (m, 2H). ^{13}C APT NMR ($CDCl_3$, 101 MHz): δ 190.01, 157.23, 154.85 (d, *J* = 260.6 Hz), 152.67 (d, *J* = 6.1 Hz), 142.52, 129.79 (d, *J* = 20.2 Hz), 129.16 (d, *J* = 7.1 Hz), 128.51(2C), 128.40(2C), 125.81, 111.73 (d, *J* = 17.2 Hz), 108.16 (d, J = 5.1 Hz), 39.56, 35.83, 31.29, 28.78, 23.72. Purity of >95% as determined by LC-MS.

1-(5-Fluorobenzo[*d*]oxazol-2-yl)-6-phenylhexan-1-ol (135)

The title compound was synthesized from 2-hydroxy-7-phenylheptanenitrile (**124**, 124 mg, 0.61 mmol) and commercially available 2-amino-4-fluorophenol (72 mg, 0.57 mmol) according to the procedure described for compound **132**. This yielded 1-(5-fluorobenzo[*d*]oxazol-2-yl)-6-phenylhexan-1-ol (133 mg, 0.42 mmol, 75%). ^{1}H NMR ($CDCl_3$, 400 MHz): δ 7.45 (dd, *J* = 8.9, 4.2 Hz, 1H), 7.39 (dd, *J* = 8.3, 2.6 Hz, 1H), 7.30 – 7.22 (m, 2H), 7.20 – 7.12 (m, 3H), 7.08 (td, *J* = 9.1, 2.6 Hz, 1H), 4.94 (dd, *J* = 7.6, 5.1 Hz, 1H), 2.70 (bs, 1H), 2.60 (t, *J* = 7.8 Hz, 2H), 2.12 – 1.87 (m, 2H), 1.70 – 1.57 (m, 2H), 1.56 – 1.45 (m, 2H), 1.45 – 1.33 (m, 2H). ^{13}C BBDEC NMR ($CDCl_3$, 101 MHz): δ 169.65, 160.15 (d, *J* = 241.4 Hz), 147.24 (d, *J* = 1.0 Hz), 142.65, 141.35 (d, *J* = 13.1 Hz), 128.51(2C), 128.39(2C), 125.78, 113.05 (d, *J* = 26.3 Hz), 111.26 (d, *J* = 10.1 Hz), 106.66 (d, *J* = 25.3 Hz), 68.21, 35.93, 35.58, 31.39, 29.01, 24.89.

1-(5-Fluorobenzo[*d*]oxazol-2-yl)-6-phenylhexan-1-one (10)

The title compound was synthesized from 1-(5-fluorobenzo[*d*]oxazol-2-yl)-6-phenylhexan-1-ol (**135**, 44 mg, 0.14 mmol) according to the procedure described for compound **7**. This yielded 1-(5-fluorobenzo[*d*]oxazol-2-yl)-6-phenylhexan-1-one (33 mg, 0.10 mmol, 74%). HRMS (ESI+) m/z: calculated for $C_{19}H_{19}FNO_2$ ([M + H]), 312.1394; found, 312.1395. ^{1}H NMR ($CDCl_3$, 400 MHz): δ 7.61 (dd, *J* = 9.0, 4.2 Hz, 1H), 7.56 (dd, *J* = 8.0, 2.5 Hz, 1H), 7.32 – 7.24 (m, 2H), 7.21 – 7.13 (m, 3H), 3.20 (t, *J* = 7.4 Hz, 2H), 2.64 (t, *J* = 7.5 Hz, 2H), 1.84 (p, *J* = 7.5 Hz, 2H), 1.75 – 1.63 (m, 2H), 1.52 – 1.41 (m, 2H). ^{13}C BBDEC NMR ($CDCl_3$, 101 MHz): δ 190.10, 160.66 (d, *J* = 244.4 Hz), 158.69, 147.20 (d, *J* = 1.0 Hz), 142.53, 141.35 (d, *J* = 14.1 Hz), 128.53(2C), 128.42(2C), 125.84, 116.97 (d, *J* = 27.3 Hz), 112.71 (d, *J* = 10.1 Hz), 108.28 (d, *J* = 25.3 Hz), 39.63, 35.85, 31.31, 28.82, 23.75. Purity of >95% as determined by LC-MS.

2-Amino-5-fluorophenol (136)

The title compound was synthesized from commercially available 5-fluoro-2-nitrophenol (500 mg, 3.18 mmol) according to the procedure described for compound **131**. This yielded 2-amino-5-fluorophenol (388 mg, 3.05 mmol, 96%). ^{1}H NMR (DMSO-d6, 400 MHz): δ 6.53 (dd, *J* = 8.3, 6.3 Hz, 1H), 6.46 (dd, *J* = 10.3, 2.6 Hz, 1H), 6.35

(td, *J* = 8.7, 2.7 Hz, 1H). ^{13}C APT NMR (DMSO-d6, 101 MHz): δ 154.63 (d, *J* = 230.8 Hz), 144.99, 133.47, 114.32 (d, *J* = 9.3 Hz), 105.16 (d, *J* = 21.3 Hz), 102.28 (d, *J* = 24.9 Hz).

1-(6-Fluorobenzo[*d*]oxazol-2-yl)-6-phenylhexan-1-ol (137)

The title compound was synthesized from 2-hydroxy-7-phenylheptanenitrile (**124**, 110 mg, 0.54 mmol) and 2-amino-5-fluorophenol (**136**, 72 mg, 0.57 mmol) according to the procedure described for compound **132**. This yielded 1-(6-fluorobenzo[*d*]oxazol-2-yl)-6-phenylhexan-1-ol (66 mg, 0.21 mmol, 39%). ^{1}H NMR ($CDCl_3$, 400 MHz): δ 7.62 (dd, *J* = 8.8, 4.8 Hz, 1H), 7.29 – 7.25 (m, 2H), 7.24 – 7.21 (m, 1H), 7.19 – 7.13 (m, 3H), 7.08 (ddd, *J* = 9.5, 8.7, 2.4 Hz, 1H), 4.93 (dd, *J* = 7.6, 5.2 Hz, 1H), 2.59 (t, *J* = 6.4 Hz, 2H), 2.08 – 1.89 (m, 2H), 1.63 (p, *J* = 7.8 Hz, 2H), 1.55 – 1.46 (m, 2H), 1.44 – 1.36 (m, 2H). ^{13}C APT NMR ($CDCl_3$, 101 MHz): δ 168.45 (d, *J* = 4.0 Hz), 160.72 (d, *J* = 244.4 Hz), 150.84 (d, J = 15.2 Hz), 142.65, 136.83 (d, *J* = 1.0 Hz), 128.50(2C), 128.38(2C), 125.78, 120.41 (d, *J* = 10.1 Hz), 112.69 (d, *J* = 24.2 Hz), 99.01 (d, *J* = 28.3 Hz), 68.11, 35.93, 35.52, 31.38, 29.01, 24.92.

1-(6-Fluorobenzo[*d*]oxazol-2-yl)-6-phenylhexan-1-one (11)

The title compound was synthesized from 1-(6-fluorobenzo[*d*]oxazol-2-yl)-6-phenylhexan-1-ol (**137**, 44 mg, 0.14 mmol) according to the procedure described for compound **7**. This yielded 1-(6-fluorobenzo[*d*]oxazol-2-yl)-6-phenylhexan-1-one (37 mg, 0.12 mmol, 85%). HRMS (ESI+) m/z: calculated for $C_{19}H_{19}FNO_2$ ([M + H]), 312.1394; found, 312.1393. ^{1}H NMR ($CDCl_3$, 400 MHz): δ 8.23 – 8.13 (m, 1H), 8.01 – 7.93 (m, 1H), 7.61 – 7.48 (m, 2H), 7.31 – 7.23 (m, 2H), 7.21 – 7.13 (m, 3H), 3.27 (t, *J* = 7.4 Hz, 2H), 2.63 (t, *J* = 7.8 Hz, 2H), 1.84 (p, *J* = 7.8 Hz, 2H), 1.70 (p, *J* = 7.8 Hz, 2H), 1.54 – 1.42 (m, 2H). ^{13}C APT NMR ($CDCl_3$, 101 MHz): δ 189.79, 162.71 (d, *J* = 250.5 Hz), 158.04 (d, *J* = 4.0 Hz), 151.03 (d, *J* = 15.2 Hz), 142.50, 136.98 (d, *J* = 1.0 Hz), 128.49(2C), 128.38(2C), 125.80, 123.11 (d, *J* = 10.1 Hz), 114.66 (d, *J* = 25.3 Hz), 99.73 (d, *J* = 27.3 Hz), 39.48, 35.82, 31.25, 28.81, 23.79. Purity of >95% as determined by LC-MS.

1-(7-Fluorobenzo[*d*]oxazol-2-yl)-6-phenylhexan-1-ol (138)

The title compound was synthesized from 2-hydroxy-7-phenylheptanenitrile (**124**, 124 mg, 0.61 mmol) and commercially available 2-amino-6-fluorophenol (75 mg, 0.59 mmol) according to the procedure described for compound **125**. This yielded 1-(7-fluorobenzo[*d*]oxazol-2-yl)-6-phenylhexan-1-ol (157 mg, 0.50 mmol, 85%). ^{1}H NMR ($CDCl_3$, 400 MHz): δ 7.50 (dd, *J* = 8.0, 0.9 Hz, 1H), 7.33 – 7.22 (m, 3H), 7.20 – 7.13 (m, 3H), 7.13 – 7.06 (m, 1H), 4.97 (dd, *J* = 7.7, 5.1 Hz, 1H), 3.06 (bs, 1H), 2.60 (t, *J* = 7.9 Hz, 2H), 2.19 – 1.88 (m, 2H), 1.73 – 1.58 (m, 2H), 1.58 – 1.46 (m, 2H), 1.46 – 1.33 (m, 2H). ^{13}C BBDEC NMR ($CDCl_3$, 101 MHz): δ 168.34, 147.16 (d, *J* = 253.5 Hz), 143.82 (d, *J* = 2.0 Hz), 142.66, 138.05 (d, *J* = 11.1 Hz), 128.51(2C), 128.38(2C), 125.78, 125.15 (d, *J* = 5.0 Hz), 115.93 (d, *J* = 4.0 Hz), 112.17 (d, *J* = 16.2 Hz), 68.13, 35.93, 35.60, 31.38, 29.00, 24.90.

1-(7-Fluorobenzo[*d*]oxazol-2-yl)-6-phenylhexan-1-one (12)

The title compound was synthesized from 1-(7-fluorobenzo[*d*]oxazol-2-yl)-6-phenylhexan-1-ol (**138**, 46 mg, 0.15 mmol) according to the procedure described for compound **1**. This yielded 1-(7-fluorobenzo[*d*]oxazol-2-yl)-6-phenylhexan-1-one (39 mg, 0.13 mmol, 86%). HRMS (ESI+) m/z: calculated for $C_{19}H_{19}FNO_2$ ([M + H]), 312.1394; found, 312.1395. ^{1}H NMR ($CDCl_3$, 400 MHz): δ 7.68 (dd, *J* = 8.1, 1.0 Hz, 1H), 7.41 (td, *J* = 8.2, 4.5 Hz, 1H), 7.31 – 7.24 (m, 3H), 7.21 – 7.14 (m, 3H), 3.22 (t, *J* = 7.4 Hz, 2H), 2.64 (t, *J* = 7.9 Hz, 2H), 1.85 (p, *J* = 7.5 Hz, 2H), 1.74 – 1.65 (m, 2H), 1.52 – 1.41 (m, 2H). ^{13}C BBDEC NMR ($CDCl_3$, 101 MHz): δ 189.70, 157.49, 147.54 (d, *J* = 255.5 Hz), 143.65 (d, *J* = 1.0 Hz), 142.53, 138.34 (d, *J* = 11.1 Hz) 128.53(2C), 128.42(2C), 126.26 (d, *J* = 6.1 Hz), 125.84, 118.10 (d, *J* = 4.04 Hz), 114.89 (d, *J* = 16.2 Hz), 39.84, 35.85, 31.31, 28.81, 23.72. Purity of >95% as determined by LC-MS.

1-(5-Nitrobenzo[*d*]oxazol-2-yl)-6-phenylhexan-1-ol (139)

The title compound was synthesized from 2-hydroxy-7-phenylheptanenitrile (**124**, 131 mg, 0.64 mmol) and commercially available 2-amino-4-nitrophenol (99 mg, 0.64 mmol) according to the procedure described for compound **125**. This yielded 1-(5-nitrobenzo[*d*]oxazol-2-yl)-6-phenylhexan-1-ol (120 mg, 0.35 mmol, 55%). ^{1}H NMR ($CDCl_3$, 400 MHz): δ 8.58 (d, *J* = 2.2 Hz, 1H), 8.30 (dd, *J* = 8.9, 2.2 Hz, 1H), 7.62 (d, *J* = 8.9 Hz, 1H), 7.30 – 7.23 (m, 2H), 7.18 – 7.13 (m, 3H), 5.01 (dd, *J* = 7.7, 5.2 Hz, 1H), 2.60 (t, *J* = 7.2 Hz, 2H), 2.11 – 1.93 (m, 2H), 1.64 (p, *J* = 7.8 Hz, 2H), 1.57 – 1.50 (m, 2H), 1.45 – 1.37 (m, 2H). ^{13}C APT NMR ($CDCl_3$, 101 MHz): δ 171.10, 154.28, 145.41, 142.49, 140.96, 128.42(2C), 128.33(2C), 125.75, 121.43, 116.49, 111.18, 68.06, 35.84, 35.41, 31.27, 28.90, 24.87.

1-(5-Nitrobenzo[*d*]oxazol-2-yl)-6-phenylhexan-1-one (13)

The title compound was synthesized from 1-(5-nitrobenzo[*d*]oxazol-2-yl)-6-phenylhexan-1-ol (**139**, 74 mg, 0.22 mmol) according to the procedure described for compound **7**. This yielded 1-(5-nitrobenzo[*d*]oxazol-2-yl)-6-phenylhexan-1-one (55 mg, 0.16 mmol, 74%). HRMS (ESI+) m/z: calculated for $C_{38}H_{37}N_4O_8$ ([2M + H]), 677.2606; found, 677.2605. ^{1}H NMR ($CDCl_3$, 400 MHz): δ 8.79 (d, *J* = 2.2 Hz, 1H), 8.47 (dd, *J* = 9.0, 2.3 Hz, 1H), 7.79 (d, *J* = 9.1 Hz, 1H), 7.29 – 7.24 (m, 2H), 7.21 – 7.15 (m, 3H), 3.24 (t, *J* = 7.4 Hz, 2H), 2.64 (t, *J* = 7.2 Hz, 2H), 1.86 (p, *J* = 7.5 Hz, 2H), 1.76 – 1.66 (m, 2H), 1.53 – 1.43 (m, 2H) ^{13}C APT NMR ($CDCl_3$, 101 MHz): δ 189.60, 159.38, 153.98, 146.13, 142.38, 140.83, 128.45(2C), 128.36(2C), 125.80, 124.05, 118.84, 112.55, 39.74, 35.76, 31.19, 28.71, 23.61. Purity of >95% as determined by LC-MS.

1-(6-Nitrobenzo[*d*]oxazol-2-yl)-6-phenylhexan-1-ol (140)

The title compound was synthesized from 2-hydroxy-7-phenylheptanenitrile (**124**, 100 mg, 0.49 mmol) and commercially available 2-amino-5-nitrophenol (76 mg, 0.49 mmol) according to the procedure described for compound **125**. This yielded 1-(6-nitrobenzo[*d*]oxazol-2-yl)-6-phenylhexan-1-ol (59 mg, 0.17 mmol, 35%). ^{1}H NMR ($CDCl_3$, 400 MHz): δ 8.42 (d, *J* = 2.1 Hz, 1H), 8.30 (dd, *J* = 8.8, 2.1 Hz, 1H), 7.80 (d, *J* = 8.8 Hz, 1H), 7.28 – 7.22 (m, 2H), 7.18 – 7.12 (m, 3H), 5.01 (dd, *J* = 7.7, 5.1 Hz, 1H), 2.60 (t, *J* = 7.6 Hz, 2H), 2.12 – 1.93 (m, 2H), 1.64 (p, *J* = 7.8 Hz, 2H), 1.57 – 1.49 (m, 2H), 1.45 – 1.38 (m, 2H). ^{13}C APT NMR ($CDCl_3$, 101 MHz): δ 172.53, 150.10, 145.85, 145.50, 142.54, 128.48(2C), 128.40(2C), 125.82, 120.85, 120.21, 107.65, 68.25, 35.90, 35.55, 31.32, 28.94, 24.87.

1-(6-Nitrobenzo[*d*]oxazol-2-yl)-6-phenylhexan-1-one (14)

The title compound was synthesized from 1-(6-nitrobenzo[*d*]oxazol-2-yl)-6-phenylhexan-1-ol (**140**, 40 mg, 0.12 mmol) according to the procedure described for compound **7**. This yielded 1-(6-nitrobenzo[*d*]oxazol-2-yl)-6-phenylhexan-1-one (35 mg, 0.10 mmol, 86%). HRMS (ESI+) m/z: calculated for $C_{38}H_{37}N_4O_8$ ([2M + H]), 677.2606; found, 677.2605. ^{1}H NMR ($CDCl_3$, 400 MHz): δ 8.55 (s, 1H), 8.39 (d, *J* = 8.9 Hz, 1H), 8.02 (d, *J* = 8.9 Hz, 1H), 7.30 – 7.25 (m, 2H), 7.21 – 7.15 (m, 3H), 3.23 (t, *J* = 7.3 Hz, 2H), 2.64 (t, *J* = 7.7 Hz, 2H), 1.86 (p, *J* = 7.5 Hz, 2H), 1.71 (p, *J* = 7.6 Hz, 2H), 1.53 – 1.43 (m, 2H). ^{13}C APT NMR ($CDCl_3$, 101 MHz): δ 189.50, 160.31, 149.92, 147.49, 145.34, 142.38, 128.45(2C), 128.37(2C), 125.82, 122.69, 121.43, 108.76, 39.83, 35.76, 31.17, 28.72, 23.59. Purity of >95% as determined by LC-MS.

1-(6-Bromobenzo[*d*]oxazol-2-yl)-6-phenylhexan-1-ol (141)

The title compound was synthesized from 2-hydroxy-7-phenylheptanenitrile (**124**, 124 mg, 0.61 mmol) and commercially available 2-amino-5-bromophenol (93 mg, 0.50 mmol) according to the procedure described for compound **132**. This yielded 1-(6-bromobenzo[*d*]oxazol-2-yl)-6-phenylhexan-1-ol (116 mg, 0.31 mmol, 62%). ^{1}H NMR ($CDCl_3$, 400 MHz): δ 7.84 (d, *J* = 1.9 Hz, 1H), 7.46 (dd, *J* = 8.6, 1.9 Hz, 1H), 7.40 (d, *J* = 8.6 Hz, 1H), 7.30 – 7.22 (m, 2H), 7.21 – 7.11 (m, 3H), 4.94 (dd, *J* = 7.6, 5.1 Hz, 1H), 2.60 (t, *J* = 7.8 Hz, 2H), 2.60 (bs, 1H), 2.16 – 1.85 (m, 2H), 1.63 (p, *J* = 7.6 Hz, 2H), 1.57 – 1.45 (m, 2H), 1.45 – 1.34 (m, 2H). ^{13}C BBDEC NMR ($CDCl_3$, 101 MHz): δ

169.03, 149.94, 142.64, 142.18, 128.51(2C), 128.41, 128.39(2C), 125.79, 123.21, 117.44, 112.18, 68.16, 35.93, 35.57, 31.38, 29.00, 24.88.

1-(6-Bromobenzo[*d*]oxazol-2-yl)-6-phenylhexan-1-one (15)

The title compound was synthesized from 1-(6-bromobenzo[*d*]oxazol-2-yl)-6-phenylhexan-1-ol (**141**, 43 mg, 0.11 mmol) according to the procedure described for compound **7**. This yielded 1-(6-bromobenzo[*d*]oxazol-2-yl)-6-phenylhexan-1-one (38 mg, 0.10 mmol, 89%). HRMS (ESI+) m/z: calculated for $C_{19}H_{19}BrNO_2$ ([M + H]), 372.0594 and 374.0573; found, 372.0596 and 374.0575. ^{1}H NMR ($CDCl_3$, 400 MHz): δ 8.03 (d, *J* = 1.9 Hz, 1H), 7.64 (dd, *J* = 8.8, 1.8 Hz, 1H), 7.54 (d, *J* = 8.7 Hz, 1H), 7.31 – 7.23 (m, 2H), 7.21 – 7.14 (m, 3H), 3.20 (t, *J* = 7.4 Hz, 2H), 2.64 (t, *J* = 7.7 Hz, 2H), 1.84 (p, *J* = 7.5 Hz, 2H), 1.75 – 1.63 (m, 2H), 1.52 – 1.41 (m, 2H). ^{13}C APT NMR ($CDCl_3$, 101 MHz): δ 190.09, 158.00, 149.77, 142.52, 142.13, 131.77, 128.53(2C), 128.42(2C), 125.85, 125.23, 118.67, 113.38, 39.68, 35.85, 31.30, 28.81, 23.74. Purity of >95% as determined by LC-MS.

2-Amino-6-bromophenol (142)

To a solution of commercially available 2-bromo-6-nitrophenol (200 mg, 0.92 mmol) in EtOH (3 mL) under argon atmosphere was added $SnCl_2$ (870 mg, 4.59 mmol) and the reaction mixture was heated to 70°C. After full conversion (5 minutes) the reaction mixture was cooled to rt and poured into ice water (20 mL). The pH was set to 10 (3M NaOH) and the mixture was stirred for thirty minutes. The water layer was extracted with 3× 30 mL EtOAc. The organic layer was washed with 50 mL brine, treated with charcoal and filtered, dried ($MgSO_4$), filtered and concentrated *in vacuo* to yield 2-amino-6-bromophenol (42 mg, 0.22 mmol, 25%). ^{1}H NMR (MeOD, 400 MHz): δ 7.07 (dd, *J* = 8.1, 1.5 Hz, 1H), 6.93 (dd, *J* = 7.9, 1.4 Hz, 1H), 6.67 (t, *J* = 8.0 Hz, 1H). ^{13}C APT NMR (MeOD, 101 MHz): δ 145.56, 132.00, 127.50, 122.52, 119.45, 111.94.

1-(7-Bromobenzo[*d*]oxazol-2-yl)-6-phenylhexan-1-ol (143)

The title compound was synthesized from 2-hydroxy-7-phenylheptanenitrile (**124**, 98 mg, 0.49 mmol) and 2-amino-6-bromophenol (**142**, 92 mg, 0.49 mmol) according to the procedure described for compound **125**. This yielded 1-(7-bromobenzo[*d*]oxazol-2-yl)-6-phenylhexan-1-ol (132 mg, 0.36 mmol, 73%). ^{1}H NMR ($CDCl_3$, 400 MHz): δ 7.61 (dd, *J* = 7.9, 1.0 Hz, 1H), 7.46 (dd, *J* = 8.0, 1.0 Hz, 1H), 7.29 – 7.22 (m, 2H), 7.22 – 7.11 (m, 4H), 4.97 (dd, *J* = 7.8, 5.1 Hz, 1H), 2.58 (t, *J* = 7.6 Hz, 2H), 2.11 – 1.91 (m, 2H), 1.67 – 1.58 (m, 2H), 1.56 – 1.47 (m, 2H), 1.43 – 1.37 (m, 2H). ^{13}C APT NMR ($CDCl_3$, 101 MHz): δ 168.30, 148.97, 142.60, 141.12, 128.44(2C), 128.31(2C), 125.80, 119.09, 102.74, 67.99, 35.86, 35.49, 31.31, 28.93, 24.95.

1-(7-Bromobenzo[*d*]oxazol-2-yl)-6-phenylhexan-1-one (16)

The title compound was synthesized from 1-(7-bromobenzo[*d*]oxazol-2-yl)-6-phenylhexan-1-ol (**143**, 37 mg, 0.10 mmol) according to the procedure described for compound **1**. This yielded 1-(7-bromobenzo[*d*]oxazol-2-yl)-6-phenylhexan-1-one (41 mg, 0.13 mmol, 66%). HRMS (ESI+) m/z: calculated for $C_{19}H_{19}BrNO_2$ ([M + H]), 372.0594 and 374.0573; found, 372.0596 and 374.0574. ^{1}H NMR (CDCl3, 400 MHz): δ 7.83 (dd, J = 8.1, 1.0 Hz, 1H), 7.68 (dd, J = 8.0, 1.0 Hz, 1H), 7.35 (t, J = 8.0 Hz, 1H), 7.30 – 7.25 (m, 2H), 7.20 – 7.16 (m, 3H), 3.20 (t, J = 7.4 Hz, 2H), 2.63 (t, J = 7.6 Hz, 2H), 1.85 (p, *J* = 7.5 Hz, 2H), 1.74 – 1.65 (m, 2H), 1.52 – 1.43 (m, 2H). ^{13}C APT NMR ($CDCl_3$, 101 MHz): δ 189.67, 157.18, 149.16, 142.54, 141.24, 131.57, 128.53(2C), 128.42(2C), 126.96, 125.84, 121.37, 103.90, 39.77, 35.85, 31.30, 28.82, 23.80. Purity of 95% as determined by LC-MS.

2-Hydroxy-4-phenylbutanenitrile (144)

The title compound was synthesized from commercially available 3-phenylpropanal (1.00 g 7.45 mmol) according to the previously reported procedure.[12] This yielded 2-hydroxy-4-phenylbutanenitrile (810 mg, 5.02 mmol, 68%). ^{1}H NMR ($CDCl_3$, 400 MHz): δ 7.38 – 7.33 (m, 2H), 7.30 – 7.23 (m, 3H), 4.40 (t, *J* = 6.8 Hz, 1H), 4.19

(bs, 1H), 2.83 (t, *J* = 8.0 Hz, 2H), 2.18 – 2.07 (m, 2H). ^{13}C APT NMR ($CDCl_3$, 101 MHz): δ 139.56, 128.54(2C), 128.40(2C), 126.35, 119.96, 60.02, 36.28, 30.46.

1-(Oxazolo[4,5-*b*]pyridin-2-yl)-3-phenylpropan-1-ol (145)

The title compound was synthesized from 2-hydroxy-4-phenylbutanenitrile (**144**, 190 mg, 1.18 mmol) and commercially available 2-amino-3-hydroxypyridine (142 mg, 1.29 mmol) according to the procedure described for compound **125**. This yielded 1-(oxazolo[4,5-*b*]pyridin-2-yl)-3-phenylpropan-1-ol (44 mg, 0.17 mmol, 15%). ^{1}H NMR ($CDCl_3$, 400 MHz): δ 8.52 (dd, *J* = 4.9, 1.4 Hz, 1H), 7.78 (dd, *J* = 8.2, 1.4 Hz, 1H), 7.30 – 7.25 (m, 2H), 7.24 – 7.19 (m, 3H), 7.19 – 7.13 (m, 1H), 5.06 (dd, *J* = 7.8, 5.0 Hz, 1H), 4.31 (bs, 1H), 2.92 – 2.79 (m, 2H), 2.47 – 2.26 (m, 2H). ^{13}C BBDEC NMR ($CDCl_3$, 101 MHz): δ 171.12, 154.90, 146.51, 143.15, 140.90, 128.68(2C), 128.53(2C), 126.16, 120.40, 118.83, 67.33, 36.91, 31.17.

1-(Oxazolo[4,5-*b*]pyridin-2-yl)-3-phenylpropan-1-one (106)

The title compound was synthesized from 1-(oxazolo[4,5-*b*]pyridin-2-yl)-3-phenylpropan-1-ol (**145**, 43.8 mg, 0.17 mmol) according to the procedure described for compound **1**. This yielded 1-(oxazolo[4,5-*b*]pyridin-2-yl)-3-phenylpropan-1-one (40 mg, 0.16 mmol, 93%). HRMS (ESI+) m/z: calculated for $C_{15}H_{13}N_2O_2$ ([M + H]), 253.0972; found, 253.0970. ^{1}H NMR ($CDCl_3$, 400 MHz): δ 8.76 (dd, *J* = 4.8, 1.5 Hz, 1H), 8.00 (dd, *J* = 8.3, 1.5 Hz, 1H), 7.50 (dd, *J* = 8.3, 4.7 Hz, 1H), 7.34 – 7.27 (m, 4H), 7.25 – 7.16 (m, 1H), 3.63 (t, *J* = 7.7 Hz, 2H), 3.16 (t, *J* = 7.6 Hz, 2H). ^{13}C BBDEC NMR ($CDCl_3$, 101 MHz): δ 189.38, 158.53, 154.20, 148.90, 143.77, 140.10, 128.72(2C), 128.58(2C), 126.53, 123.36, 120.44, 41.43, 29.70. Purity of >95% as determined by LC-MS.

2-Hydroxy-5-phenylpentanenitrile (146)

The title compound was synthesized commercially available 4-phenylbutan-1-ol (500 mg, 3.33 mmol) according to the previously reported 2 step procedure.[12] This yielded 2-hydroxy-5-phenylpentanenitrile (439 mg, 2.51 mmol, 75% over 2 steps). ^{1}H NMR ($CDCl_3$, 400 MHz): δ 7.32 – 7.25 (m, 2H), 7.22 – 7.14 (m, 3H), 4.46 – 4.38 (m, 1H), 3.10 (bs, 1H), 2.69 – 2.65 (m, 2H), 1.90 – 1.74 (m, 4H). ^{13}C APT NMR ($CDCl_3$, 101 MHz): δ 141.24, 128.59(2C), 128.49(2C), 126.23, 120.04, 61.16, 35.10, 34.61, 26.27.

1-(Oxazolo[4,5-*b*]pyridin-2-yl)-4-phenylbutan-1-ol (147)

The title compound was synthesized from 2-hydroxy-5-phenylpentanenitrile (**146**, 206 mg, 1.18 mmol) and commercially available 2-amino-3-hydroxypyridine (129 mg, 1.17 mmol) according to the procedure described for compound **125**. This yielded 1-(oxazolo[4,5-*b*]pyridin-2-yl)-4-phenylbutan-1-ol (56 mg, 0.21 mmol, 18%). ^{1}H NMR ($CDCl_3$, 400 MHz): δ 8.48 (dd, *J* = 4.9, 1.5 Hz, 1H), 7.77 (dd, *J* = 8.2, 1.5 Hz, 1H), 7.27 – 7.21 (m, 3H), 7.19 – 7.12 (m, 3H), 5.08 (dd, *J* = 7.5, 5.5 Hz, 1H), 4.62 (bs, 1H), 2.67 (t, *J* = 7.6 Hz, 2H), 2.12 – 1.98 (m, 2H), 1.94 – 1.78 (m, 2H). ^{13}C APT NMR ($CDCl_3$, 101 MHz): δ 171.31, 154.87, 146.35, 143.05, 141.86, 128.48(2C), 128.39(2C), 125.90, 120.31, 118.84, 67.91, 35.51, 34.96, 26.80.

1-(Oxazolo[4,5-*b*]pyridin-2-yl)-4-phenylbutan-1-one (107)

The title compound was synthesized from 1-(oxazolo[4,5-*b*]pyridin-2-yl)-4-phenylbutan-1-ol (**147**, 52.4 mg, 0.20 mmol) according to the procedure described for compound **1**. This yielded 1-(oxazolo[4,5-*b*]pyridin-2-yl)-4-phenylbutan-1-one (22 mg, 0.08 mmol, 42%). HRMS (ESI+) m/z: calculated for $C_{16}H_{15}N_2O_2$ ([M + H]), 267.1128; found, 267.1126. ^{1}H NMR ($CDCl_3$, 400 MHz): δ 8.76 (dd, *J* = 4.8, 1.5 Hz, 1H), 7.99 (dd, *J* = 8.3, 1.5 Hz, 1H), 7.49 (dd, *J* = 8.3, 4.8 Hz, 1H), 7.31 – 7.25 (m, 2H), 7.24 – 7.14 (m, 3H), 3.31 (t, *J* = 7.3 Hz, 2H), 2.76 (t, *J* = 7.6 Hz, 2H), 2.22 – 2.11 (m, 2H). ^{13}C BBDEC NMR ($CDCl_3$, 101 MHz): δ 190.12, 158.58, 154.22, 148.85, 143.72, 141.19, 128.64(2C), 128.58(2C), 123.29, 120.40, 39.25, 35.12, 25.41. Purity of 94% as determined by LC-MS. Spectroscopic data are in agreement with reported literature.[14]

2-Hydroxy-6-phenylhexanenitrile (148)

The title compound was synthesized from commercially available 5-phenylpentanol (513 mg 3.12 mmol) according to the previously reported 2 step procedure.[12] This yielded 2-hydroxy-6-phenylhexanenitrile (318 mg, 1.68 mmol, 54% over 2 steps). ^{1}H NMR ($CDCl_3$, 400 MHz): δ 7.33-7.19 (m, 5H), 4.43 (bs, 1H), 4.18-4.12 (m, 1H), 2.66 (t, *J* = 7.6 Hz, 2H), 1.86 (q, *J* = 7.2 Hz, 2H), 1.70 (p, *J* = 7.6 Hz, 2H), 1.55 (p, *J* = 7.6 Hz, 2H). ^{13}C APT NMR ($CDCl_3$, 101 MHz): δ 141.96, 128.81(2C), 128.32(2C), 125.79, 120.20, 60.92, 35.56, 34.90, 30.72, 24.21.

1-(Oxazolo[4,5-*b*]pyridin-2-yl)-5-phenylpentan-1-ol (149)

The title compound was synthesized from 2-hydroxy-6-phenylhexanenitrile (**148**, 174 mg, 0.92 mmol) and commercially available 2-amino-3-hydroxypyridine (102 mg, 0.93 mmol) according to the procedure described for compound **125**. This yielded 1-(oxazolo[4,5-*b*]pyridin-2-yl)-5-phenylpentan-1-ol (51 mg, 0.18 mmol, 20%). ^{1}H NMR ($CDCl_3$, 400 MHz): δ 8.49 (dd, *J* = 5.0, 1.4 Hz, 1H), 7.79 (dd, *J* = 8.2, 1.4 Hz, 1H), 7.29 – 7.20 (m, 4H), 7.18 – 7.10 (m, 3H), 5.05 (dd, *J* = 7.4, 5.6 Hz, 1H), 2.60 (t, *J* = 7.6 Hz, 2H), 2.12 – 1.98 (m, 2H), 1.72 – 1.62 (m, 2H), 1.60 – 1.49 (m, 2H). ^{13}C APT NMR ($CDCl_3$, 101 MHz): δ 170.88, 154.90, 146.59, 143.08, 142.26, 128.38(2C), 128.30(2C), 125.74, 120.31, 118.68, 68.14, 35.71, 35.34, 31.12, 24.57.

1-(Oxazolo[4,5-*b*]pyridin-2-yl)-5-phenylpentan-1-one (108)

The title compound was synthesized from 1-(oxazolo[4,5-*b*]pyridin-2-yl)-5-phenylpentan-1-ol (**149**, 40 mg, 0.14 mmol) according to the procedure described for compound **1**. This yielded 1-(oxazolo[4,5-*b*]pyridin-2-yl)-5-phenylpentan-1-one (35 mg, 0.10 mmol, 86%). HRMS (ESI+) m/z: calculated for $C_{17}H_{17}N_2O_2$ ([M + H]), 281.1285; found, 281.1282. ^{1}H NMR ($CDCl_3$, 400 MHz): δ 8.75 (dd, *J* = 4.8, 1.5 Hz, 1H), 8.00 (dd, *J* = 8.3, 1.4 Hz, 1H), 7.49 (dd, *J* = 8.3, 4.8 Hz, 1H), 7.30 – 7.26 (m, 2H), 7.23 – 7.16 (m, 3H), 3.31 (t, *J* = 7.2 Hz, 2H), 2.69 (t, *J* = 7.5 Hz, 2H), 1.93 – 1.83 (m, 2H), 1.81 – 1.72 (m, 2H). ^{13}C APT NMR ($CDCl_3$, 101 MHz): δ 190.23, 158.61, 154.26, 148.85, 143.73, 142.01, 128.66(2C), 128.44(2C), 125.92, 123.26, 120.35, 39.72, 35.69, 30.87, 23.53. Purity of >95% as determined by LC-MS. Spectroscopic data are in agreement with reported literature.[14]

2-Hydroxy-8-phenyloctanenitrile (150)

The title compound was synthesized from commercially available 7-phenylheptan-1-ol (500 mg, 2.60 mmol) according to the previously reported 2 step procedure.[12] This yielded 2-hydroxy-8-phenyloctanenitrile (430 mg, 1.98 mmol, 76% over 2 steps). ^{1}H NMR ($CDCl_3$, 400 MHz): δ 7.29 – 7.20 (m, 2H), 7.18 – 7.10 (m, 3H), 4.34 (q, *J* = 6.1 Hz, 1H), 3.86 – 3.78 (bs, 1H), 2.57 (t, *J* = 7.7 Hz, 2H), 1.75 (q, J = 7.2 Hz, 2H), 1.59 (t, J = 7.5 Hz, 2H), 1.49 – 1.38 (m, 2H), 1.37 – 1.27 (m, 4H). ^{13}C BBDEC NMR ($CDCl_3$, 101 MHz): δ 142.51, 128.31(2C), 128.20(2C), 125.58, 120.14, 60.97, 35.76, 34.85, 31.20, 28.88, 28.68, 24.40.

1-(Oxazolo[4,5-*b*]pyridin-2-yl)-7-phenylheptan-1-ol (151)

The title compound was synthesized from 2-hydroxy-8-phenyloctanenitrile (**150**, 231 mg, 1.06 mmol) and commercially available 2-amino-3-hydroxypyridine (101 mg, 0.92 mmol) according to the procedure described for compound **125**. This yielded 1-(oxazolo[4,5-*b*]pyridin-2-yl)-7-phenylheptan-1-ol (38 mg, 0.12 mmol, 13%). ^{1}H NMR ($CDCl_3$, 400 MHz): 8.53 (dd, *J* = 4.9, 1.4 Hz, 1H), 7.81 (dd, *J* = 8.1, 1.4 Hz, 1H), 7.30 – 7.23 (m, 3H), 7.19 – 7.13 (m, 3H), 5.03 (dd, *J* = 7.6, 5.3 Hz, 1H), 3.91 (bs, 1H), 2.58 (t, *J* = 7.8 Hz, 2H), 2.10 – 1.91 (m, 2H), 1.65 – 1.54 (m, 2H), 1.54 – 1.44 (m, 2H), 1.41 – 1.29 (m, 4H). δ ^{13}C APT NMR ($CDCl_3$, 101 MHz): δ 171.29, 154.97, 146.54, 143.15, 142.82, 128.48(2C), 128.34(2C), 125.70, 120.37, 118.82, 68.21, 36.01, 35.54, 31.48, 29.27, 29.20, 24.96. Spectroscopic data are in agreement with reported literature.[14]

1-(Oxazolo[4,5-*b*]pyridin-2-yl)-7-phenylheptan-1-one (109)

The title compound was synthesized from 1-(oxazolo[4,5-*b*]pyridin-2-yl)-7-phenylheptan-1-ol (**151**, 38 mg, 0.12 mmol) according to the procedure described for compound **1**. This yielded 1-(oxazolo[4,5-*b*]pyridin-2-yl)-7-

phenylheptan-1-one (23 mg, 0.07 mmol, 61%). HRMS (ESI+) m/z: calculated for $C_{19}H_{21}N_2O_2$ ([M + H]), 309.1598; found, 309.1596. ^{1}H NMR ($CDCl_3$, 400 MHz): δ 8.77 (dd, *J* = 4.8, 1.5 Hz, 1H), 8.00 (dd, *J* = 8.3, 1.5 Hz, 1H), 7.50 (dd, *J* = 8.3, 4.8 Hz, 1H), 7.30 – 7.23 (m, 2H), 7.20 – 7.13 (m, 3H), 3.27 (t, *J* = 7.4 Hz, 2H), 2.61 (t, *J* = 7.5 Hz, 2H), 1.83 (p, *J* = 7.4 Hz, 2H), 1.70 – 1.59 (m, 2H), 1.51 – 1.35 (m, 4H). ^{13}C BBDEC NMR ($CDCl_3$, 101 MHz): δ 190.48, 158.68, 154.25, 148.81, 143.77, 142.75, 128.51(2C), 128.37(2C), 125.74, 123.30, 120.47, 39.91, 35.98, 31.38, 29.08, 29.05, 23.86. Purity of 94% as determined by LC-MS. Spectroscopic data are in agreement with reported literature.[14]

2-Hydroxy-9-phenylnonanenitrile (152)

The title compound was synthesized from commercially available 8-phenyloctan-1-ol (1.00 g 4.85 mmol) according to the previously reported 2 step procedure. This yielded 2-hydroxy-9-phenylnonanenitrile (850 mg, 4.11 mmol, 85% over 2 steps). ^{1}H NMR ($CDCl_3$, 400 MHz): δ 7.32 – 7.23 (m, 2H), 7.22 – 7.13 (m, 3H), 4.46 (t, *J* = 6.7 Hz, 1H), 2.60 (t, *J* = 7.9 Hz, 2H), 2.44 (bs, 1H), 1.90 – 1.77 (m, 2H), 1.67 – 1.55 (m, 2H), 1.54 – 1.43 (m, 2H), 1.39 – 1.28 (m, 6H). ^{13}C APT NMR ($CDCl_3$, 101 MHz): δ 142.86, 128.52(2C), 128.38(2C), 125.74, 120.03, 61.50, 36.03, 35.32, 31.53, 29.31, 29.19, 28.95, 24.60.

1-(Oxazolo[4,5-*b*]pyridin-2-yl)-8-phenyloctan-1-ol (153)

The title compound was synthesized from 2-hydroxy-7-phenylheptanenitrile (**152**, 337 mg, 1.46 mmol) and commercially available 2-amino-3-hydroxypyridine (159 mg, 1.44 mmol) according to the procedure described for compound **125**. This yielded 1-(oxazolo[4,5-*b*]pyridin-2-yl)-8-phenyloctan-1-ol (104 mg, 0.32 mmol, 22%). ^{1}H NMR ($CDCl_3$, 400 MHz): δ 8.49 (dd, *J* = 4.9, 1.4 Hz, 1H), 7.79 (dd, *J* = 8.1, 1.4 Hz, 1H), 7.28 – 7.23 (m, 3H), 7.18 – 7.13 (m, 3H), 5.05 (dd, *J* = 7.4, 5.6 Hz, 1H), 4.55 (bs, 1H), 2.57 (t, *J* = 8.0 Hz, 2H), 2.12 – 1.90 (m, 2H), 1.63 – 1.53 (m, 2H), 1.53 – 1.40 (m, 2H), 1.39 – 1.20 (m, 6H). ^{13}C APT NMR ($CDCl_3$, 101 MHz): δ 171.46, 154.92, 146.34, 143.05, 142.87, 128.44(2C), 128.28(2C), 125.62, 120.26, 118.79, 68.06, 35.99, 35.47, 31.53, 29.37, 29.30, 29.26, 25.05. Spectroscopic data are in agreement with reported literature.[14]

1-(Oxazolo[4,5-*b*]pyridin-2-yl)-8-phenyloctan-1-one (110)

The title compound was synthesized from 1-(oxazolo[4,5-*b*]pyridin-2-yl)-8-phenyloctan-1-ol (**153**, 50 mg, 0.15 mmol) according to the procedure described for compound **1**. This yielded 1-(oxazolo[4,5-*b*]pyridin-2-yl)-8-phenyloctan-1-one (42 mg, 0.13 mmol, 84%). HRMS (ESI+) m/z: calculated for $C_{20}H_{23}N_2O_2$ ([M + H]), 323.1754; found, 323.1755. ^{1}H NMR ($CDCl_3$, 400 MHz): δ 8.76 (dd, *J* = 4.8, 1.4 Hz, 1H), 8.00 (dd, *J* = 8.3, 1.5 Hz, 1H), 7.50 (dd, *J* = 8.3, 4.8 Hz, 1H), 7.30 – 7.24 (m, 2H), 7.20 – 7.13 (m, 3H), 3.27 (t, *J* = 7.4 Hz, 2H), 2.60 (t, *J* = 7.8 Hz, 2H), 1.82 (p, *J* = 7.4 Hz, 2H), 1.62 (p, *J* = 7.6 Hz, 2H), 1.48 – 1.30 (m, 6H). ^{13}C APT NMR ($CDCl_3$, 101 MHz): δ 190.58, 158.65, 154.30, 148.89, 143.74, 142.91, 128.53(2C), 128.37(2C), 125.71, 123.30, 120.41, 39.95, 36.06, 31.56, 29.33, 29.22, 29.14, 23.95. Purity of >95% as determined by LC-MS. Spectroscopic data are in agreement with reported literature.[14]

References

1. Katona, I.; Freund, T. F. Multiple functions of endocannabinoid signaling in the brain. *Annu. Rev. Neurosci.* **2012**, *35*, 529-558.
2. Tanimura, A.; Yamazaki, M.; Hashimotodani, Y.; Uchigashima, M.; Kawata, S.; Abe, M.; Kita, Y.; Hashimoto, K.; Shimizu, T.; Watanabe, M.; Sakimura, K.; Kano, M. The endocannabinoid 2-arachidonoylglycerol produced by diacylglycerol lipase alpha mediates retrograde suppression of synaptic transmission. *Neuron* **2010**, *65*, 320-327.
3. Gao, Y.; Vasilyev, D. V.; Goncalves, M. B.; Howell, F. V.; Hobbs, C.; Reisenberg, M.; Shen, R.; Zhang, M. Y.; Strassle, B. W.; Lu, P.; Mark, L.; Piesla, M. J.; Deng, K.; Kouranova, E. V.; Ring, R. H.; Whiteside, G. T.; Bates, B.; Walsh, F. S.; Williams, G.; Pangalos, M. N.; Samad, T. A.; Doherty, P. Loss of retrograde endocannabinoid signaling and reduced adult neurogenesis in diacylglycerol lipase knock-out mice. *J. Neurosci.* **2010**, *30*, 2017-2024.
4. Hsu, K. L.; Tsuboi, K.; Adibekian, A.; Pugh, H.; Masuda, K.; Cravatt, B. F. DAGLbeta inhibition perturbs a lipid network involved in macrophage inflammatory responses. *Nat. Chem. Biol.* **2012**, *8*, 999-1007.
5. Di Marzo, V. Targeting the endocannabinoid system: to enhance or reduce? *Nat. Rev. Drug Discovery,* **2008**, *7*, 438-455.
6. Rouzer, C. A.; Marnett, L. J. Endocannabinoid oxygenation by cyclooxygenases, lipoxygenases, and cytochromes P450: cross-talk between the eicosanoid and endocannabinoid signaling pathways. *Chem. Rev.* **2011**, *111*, 5899-5921.
7. Kohnz, R. A.; Nomura, D. K. Chemical approaches to therapeutically target the metabolism and signaling of the endocannabinoid 2-AG and eicosanoids. *Chem. Soc. Rev.* **2014**, *43*, 6859-6869.
8. Alhouayek, M.; Muccioli, G. G. COX-2-derived endocannabinoid metabolites as novel inflammatory mediators. *Trends Pharmacol. Sci.* **2014**, *35*, 284-292.
9. Nomura, D. K.; Morrison, B. E.; Blankman, J. L.; Long, J. Z.; Kinsey, S. G.; Marcondes, M. C.; Ward, A. M.; Hahn, Y. K.; Lichtman, A. H.; Conti, B.; Cravatt, B. F. Endocannabinoid hydrolysis generates brain prostaglandins that promote neuroinflammation. *Science* **2011**, *334*, 809-813.
10. Di Marzo, V. Endocannabinoid signaling in the brain: biosynthetic mechanisms in the limelight. *Nat. Neurosci.* **2011**, *14*, 9-15.
11. Murataeva, N.; Straiker, A.; Mackie, K. Parsing the players: 2-arachidonoylglycerol synthesis and degradation in the CNS. *Br. J. Pharmacol.* **2014**, *171*, 1379-1391.
12. Baggelaar, M. P.; Janssen, F. J.; van Esbroeck, A. C.; den Dulk, H.; Allara, M.; Hoogendoorn, S.; McGuire, R.; Florea, B. I.; Meeuwenoord, N.; van den Elst, H.; van der Marel, G. A.; Brouwer, J.; Di Marzo, V.; Overkleeft, H. S.; van der Stelt, M. Development of an activity-based probe and in silico design reveal highly selective inhibitors for diacylglycerol lipase-alpha in brain. *Angew. Chem. Int. Ed.* **2013**, *52*, 12081–12085.
13. Baggelaar, M. P.; Chameau, P. J.; Kantae, V.; Hummel, J.; Hsu, K. L.; Janssen, F.; van der Wel, T.; Soethoudt, M.; Deng, H.; den Dulk, H.; Allara, M.; Florea, B. I.; Di Marzo, V.; Wadman, W. J.; Kruse, C. G.; Overkleeft, H. S.; Hankemeier, T.; Werkman, T. R.; Cravatt, B. F.; van der Stelt, M. Highly selective, reversible inhibitor identified by comparative chemoproteomics modulates diacylglycerol lipase activity in neurons. *J. Am. Chem. Soc.* **2015**, *137*, 8851–8857.
14. Boger, D. L.; Sato, H.; Lerner, A. E.; Hedrick, M. P.; Fecik, R. A.; Miyauchi, H.; Wilkie, G. D.; Austin, B. J.; Patricelli, M. P.; Cravatt, B. F. Exceptionally potent inhibitors of fatty acid amide hydrolase: the enzyme responsible for degradation of endogenous oleamide and anandamide. *Proc. Natl. Acad. Sci. U.S.A.* **2000**, *97*, 5044-5049.
15. Edwards, P. D.; Wolanin, D. J.; Andisik, D. W.; Davis, M. W. Peptidyl alpha-ketoheterocyclic inhibitors of human neutrophil elastase. 2. Effect of varying the heterocyclic ring on in vitro potency. *J. Med. Chem.* **1995**, *38*, 76-85.
16. Edwards, P. D.; Zottola, M. A.; Davis, M.; Williams, J.; Tuthill, P. A. Peptidyl alpha-ketoheterocyclic inhibitors of human neutrophil elastase. 3. In vitro and in vivo potency of a series of peptidyl alpha-ketobenzoxazoles. *J. Med. Chem.* **1995**, *38*, 3972-3982.
17. Edwards, P. D., Meyer, E.F., Vijayalakshmi, J. , Tuthill, P.A., Andisik, D. A., Gomes, B., Strimpler, A. . Design, synthesis, and kinetic evaluation of a unique class of elastase inhibitors, the peptidyl a-ketobenzoxazoles, and the x-ray crystal structure of the covalent complex between porcine pancreatic elastase and Ac-Ala-Pro-Val-2-benzoxazole *J. Am. Chem. Soc* **1992**, *114*, 1854-1863.

18. Costanzo, M. J.; Maryanoff, B. E.; Hecker, L. R.; Schott, M. R.; Yabut, S. C.; Zhang, H. C.; Andrade-Gordon, P.; Kauffman, J. A.; Lewis, J. M.; Krishnan, R.; Tulinsky, A. Potent thrombin inhibitors that probe the S1 subsite: tripeptide transition state analogues based on a heterocycle-activated carbonyl group. *J. Med. Chem.* **1996**, *39*, 3039-3043.
19. Costanzo, M. J.; Almond, H. R., Jr.; Hecker, L. R.; Schott, M. R.; Yabut, S. C.; Zhang, H. C.; Andrade-Gordon, P.; Corcoran, T. W.; Giardino, E. C.; Kauffman, J. A.; Lewis, J. M.; de Garavilla, L.; Haertlein, B. J.; Maryanoff, B. E. In-depth study of tripeptide-based alpha-ketoheterocycles as inhibitors of thrombin. Effective utilization of the S1' subsite and its implications to structure-based drug design. *J. Med. Chem.* **2005**, *48*, 1984-2008.
20. Lin, J.; Deng, H.; Jin, L.; Pandey, P.; Quinn, J.; Cantin, S.; Rynkiewicz, M. J.; Gorga, J. C.; Bibbins, F.; Celatka, C. A.; Nagafuji, P.; Bannister, T. D.; Meyers, H. V.; Babine, R. E.; Hayward, N. J.; Weaver, D.; Benjamin, H.; Stassen, F.; Abdel-Meguid, S. S.; Strickler, J. E. Design, synthesis, and biological evaluation of peptidomimetic inhibitors of factor XIa as novel anticoagulants. *J. Med. Chem.* **2006**, *49*, 7781-7791.
21. Akahoshi, F.; Ashimori, A.; Sakashita, H.; Yoshimura, T.; Imada, T.; Nakajima, M.; Mitsutomi, N.; Kuwahara, S.; Ohtsuka, T.; Fukaya, C.; Miyazaki, M.; Nakamura, N. Synthesis, structure-activity relationships, and pharmacokinetic profiles of nonpeptidic alpha-keto heterocycles as novel inhibitors of human chymase. *J. Med. Chem.* **2001**, *44*, 1286-1296.
22. Costanzo, M. J.; Yabut, S. C.; Almond, H. R., Jr.; Andrade-Gordon, P.; Corcoran, T. W.; De Garavilla, L.; Kauffman, J. A.; Abraham, W. M.; Recacha, R.; Chattopadhyay, D.; Maryanoff, B. E. Potent, small-molecule inhibitors of human mast cell tryptase. Antiasthmatic action of a dipeptide-based transition-state analogue containing a benzothiazole ketone. *J. Med. Chem.* **2003**, *46*, 3865-3876.
23. Tavares, F. X.; Deaton, D. N.; Miller, A. B.; Miller, L. R.; Wright, L. L. Ketoheterocycle-based inhibitors of cathepsin K: a novel entry into the synthesis of peptidic ketoheterocycles. *Bioorg. Med. Chem. Lett.* **2005**, *15*, 3891-3895.
24. Maryanoff, B. E.; Costanzo, M. J. Inhibitors of proteases and amide hydrolases that employ an alpha-ketoheterocycle as a key enabling functionality. *Bioorg. Med. Chem.* **2008**, *16*, 1562-1595.
25. Commercially available from Aldrich as ALD00032 and also known as OL-100 first prepared and examined as disclosed in reference 14. .
26. Boger, D. L.; Miyauchi, H.; Du, W.; Hardouin, C.; Fecik, R. A.; Cheng, H.; Hwang, I.; Hedrick, M. P.; Leung, D.; Acevedo, O.; Guimaraes, C. R.; Jorgensen, W. L.; Cravatt, B. F. Discovery of a potent, selective, and efficacious class of reversible alpha-ketoheterocycle inhibitors of fatty acid amide hydrolase effective as analgesics. *J. Med. Chem.* **2005**, *48*, 1849-1856.
27. DeMartino, J. K.; Garfunkle, J.; Hochstatter, D. G.; Cravatt, B. F.; Boger, D. L. Exploration of a fundamental substituent effect of alpha-ketoheterocycle enzyme inhibitors: Potent and selective inhibitors of fatty acid amide hydrolase. *Bioorg. Med. Chem. Lett.* **2008**, *18*, 5842-5846.
28. Ezzili, C.; Mileni, M.; McGlinchey, N.; Long, J. Z.; Kinsey, S. G.; Hochstatter, D. G.; Stevens, R. C.; Lichtman, A. H.; Cravatt, B. F.; Bilsky, E. J.; Boger, D. L. Reversible competitive alpha-ketoheterocycle inhibitors of fatty acid amide hydrolase containing additional conformational constraints in the acyl side chain: orally active, long-acting analgesics. *J. Med. Chem.* **2011**, *54*, 2805-2822.
29. Hardouin, C.; Kelso, M. J.; Romero, F. A.; Rayl, T. J.; Leung, D.; Hwang, I.; Cravatt, B. F.; Boger, D. L. Structure-activity relationships of alpha-ketooxazole inhibitors of fatty acid amide hydrolase. *J. Med. Chem.* **2007**, *50*, 3359-3368.
30. Kimball, F. S.; Romero, F. A.; Ezzili, C.; Garfunkle, J.; Rayl, T. J.; Hochstatter, D. G.; Hwang, I.; Boger, D. L. Optimization of alpha-ketooxazole inhibitors of fatty acid amide hydrolase. *J. Med. Chem.* **2008**, *51*, 937-947.
31. Leung, D.; Du, W.; Hardouin, C.; Cheng, H.; Hwang, I.; Cravatt, B. F.; Boger, D. L. Discovery of an exceptionally potent and selective class of fatty acid amide hydrolase inhibitors enlisting proteome-wide selectivity screening: concurrent optimization of enzyme inhibitor potency and selectivity. *Bioorg. Med. Chem. Lett.* **2005**, *15*, 1423-1428.
32. Romero, F. A.; Hwang, I.; Boger, D. L. Delineation of a fundamental alpha-ketoheterocycle substituent effect for use in the design of enzyme inhibitors. *J. Am. Chem. Soc.* **2006**, *128*, 14004-14005.
33. Garfunkle, J.; Ezzili, C.; Rayl, T. J.; Hochstatter, D. G.; Hwang, I.; Boger, D. L. Optimization of the central heterocycle of alpha-ketoheterocycle inhibitors of fatty acid amide hydrolase. *J. Med. Chem.* **2008**, *51*, 4392-4403.
34. Talylor, P. J.; Wait, A. R. σ_i Values for heterocycles. *J. Chem. Soc. Perkin. Trans. 2* **1986**, 1765-1770.

CHAPTER 4

α-Keto heterocycles as highly selective and drug-like *sn*-1 diacylglycerol lipase α inhibitors*

Introduction

Sn-1 diacylglycerol lipase (DAGL) inhibitors have been utilized to study the role of the endocannabinoid 2-arachidonoylglycerol (2-AG) in several (patho)physiological processes. Perturbation of 2-AG biosynthesis reduces cannabinoid receptors (CB1R and CB2R) signaling and decreases eicosanoid formation in a tissue dependent manner. As such, disruption of DAGL activity has shown potential therapeutic benefits in the treatment of obesity & metabolic syndrome,[1,2] diabetes,[3] constipation,[4] nicotine addiction,[5] pathological pain,[6] and (neuro)inflammation.[7–9]

The reversible α-ketoheterocycle LEI104 (**1**) has been discovered as a selective inhibitor for DAGLα (Chapter 2).[10] Detailed structure-activity relationship (SAR) studies on LEI104 (**1**) provided highly valuable information for the structural requirements for DAGLα inhibition (Chapter 3).[11] Using this information, a homology model was validated which led to the discovery of LEI105 (**2**), a potent and selective DAGLα and DAGLβ inhibitor (see Table 1).[12] Introduction of the *p*-tolyl substituent of LEI105 (**2**) was crucial for obtaining selectivity over fatty acid amide hydrolase (FAAH) and increased potency 6 fold compared to LEI104.[12] On the other hand, lipophilicity increased almost 250 fold (Table 1). Lipophilicity is reported as one of the most important parameters to control during lead optimization.[13] High lipophilicity is associated with solubility issues, increased aspecific binding (to unwanted off-targets), human ether-a-go-go-related potassium channel protein (hERG) channel affinity,[14,15] toxicity by promoting cellular phospholipidosis[16] and increased cytochrome P450 (CYP) liability.[17] Hence, the sub-optimal drug-like properties of LEI105 hamper its widespread use as a drug candidate.

* Published as part of: Janssen, F. J.; Baggelaar, M. P.; Hummel, J. J. A; van Boeckel, C. A. A.; van der Stelt, M. Pharmaceutically active compounds as DAG-lipase inhibitors, European Patent Number EP15169052.6. Filing date 23 May **2016**. Publication date 22 November **2016**. Ming Jiang is kindly acknowledged for synthesis, characterization and biological assessment of multiple inhibitors reported in this chapter.

As such, lipophilic efficiency (LipE, which is calculated by pIC_{50} - cLogP) is an important objective in lead generation and optimization programmes.[13] Typically LipE of 5 or greater is required for drug candidates.[13] Here, an optimization of LEI105 is reported, by combined activity-based protein profiling (ABPP) and LipE guided structure-based design. The identification of a highly efficient C2 acyl spacer, followed by careful selection of the most selective and efficient substituted heterocyclic scaffold led to the discovery of LEI107 (**16**), a highly selective DAGLα inhibitor with drug-like properties.

Results

LEI105 (**2**) showed a marked decrease in LipE 2.1, versus 3.4 for LEI104 (Table 1), hence an optimization program on LEI105 was initiated in order to reduce lipophilicity while maintaining potency. The LEI105 derivatives were synthesized according to previously reported procedures.[10–12] In brief, an alcohol precursor (usually commercially available) was oxidized by Swern oxidation (Scheme 1a) to the corresponding aldehyde and treated with potassium cyanide (b) to yield the cyanohydrin as key intermediate. The cyanohydrin was converted to the corresponding Pinner salt using dry acidic conditions in EtOH (c), followed by reflux with a corresponding aminohydroxypyridine, in EtOH with pyridine (d). The obtained alcohol was oxidized to the ketone by Dess-Martin Periodinane (DMP) oxidation (e).

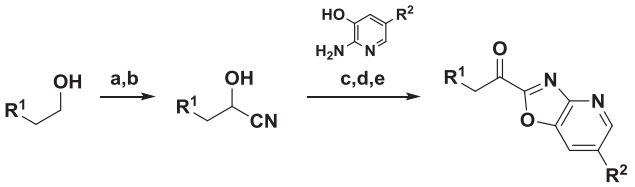

Scheme 1. General synthetic approach towards LEI105 derivatives **3**-**18**. **a)** DMSO, $(COCl)_2$, DCM, Et_3N, -78°C. **b)** KCN, THF/H_2O, rt. **c)** AcCl, EtOH, 0°C to rt. **d)** Corresponding aminohydroxypyridine, EtOH, Pyr., 80°C. **e)** DMP, DCM, rt.

Optimization of the 2-acyl substituent

During the investigation of the SAR of LEI104, longer spacers length increased potency, but not necessarily LipE (Chapter 3).[11] Therefore the effect of LEI105 spacer length was systematically reduced. Compounds **4,** containing a C3 methylene spacer is 2.5 times more efficient than LEI105. To gain activity while reducing lipophilicity, incorporation of an electron withdrawing trifluoromethyl (CF_3) spacer was envisioned. To test this hypothesis, **7** and **8** were synthesized. Water free nitrilation of commercially available 3,3,3-trifluoropropanol followed by the standard synthesis procedures of Scheme 1 yielded **7**. The synthesis of cyanohydrin precursor of **8** was optimized through a TEMPO NaOCl oxidation from commercially available 4,4,4-trifluorobutanol (DMP oxidation was very low yielding, other oxidants were uniformly unsuccessful). Room temperature evaporation of the corresponding aldehyde *in vacuo* followed by direct nitrilation and additional steps (Scheme

1c-e) yielded **8**. Compound **7** appeared unstable, whereas compound **8** showed tremendous improvement in overall LipE and displayed no stability issues upon workup. The lack of stability of **7** could be explained by the CF_3 being positioned too close to the ketone warhead. Conformational restriction was investigated with derivatives **9**-**12**, as such biphenylethers were incorporated to mimic the natural substrate fatty acid chains. The alcohol precursors of **9**-**12** were not commercially available and were synthesized in three steps from the corresponding fluorobenzaldehyde by nucleophilic aromatic substitution with phenol, followed by Wittig-Horner olefination and lithium aluminium hydride (LAH) reduction to the corresponding alcohol (see Experimental). Subsequently, the 5-step general synthesis (Scheme 1) yielded **9**-**12**. Biphenylethers **9**-**11** had significantly decreased LipE, whereas compound **6** showed minor LipE improvement (LipE = 2.42).

Table 1. Optimization of the 2-acyl substituent derivatives **3**-**12**.

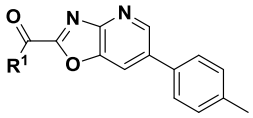

Entry	Structure	DAGLα (pIC_{50} ± SEM)	cLogP	LipE
1 (LEI104)[10,12]	-	7.43 ± 0.05	4.07	3.36
2 (LEI105)[12]	-$C_5H_{10}Ph$	8.52 ± 0.06	6.46	2.06
3	-C_4H_8Ph	7.84 ± 0.04	5.93	1.91
4	-C_3H_4Ph	7.86 ± 0.08	5.40	2.46
5	-C_2H_4Ph	7.22 ± 0.11	5.02	2.20
6	-C_1H_2Ph	6.31 ± 0.09	4.69	1.62
7	-$C_1H_2CF_3$	5.76 ± 0.07	3.21	2.55
8	-$C_2H_4CF_3$	7.83 ± 0.07	3.69	4.14
9	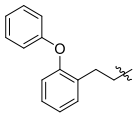	8.02 ± 0.08	7.12	0.90
10	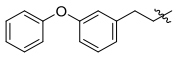	8.43 ± 0.08	7.12	1.31
11	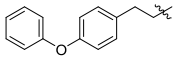	8.29 ± 0.08	7.12	1.17
12	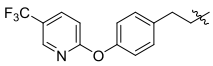	9.07 ± 0.06	6.65	2.42

Optimization of the heterocyclic scaffold

Previously, the oxazolopyridine scaffold was found most optimal (Chapter 3), therefore the effect of the scaffold substituent pattern was investigated. As a starting point, compound **8** was selected due to its highest LipE. Electron donating and withdrawing substituents, methoxy and cyano functionalities were introduced in compounds **13**, **14** and **15** to assess the electronic effects of the phenyl ring and simultaneously decrease inhibitor lipophilicity. Of note, the *p*-chloro substituted aminohydroxypyridine precursor of **13** was obtained through a HBr/AcOH deprotection from its corresponding benzyl protected precursor (standard Pd/H_2 hydrogenation conditions consistently resulted in a loss of the chlorine substituent). Compound **14** showed a thousand-fold increase in LipE compared to LEI105 (**2**). To increase metabolic stability, the *p*-methyl group of **8** was replaced with *p*-fluoro (**16**), *p*-chloro (**17**), *p*,*m*-dioxymethylene (**18**). Assessment of these compounds in the colorimetric activity assay shows that compound **16** is most potent (pIC_{50} = 8.59 ± 0.04) in this study and displays the highest LipE (5.25).

Natural substrate DAGLα activity assay

To assess if the inhibitors were able to block conversion of the natural substrate of DAGLα, all compounds were measured in a previously reported 96-well plate DAGLα natural substrate activity (N = 2, n = 2).[18] In brief, the assay is based on the conversion of 1-stearoyl-2-arachidonoyl-*sn*-glycerol (SAG) by HEK293T cell membrane fractions overexpressing hDAGLα. The formation of 2-AG from SAG is coupled via glycerol formation to a fluorescent readout using an additional 4 enzyme cascade.[18] In this assay, the 2-acyl trifluoromethyl spacer (**8**) was equally potent compared to the original spacer of LEI105 (**2**, Table 2). Compounds **16** and **17** were highly potent and inhibited the conversion of SAG to 2-AG by DAGLα *in vitro* with pIC_{50} values of 7.92 ± 0.10 and 8.11 ± 0.07 respectively (Table 2)

Table 2. Optimization of the heterocyclic scaffold. *LEI105 was measured on ABPP in a 5 point 5 fold dilution array, whereas all other compounds were measured in the general 10 fold dilution used in other biochemical activity assays (colorimetric PNP and SAG). Colorimetric PNP assay N = 2, n = 2. ABPP, N = 3. ****16** is measured N = 1.

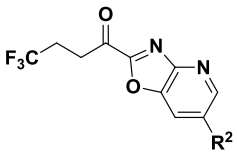

Entry	Structure	DAGLα (pIC_{50} ± SEM)			cLogP	LipE
		PNP	SAG	ABPP		
2 (LEI105)	-	8.52 ± 0.06	7.9 ± 0.1	7.5 ± 0.1*	6.46	2.06
8		7.83 ± 0.07	8.01 ± 0.13	7.0 ± 0.1	3.69	4.14
13	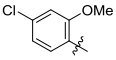	8.41 ± 0.05	7.96 ± 0.12	7.1 ± 0.1	3.44	4.97
14		7.79 ± 0.03	7.06 ± 0.15	6.5 ± 0.1	2.63	5.16
15	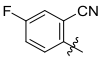	7.61 ± 0.06	N.D.	N.D.	2.78	4.83
16 (LEI107)		8.59 ± 0.04	7.92 ± 0.10**	7.2 ± 0.1	3.34	5.25
17		8.57 ± 0.07	8.11 ± 0.07	7.1 ± 0.1	3.91	4.66
18		8.16 ± 0.04	7.66 ± 0.14	6.5 ± 0.1	3.23	4.56

Activity-based protein profiling

Introduction of the *p*-tolyl substituent in LEI105 was shown to be crucial for obtaining selectivity over FAAH.[12] To determine if compounds **16** and **17** are selective over FAAH, and other enzymes involved in the endocannabinoid system, **16** and **17** were measured in mouse brain membrane homogenate using two broad-spectrum probes MB064 and TAMRA-FP, as previously reported (N = 3).[10,12,19] Both compounds **16** and **17** displayed a highly selective profile, as no significant reduction of other bands than DAGLα and DAGLα* was observed in this ABPP setting. Of note, compound **16** was screened at a concentration of 100 µM on broad-spectrum probe TAMRA-FP, showing no observable off-target activity. Consequently, compound **16** has a selectivity window of >1000 over off-targets of broad-spectrum serine hydrolase probe TAMRA-FP, including endocannabinoid system related ABHD6, ABHD12, monoacylglycerol lipase (MAGL) and FAAH as assessed by in-gel fluorescence scanning. Chemoproteomics might be applied to further investigate this highly selective profile. Due to combination of high potency, selectivity and LipE, compound **16** was named LEI107.

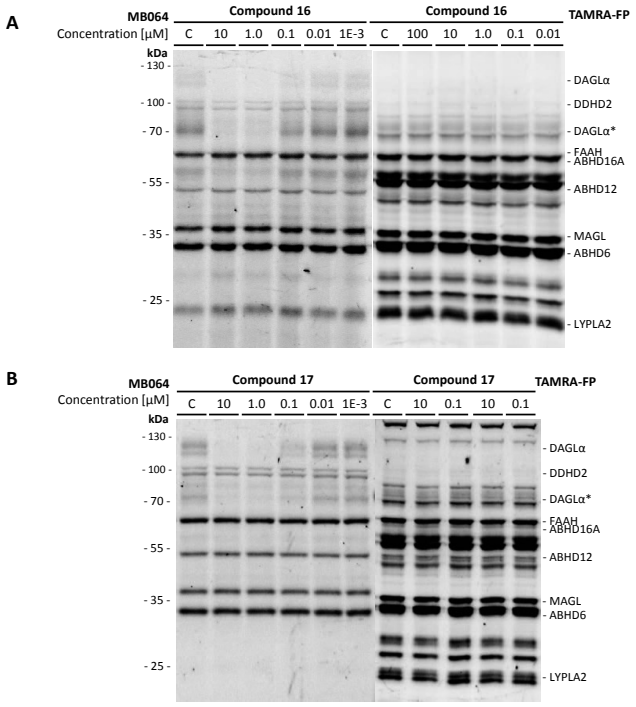

Figure 1. **A)** Characterization of compound **16** on ABPP with probes MB064 (left) and TAMRA-FP (right). pIC_{50} DAGLα* of **16** = 7.2 ± 0.1 (N = 3). Compound **16** shows no reduction of probe labeling on ABHD6 and others at 10 μM inhibitor concentration using MB064, and on FAAH labeling and others at 100 μM inhibitor concentration using TAMRA-FP (N = 3). Of note, left panel DAGLα < DAGLα*, the exact mechanism for DAGLα* formation is unknown to date but absence of DAGLα* is also observed in DAGLα KO mice.[11] **B)** Characterization of compound **17** on ABPP with probes MB064 (left) and TAMRA-FP (right). pIC_{50} DAGLα of **17** = 7.1 ± 0.1 (N = 3). Compound **17** shows no effect on ABHD6 and FAAH (and any other protein tested) at 10 μM concentration (N = 3).

Conclusions

To conclude, the sub-optimal lipophilicity of LEI105 was improved by LipE guided structure-based design in combination with ABPP. First, optimization of the 2-acyl substituent led to a potent trifluorobutanoyl spacer with significantly improved LipE. Second, investigation of the heterocyclic scaffold showed that a *p*-fluorophenyl substituent was optimal, yielding LEI107 (**16**), an α-keto heterocycle with drug-like properties and high potency in a DAGLα natural substrate activity assay. Projecting forward, it is important to test whether LEI107 is a dual inhibitor of DAGLα and DAGLβ.[12] Due to its optimized physicochemical properties, LEI107 can now be fully characterized on early absorption, distribution, metabolism and extraction (ADME) properties. Moreover, both *in vivo* stability and CYP liability are also important. LEI107 can be a highly important inhibitor for studying the role of the 2-AG perturbation in many pathophysiological conditions including (mouse models of) obesity, Alzheimer's and Parkinson's disease.[20] Important to keep in mind, possible hemiacetal formation can occur at

the ketone. Therefore, its consequences with regard to *in vivo* stability need to be investigated. Due to the covalent reversible binding mode of α-keto heterocycles, LEI107 could shed light on whether a therapeutic window for DAGL inhibition can be established, with regard to possible CNS mediated side-effects.

Experimental

Experimental procedures biochemistry

Cloning procedures

Cloning procedures were performed as previously reported.[12] In brief, full-length human hDAGL-α cDNA was purchased from Biosource and cloned into mammalian expression vector pcDNA3.1, containing genes for ampicillin and neomycin resistance. The empty vector was used as a negative control (mock). All plasmids were grown in XL-10 Z-competent cells and prepped (Maxi Prep, Qiagen). The sequences were confirmed by sequence analysis at the Leiden Genome Technology Centre.

Cell culture and membrane preparation

Cell culture and membrane preperations were performed as previously reported.[12] In brief, HEK293T cells were grown in DMEM with stable glutamine and phenol red (PAA) with 10% new born calf serum, penicillin, and streptomycin. Cells were passaged every 2−3 days by resuspension in medium and seeding to the appropriate confluence. Membranes were prepared from transiently transfected HEK293T cells. 24 Hours prior to transfection, 10^7 cells were seeded in a 15 cm Petri dish. Cells were transfected by the addition of a 3:1 mixture of polyethyleneimine (60 μg) and plasmid DNA (20 μg) in 2 mL of serum free medium. The medium was refreshed after 24 h, and after 72 h the cells were harvested by suspending them in 20 mL of medium. The supernatant was removed by centrifuge for 10 min at 1000 rpm. The cell pellet quickly frozen in liquid nitrogen and stored at −80 °C until use. Cell pellets were thawed on ice and suspended in lysis buffer A (20 mM HEPES, pH 7.2, 2 mM DTT, 0.25 M sucrose, 1 mM $MgCl_2$, 1× cocktail (Roche cOmplete EDTA free), 25 U/mL Benzonase). The suspension was homogenized by polytrone (3 × 7 s) and incubated for 30 min on ice. The membrane fraction was separated by ultracentrifuge (100.000g, 30 min, 4 °C, Beckman Coulter, type Ti70 rotor) and the pellet was resuspended in lysis buffer B (20 mM HEPES, pH 7.2, 2 mM DTT, 1× cocktail (Roche cOmplete EDTA free)). The protein concentration was determined with Qubit protein assay (Invitrogen). The total protein concentration was diluted to 1 mg/mL and the samples were quickly frozen in liquid nitrogen and stored in small aliquots at −80 °C until use.

Biochemical hDAGLα activity assay

The biochemical hDAGL-α activity assay was performed as previously reported.[12] In brief, the biochemical hDAGL-α activity assay is based on the hydrolysis of *para*-nitrophenylbutyrate (PNP-butyrate) by membrane preparations from HEK293T cells transiently transfected with hDAGL-α. Reactions (200 μL) were performed in a flat bottom Greiner 96-wells plates, 50 mM HEPES pH 7.2 buffer with 0.05 μg/μL (final protein concentration) hDAGL-α transfected membrane fractions.

Biochemical hDAGLα natural substrate assay

The natural substrate assay for DAGLα was performed as previously reported.[18]

Biochemical ABPP assay

The biochemical ABPP assay on mouse brain proteome was performed as previously reported.[10,12]

Experimental procedures chemistry

General Remarks

All reactions were performed using oven- or flame-dried glassware and dry solvents. Reagents were purchased from Sigma-Aldrich, Acros, and Merck and used without further purification unless noted otherwise. All

moisture sensitive reactions were performed under an argon atmosphere. Traces of water were removed from starting compounds by co-evaporation with toluene. ^{1}H and ^{13}C NMR spectra were recorded on a Bruker AV 400 MHz spectrometer at 400.2 (^{1}H) and 100.6 (^{13}C) MHz using the reported deuterated solvent. Chemical shift values are reported in ppm with tetramethylsilane or solvent resonance as the internal standard ($CDCl_3$: δ 7.26 for ^{1}H, δ 77.16 for ^{13}C; CD_3OD: δ 3.31 for 1H, δ 49.00 for ^{13}C). Data are reported as follows: chemical shifts (δ), multiplicity (s = singlet, d = doublet, dd = double doublet, td = triple doublet, t = triplet, q = quartet, quintet = quint, b = broad, m = multiplet), coupling constants J (*Hz*), and integration. High resolution mass spectra were recorded on a Thermo Scientific LTQ Orbitrap XL. Compound purity (>95% unless stated otherwise) was measured by liquid chromatography on a Finnigan Surveyor LC-MS system, equipped with a C18 column. Flash chromatography was performed using SiliCycle silica gel type SiliaFlash P60 (230−400 mesh). TLC analysis was performed on Merck silica gel 60/Kieselguhr F254, 0.25 mm. Compounds were visualized using either Seebach's reagent (a mixture of phosphomolybdic acid (25 g), cerium(IV) sulfate (7.5 g), H_2O (500 mL), and H_2SO_4 (25 mL)) or a $KMnO_4$ stain (K_2CO_3 (40 g), $KMnO_4$ (6 g), and H_2O (600 mL)).

2-Hydroxy-7-phenylheptanenitrile (19)

The title compound was synthesized from commercially available 6-phenylhexan-1-ol (1.70 g, 9.51 mmol) to yield 2-hydroxy-7-phenylheptanenitrile (1.67 g, 8.22 mmol, 86% over 2 steps) using previously reported procedures. Spectroscopic data are in agreement with those previously reported.[10]

1-(6-(*p*-Tolyl)oxazolo[4,5-*b*]pyridin-2-yl)-6-phenylhexan-1-ol (20)

The title compound was synthesized from 2-hydroxy-7-phenylheptanenitrile (**19**) as previously reported. Spectroscopic data are in agreement with those previously reported.[12]

1-(6-(*p*-Tolyl)oxazolo[4,5-*b*]pyridin-2-yl)-6-phenylhexan-1-one (2)

The title compound was synthesized from 1-(6-(*p*-tolyl)oxazolo[4,5-*b*]pyridin-2-yl)-6-phenylhexan-1-ol (**20**) by DMP oxidation as previously reported. Spectroscopic data are in agreement with those previously reported.[12]

2-Hydroxy-6-phenylhexanenitrile (21)

The title compound was synthesized from commercially available 5-phenylpentan-1-ol according to the previously reported procedures.[10,11]

5-Phenyl-1-(6-(*p*-tolyl)oxazolo[4,5-*b*]pyridin-2-yl)pentan-1-ol (22)

The title compound was synthesized from 2-hydroxy-6-phenylhexanenitrile (**21**, 88 mg, 0.47 mmol) and 2-amino-5-(*p*-tolyl)pyridin-3-ol (62 mg, 0.31 mmol) according to procedure described for compound **20**. This yielded 5-phenyl-1-(6-(*p*-tolyl)oxazolo[4,5-*b*]pyridin-2-yl)pentan-1-ol (21 mg, 0.056 mmol, 18 %). ^{1}H NMR ($CDCl_3$, 400 MHz): δ 8.75 (d, *J* = 2.0 Hz, 1H), 7.94 (d, *J* = 1.9 Hz, 1H), 7.53 – 7.44 (m, 2H), 7.33 – 7.28 (m, 2H), 7.26 – 7.21 (m, 2H), 7.20 – 7.10 (m, 3H), 5.04 (dd, *J* = 7.6, 5.2 Hz, 1H), 3.71 (bs, 1H), 2.63 (t, *J* = 7.6 Hz, 2H), 2.42 (s, 3H), 2.17 – 1.97 (m, 2H), 1.77 – 1.49 (m, 4H). ^{13}C BBDEC NMR ($CDCl_3$, 101 MHz): δ 171.26, 153.96, 145.68, 143.58, 142.40, 138.45, 134.77, 134.63, 130.09(2C), 128.50(2C), 128.41(2C), 127.50(2C), 125.84, 116.87, 68.27, 35.85, 35.46, 31.27, 24.75, 21.29.

5-Phenyl-1-(6-(*p*-tolyl)oxazolo[4,5-*b*]pyridin-2-yl)pentan-1-one (3)

The title compound was synthesized from 5-phenyl-1-(6-(*p*-tolyl)oxazolo[4,5-*b*]pyridin-2-yl)pentan-1-ol (**22**, 20 mg, 0.054 mmol) according to procedure described for compound 1. This yielded 5-phenyl-1-(6-(*p*-tolyl)oxazolo[4,5-*b*]pyridin-2-yl)pentan-1-one (19 mg, 0.051 mmol, 95%). HRMS (ESI+) m/z: calculated for $C_{24}H_{23}N_2O_2$ ([M + H]), 371.1754; found, 371.1754. ^{1}H NMR ($CDCl_3$, 400 MHz): δ 8.98 (s, 1H), 8.09 (s, 1H), 7.56 – 7.51 (m, 2H), 7.34 (d, *J* = 7.9 Hz, 2H), 7.31 – 7.24 (m, 3H), 7.23 – 7.14 (m, 3H), 3.32 (t, *J* = 7.2 Hz, 2H), 2.70 (t, *J* =

7.5 Hz, 2H), 2.44 (s, 3H), 1.94 – 1.83 (m, 2H), 1.84 – 1.71 (m, 2H). ^{13}C BBDEC NMR ($CDCl_3$, 101 MHz): δ 190.23, 158.72, 153.13, 153.11, 148.22, 148.10, 142.07, 139.15, 134.13, 130.25(2C), 128.55(2C), 128.49(2C), 127.66(2C), 125.96, 117.80, 39.73, 35.75, 30.96, 23.63, 21.36. Purity of 80% as determined by LC-MS.

2-Hydroxy-5-phenylpentanenitrile (23)

The title compound was synthesized as previously reported.[11]

4-Phenyl-1-(6-(*p*-tolyl)oxazolo[4,5-*b*]pyridin-2-yl)butan-1-ol (24)

The title compound was synthesized from 2-hydroxy-5-phenylpentanenitrile (**23**, 108 mg, 0.62 mmol) and 2-amino-5-(*p*-tolyl)pyridin-3-ol (87 mg, 0.44 mmol) according to procedure described for compound **20**. This yielded 4-phenyl-1-(6-(*p*-tolyl)oxazolo[4,5-*b*]pyridin-2-yl)butan-1-ol (20 mg, 0.056 mmol, 13%). ^{1}H NMR ($CDCl_3$, 400 MHz): δ 8.74 (dd, *J* = 5.0, 1.9 Hz, 1H), 7.93 (d, *J* = 1.9 Hz, 1H), 7.49 – 7.45 (m, 2H), 7.32 – 7.22 (m, 4H), 7.20 – 7.11 (m, 3H), 5.05 (dd, *J* = 7.6, 5.1 Hz, 1H), 2.70 (t, *J* = 7.6 Hz, 2H), 2.42 (s, 3H), 2.18 – 1.97 (m, 2H), 1.95 – 1.79 (m, 2H). ^{13}C BBDEC NMR ($CDCl_3$, 101 MHz): δ 171.20, 153.92, 145.66, 143.58, 141.83, 138.46, 134.80, 134.60, 130.09(2C), 128.54(2C), 128.48(2C), 127.51(2C), 126.02, 116.91, 68.20, 35.57, 35.07, 26.77, 21.29.

4-Phenyl-1-(6-(*p*-tolyl)oxazolo[4,5-*b*]pyridin-2-yl)butan-1-one (4)

The title compound was synthesized from 4-phenyl-1-(6-(*p*-tolyl)oxazolo[4,5-*b*]pyridin-2-yl)butan-1-ol (**24**, 19 mg, 0.053 mmol) according to procedure described for compound **2**. This yielded 4-phenyl-1-(6-(*p*-tolyl)oxazolo[4,5-*b*]pyridin-2-yl)butan-1-one (6 mg, 0.017 mmol, 32%). HRMS (ESI+) m/z: calculated for $C_{23}H_{21}N_2O_2$ ([M + H]), 357.1598; found, 357.1597. ^{1}H NMR ($CDCl_3$, 400 MHz): δ 8.97 (d, *J* = 1.3 Hz, 1H), 8.09 (d, *J* = 2.0 Hz, 1H), 7.61 – 7.50 (m, 2H), 7.37 – 7.27 (m, 4H), 7.25 – 7.14 (m, 3H), 3.31 (t, *J* = 7.4 Hz, 2H), 2.77 (t, *J* = 7.6 Hz, 2H), 2.44 (s, 3H), 2.26 – 2.10 (m, 2H). ^{13}C BBDEC NMR ($CDCl_3$, 101 MHz): δ 190.07, 158.70, 153.11, 148.30, 144.21, 141.25, 139.16, 137.68, 134.10, 130.26(2C), 128.67(2C), 128.61(2C), 127.66(2C), 126.26, 117.85, 39.24, 35.17, 25.51, 21.35. Purity of 95% as determined by LC-MS.

2-Hydroxy-4-phenylbutanenitrile (25)

The title compound was synthesized as previously reported.[11]

3-Phenyl-1-(6-(*p*-tolyl)oxazolo[4,5-*b*]pyridin-2-yl)propan-1-ol (26)

The title compound was synthesized from 2-hydroxy-4-phenylbutanenitrile (**25**, 114 mg, 0.71 mmol) and 2-amino-5-(*p*-tolyl)pyridin-3-ol (84 mg, 0.42 mmol) according to procedure described for compound **20**. This yielded 3-phenyl-1-(6-(*p*-tolyl)oxazolo[4,5-*b*]pyridin-2-yl)propan-1-ol (24 mg, 0.071 mmol, 17%). ^{1}H NMR ($CDCl_3$, 400 MHz): δ 8.74 (d, *J* = 1.9 Hz, 1H), 7.92 (d, *J* = 1.9 Hz, 1H), 7.52 – 7.43 (m, 2H), 7.32 – 7.28 (m, 2H), 7.27 – 7.21 (m, 4H), 7.19 – 7.13 (m, 1H), 5.04 (dd, *J* = 7.9, 4.9 Hz, 1H), 3.75 (bs, 1H), 2.89 (t, *J* = 7.7 Hz, 2H), 2.42 (s, 3H), 2.40 – 2.28 (m, 2H). ^{13}C BBDEC NMR ($CDCl_3$, 101 MHz): δ 171.12, 153.90, 145.67, 143.60, 140.86, 138.48, 134.83, 134.60, 130.10(2C), 128.71(2C), 128.59(2C), 127.51(2C), 126.22, 116.88, 67.46, 36.96, 31.16, 21.29.

3-Phenyl-1-(6-(*p*-tolyl)oxazolo[4,5-*b*]pyridin-2-yl)propan-1-one (5)

The title compound was synthesized from 3-phenyl-1-(6-(*p*-tolyl)oxazolo[4,5-*b*]pyridin-2-yl)propan-1-ol (**26**, 23 mg, 0.067 mmol) according to procedure described for compound **2**. This yielded 3-phenyl-1-(6-(*p*-tolyl)oxazolo[4,5-*b*]pyridin-2-yl)propan-1-one (15 mg, 0.044 mmol, 65%). HRMS (ESI+) m/z: calculated for $C_{22}H_{19}N_2O_2$ ([M + H]), 343.1441; found, 343.1441. ^{1}H NMR ($CDCl_3$, 400 MHz): δ 8.97 (d, *J* = 2.0 Hz, 1H), 8.09 (d, *J* = 2.0 Hz, 1H), 7.58 – 7.50 (m, 2H), 7.36 – 7.27 (m, 4H), 7.27 – 7.17 (m, 1H), 3.64 (t, *J* = 7.4 Hz, 2H), 3.17 (t, *J* = 7.6 Hz, 2H), 2.44 (s, 3H). ^{13}C BBDEC NMR ($CDCl_3$, 101 MHz): δ 189.30, 158.63, 153.06, 148.33, 144.26, 140.16, 139.18, 137.74, 134.06, 130.26(2C), 128.74(2C), 128.60(2C), 127.65(2C), 126.54, 117.88, 41.40, 29.77, 21.35. Purity of 92% as determined by LC-MS.

2-Hydroxy-3-phenylpropanenitrile (27)

The title compound was synthesized from commercially available 2-phenylacetaldehyde (1.27 g, 10.53 mmol) according to the previously reported procedure.[1] This yielded 2-hydroxy-3-phenylpropanenitrile (610 mg, 4.14 mmol, 39%). ^{1}H NMR ($CDCl_3$, 400 MHz): δ 7.39 – 7.24 (m, 5H), 4.62 (t, *J* = 6.5 Hz, 1H), 3.10 (d, *J* = 6.5 Hz, 2H), 2.88 (bs, 1H). ^{13}C BBDEC NMR ($CDCl_3$, 101 MHz): 133.92, 129.82(2C), 129.05(2C), 127.97, 119.44, 62.27, 41.45.

2-Phenyl-1-(6-(*p*-tolyl)oxazolo[4,5-*b*]pyridin-2-yl)ethan-1-ol (28)

The title compound was synthesized from 2-hydroxy-3-phenylpropanenitrile (**27**, 112 mg, 0.76 mmol) and 2-amino-5-(*p*-tolyl)pyridin-3-ol (93 mg, 0.46 mmol) according to procedure described for compound **20**. This yielded 2-phenyl-1-(6-(*p*-tolyl)oxazolo[4,5-*b*]pyridin-2-yl)ethan-1-ol (29 mg, 0.087 mmol, 19%). ^{1}H NMR ($CDCl_3$, 400 MHz): δ 8.72 (d, *J* = 1.9 Hz, 1H), 7.95 (d, *J* = 1.9 Hz, 1H), 7.55 – 7.45 (m, 2H), 7.36 – 7.19 (m, 7H), 5.26 (dd, *J* = 7.8, 5.0 Hz, 1H), 3.42 (dd, J = 13.9, 5.0 Hz, 1H), 3.30 (dd, J = 13.9, 7.8 Hz, 1H), 2.43 (s, 3H). ^{13}C BBDEC NMR ($CDCl_3$, 101 MHz): δ 170.24, 153.92, 145.76, 143.52, 138.47, 136.07, 134.85, 134.58, 130.09(2C), 129.65(2C), 128.76(2C), 127.51(2C), 127.22, 116.89, 69.28, 41.90, 29.82.

2-Phenyl-1-(6-(*p*-tolyl)oxazolo[4,5-*b*]pyridin-2-yl)ethan-1-one (6)

The title compound was synthesized from 2-phenyl-1-(6-(*p*-tolyl)oxazolo[4,5-*b*]pyridin-2-yl)ethan-1-ol (**28**, 20 mg, 0.061 mmol) according to procedure described for compound **2**. This yielded 2-phenyl-1-(6-(*p*-tolyl)oxazolo[4,5-*b*]pyridin-2-yl)ethan-1-one (12 mg, 0.037 mmol, 60%). HRMS (ESI+) m/z: calculated for $C_{21}H_{17}N_2O_2$ ([M + H]), 329.1285; found, 329.1283. ^{1}H NMR ($CDCl_3$, 400 MHz): δ 8.98 (d, *J* = 2.0 Hz, 1H), 8.08 (d, *J* = 2.0 Hz, 1H), 7.56 – 7.51 (m, 2H), 7.48 – 7.42 (m, 2H), 7.40 – 7.27 (m, 5H), 4.57 (s, 2H), 2.44 (s, 4H). ^{13}C BBDEC NMR ($CDCl_3$, 101 MHz): δ 187.23, 158.63, 153.11, 148.41, 144.51, 139.20, 137.82, 134.07, 132.47, 130.26(2C), 130.15(2C), 129.37, 128.97(2C), 127.66(2C), 117.88, 46.19, 21.35. Purity of >95% as determined by LC-MS (44:56 enol/ketone).

4,4,4-Trifluoro-2-hydroxybutanenitrile (29)

The title compound was synthesized from commercially available 3,3,3-trifluoropropanol (1 g, 8.92 mmol) according to previously reported nitrilation procedures with only THF as solvent.[1] This yielded 4,4,4-trifluoro-2-hydroxybutanenitrile (137 mg, 0.99 mmol, 10%). ^{1}H NMR ($CDCl_3$, 400 MHz): δ 5.14 (bs, 1H), 4.82 (t, *J* = 6.6 Hz, 1H), 2.77 – 2.65 (m, 2H). ^{13}C BBDEC NMR ($CDCl_3$, 101 MHz): δ 124.47 (q, *J* = 277.0 Hz), 120.34, 39.15 (q, *J* = 29.3 Hz), 36.57 (q, *J* = 3.0 Hz).

3,3,3-Trifluoro-1-(6-(*p*-tolyl)oxazolo[4,5-*b*]pyridin-2-yl)propan-1-ol (30)

The title compound was synthesized from 4,4,4-trifluoro-2-hydroxybutanenitrile (**29**, 130 mg, 0.94 mmol) and 2-amino-5-(*p*-tolyl)pyridin-3-ol (120 mg, 0.60 mmol) according to procedure described for compound **20**. This yielded 3,3,3-trifluoro-1-(6-(*p*-tolyl)oxazolo[4,5-*b*]pyridin-2-yl)propan-1-ol (7 mg, 0.022 mmol, 4%). ^{1}H NMR ($CDCl_3$, 400 MHz): δ 8.77 (d, *J* = 2.0 Hz, 1H), 8.33 (d, *J* = 2.0 Hz, 1H), 7.65 – 7.58 (m, 2H), 7.34 (d, *J* = 7.9 Hz, 2H), 5.31 (dd, *J* = 8.7, 4.3 Hz, 1H), 2.41 (s, 3H), 2.36 – 2.15 (m, 2H). ^{13}C BBDEC NMR (MeOD, 101 MHz): δ 161.67, 146.19, 145.29, 139.73, 136.79, 135.50, 131.00(2C), 128.48(2C), 124.17 (q, *J* = 269.7 Hz), 118.76, 61.54, 39.55 (q, *J* = 30.3 Hz), 37.53 (q, *J* = 4.04 Hz), 21.16.

3,3,3-Trifluoro-1-(6-(*p*-tolyl)oxazolo[4,5-*b*]pyridin-2-yl)propan-1-one (7)

The title compound was synthesized from 3,3,3-trifluoro-1-(6-(*p*-tolyl)oxazolo[4,5-*b*]pyridin-2-yl)propan-1-ol (**30**, 7 mg, 0.022 mmol) according to procedure described for compound **2**. This yielded 3,3,3-trifluoro-1-(6-(*p*-tolyl)oxazolo[4,5-*b*]pyridin-2-yl)propan-1-one (3 mg, 9.4 µmol, 43%). HRMS (ESI+) m/z: calculated for $C_{16}H_{14}F_3N_2O_3$ ([M + H_3O]), 339.0951; found, 339.0949. ^{1}H NMR ($CDCl_3$, 400 MHz): δ 9.06 (bs, 1H), 8.15 (bs, 1H), 7.59 – 7.51 (m, 2H), 7.36 (d, *J* = 7.9 Hz, 2H), 4.19 (q, *J* = 9.8 Hz, 2H), 2.45 (s, 3H).^{13}C BBDEC NMR ($CDCl_3$, 101

MHz): δ 179.36 (q, *J* = 2.7 Hz), 173.18, 157.74, 157.73, 139.41, 133.75, 130.26(2C), 127.62(2C), 127.43, 123.31 (q, *J* = 277.8 Hz), 117.84, 117.82, 42.89 (q, *J* = 29.9 Hz), 21.30. **Final compound not stable.**

5,5,5-Trifluoro-2-hydroxypentanenitrile (31)

To a vigorously stirred solution of commercially available 4,4,4-trifluorobutanol (5.0 g, 39 mmol) in CH_2Cl_2 (100 mL) was added KBr (485 mg, 4.08 mmol), TEMPO (30 mg, 0.005 mmol) and a solution of NaOCl (59 mmol) in 10% sat. $NaHCO_3$ (aq). After complete conversion (2 h), the organic layer was separated and the aquous layer was extracted 2x with 50 mL CH_2Cl_2. The combined organic layers were dried over Na_2SO_4, filtered, after which THF (100 mL) was added. CH_2Cl_2 was evaporated at rt, 300 mbar, whereafter nitrilation was performed as previously reported.[1] The product was purified by flash chromatography (Et_2O/ pentane) and evaporated at rt to obtain 5,5,5-trifluoro-2-hydroxypentanenitrile (3.53 g, 23.1 mmol, 59%). ^{1}H NMR ($CDCl_3$, 400 MHz): δ 4.62 (t, *J* = 6.1 Hz, 1H), 2.93 (bs, 1H), 2.46 – 2.28 (m, 2H), 2.17 – 2.09 (m, 2H). ^{13}C BBDEC NMR ($CDCl_3$, 101 MHz): δ 126.57 (q, *J* = 275.9 Hz), 118.93, 59.63, 29.20 (q, *J* = 30.1 Hz), 27.91 (q, *J* = 3.1 Hz).

4,4,4-Trifluoro-1-(6-(*p*-tolyl)oxazolo[4,5-*b*]pyridin-2-yl)butan-1-ol (32)

The title compound was synthesized from 5,5,5-trifluoro-2-hydroxypentanenitrile (**31**, 117 mg, 0,76 mmol) and 2-amino-5-(*p*-tolyl)pyridin-3-ol (85 mg, 0.42 mmol) according to procedure described for compound **20**. This yielded 4,4,4-trifluoro-1-(6-(*p*-tolyl)oxazolo[4,5-*b*]pyridin-2-yl)butan-1-ol (6 mg, 0.017 mmol, 4%). ^{1}H NMR ($CDCl_3$, 400 MHz): δ 8.78 (d, *J* = 1.9 Hz, 1H), 7.98 (d, *J* = 1.8 Hz, 1H), 7.53 – 7.46 (m, 2H), 7.36 – 7.29 (m, 2H), 5.13 (dd, *J* = 8.0, 3.8 Hz, 1H), 3.79 (bs, 1H), 2.43 (s, 3H), 2.41 – 2.23 (m, 2H). ^{13}C BBDEC NMR ($CDCl_3$, 101 MHz): δ 169.81, 153.65, 146.04, 143.74, 138.63, 135.20, 134.48, 130.15(2C), 127.54(2C), 127.1 (q, *J* = 276.7 Hz), 117.04, 66.67, 29.66 (q, *J* = 30.3 Hz), 27.82 (q, *J* = 3.0 Hz), 21.30.

4,4,4-Trifluoro-1-(6-(*p*-tolyl)oxazolo[4,5-*b*]pyridin-2-yl)butan-1-one (8)

The title compound was synthesized from 4,4,4-trifluoro-1-(6-(*p*-tolyl)oxazolo[4,5-*b*]pyridin-2-yl)butan-1-ol (**32,** 6 mg, 0.017 mmol) according to procedure described for compound **2**. This yielded 4,4,4-trifluoro-1-(6-(*p*-tolyl)oxazolo[4,5-*b*]pyridin-2-yl)butan-1-one (4 mg, 0.012 mmol, 70%). HRMS (ESI+) m/z: calculated for $C_{17}H_{14}F_3N_2O_2$ ([M + H]), 335.1002; found, 335.1003. ^{1}H NMR ($CDCl_3$, 400 MHz): δ 9.01 (d, *J* = 2.1 Hz, 1H), 8.12 (d, *J* = 2.1 Hz, 1H), 7.58 – 7.50 (m, 2H), 7.35 (d, *J* = 8.0 Hz, 2H), 3.60 (t, *J* = 7.6 Hz, 2H), 2.76 – 2.61 (m, 2H), 2.45 (s, 3H). ^{13}C BBDEC NMR ($CDCl_3$, 101 MHz): δ 186.61, 158.08, 152.80, 148.68, 141.98, 139.34, 138.11, 131.98, 130.31(2C), 127.68(2C), 126.69 (q, *J* = 277.8 Hz), 117.95, 32.76 (q, *J* = 3.0 Hz), 28.03 (q, *J* = 30.5 Hz), 21.36. Purity of >95% as determined by LC-MS.

2-Phenoxybenzaldehyde (33)

K_2CO_3 (22 g, 159 mmol) was added to a stirred solution of phenol (7.60 g, 81 mmol) in THF (100 mL) at reflux. After 1 h 2-fluorobenzaldehyde (8.49 mL, 101 mmol) was added and the reaction mixture was refluxed for an additional 24 h. Upon completion the mixture was cooled to rt and concentrated *in vacuo*. Saturated $NaHCO_3$ (100 mL) was added and product was extracted using EtOAc (3 x 80 mL). The combined organic layers were washed with brine, dried, *concentrated in vacuo* and purified by flash chromatography to yield 2-phenoxybenzaldehyde (8.05 g, 40,6 mmol, 50%). ^{1}H NMR ($CDCl_3$, 400 MHz): δ 10.52 (s, 1H), 7.94 (dd, *J* = 7.8, 1.8 Hz, 1H), 7.54 – 7.48 (m, 1H), 7.43 – 7.36 (m, 2H), 7.22 – 7.15 (m, 2H), 7.10 – 7.04 (m, 2H), 6.90 (d, *J* = 8.4, 1H).

Methyl 3-(2-phenoxyphenyl)acrylate (34)

n-BuLi (30.6 ml, 76 mmol) was added dropwise over 10 minutes to a cooled solution (-80 °C) of methyl 2-(dimethoxyphosphoryl)acetate (11.04 mL, 76 mmol) in THF (100 mL) and the resulting mixture was stirred for 1 h. 2-Phenoxybenzaldehyde (**33**, 7.57 g, 38.2 mmol) was added and the reaction mixture was slowly warmed to rt and stirred overnight. Upon completion the mixture was concentrated *in vacuo*, saturated $NaHCO_3$ (80 mL)

was added and product was extracted using EtOAc (3 x 50 mL). The combined organic layers were washed with brine, dried, concentrated *in vacuo* and purified by flash chromatography to yield methyl 3-(2-phenoxyphenyl)acrylate (6.6 g, 26.0 mmol, 68%). ^{1}H NMR ($CDCl_3$, 400 MHz): δ 8.03 (d, *J* = 16.2 Hz, 1H), 7.62 (dd, *J* = 7.8, 1.7 Hz, 1H), 7.39 –6.81 (m, 8H), 6.57 (d, *J* = 16.2, 1H), 3.79 (s, 3H).

3-(2-Phenoxyphenyl)propan-1-ol (35)

Lithium aluminum hydride (22,71 ml, 54,5 mmol) was added to a stirred and cooled solution (0 °C) of methyl 3-(2-phenoxyphenyl)acrylate (**34**, 6.6 g, 26,0 mmol) in THF (100 mL) over 10 minutes. The reaction mixture was stirred for 2 hours and upon completion the mixture was concentrated *in vacuo*, saturated $NaHCO_3$ (80 mL) was added and product was extracted using EtOAc (3 x 50 mL). The combined organic layers were washed with brine, dried, concentrated *in vacuo* and purified by flash chromatography to yield 3-(2-phenoxyphenyl)propan-1-ol (1.3 g, 5.69 mmol, 22%). ^{1}H NMR ($CDCl_3$, 400 MHz): δ 7.34 – 7.26 (m, 3H), 7.17 (td, *J* = 7.7, 1.8 Hz, 1H), 7.11 – 7.04 (m, 2H), 6.96 – 6.91 (m, 2H), 6.88 (dd, *J* = 8.1, 1.3 Hz, 1H), 3.63 (t, *J* = 6.3 Hz, 2H), 2.73 (t, *J* = 7.2 Hz, 2H), 1.94 – 1.82 (m, 2H), 1.76 (bs, 1H). ^{13}C NMR ($CDCl_3$, 101 MHz): δ 157.82, 154.69, 133.25, 130.87, 129.87(2C), 127.56, 124.13, 122.89, 119.56, 117.89(2C), 62.21, 33.20, 26.31.

2-Hydroxy-4-(2-phenoxyphenyl)butanenitrile (36)

The title compound was synthesized from 3-(2-phenoxyphenyl)propan-1-ol (**35**, 1.3 g, 5.69 mmol) according to the previously reported 2 step procedure.[1] This yielded 2-hydroxy-4-(2-phenoxyphenyl)butanenitrile (727.9 mg, 2.87 mmol, 50%, 2 steps). ^{1}H NMR ($CDCl_3$, 400 MHz): δ 7.36 – 7.30 (m, 2H), 7.27 (dd, *J* = 7.5, 1.8 Hz, 1H), 7.21 (td, *J* = 7.8, 1.8 Hz, 1H), 7.12 – 7.07 (m, 2H), 6.96 – 6.93 (m, 2H), 6.88 (dd, *J* = 8.2, 1.2 Hz, 1H), 4.42 (q, *J* = 6.3 Hz, 1H), 2.87 (t, *J* = 7.4 Hz, 2H), 2.28 – 2.07 (m, 2H). ^{13}C NMR ($CDCl_3$, 101 MHz): δ 157.32, 154.88, 131.03, 130.89, 130.00(2C), 128.35, 124.22, 123.32, 119.84, 119.41, 118.13(2C), 60.67, 35.67, 25.61.

3-(2-Phenoxyphenyl)-1-(6-(*p*-tolyl)oxazolo[4,5-*b*]pyridin-2-yl)propan-1-ol (37)

The title compound was synthesized from 2-hydroxy-4-(2-phenoxyphenyl)butanenitrile (**36**, 144.6 mg, 0.571 mmol) and 2-amino-5-(*p*-tolyl)pyridin-3-ol (84.6 mg, 0.422 mmol) according to the procedure described for compound **20**. This yielded 3-(2-phenoxyphenyl)-1-(6-(*p*-tolyl)oxazolo[4,5-*b*]pyridin-2-yl)propan-1-ol (35.9 mg, 0.082 mmol, 19%). ^{1}H NMR ($CDCl_3$, 400 MHz): δ 8.74 (d, *J* = 2.0 Hz, 1H), 7.85 (d, *J* = 2.0 Hz, 1H), 7.47 (d, *J* = 7.9 Hz, 2H), 7.33 – 7.27 (m, 5H), 7.17 – 7.11 (m, 1H), 7.07 – 7.01 (m, 2H), 6.92 (d, *J* = 8.0 Hz, 2H), 6.85 (d, *J* = 8.0 Hz, 1H), 5.02 (dd, *J* = 7.9, 4.8 Hz, 1H), 3.49 (bs, 1H), 2.90 (t, *J* = 7.6 Hz, 2H), 2.43 (s, 3H), 2.40 – 2.28 (m, 2H). ^{13}C NMR ($CDCl_3$, 101 MHz): δ 170.93, 170.90, 157.63, 154.80, 153.94, 145.65, 143.55, 138.42, 134.67, 132.18, 131.12, 130.08(2C), 129.85(2C), 127.84, 127.50(2C), 124.06, 122.94, 119.44, 118.00(2C), 116.79, 67.61, 35.70, 25.81, 21.30.

3-(2-phenoxyphenyl)-1-(6-(*p*-tolyl)oxazolo[4,5-*b*]pyridin-2-yl)propan-1-one (9)

The title compound was synthesized from 3-(2-phenoxyphenyl)-1-(6-(*p*-tolyl)oxazolo[4,5-*b*]pyridin-2-yl)propan-1-ol (**37**, 24.1 mg, 0.055 mmol) according to the procedure described for compound **2**. This yielded 3-(2-phenoxyphenyl)-1-(6-(*p*-tolyl)oxazolo[4,5-*b*]pyridin-2-yl)propan-1-one (13.7 mg, 0.032 mmol, 57%). HRMS (ESI+) m/z: calculated for $C_{28}H_{23}N_2O_3$ ([M + H]), 435.1703; found, 435.1699. ^{1}H NMR ($CDCl_3$, 400 MHz): δ 8.96 (d, *J* = 2.0 Hz, 1H), 8.05 (d, *J* = 2.0 Hz, 1H), 7.56 – 7.49 (m, 2H), 7.38 – 7.27 (m, 5H), 7.21 – 7.14 (m, 1H), 7.10 – 7.02 (m, 2H), 6.99 – 6.93 (m, 2H), 6.89 – 6.83 (m, 1H), 3.65 (t, *J* = 7.4 Hz, 2H), 3.20 (t, *J* = 7.4 Hz, 2H), 2.44 (s, 3H). ^{13}C NMR ($CDCl_3$, 101 MHz): δ 189.42, 158.62, 157.38, 155.05, 153.11, 148.24, 144.14, 139.12, 137.57, 134.10, 131.31, 130.92(2C), 130.24(2C), 129.87, 128.11, 127.64(2C), 123.89, 123.10, 119.03, 118.34(2C), 117.79, 40.23, 24.89, 21.35. Purity of >95% as determined by LC-MS.

Methyl 3-(3-phenoxyphenyl)acrylate (38)

The title compound was synthesized from commercially available 3-phenoxybenzaldehyde (3.0 ml, 17,36 mmol) according to the procedure described for compound **34**. This yielded methyl 3-(3-phenoxyphenyl)acrylate (4,53 g, 17,81 mmol, 103%). ^{1}H NMR ($CDCl_3$, 400 MHz): δ 7.60 (d, *J* = 16.0 Hz, 1H), 7.30 – 7.22 (m, 2H), 7.20 (d, *J* = 7.9 Hz, 1H), 7.17 – 7.10 (m, 2H), 7.08 – 7.01 (m, 1H), 6.99 – 6.90 (m, 3H), 6.36 (d, *J* = 16.0 Hz, 1H), 3.68 (s, 3H). ^{13}C NMR ($CDCl_3$, 101 MHz): δ 166.34, 157.37, 156.33, 143.48, 135.83, 129.72, 129.47(2C), 123.21, 122.53, 119.95, 118.65(2C), 118.21, 117.51, 51.01.

3-(3-Phenoxyphenyl)propan-1-ol (39)

The title compound was synthesized from methyl 3-(3-phenoxyphenyl)acrylate (**38**, 4.50 g, 17.70 mmol) according to the procedure described for compound **35**. This yielded 3-(3-phenoxyphenyl)propan-1-ol (3.15 g, 13.80 mmol, 78%). ^{1}H NMR ($CDCl_3$, 400 MHz): δ 7.36 – 7.28 (m, 2H), 7.28 – 7.21 (m, 1H), 7.12 – 7.06 (m, 1H), 7.03 – 6.97 (m, 2H), 6.96 – 6.92 (m, 1H), 6.89 – 6.80 (m, 2H), 3.67 (t, *J* = 6.4 Hz, 2H), 2.68 (t, *J* = 6.8 Hz, 2H), 1.92 – 1.83 (m, 2H), 1.56 (bs, 1H). ^{13}C NMR ($CDCl_3$, 101 MHz): δ 157.43, 157.40, 144.06, 129.85(2C), 129.75, 123.51, 123.28, 119.04, 118.96(2C), 116.47, 62.33, 34.17, 32.09.

2-Hydroxy-4-(3-phenoxyphenyl)butanenitrile (40)

The title compound was synthesized from 3-(3-phenoxyphenyl)propan-1-ol (**39**, 3.1 g, 13.58 mmol) according to the procedure described for compound **19**. This yielded 2-hydroxy-4-(3-phenoxyphenyl)butanenitrile (2.10 g, 8.29 mmol, 61% over 2 steps). ^{1}H NMR ($CDCl_3$, 400 MHz): δ 7.37 – 7.31 (m, 2H), 7.29 – 7.23 (m, 1H), 7.14 – 7.09 (m, 1H), 7.02 – 6.98 (m, 2H), 6.94 (dt, *J* = 7.6, 1.3 Hz, 1H), 6.88 – 6.84 (m, 2H), 4.43 (t, J = 6.3 Hz, 1H), 3.03 (bs, 1H), 2.88 – 2.72 (m, 2H), 2.24 – 2.06 (m, 2H). ^{13}C NMR ($CDCl_3$, 101 MHz): δ 157.72, 157.09, 141.78, 130.11, 129.92(2C), 123.53, 123.40, 119.87, 119.08(2C), 118.90, 116.96, 60.42, 36.54, 30.63.

3-(3-Phenoxyphenyl)-1-(6-(*p*-tolyl)oxazolo[4,5-*b*]pyridin-2-yl)propan-1-ol (41)

The title compound was synthesized from 2-hydroxy-4-(3-phenoxyphenyl)butanenitrile (**40**, 184.1 mg, 0.727 mmol) and 2-amino-5-(*p*-tolyl)pyridin-3-ol (91.3 mg, 0.456 mmol) according to the procedure described for compound **20**. This yielded 3-(3-phenoxyphenyl)-1-(6-(*p*-tolyl)oxazolo[4,5-*b*]pyridin-2-yl)propan-1-ol (41.9 mg, 0.096 mmol, 21%). ^{1}H NMR ($CDCl_3$, 400 MHz): δ 8.70 (d, *J* = 1.9 Hz, 1H), 7.89 (d, *J* = 1.9 Hz, 1H), 7.44 (d, *J* = 7.9 Hz, 2H), 7.34 – 7.24 (m, 4H), 7.20 (t, *J* = 7.9 Hz, 1H), 7.07 (t, *J* = 7.5 Hz, 1H), 7.00 – 6.90 (m, 4H), 6.79 (dd, *J* = 8.0, 2.4 Hz, 1H), 5.07 (dd, *J* = 7.7, 5.0 Hz, 1H), 4.36 (bs, 1H), 2.90 – 2.81 (m, 2H), 2.41 (s, 3H), 2.38 – 2.28 (m, 2H). ^{13}C NMR ($CDCl_3$, 101 MHz): δ 171.27, 157.38, 157.26, 153.75, 145.55, 143.53, 143.05, 138.44, 134.79, 134.49, 130.06(2C), 129.82(2C), 129.78, 127.48(2C), 123.65, 123.26, 119.16, 118.92(2C), 116.91, 116.58, 67.34, 36.74, 31.09, 21.28.

3-(3-Phenoxyphenyl)-1-(6-(*p*-tolyl)oxazolo[4,5-*b*]pyridin-2-yl)propan-1-one (10)

The title compound was synthesized from 3-(3-phenoxyphenyl)-1-(6-(*p*-tolyl)oxazolo[4,5-*b*]pyridin-2-yl)propan-1-ol (**41**, 24.1 mg, 0.055 mmol) according to the procedure described for compound **2**. This yielded 3-(3-phenoxyphenyl)-1-(6-(*p*-tolyl)oxazolo[4,5-*b*]pyridin-2-yl)propan-1-one (13.7 mg, 0.032 mmol, 57%). HRMS (ESI+) m/z: calculated for $C_{28}H_{23}N_2O_3$ ([M + H]), 435.1703; found, 435.1701. ^{1}H NMR ($CDCl_3$, 400 MHz): δ 8.97 (d, *J* = 2.0 Hz, 1H), 8.09 (d, *J* = 2.0 Hz, 1H), 7.58 – 7.49 (m, 2H), 7.38 – 7.30 (m, 4H), 7.29 – 7.22 (m, 1H), 7.13 – 7.06 (m, 1H), 7.05 – 6.98 (m, 3H), 6.94 (t, *J* = 2.0 Hz, 1H), 6.85 (ddd, *J* = 8.3, 2.6, 1.0 Hz, 1H), 3.62 (t, *J* = 7.6 Hz, 2H), 3.14 (t, *J* = 7.6 Hz, 2H), 2.44 (s, 3H). ^{13}C NMR ($CDCl_3$, 101 MHz): 189.11, 158.54, 157.58, 157.19, 153.03, 148.39, 144.24, 142.17, 139.18, 137.74, 134.04, 130.26(2C), 130.00, 129.87(2C), 127.65(2C), 123.41, 123.38, 119.07(2C), 118.98, 117.85, 116.91, 41.17, 29.58, 21.36. Purity of >95% as determined by LC-MS.

Methyl 3-(4-phenoxyphenyl)acrylate (42)

The title compound was synthesized from commercially available 4-phenoxybenzaldehyde (0.88 mL, 5.05 mmol) according to the procedure described for compound **34**. This yielded methyl 3-(4-phenoxyphenyl)acrylate (1.14 g, 4.50 mmol, 89%). ^{1}H NMR ($CDCl_3$, 400 MHz): δ 7.65 (d, *J* = 16.0 Hz, 1H), 7.48 – 7.42 (m, 2H), 7.37 – 7.31 (m, 2H), 7.17 – 7.10 (m, 1H), 7.05 – 6.99 (m, 2H), 6.98 – 6.91 (m, 2H), 6.33 (d, *J* = 16.0 Hz, 1H), 3.77 (s, 3H). ^{13}C NMR ($CDCl_3$, 101 MHz): δ 167.45, 159.46, 156.06, 144.05, 129.90(2C), 129.73(2C), 129.08, 124.08, 119.64(2C), 118.33(2C), 116.39, 51.56.

3-(4-Phenoxyphenyl)propan-1-ol (43)

Catalytic Pd/C was added to a solution of methyl 3-(4-phenoxyphenyl)acrylate (**42**, 1.14 g, 4.48 mmol) in MeOH (50 mL) and the mixture was stirred under H_2 (g) for 6 days. Upon completion the mixture was concentrated *in vacuo* and purified by flash chromatography to yield methyl 3-(4-phenoxyphenyl)propanoate. This was directly converted to the title compound according to the procedure described for compound **35.** This yielded 3-(4-phenoxyphenyl)propan-1-ol (0.545 g, 2.39 mmol, 53% over 2 steps). ^{1}H NMR ($CDCl_3$, 400 MHz): δ 7.31 – 7.23 (m, 2H), 7.14 – 7.09 (m, 2H), 7.03 (tt, *J* = 7.3, 1.1 Hz, 1H), 6.99 – 6.93 (m, 2H), 6.93 – 6.87 (m, 2H), 3.62 (t, *J* = 6.5 Hz, 2H), 2.84 (bs, 1H), 2.64 (t, *J* = 7.5 Hz, 2H), 1.90 – 1.77 (m, 2H). ^{13}C NMR ($CDCl_3$, 101 MHz): δ 157.54, 155.09, 136.84, 129.67(2C), 129.61(2C), 122.94, 119.02(2C), 118.48(2C), 61.87, 34.24, 31.29.

2-Hydroxy-4-(4-phenoxyphenyl)butanenitrile (44)

The title compound was synthesized from 3-(4-phenoxyphenyl)propan-1-ol (**43**, 0.544 g, 2.39 mmol) according to the procedure described for compound **19**. This yielded 2-hydroxy-4-(4-phenoxyphenyl)butanenitrile (0.563 g, 2.22 mmol, 93% over 2 steps). ^{1}H NMR ($CDCl_3$, 400 MHz): δ 7.33 – 7.25 (m, 2H), 7.16 – 7.10 (m, 2H), 7.09 – 7.04 (m, 1H), 7.00 – 6.95 (m, 2H), 6.95 – 6.89 (m, 2H), 4.40 (t, *J* = 6.8 Hz, 1H), 3.82 (bs, 1H), 2.86 – 2.71 (m, 2H), 2.22 – 2.01 (m, 2H). ^{13}C NMR ($CDCl_3$, 101 MHz): δ 157.26, 155.73, 134.52, 129.78(2C), 129.75(2C), 123.25, 120.07, 119.18(2C), 118.71(2C), 60.20, 36.59, 29.91.

3-(4-Phenoxyphenyl)-1-(6-(*p*-tolyl)oxazolo[4,5-*b*]pyridin-2-yl)propan-1-ol (45)

The title compound was synthesized from 2-hydroxy-4-(4-phenoxyphenyl)butanenitrile (**44**, 126.9 mg, 0.501 mmol) and 2-amino-5-(*p*-tolyl)pyridin-3-ol (83.0 mg, 0.415 mmol) according to the procedure described for compound **20**. This yielded 3-(4-phenoxyphenyl)-1-(6-(*p*-tolyl)oxazolo[4,5-*b*]pyridin-2-yl)propan-1-ol (28.4 mg, 0.065 mmol, 16%). ^{1}H NMR ($CDCl_3$, 400 MHz): δ 8.73 (d, *J* = 1.9 Hz, 1H), 7.91 (d, *J* = 2.0 Hz, 1H), 7.49 – 7.42 (m, 2H), 7.34 – 7.27 (m, 4H), 7.22 – 7.16 (m, 2H), 7.11 – 7.03 (m, 1H), 6.99 – 6.93 (m, 2H), 6.93 – 6.87 (m, 2H), 5.08 (dd, J = 7.8, 5.0 Hz, 1H), 4.14 (bs, 1H), 2.88 (t, *J* = 7.7 Hz, 2H), 2.42 (s, 3H), 2.40 – 2.28 (m, 2H). ^{13}C NMR ($CDCl_3$, 101 MHz): δ 171.19, 157.53, 155.49, 153.85, 145.65, 143.55, 138.46, 135.81, 134.79, 134.54, 130.08(2C), 129.94(2C), 129.79(2C), 127.50(2C), 123.12, 119.13(2C), 118.70(2C), 116.85, 67.35, 37.03, 30.45, 21.29.

3-(4-phenoxyphenyl)-1-(6-(*p*-tolyl)oxazolo[4,5-*b*]pyridin-2-yl)propan-1-one (11)

The title compound was synthesized from 3-(4-phenoxyphenyl)-1-(6-(*p*-tolyl)oxazolo[4,5-*b*]pyridin-2-yl)propan-1-ol (**45**, 21.3 mg, 0.049 mmol) according to the procedure described for compound **2**. This yielded 3-(4-phenoxyphenyl)-1-(6-(*p*-tolyl)oxazolo[4,5-*b*]pyridin-2-yl)propan-1-one (12.9 mg, 0.030 mmol, 61%). HRMS (ESI+) m/z: calculated for $C_{28}H_{23}N_2O_3$ ([M + H]), 435.1703; found, 435.1700. ^{1}H NMR ($CDCl_3$, 400 MHz): 9.00 – 8.95 (m, 1H), 8.11 – 8.06 (m, 1H), 7.57 – 7.51 (m, 2H), 7.36 – 7.28 (m, 4H), 7.28 – 7.22 (m, 2H), 7.11 – 7.05 (m, 1H), 7.01 – 6.92 (m, 4H), 3.63 (t, *J* = 7.5 Hz, 2H), 3.15 (t, *J* = 7.5 Hz, 2H), 2.44 (s, 3H). ^{13}C NMR ($CDCl_3$, 101 MHz): δ 189.30, 158.58, 157.50, 155.76, 153.05, 148.38, 144.24, 139.17, 137.74, 135.05, 134.04, 130.25(2C), 129.88(2C), 129.82(2C), 127.64(2C), 123.19, 119.26(2C), 118.77(2C), 117.85, 41.52, 29.07, 21.36. Purity of >95% as determined by LC-MS.

3-(4-((5-(Trifluoromethyl)pyridin-2-yl)oxy)phenyl)propan-1-ol (46)

The title compound was synthesized from 4-(3-hydroxypropyl)phenol (1.311 g, 8.61 mmol), 2-fluoro-5-(trifluoromethyl)pyridine (1.49 g, 9,03 mmol) and K_2CO_3 (1.2 g, 8.68 mmol) according to the procedure described for compound **35**. This yielded 3-(4-((5-(trifluoromethyl)pyridin-2-yl)oxy)phenyl)propan-1-ol (2.15 g, 7.24 mmol, 84%). ^{1}H NMR ($CDCl_3$, 400 MHz): δ 8.47 – 8.41 (m, 1H), 7.89 (dd, *J* = 8.7, 2.5 Hz, 1H), 7.29 – 7.23 (m, 2H), 7.09 – 7.04 (m, 2H), 7.02 – 6.96 (m, 1H), 3.71 (t, *J* = 6.4 Hz, 2H), 2.78 – 2.70 (m, 2H), 1.96 – 1.86 (m, 2H), 1.58 (bs, 1H). ^{13}C NMR ($CDCl_3$, 101 MHz): δ 166.09, 151.30, 145.61 (q, *J* = 4.3 Hz), 139.19, 136.77 (q, *J* = 3.1 Hz), 129.89(2C), 123.82 (q, *J* = 272.4 Hz), 121.48 (q, *J* = 33.3 Hz), 121.46(2C), 111.36, 62.30, 34.25, 31.61.

2-Hydroxy-4-(4-((5-(trifluoromethyl)pyridin-2-yl)oxy)phenyl)butanenitrile (47)

The title compound was synthesized from 3-(4-((5-(trifluoromethyl)pyridin-2-yl)oxy)phenyl)propan-1-ol (**46**, 1.38 g, 4.64 mmol) according to the previously described general synthesis scheme. This yielded 2-hydroxy-4-(4-((5-(trifluoromethyl)pyridin-2-yl)oxy)phenyl)butanenitrile (1.20 g, 3.72 mmol, 69%). ^{1}H NMR ($CDCl_3$, 400 MHz): δ 8.47 – 8.40 (m, 1H), 7.91 (dd, *J* = 8.7, 2.5 Hz, 1H), 7.27 (dd, *J* = 6.7, 1.8 Hz, 2H), 7.13 – 7.05 (m, 2H), 7.03 – 6.98 (m, 1H), 4.45 (t, *J* = 6.7 Hz, 1H), 2.95 – 2.79 (m, 2H), 2.27 – 2.11 (m, 2H). ^{13}C NMR ($CDCl_3$, 101 MHz): δ 165.91, 154.50, 151.77, 145.51 (q, *J* = 4.3 Hz), 136.99 (q, *J* = 3.4 Hz), 130.02(2C), 123.74 (q, *J* = 272.6 Hz), 121.91(2C), 121.74 (q, *J* = 33.5 Hz), 119.93, 111.47, 60.38, 36.62, 30.18.

1-(6-(*p*-Tolyl)oxazolo[4,5-*b*]pyridin-2-yl)-3-(4-((5-(trifluoromethyl)pyridin-2-yl)oxy)phenyl)propan-1-ol (48)

The title compound was synthesized from 2-hydroxy-4-(4-((5-(trifluoromethyl)pyridin-2-yl)oxy)phenyl)butanenitrile (**47**, 0.167 g, 0.518 mmol) and 2-amino-5-(*p*-tolyl)pyridin-3-ol (214 mg, 1.069 mmol) according to the procedure described for compound **20**. This yielded 1-(6-(*p*-tolyl)oxazolo[4,5-*b*]pyridin-2-yl)-3-(4-((5-(trifluoromethyl)pyridin-2-yl)oxy)phenyl)propan-1-ol (57.3 mg, 0.113 mmol, 22%). ^{1}H NMR ($CDCl_3$, 400 MHz): δ 8.84 – 8.66 (m, 1H), 8.50 – 8.36 (m, 1H), 7.94 – 7.90 (m, 1H), 7.86 (dd, J = 8.7, 2.6 Hz, 1H), 7.46 (d, J = 7.8 Hz, 2H), 7.36 – 7.23 (m, 4H), 7.11 – 7.00 (m, 2H), 6.96 (d, J = 8.6 Hz, 1H), 5.16 – 5.08 (m, 1H), 4.41 (bs, 1H), 2.92 (t, J = 7.6 Hz, 2H), 2.42 (m, 5H). ^{13}C NMR ($CDCl_3$, 101 MHz): δ 171.16, 165.98, 153.87, 151.47, 145.63, 145.56 (q, *J* = 4.0 Hz), 143.57, 138.46, 138.19, 136.75 (q, *J* = 3.0 Hz), 134.81, 134.54, 130.06(4C), 127.48(2C), 123.80 (q, *J* = 272.7 Hz), 121.50 (q, *J* = 34.3 Hz), 121.49(2C), 116.86, 111.34, 67.35, 36.83, 30.62, 21.26.

1-(6-(*p*-Tolyl)oxazolo[4,5-*b*]pyridin-2-yl)-3-(4-((5-(trifluoromethyl)pyridin-2-yl)oxy)phenyl)propan-1-one (12)

The title compound was synthesized from 1-(6-(*p*-tolyl)oxazolo[4,5-*b*]pyridin-2-yl)-3-(4-((5-(trifluoromethyl)pyridin-2-yl)oxy)phenyl)propan-1-ol (**48**, 38.5 mg, 0.076 mmol) according to the procedure described for compound **2**. This yielded 1-(6-(*p*-tolyl)oxazolo[4,5-*b*]pyridin-2-yl)-3-(4-((5-(trifluoromethyl)pyridin-2-yl)oxy)phenyl)propan-1-one (30 mg, 0.060 mmol, 78%). HRMS (ESI+) m/z: calculated for $C_{28}H_{21}F_3N_3O_3$ ([M + H]), 504.1530; found, 504.1527. ^{1}H NMR ($CDCl_3$, 400 MHz): δ 8.98 (d, *J* = 2.0 Hz, 1H), 8.46 – 8.41 (m, 1H), 8.10 (d, *J* = 2.0 Hz, 1H), 7.89 (dd, *J* = 8.7, 2.6 Hz, 1H), 7.56 – 7.51 (m, 2H), 7.35 (t, *J* = 8.5 Hz, 4H), 7.12 – 7.07 (m, 2H), 6.99 (d, *J* = 8.6 Hz, 1H), 3.67 (t, *J* = 7.5 Hz, 2H), 3.20 (t, *J* = 7.5 Hz, 2H), 2.44 (s, 3H). ^{13}C NMR ($CDCl_3$, 101 MHz): δ 189.16, 166.00, 158.59, 153.07, 151.76, 148.43, 145.63 (q, *J* = 4.3 Hz), 144.28, 139.20, 137.79, 137.40, 136,78 (q, *J* = 3.1 Hz), 134.06, 130.27(2C), 130.03(2C), 127.66(2C), 121.73(2C), 117.85, 111.41, 41.31, 29.16, 21.35. Two carbon signals (quatonary quartets of -**C**F_3 and -**C**-CF_3) not observed. Purity of >95% as determined by LC-MS.

2-Amino-5-(4-chloro-2-methoxyphenyl)pyridin-3-ol (49)

The title compound was synthesized from 3-(benzyloxy)-5-bromopyridin-2-amine (341 mg, 1.22 mmol) according to the previously reported procedure. Next the crude product (385 mg) was refluxed in HBr (0.35 mL, 48%, 2.7 eq.)/ Acetic acid (2.0 mL, 30 eq.). After complete conversion (24 h) the reaction mixture was slowly poured into excess sat. $NaHCO_3$ (aq), extracted with EtOAc, washed with brine, dried, filtered, concentrated *in*

vacuo and purified by flash chromatography to obtain 2-amino-5-(4-chloro-2-methoxyphenyl)pyridin-3-ol (128 mg, 0.51 mmol, 42%, 2 steps). ^{1}H NMR (MeOD, 400 MHz): δ 7.49 (d, *J* = 1.9 Hz, 1H), 7.21 (d, *J* = 8.1 Hz, 1H), 7.12 (d, *J* = 1.9 Hz, 1H), 7.05 (d, *J* = 2.0 Hz, 1H), 6.98 (dd, *J* = 8.1, 2.0 Hz, 1H), 3.80 (s, 3H). ^{13}C NMR (101 MHz, MeOD) δ 158.62, 150.46, 141.46, 135.51, 134.85, 131.83, 127.20, 124.82, 124.79, 121.89, 113.05, 56.37.

1-(6-(4-Chloro-2-methoxyphenyl)oxazolo[4,5-*b*]pyridin-2-yl)-4,4,4-trifluorobutan-1-ol (50)

The title compound was synthesized from 5,5,5-trifluoro-2-hydroxypentanenitrile (**31**, 92 mg, 0.60 mmol) and 2-amino-5-(4-chloro-2-methoxyphenyl)pyridin-3-ol (**49**, 80 mg, 0.32 mmol) according to procedure described for compound **20**. This yielded 1-(6-(4-chloro-2-methoxyphenyl)oxazolo[4,5-*b*]pyridin-2-yl)-4,4,4-trifluorobutan-1-ol (27 mg, 0.07 mmol, 22%). ^{1}H NMR ($CDCl_3$, 400 MHz): δ 8.60 (d, *J* = 1.9 Hz, 1H), 8.00 (d, *J* = 1.9 Hz, 1H), 7.29 – 7.22 (m, 1H), 7.07 (dd, *J* = 8.1, 1.9 Hz, 1H), 7.01 (d, *J* = 1.9 Hz, 1H), 5.18 (dd, *J* = 8.0, 4.3 Hz, 1H), 3.83 (s, 3H), 2.50 – 2.22 (m, 4H). ^{13}C BBDEC NMR ($CDCl_3$, 101 MHz): δ 157.09, 153.41, 147.48, 143.02, 135.61, 131.67, 131.16, 127.13 (q, *J* = 276.0 Hz), 124.76, 121.42, 119.93, 112.24, 55.97, 29.78 (q, *J* = 30.3 Hz), 27.79 (q, *J* = 3.03 Hz).

1-(6-(4-Chloro-2-methoxyphenyl)oxazolo[4,5-*b*]pyridin-2-yl)-4,4,4-trifluorobutan-1-one (13)

The title compound was synthesized from 1-(6-(4-chloro-2-methoxyphenyl)oxazolo[4,5-*b*]pyridin-2-yl)-4,4,4-trifluorobutan-1-ol (**50**, 27 mg, 0.07 mmol) according to procedure described for compound **2**. This yielded 1-(6-(4-chloro-2-methoxyphenyl)oxazolo[4,5-*b*]pyridin-2-yl)-4,4,4-trifluorobutan-1-one (22 mg, 0.06 mmol, 82%). LCQ (ESI+) m/z: calculated for $C_{17}H_{13}ClF_3N_2O_3$ ([M + H]), 385.06; found, 385.00. ^{1}H NMR ($CDCl_3$, 400 MHz): δ 8.86 (d, J = 1.9 Hz, 1H), 8.16 (d, *J* = 1.9 Hz, 1H), 7.32 (d, *J* = 8.1 Hz, 1H), 7.11 (dd, *J* = 8.1, 1.9 Hz, 1H), 7.04 (d, *J* = 1.9 Hz, 1H), 3.86 (s, 3H), 3.61 (t, *J* = 7.6 Hz, 2H), 2.79 – 2.59 (m, 2H). ^{13}C BBDEC NMR ($CDCl_3$, 101 MHz): δ 186.66, 158.11, 157.16, 152.63, 150.29, 143.75, 136.17, 134.18, 131.70, 126.67 (q, *J* = 276.0 Hz), 124.34, 121.56, 120.89, 112.37, 56.04, 32.75 (q, *J* = 2.7 Hz), 27.99 (q, *J* = 30.5 Hz). Purity of 95% as determined by LC-MS.

2-(6-Amino-5-hydroxypyridin-3-yl)benzonitrile (51):

The title compound was synthesized from 2-amino-5-bromopyridin-3-ol (380 mg, 1.4 mmol) and 2-cyanophenylboronic acid (300 mg, 2.0 mmol) according to the previously reported procedures.[12] This yielded 2-(6-amino-5-hydroxypyridin-3-yl)benzonitrile (90 mg, 0.42 mmol, 30%). ^{1}H NMR (400 MHz, DMSO) δ 9.90 (s, 1H), 8.02 – 7.82 (m, 1H), 7.74 (td, *J* = 7.7, 1.4 Hz, 1H), 7.66 (d, *J* = 2.1 Hz, 1H), 7.55 (d, *J* = 7.3 Hz, 1H), 7.50 (td, *J* = 7.6, 1.1 Hz, 1H), 7.09 (t, *J* = 4.6 Hz, 1H), 5.90 (s, 2H). ^{13}C NMR (101 MHz, DMSO) δ 151.38, 142.88, 139.22, 137.62, 134.38, 133.98, 129.97, 127.75, 122.78, 119.35, 118.53, 109.99.

2-(2-(4,4,4-Trifluoro-1-hydroxybutyl)oxazolo[4,5-*b*]pyridin-6-yl)benzonitrile (52)

The title compound was synthesized from 5,5,5-trifluoro-2-hydroxypentanenitrile (**31**, 83 mg, 0.54 mmol) and 2-(6-amino-5-hydroxypyridin-3-yl)benzonitrile (**51**, 127 mg, 0.60 mmol) according to procedure described for compound **19**. This yielded 2-(2-(4,4,4-trifluoro-1-hydroxybutyl)oxazolo[4,5-*b*]pyridin-6-yl)benzonitrile (48 mg, 0.138 mmol, 26%). ^{1}H NMR ($CDCl_3$, 400 MHz): δ 8.68 (d, *J* = 2.0 Hz, 1H), 8.10 (d, *J* = 2.0 Hz, 1H), 7.88 – 7.82 (m, 1H), 7.78 – 7.71 (m, 1H), 7.60 – 7.56 (m, 2H), 5.21 (dd, *J* = 8.1, 4.2 Hz, 1H), 3.56 (bs, 1H), 2.54 – 2.08 (m, 4H). ^{13}C BBDEC NMR ($CDCl_3$, 101 MHz): δ 175.24, 155.42, 146.75, 143.00, 141.38, 134.16, 133.45, 131.30, 130.60, 128.85, 127.10 (q, J = 276.7 Hz), 119.03, 118.19, 111.93, 70.22. 29.68 (q, J = 29.3 Hz). 27.78 (q, J = 3.0 Hz).

2-(2-(4,4,4-Trifluorobutanoyl)oxazolo[4,5-*b*]pyridin-6-yl)benzonitrile (14)

The title compound was synthesized from 2-(2-(4,4,4-trifluoro-1-hydroxybutyl)oxazolo[4,5-*b*]pyridin-6-yl)benzonitrile (**52**, 40 mg, 0.115 mmol) according to procedure described for compound **2** This yielded 2-(2-(4,4,4-trifluoro-1-hydroxybutyl)oxazolo[4,5-*b*]pyridin-6-yl)benzonitrile (17 mg, 0.049 mmol, 43%). HRMS (ESI+) m/z: calculated for $C_{17}H_{11}F_3N_3O_2$ ([M + H]), 346.0798; found, 346.0799. ^{1}H NMR ($CDCl_3$, 400 MHz): δ 8.92 (d, *J* =

2.1 Hz, 1H), 8.27 (d, *J* = 2.1 Hz, 1H), 7.89 (dd, *J* = 8.1, 1.4 Hz, 1H), 7.79 (td, *J* = 7.7, 1.4 Hz, 1H), 7.65 – 7.59 (m, 2H), 3.63 (t, *J* = 7.5 Hz, 2H), 2.77 – 2.62 (m, 2H). ^{13}C BBDEC NMR ($CDCl_3$, 101 MHz): δ 186.48, 158.79, 154.10, 149.37, 143.51, 140.55, 134.49, 134.28, 133.56, 130.58, 129.41, 126.63 (q, *J* = 2717.1 Hz), 120.62, 117.87, 112.09, 32.87 (q, *J* = 2.9 Hz), 27.94 (q, *J* = 30.4 Hz). Purity of 95% as determined by LC-MS.

2-(6-Amino-5-hydroxypyridin-3-yl)-5-fluorobenzonitrile (53)

The title compound was synthesized from 2-amino-5-bromopyridin-3-ol and 2-cyano-4-fluorophenylboronic acid according to the previously reported procedures.[12]

5-Fluoro-2-(2-(4,4,4-trifluoro-1-hydroxybutyl)oxazolo[4,5-b]pyridin-6-yl)benzonitrile (**54**)

The title compound was synthesized from 5,5,5-trifluoro-2-hydroxypentanenitrile (**31**, 222 mg, 1.448mmol) and 2-(6-amino-5-hydroxypyridin-3-yl)-5-fluorobenzonitrile (**53**, 83 mg, 0.362mmol) according to procedure described for compound **19**. This yielded 5-fluoro-2-(2-(4,4,4-trifluoro-1-hydroxybutyl)oxazolo[4,5-*b*]pyridin-6-yl)benzonitrile (16 mg, 0.044 mmol, 12%).^{1}H NMR (MeOD, 400 MHz) δ 8.69 (d, *J* = 1.9 Hz, 1H), 8.37 (d, *J* = 1.9 Hz, 1H), 7.75 (td, *J* = 6.8, 5.1, 2.5 Hz, 2H), 7.65 – 7.56 (m, 1H), 5.10 – 5.04 (m, 1H), 2.54 – 2.41 (m, 2H), 2.40 – 2.18 (m, 2H).^{13}C NMR (MeOD, 101 MHz) δ 173.19, 164.73 (d, *J* = 249.6 Hz), 156.31, 147.50, 144.36, 138.97 (d, *J* = 3.7 Hz), 134.26 (d, *J* = 8.6 Hz), 132.53, 130.14 (q, *J* = 275.7 Hz), 122.21 (d, *J* = 21.2 Hz), 121.74 (d, *J* = 25.9 Hz), 121.14, 118.01 (2.4 Hz), 114.67(d, *J* = 9.6Hz), 67.14, 30.60(q, *J* = 29.3 Hz), 28.55(q, *J* = 3.0 Hz)

5-Fluoro-2-(2-(4,4,4-trifluorobutanoyl)oxazolo[4,5-b]pyridin-6-yl)benzonitrile (**15**)

The title compound was synthesized from 5-fluoro-2-(2-(4,4,4-trifluoro-1-hydroxybutyl)oxazolo[4,5-*b*]pyridin-6-yl)benzonitrile (**54**, 28 mg, 0.077 mmol) according to procedure described for compound **2**. This yielded 5-fluoro-2-(2-(4,4,4-trifluorobutanoyl)oxazolo[4,5-b]pyridin-6-yl)benzonitrile (2 mg, 0.005mmol, 7%). LCQ (ESI+) m/z: calculated for $C_{16}H_{10}F_2N_2O_2$ ([M + H]), 363.27; found, 364.20. ^{1}H NMR (CDCl3, 400 MHz) δ 8.88 (d, *J* = 2.0 Hz, 1H), 8.22 (d, *J* = 2.0 Hz, 1H), 7.64 – 7.55 (m, 2H), 7.54 – 7.45 (m, 1H), 3.62 (t, *J* = 7.5 Hz, 2H), 2.70 (qt, *J* = 10.6, 7.6 Hz, 2H). ^{13}C NMR ($CDCl_3$, 151 MHz) δ 186.50, 163.13 (d, *J* = 249.53 Hz), 158.81, 154.20, 149.31, 143.43, 136.95(d, *J* = 4.08 Hz), 133.46, 132.68 (d, *J* = 8.46 Hz), 127.51 (q, *J* = 275.48 Hz), 121.47 (d, *J* = 21.47 Hz), 121.24 (d, *J* = 24.90 Hz), 120.64, 116.75 (d, *J* = 2.6 Hz), 113.60 (d, *J* = 9.34 Hz), 32.90 (q, *J* = 2.99 Hz), 27.98 (q, *J* = 30.8 Hz). Purity of 93% as determined by LC-MS. **Final compound not stable upon storage.**

2-Amino-5-(4-fluorophenyl)pyridin-3-ol (**55**)

The title compound was synthesized from 3-(benzyloxy)-5-bromopyridin-2-amine (300 mg, 1.07 mmol) according to the previously reported procedures.[12] This yielded 2-amino-5-(4-fluorophenyl)pyridin-3-ol (143 mg, 0.71 mmol, 66%, 2 steps). ^{1}H NMR (MeOD, 400 MHz) δ 7.62 (d, *J* = 2.0 Hz, 1H), 7.55 – 7.45 (m, 2H), 7.19 – 7.08 (m, 3H), 3.35 (s, 1H). ^{13}C NMR (MeOD, 101 MHz) δ 164.77(d, *J* = 246.3 Hz), 151.12, 135.99, 134.26, 128.97(2C, d, *J* = 8.0 Hz) 127.75, 118.91, 116.67(2C, d, *J* = 21.6 Hz).

4,4,4-Trifluoro-1-(6-(4-fluorophenyl)oxazolo[4,5-b]pyridin-2-yl)butan-1-ol (56)

The title compound was synthesized from 5,5,5-trifluoro-2-hydroxypentanenitrile (**31**, 270 mg, 1.76 mmol) and 2-amino-5-(4-fluorophenyl)pyridin-3-ol (**55**, 90 mg, 0.44 mmol) according to procedure described for compound **20**. This yielded 4,4,4-trifluoro-1-(6-(4-fluorophenyl)oxazolo[4,5-b]pyridin-2-yl)butan-1-ol (16 mg, 0.5 mmol, 11%). ^{1}H NMR (MeOD, 400 MHz) δ 8.75 (d, *J* = 2.0 Hz, 1H), 8.33 (d, *J* = 2.0 Hz, 1H), 7.80 – 7.70 (m, 2H), 7.31 – 7.18 (m, 2H), 5.04 (dd, *J* = 8.2, 4.8 Hz, 1H), 2.52 – 2.38 (m, 2H), 2.36 – 2.17 (m, 2H). ^{13}C NMR (MeOD, 101 MHz) δ 172.29, 165.75(d, 247.3Hz), 155.22, 146.09, 145.07, 135.54, 134.85(d, 3.4 Hz), 130.72(2C, d, 8.2 Hz), 130.15(q, 276.1 Hz), 118.93, 117.22(2C, d, 22.0 Hz), 67.11, 30.77(q, 29.3 Hz), 28.57(q, 2.8 Hz).

4,4,4-Trifluoro-1-(6-(4-fluorophenyl)oxazolo[4,5-b]pyridin-2-yl)butan-1-one (**16, LEI107**)

The title compound was synthesized from 4,4,4-trifluoro-1-(6-(4-fluorophenyl)oxazolo[4,5-*b*]pyridin-2-yl)butan-1-ol (**56**, 10 mg, 0.029 mmol) according to procedure described for compound **2**. This yielded 4,4,4-trifluoro-1-(6-(4-fluorophenyl)oxazolo[4,5-b]pyridin-2-yl)butan-1-one (3 mg, 0.01mmol, 30%). LCQ (ESI+) m/z: calculated for $C_{16}H_{11}F_2N_2O_2$ ([M + H]), 339.07; found, 339.07. ^{1}H NMR ($CDCl_3$, 400 MHz) δ 8.97 (d, *J* = 2.1 Hz, 1H), 8.10 (d, *J* = 2.1 Hz, 1H), 7.65 – 7.59 (m, 2H), 7.25 – 7.21 (m, 2H), 3.66 – 3.57 (m, 2H), 2.74 – 2.63 (m, 2H). ^{13}C NMR (101 MHz, $CDCl_3$) δ 186.46, 164.64(d, 249.53 Hz), 158.24, 153.10, 148.61, 144.26, 137.01, 133.01, 129.56(2C, d, 8.4 Hz), 127.76(q, 276.75 Hz), 118.01, 116.68(2C, d, 21.9 Hz), 32.67(q, 2.7 Hz), 28.03(q, 30.2 Hz). Purity of 95% as determined by LC-MS.

2-Amino-5-(4-chlorophenyl)pyridin-3-ol (57)

The title compound was synthesized from 3-(benzyloxy)-5-bromopyridin-2-amine (303 mg, 1.09 mmol) according to the previously reported procedures.[12] This yielded 2-amino-5-(4-chlorophenyl)pyridin-3-ol (60 mg, 0.27 mmol, 25%, 2 steps). ^{1}H NMR (MeOD, 400 MHz): δ 7.67 – 7.61 (m, 1H), 7.48 – 7.44 (m, 2H), 7.39 – 7.35 (m, 2H), 7.16 (d, *J* = 2.0 Hz, 1H). ^{13}C NMR (101 MHz, MeOD) δ 151.24, 138.10, 133.75, 133.70, 130.17, 129.96(2C), 128.50(2C), 127.14, 118.65.

1-(6-(4-Chlorophenyl)oxazolo[4,5-*b*]pyridin-2-yl)-4,4,4-trifluorobutan-1-ol (58)

The title compound was synthesized from 5,5,5-trifluoro-2-hydroxypentanenitrile (**31**, 62 mg, 0.41 mmol) and 2-amino-5-(4-chlorophenyl)pyridin-3-ol (**57**, 60 mg, 0.27 mmol) according to procedure described for compound **20**. This yielded 1-(6-(4-chlorophenyl)oxazolo[4,5-*b*]pyridin-2-yl)-4,4,4-trifluorobutan-1-ol (15 mg, 0.04 mmol, 15%). ^{1}H NMR ($CDCl_3$, 400 MHz): δ 8.73 (d, *J* = 2.0 Hz, 1H), 7.97 (d, *J* = 2.0 Hz, 1H), 7.54 – 7.46 (m, 4H), 5.17 (dd, *J* = 8.1, 4.1 Hz, 1H), 2.52 – 2.20 (m, 4H). ^{13}C BBDEC NMR ($CDCl_3$, 101 MHz): δ 170.67, 153.98, 145.78, 143.61, 135.68, 135.01, 134.04, 131.19, 129.67, 128.91, 127.08 (q, *J* = 276.7 Hz), 117.30, 66.60, 29.66 (q, *J* = 30.3 Hz), 27.77 (q, *J* = 3.0 Hz)

1-(6-(4-Chlorophenyl)oxazolo[4,5-*b*]pyridin-2-yl)-4,4,4-trifluorobutan-1-one (17)

The title compound was synthesized from 1-(6-(4-chlorophenyl)oxazolo[4,5-*b*]pyridin-2-yl)-4,4,4-trifluorobutan-1-ol (**58**, 15 mg, 0.04 mmol) according to procedure described for compound **2**. This yielded 1-(6-(4-chlorophenyl)oxazolo[4,5-*b*]pyridin-2-yl)-4,4,4-trifluorobutan-1-one (5.2 mg, 0.02 mmol, 35%). LCQ (ESI+) m/z: calculated for $C_{16}H_{11}ClF_3N_2O_2$ ([M + H]), 355.05; found, 355.07. ^{1}H NMR ($CDCl_3$, 400 MHz): δ 8.98 (bs, 1H), 8.12 (d, *J* = 1.8 Hz, 1H), 7.64 – 7.55 (m, 2H), 7.55 – 7.48 (m, 2H), 3.61 (t, *J* = 7.6 Hz, 2H), 2.78 – 2.60 (m, 2H). ^{13}C BBDEC NMR ($CDCl_3$, 101 MHz): δ 186.38, 158.28, 153.15, 148.18, 144.08, 141.44, 136.53, 135.21, 135.16, 129.58, 129.06, 126.69 (q, *J* = 276.0 Hz), 118.24, 32.55 (q, *J* = 3.0 Hz), 27.68 (q, *J* = 30.4 Hz). Purity of 95% as determined by LC-MS.

2-Amino-5-(benzo[*d*][1,3]dioxol-5-yl)pyridin-3-ol (59)

The title compound was synthesized from 3-(benzyloxy)-5-bromopyridin-2-amine (279 mg, 1.00 mmol) according to the previously reported procedures.[12] This yielded 2-amino-5-(benzo[*d*][1,3]dioxol-5-yl)pyridin-3-ol (202 mg, 0.88 mmol, 88%, 2 steps). ^{1}H NMR (MeOD, 400 MHz) δ 7.57 (d, *J* = 2.0 Hz, 1H), 7.09 (d, *J* = 1.9 Hz, 1H), 7.00 – 6.92 (m, 2H), 6.85 (d, *J* = 7.9 Hz, 1H), 5.96(s, 2H). ^{13}C NMR (MeOD , 101 MHz) δ 150.40, 149.75, 148.45, 142.73, 133.42, 131.99, 128.65, 120.70, 119.38, 109.58, 107.64, 102.54.

1-(6-(Benzo[*d*][1,3]dioxol-5-yl)oxazolo[4,5-*b*]pyridin-2-yl)-4,4,4-trifluorobutan-1-ol (60)

The title compound was synthesized from 5,5,5-trifluoro-2-hydroxypentanenitrile (**31**, 239 mg, 1.56 mmol) and 2-amino-5-(4-fluorophenyl)pyridin-3-ol (**59**, 90 mg, 0.39 mmol) according to procedure described for compound **20**. This yielded 1-(6-(benzo[*d*][1,3]dioxol-5-yl)oxazolo[4,5-*b*]pyridin-2-yl)-4,4,4-trifluorobutan-1-ol

(10 mg, 0.027 mmol, 7%). ^{1}H NMR (MeOD, 400 MHz) δ 8.70 (d, *J* = 2.0 Hz, 1H), 8.26 (d, *J* = 2.0 Hz, 1H), 7.24 – 7.16 (m, 2H), 6.98 – 6.93 (m, 1H), 6.02 (s, 2H), 5.07 – 4.96 (m, 1H), 2.48-2.27 (m, 4H).

1-(6-(Benzo[*d*][1,3]dioxol-5-yl)oxazolo[4,5-*b*]pyridin-2-yl)-4,4,4-trifluorobutan-1-one (18)

The title compound was synthesized from 1-(6-(benzo[*d*][1,3]dioxol-5-yl)oxazolo[4,5-b]pyridin-2-yl)-4,4,4-trifluorobutan-1-ol (**60**, 14 mg, 0.038 mmol) according to procedure described for compound **2**. This yielded 1-(6-(benzo[*d*][1,3]dioxol-5-yl)oxazolo[4,5-*b*]pyridin-2-yl)-4,4,4-trifluorobutan-1-one (4 mg, 0.01mmol, 29%). LCQ (ESI+) m/z: calculated for $C_{17}H_{12}F_3N_2O_4$ ([M + H]), 365.07; found, 365.13. ^{1}H NMR ($CDCl_3$, 400 MHz) δ 8.95 (d, *J* = 2.0 Hz, 1H), 8.06 (d, *J* = 2.0 Hz, 1H), 7.16 – 7.08 (m, 2H), 7.01 – 6.94 (m, 1H), 6.08 (s, 2H), 3.61 (t, *J* = 7.6 Hz, 2H), 2.69 (m, 2H). ^{13}C NMR ($CDCl_3$, 151 MHz) δ 186.60, 158.06, 152.75, 148.91, 148.71, 148.60, 144.35, 137.87, 130.90, 127.59(d, 276.1 Hz), 121.91, 117.77, 109.34, 108.04, 101.82, 32.76(q, 2.9 Hz), 28.31(q, 30.3 Hz). Purity of 95% as determined by LC-MS.

References

1. Bisogno, T. *et al.* Synthesis and pharmacological activity of a potent inhibitor of the biosynthesis of the endocannabinoid 2-arachidonoylglycerol. *ChemMedChem* **4,** 946–950 (2009).
2. Bisogno, T. *et al.* A novel fluorophosphonate inhibitor of the biosynthesis of the endocannabinoid 2-arachidonoylglycerol with potential anti-obesity effects. *Br. J. Pharmacol.* **169,** 784–793 (2013).
3. Powell, D. R. *et al.* Diacylglycerol Lipase a Knockout Mice Demonstrate Metabolic and Behavioral Phenotypes Similar to Those of Cannabinoid Receptor 1 Knockout Mice. *Front. Endocrinol.* **6,** 86 (2015).
4. Bashashati, M. *et al.* Inhibiting endocannabinoid biosynthesis: A novel approach to the treatment of constipation. *Br. J. Pharmacol.* 3099–3111 (2015). doi:10.1111/bph.13114
5. Buczynski, M. W. *et al.* Diacylglycerol lipase disinhibits VTA dopamine neurons during chronic nicotine exposure. *Proc. Natl. Acad. Sci. U.S.A.* **113,** 1086–1091 (2016).
6. Wilkerson, J. L. *et al.* Diacylglycerol lipase beta inhibition reverses nociceptive behavior in mouse models of inflammatory and neuropathic pain. *Br. J. Pharmacol.* **173,** 1678–1692 (2016).
7. Hsu, K. L. *et al.* DAGLβ inhibition perturbs a lipid network involved in macrophage inflammatory responses. *Nat. Chem. Biol.* **8,** 999–1007 (2012).
8. Ogasawara, D. *et al.* Rapid and profound rewiring of brain lipid signaling networks by acute diacylglycerol lipase inhibition. *Proc. Natl. Acad. Sci. U.S.A.* **113,** (2015).
9. Valdeolivas, S. *et al.* The inhibition of 2-arachidonoyl-glycerol (2-AG) biosynthesis, rather than enhancing striatal damage, protects striatal neurons from malonate-induced death: a potential role of cyclooxygenase-2-dependent metabolism of 2-AG. *Cell Death Dis.* **4,** e862 (2013).
10. Baggelaar, M. P. *et al.* Development of an activity-based probe and in silico design reveal highly selective inhibitors for diacylglycerol lipase-a in brain. *Angew. Chem. Int. Ed.* **52,** 12081–12085 (2013).
11. Janssen, F. J. *et al.* Comprehensive Analysis of Structure-Activity Relationships of α-Ketoheterocycles as sn-1-Diacylglycerol Lipase α Inhibitors. *J. Med. Chem.* **58,** 9742–9753 (2015).
12. Baggelaar, M. P. *et al.* Highly Selective, Reversible Inhibitor Identified by Comparative Chemoproteomics Modulates Diacylglycerol Lipase Activity in Neurons. *J. Am. Chem. Soc.* **137,** 8851–8857 (2015).
13. Leeson, P. D. & Springthorpe, B. The influence of drug-like concepts on decision-making in medicinal chemistry. *Nat. Rev. Drug Discov.* **6,** 881–90 (2007).
14. Shamovsky, I. *et al.* Overcoming undesirable hERG potency of chemokine receptor antagonists using baseline lipophilicity relationships. *J. Med. Chem.* **51,** 1162–1178 (2008).
15. Waring, M. J. & Johnstone, C. A quantitative assessment of hERG liability as a function of lipophilicity. *Bioorganic Med. Chem. Lett.* **17,** 1759–1764 (2007).
16. Hanumegowda, U. M. *et al.* Phospholipidosis as a function of basicity, lipophilicity, and volume of distribution of compounds. *Chem. Res. Toxicol.* **23,** 749–755 (2010).
17. Lewis, D. F. V, Jacobs, M. N. & Dickins, M. Compound lipophilicity for substrate binding to human P450s in drug metabolism. *Drug Discov. Today* **9,** 530–537 (2004).
18. Van Der Wel, T. *et al.* A natural substrate-based fluorescence assay for inhibitor screening on diacylglycerol lipase α. *J. Lipid Res.* **56,** 927–935 (2015).
19. Janssen, F. J. *et al.* Discovery of glycine sulfonamides as dual inhibitors of sn-1-diacylglycerol lipase α and α/β hydrolase domain 6. *J. Med. Chem.* **57,** 6610–6622 (2014).
20. Janssen, F. J. & van der Stelt, M. Inhibitors of diacylglycerol lipases in neurodegenerative and metabolic disorders. *Bioorg. Med. Chem. Lett.* **26,** 3831–3837 (2016).

CHAPTER 5

Discovery of glycine sulfonamides as dual inhibitors of *sn*-1 diacylglycerol lipase α and α/β hydrolase domain 6*

Introduction

Diacylglycerol lipases (DAGL) are responsible for the synthesis of the endogenous signaling lipid 2-arachidonoylglycerol (2-AG) in the brain and immune system.[1] 2-AG activates the cannabinoid type 1 receptor (CB1R), which is also the target of Δ^9-tetrahydrocannabinol, the main psychoactive compound in marijuana. 2-AG functions as a retrograde messenger and modulates synaptic plasticity at both GABAergic and glutamatergic synapses by inhibiting neurotransmitter release in various regions of the central nervous system. It is involved in a broad array of neurophysiological functions, such as adult neurogenesis, modulation of reward-related behavior, memory formation, pain sensation and appetite.[2,3] Activation of CB1R via 2-AG has been implicated in various disorders, including obesity and nicotine addiction.[4] In addition, 2-AG is a precursor for pro-inflammatory prostaglandins in animal models of neuroinflammation.[4-7] As a consequence, inhibitors of 2-AG biosynthesis may become useful for therapeutic intervention in various human diseases.[8,9] DAGLs are intracellular, multi-domain integral membrane proteins that produce 2-AG. Two homologous isoforms are known: *sn*-1 diacylglycerol lipase-α (DAGLα) and *sn*-1 diacylglycerol lipase-β (DAGLβ). The DAG lipases share extensive homology, but differ in size: ~120 and ~70 kD for DAGLα and DAGLβ respectively. DAG lipases employ the typical Ser-His-Asp catalytic triad to specifically hydrolyze the ester bond of *sn*-1 acyl chains from arachidonate-containing diacylglycerols. Studies with DAGL-KO mice have shown that DAGLα controls to a large extent the formation of 2-AG in the central nervous system whereas DAGLβ partakes in 2-AG production in the periphery during inflammation.[10]

* Janssen, F.J., Deng, H., Baggelaar, M.P., Allarà, M., van der Wel, T., den Dulk, H., Ligresti, A., van Esbroeck, A.C.M., McGuire, R., Di Marzo, V., Overkleeft, H.S., van der Stelt, M. Discovery of glycine sulfonamides as dual inhibitors of *sn*-1-diacylglycerol lipase α and α/β hydrolase domain 6. *J. Med. Chem.* **57**, 6610-6622 (**2014**).

Selective chemical tools (*i.e.* inhibitors and activity-based probes) for DAGLα and DAGLβ can be used to obtain a better understanding of the physiological role of 2-AG. Such chemical tools provide a critical counterpart of the DAGL-KO mice and allow the examination of acute versus congenital inhibition. Currently, several different classes of DAGL-inhibitors have been reported. These are a) α-ketoheterocycles,[11] *b*) fluorophosphonates,[12-14] *c*) beta-lactones,[10,15] *d*) bis-oximino-carbamates,[10] and *e*) 1,2,3-triazole ureas. The latter have recently been described as non-brain-penetrable subtype selective DAGLβ inhibitors, which cross-react with α/β hydrolase domain 6 (ABHD6).[16] This is an enzyme responsible for 2-AG hydrolysis and is involved in obesity-related metabolic disorders.[17] Most of the reported inhibitors are lipid-based molecules with chemically reactive warheads that appear not to be sufficiently efficacious and selective over other lipases and/or lack *in vivo* activity on DAGL. Thus, there is a need for new, subtype selective DAGL-inhibitors, which can be used to study the function of DAGLα and DAGLβ in animal models of disease.

DAGLs belong to the class of serine hydrolases, which contains more than 200 members with various physiological functions.[18] In order to gain insight in the biological role of a specific serine hydrolase, it is important to know the selectivity of the chemical tool that is used to study the role of a particular enzyme. Activity-based protein profiling (ABPP) is often used to characterize the selectivity and activity of serine hydrolase inhibitors in proteome wide screens using tagged fluorophosphonates (FP) as broad-spectrum activity-based probes.[19] However, DAGLα does not react with such FP-probes. To overcome this shortcoming, a bodipy tagged tetrahydrolipstatin based β-lactone probe MB064 was recently developed,[11] which is able to detect endogenous DAGLα expressed in brain. Probe MB064 was used in conjunction with a commercially available fluorophosphonate TAMRA-FP, to assess the activity and selectivity of novel DAGLα inhibitors. For example, α-ketoheterocycles were identified as a potent class of DAGLα inhibitors with fatty acid amide hydrolase (FAAH) as the only off-target of LEI104 in mouse brain, as assessed by competitive ABPP. This demonstrated the power of comparative ABPP to rapidly identify and characterize novel hits.[11]

Recently, researchers from Bristol-Myers Squibb disclosed a new reversible class of DAGLα inhibitors.[20,21] They performed a high throughput screening campaign and prioritized the glycine sulfonamide series as an initial lead for chemical optimization (see also Chapter 6). Compounds **2a-c** (Figure 1) were shown to be active on recombinant human DAGL and were selective over pancreatic lipase and monoacylglycerol (MAG) lipase, the main enzyme in the central nervous system that hydrolyzes 2-AG. Due to the lack of an obvious serine hydrolase warhead, the structure-activity relationships of this novel chemotype were investigated, using **2c** as a starting point. In addition, a broader selectivity profile over the serine hydrolase family in native brain proteome was not available.

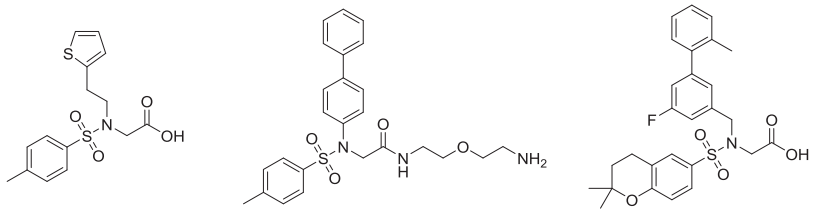

Figure 1. Glycine sulfonamides as reversible class of DAGLα inhibitors.[20, 21] Compounds **2a** (IC_{50} = 0.5 μM), **2b** (IC_{50} = 0.05 μM) and **2c** (IC_{50} = 0.02 μM) were initial leads for chemical optimization.[20, 21]

Here, the first study of structure-activity relationships of glycine sulfonamide DAGLα inhibitors is reported, together with the assessment of the selectivity profile over brain membrane proteome using comparative ABPP with MB064 (**1**) and TAMRA-FP. Chemical optimization of the sulfonamide series led to the discovery of **15**, which is a potent DAGLα inhibitor. This study confirmed that glycine sulfonamides are selective over MAGL, but ABPP assays revealed that **15** is also a potent ABHD6 inhibitor. Since ABHD6, a general lysophospholipid hydrolase, is strongly linked to high-fat-diet induced obesity, hepatic steatosis and insulin resistance,[17] this dual inhibition profile may be beneficial for the treatment of obesity-related disorders.

Results

To systematically investigate the structure-activity relationships of glycine sulfonamide series, a general synthetic scheme was developed that allowed for rapid variation of different parts of the molecule. Compound **2c,** with a 2,2-dimethylchroman substituent was used as a starting point, because this was one of the most potent inhibitors reported by BMS.[21] First, the biphenyl substituent was replaced by biarylethers (**13**-**17**), which are other well-known fatty acid tail bio-isosters used in clinical candidates (e.g. PF-04457845).[22] To probe the size of the binding site, analogs were synthesized with the ether substituent at *ortho* (**13**), *meta* (**14**, **16**) and *para* (**15**, **17**) position of the first phenyl ring. Second, to reduce the polar surface area of the molecules, the sulfonamide was replaced by an amide (**19** vs **23**; **20** vs **22** and **24** vs **25**). Of note, chlorophenyl substituents at R^B were used, because they are metabolically stable analogs of the tolyl substituent in compound **2b** and are commercially available as both a sulfonoyl chlorides and acyl chlorides. Finally, since there is no obvious serine hydrolase warhead present in the starting molecule **2c**, the contribution of the carboxylic acid to its activity was investigated by replacing it by ester (**26**), alcohol (**27**), carbamate (**28**) amide (**29, 30**), nitrile (**32**), amine (**33**) and tetrazole (**34**) functionalities. To this end, reductive amination of glycine methyl ester with benzaldehydes **3-7** was performed, followed by a (sulfon)amide coupling using different acyl chlorides (4-chlorobenzoyl- and 2,6-dichlorobenzoyl chloride) and sulfonyl chlorides (4-chlorophenyl-, 2,6-dichlorophenyl- or 2,2-dimethylchroman-6-sulfonyl chloride). Hydrolysis of the glycine ester yielded final compounds **13-25**.

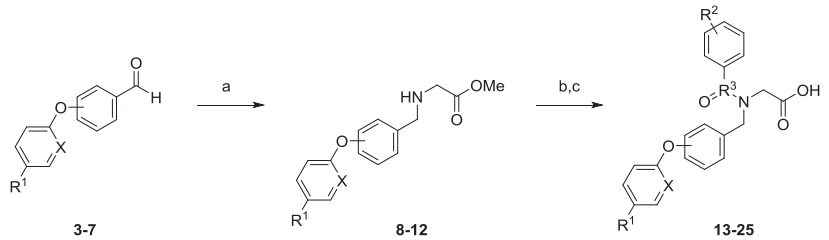

Scheme 1. Synthesis of glycine sulfonamide derivatives **13-25.** a) Methyl glycinate, AcOH, $NaCNBH_3$, MeOH, 3Å molecular sieves. rt, 27-80%, **8**: *ortho*, X = CH, R_1 = H, **9**: *meta* X = CH, R_1 = H, **10**: *para*, X = CH, R_1 = H, **11**: *meta* X = N, R_1 = CF_3, **12**: *para* X = N, R_1 = CF_3; b) acylchloride or sulfonylchloride, Et_3N, DMAP or pyridine (cat.), CH_2Cl_2, 0°C to rt. 25-94%; c) NaOH, THF, H_2O, rt, 33-92%, for the structures of final compounds **13**-**25** see Table 1.

To derivatize the carboxylic acid moiety, methyl esters **14a** and **26** were reduced and subsequent CDI coupling was performed to yield carbamate **28** (see Scheme 2A). Hydrolysis of methyl ester **20** followed by EDC coupling and deprotection provided amide **29**. In addition, reductive aminations using 2-aminoacetamide and aldehydes **4-5** were performed, followed by sulfonylchloride coupling to **30** and **31** (see Scheme 2B). Dehydration to nitriles **32** and **33a** followed by reduction or cyclization yielded amine **33** and tetrazole **34** respectively. All compounds were tested in a colorimetric, biochemical assay using *para*-nitrophenylbutyrate as substrate and HEK293T cell membranes overexpressing human DAGLα, as previously described.[11, 23]

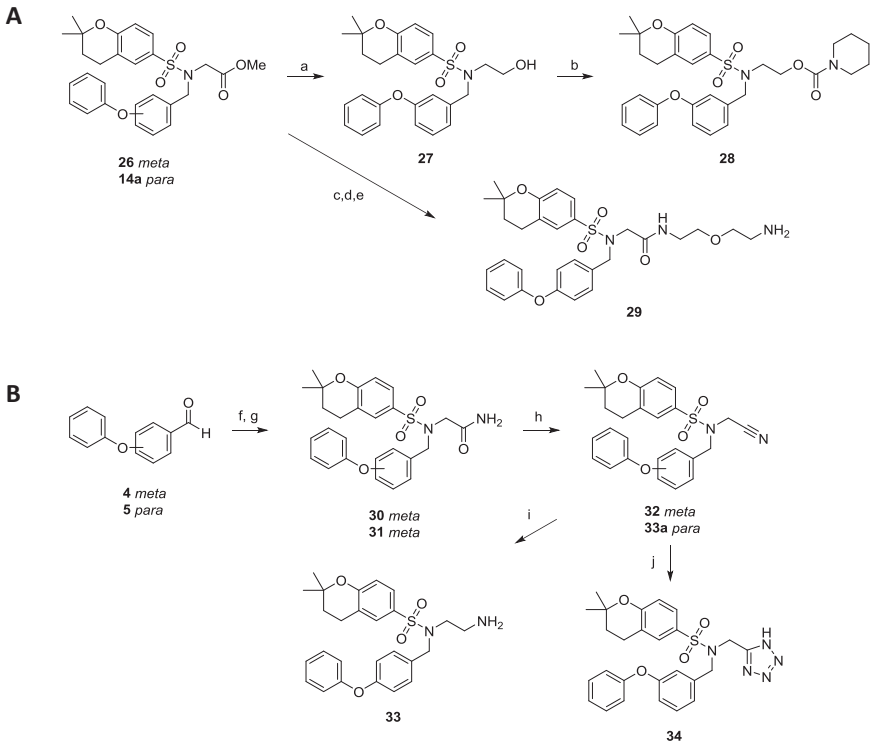

Scheme 2. Synthetic approach towards glycine sulfonamide derivatives **26**-**34. A** a) $LiBH_4$, THF, -5°C, 65%; b) CDI, DIPEA, then piperidine, CH_2Cl_2, 0°C to rt, quant; c) NaOH, THF, H_2O, rt, 90%; d) EDC, DIPEA, MeCN, then tert-butyl (2-(2-aminoethoxy)ethyl)carbamate, rt, 21%; e) TFA, CH_2Cl_2, rt, 96%. **B** f) 2-aminoacetamide, AcOH, $NaCNBH_3$, MeOH, 3Å molecular sieves. rt, 50% (*meta*, **30a**), 68% (*para*, **31a**); g) 2,2-dimethylchroman-6-sulfonyl chloride, Et_3N, pyridine (cat.), CH_2Cl_2, 0°C to rt, 42% (*meta*, **30**), 63% (*para*, **31**); h) Pyridine, TFAA, THF, 0°C to rt, 69% (*meta*, **32**), 62% (*para*, **33a**); i) borane THF complex, THF, 0°C, 54%; j) Et_3N.HCl, NaN_3, toluene, reflux, 16%;

DAGLα seems to have a large binding cavity, because *ortho* (**13**), *meta* (**14**, **16**) and *para* (**15**, **17**) substitution of the benzylamine moiety with arylethers was allowed at R^A (see Table 1). *Para* substitution was, however, preferred over *ortho* and *meta* substitution. The sulfonamides **13**-**21** and **24** were well tolerated, whereas amide derivatives **22**, **23** and **25** proved inactive. Thus, a specific orientation of the R^B substituent induced by the sulfonamide is required. The weak activity of compound **19** indicated that the steric tolerance around the sulfonamide functionality is limited, whereas a *para*-chlorophenyl group is allowed (compounds **18** and **22**). This indicated that both electron withdrawing and donating substituents (**2b**) are tolerated at R^B. Thus, the activity in this subpocket seems to be more governed by lipophilic and steric interactions than electronic interactions. In contrast, from the activity of compounds **26**-**34** it was clear that the carboxylic acid is a crucial pharmacophoric feature, because methylester **26**, alcohol **27**, primary amide **33** and tetrazole **34,** a carboxylic acid bioisoster, were all inactive. Replacement of the acid

functionality by carbamate **28**, which is a well-known warhead for serine hydrolases,[24] resulted in loss of activity. It could be that the steric hinder posed by the piperidine moiety caused the drop in activity, however, the primary amide (**30**) was also inactive. Moreover, conversion of the acid moiety into substituted amide **29**, as observed in the original hit **2b**, was detrimental for activity on DAGLα (IC_{50} > 10 μM). Alltogether, this suggests that the carboxylate of the glycine forms an important ionic interaction with a basic amino acid in the enzyme. Surprisingly, replacement of the carboxylic acid with a primary amine yielded compound **33** with an IC_{50} of 512 ± 147 nM. Compound **15** proved the most potent glycine sulfonamide derivative in the biochemical assay with an IC_{50} of 18 ± 6 nM and inhibited the hydrolysis of [^{14}C]-*sn*-1-oleoyl-2-arachidonoyl-glycerol, the natural substrate of DAGLα, with a K_i of 0.7 ± 0.08 μM.[10]

To explain the observed structure-activity-relationships, **15** was docked in a previously reported homology model of DAGLα (built from the crystal structure of the S146A mutant of *Thermomyces (Humicola) lanuginosa* lipase in complex with oleic acid, PDB code 1GT6).[11] Docking was performed using the Yasara[25] implementation of AutodockVina,[26] generating 25 high scoring poses within 1.3 kcal.mol^{-1} of the calculated binding energy minimum. Two high ranking binding poses (Figure 2) have been observed that place the carboxylic acid in very close proximity to the catalytic serine (Ser472) or histidine (His650) residues. While in both poses pi-cation interactions with the benzylphenoxy pharmacophore are observed, the interactions of the key carboxylic acid moiety differ (Figure 2A,B). In pose 1 a hydrogen bond between the carboxylic acid with the catalytic serine (Ser472) is found, while in pose 2 the carboxylic acid is in close proximity of the catalytic histidine (His650) and a neighboring His471. This may also explain the weak activity of the amine (compound **33**), because a histidine has both an acid and base functionality. The orientations of the two hydrophobic substituents differ as well in the different binding poses. In pose 1 the 2,2-dimethylchroman substituent is in a hydrophobic pocket lined by residues Leu410, Val526, Ile529 and Leu531 and the phenoxybenzyl group is directed outside of the catalytic site into a broader cavity (Figure 2C). In pose 2 the 2,2-dimethylchroman substituent is in another hydrophobic pocket that is only accessible through its perpendicular angle induced by the sulfonamide (Figure 2D). In this pose the phenoxybenzyl group is positioned in the pocket aligned by Leu410, Val526, Ile529 and Leu531. While these binding modes were among the highest ranking docking poses and are in agreement with the observed structure-activity relationships, a co-crystal structure of the glycine sulfonamide inhibitors with DAGLα is required to prove the proposed binding modes.

Table 1. Structure-activity relationship overview.

Entry	R^A	R^B	R^C	DAGLα IC_{50} ± SEM (nM)
13				185 ± 74
14	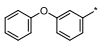			56 ± 11
15 (LEI106)	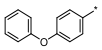			18 ± 6
16	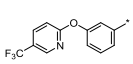			143 ± 60
17	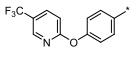			65 ± 21
18	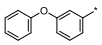			91 ± 20
19	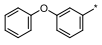			1600 ± 500
20	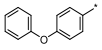			66 ± 27
21	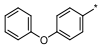			695 ± 335
22	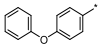			> 10^4
23	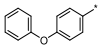			> 10^4
24	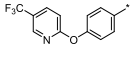			302 ± 135
25	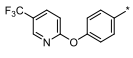			> 10^4
26				> 10^4
27				> 10^4
28				> 10^4
29				> 10^4
30				> 10^4

Entry	R^A	R^B	R^C	DAGLα IC_{50} ± SEM (nM)
32	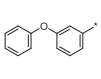			> 10^4
33	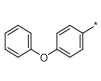			512 ± 147
34	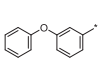			> 10^4

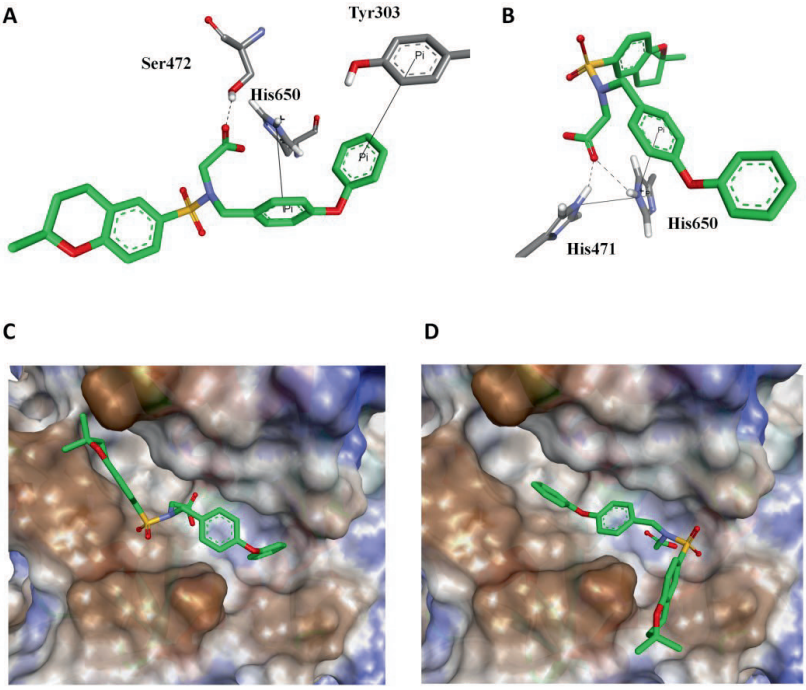

Figure 2. Two highly ranked binding poses of compound **15** in the DAGLα homology model. **A)** Binding mode 1 displaying key interactions with catalytic serine (Ser472) and histidine (His650) and a neighboring Tyr303. **B)** Binding mode 2 displaying key interactions with the catalytic histidine (His650) and a neighboring His471 **C)** Binding mode 1 in the catalytic binding site cavity. **D)** Binding mode 2 in the catalytic binding site cavity.

To determine the activity and selectivity of the glycine sulfonamide series on endogenously expressed DAGLα and other serine hydrolases in brain membrane proteome, the three most potent inhibitors **14**, **15** and **17** were incubated for 20 min with mouse brain membrane homogenates, followed by labeling of the serine hydrolases by MB064 (**1**) or FP-probe (Figure 3C,D). The non-selective lipase inhibitor, tetrahydrolipstatin (THL) was used as a positive control. All compounds were able to block the labeling of DAGLα in the mouse brain proteome in a concentration dependent manner. Complete blockade was observed at 20 μM of inhibitors **14**, **15** and **17** (Figure 3D). The order of potency was similar to that found in

the biochemical assay. Compound **15** inhibited DAGLα labeling with an IC_{50} of 124 ± 13 nM (N = 3), which is ~2.5 times more potent than compound **14** and ~6 times more potent than compound **17** (Figure 3A,B). No reduction of MAGL (protein bands 11 and 12, Figure 3C) labeling at 20 μM was observed for any of the three compounds, which is in line with the reported lack of activity of this chemical series in a biochemical assay. However, compounds **14** and **15** partially prevented labeling of an unknown off-target protein by TAMRA-FP (protein 4 in Figure 3C) and all three compounds reduced labeling of two other proteins (labeled 8 and 9 in Figure 3D) by MB064 (**1**). Protein 9 was identified as ABHD6. Hence, three off-targets for **14** and **15** and two off-targets for **17** were identified in the current setting.

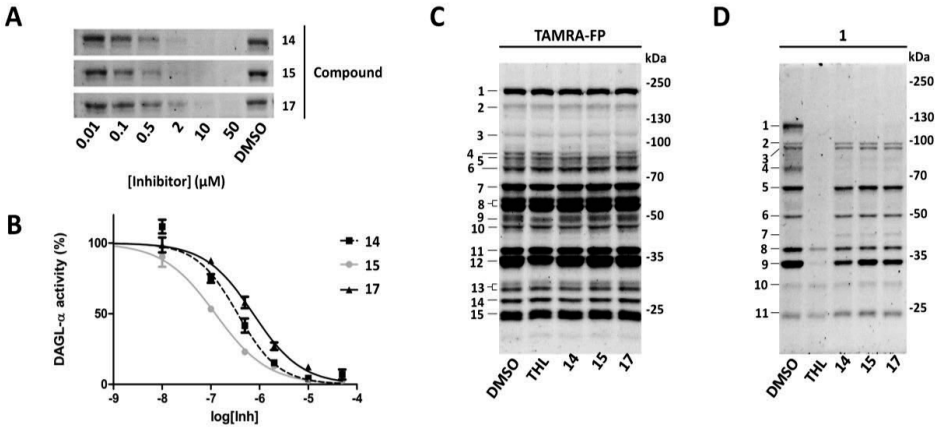

Figure 3: Activity-based protein profiling assay with TAMRA-FP and MB064 (**1**)**. A)** Concentration dependent inhibition of DAGLα in the mouse brain membrane proteome by **14**, **15** and **17**. **B)** Dose–response curves of DAGLα inhibition by **14** (black, ---■---, IC_{50} = 355 ± 54 nM), **15** (grey —●—, IC_{50} = 124 ± 13 nM) and **17** (black, —▲—, IC_{50} = 743 ± 72 nM) as measured by competitive ABPP with MB064 (**1**, SEM, N = 3). **C)** and **D)** Competitive ABPP with the DAGLα inhibitors **14**, **15** and **17** (20 μM) using ABPs carboxytetramethylrhodamine fluorophosphonate (TAMRA-FP) and MB064 (**1**) in mouse brain membrane proteome. The quantified data of the selectivity screening can be found in the supplementary information.

Since ABHD6 is a hydrolase that is capable of metabolizing 2-AG, the natural product of DAGLα, a natural substrate-based assay for ABHD6 was set up.[27] This assay employs ABHD6 to convert 2-AG into glycerol, which is coupled to the oxidation of commercially available fluorogenic Amplifu™Red via a multi-enzyme cascade (Figure 4A). It was found that membrane preparations of HEK293T cells overexpressing human ABHD6 are able to hydrolyze 2-AG with an apparent K_m of 25.4 ± 3.3 μM and a V_{max} of 5.94 ± 0.28 nmol/min/mg protein. Pre-incubation of the three inhibitors dose-dependently inhibited ABHD6 with a K_i of 0.8, 2.7 and 18.3 μM for compound **15**, **17** and **14**, respectively (Figure 4C). This indicates that the glycine sulfonamides are a class of dual inhibitors for DAGLα and ABHD6.

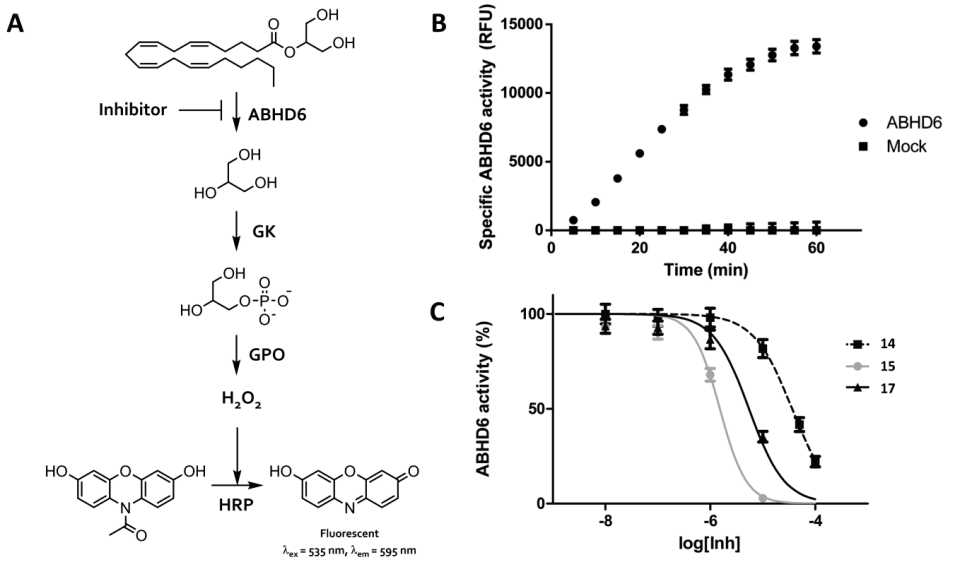

Figure 4. Biochemical hABHD6 activity assay and dose response analysis. **A)** Enzymatic activity of hABHD6 was measured in a natural substrate based activity assay as previously described.[27] **B)** Normalized and corrected (for control) fluorescence measurements over time. **C)** Concentration response analysis for ABHD6 inhibition by **14** (black, ---■---, K_i = 18.3 ± 1.8 µM), **15** (grey —●—, K_i = 0.8 ± 0.1 µM) and **17** (black, —▲—, K_i = 2.7 ± 0.4 µM) as measured by resorufin fluorescence (SEM, N = 2, n = 2).

Discussion & Conclusion

This study reports on the first structure-activity-relationship study of non-covalent small molecule inhibitors of DAGLα based on the glycine sulfonamide scaffold. It was found that *i*) the enzyme tolerates a variety of biaryl substituents, *ii*) the sulfonamide is required for inducing a specific orientation of a 2,2-dimethylchroman substituent and *iii*) a carboxylic acid is essential for its activity. Analysis of potential binding modes of the most potent inhibitor **15** in a homology model of DAGLα indicated that the carboxylic acid may interact with the catalytic Ser472 or His650 and that the two hydrophobic substituents may address different hydrophobic binding pockets.

In contrast to a previous report, which claimed that glycine sulfonamide were selective inhibitors for DAGLα, proteome-wide ABPP assay indicated that the glycine sulfonamides do interact with other proteins. Compound **15** prevented labeling of at least three other unknown proteins targeted by MB064 and TAMRA-FP. One off-target was identified as ABHD6. Using a recently developed activity assay for ABHD6 that employs 2-AG as natural substrate, it was discovered that **15** prevented the hydrolysis of 2-AG with a K_i of 0.8 ± 0.1 μM, which is very similar as for DAGLα (K_i = 0.7 ± 0.08 μM) . Thus, compound **15** is a dual inhibitor of DAGLα and ABHD6. Of note, it seems that ABHD6 is a common off-target for DAGLα inhibitors in general, because also the triazole ureas,[16] fluorophosphonates[12-14] and beta-lactones[10,15] cross-react with this enzyme. To investigate DAGL biology it is necessary to identify compounds that do not cross-react with ABHD6 and the two other unknown off-targets.

Recently it has been reported that ABHD6 is linked to metabolic disorders and is a regulator of *de novo* lipogenesis in the liver by acting as a general lysophospholipid hydrolase using *lyso*-phosphatidylglycerol, *lyso*-phosphatidylethanolamine, *lyso*-phosphatic acid and *lyso*-phosphatidyl serine as substrates. Peripheral knock-down of ABHD6 protected mice from high-fat-diet induced obesity, hepatic steatosis and insulin resistance. *In vivo* inhibition of ABHD6 with a small molecule resulted in reduced glucose intolerance and induced weight loss, thereby providing rationale for the development of small molecule inhibitors of ABHD6 for the treatment of obesity-induced metabolic disorders.[17] Since inhibition of DAGLα is also strongly linked with reduced body weight and resistance against high-fat diet induced obesity,[14] via reduced cannabinoid CB1R activation,[4,28,29] it can be envisioned that dual inhibition of both ABHD6 and DAGLα may provide additional therapeutical benefits. Since both DAGLα and ABHD6 are highly expressed in the brain, it would be of interest to develop compounds with restricted access to the central nervous system to prevent adverse neuropsychiatric side effects as previously observed with the cannabinoid CB1R antagonist Rimonabant. The glycine sulfonamide series, as exemplified by **15**, may be an interesting lead series to provide such tool compounds, because their polar surface area is quite large (> 70 $Å^2$).

In summary, this study provides the first structure-activity relationship of the glycine sulfonamide series of DAGLα inhibitors and discovered that this class of compounds is not selective over ABHD6. This provided important insights in the direction for optimization of **15**, LEI106, as a selective DAGLα tool compound. In addition, this dual DAGLα/ ABHD6 inhibition profile might provide a new lead for the treatment of diet-induced obesity and metabolic syndrome.

Experimental

Experimental procedures computational chemistry

Docking in DAGLα homology model. Docking was performed as previously reported (Chapter 2).[11]

Experimental procedures biochemistry

Cloning procedures. Full length human hDAGLα and hABHD6 cDNA was purchased from Biosource and cloned into mammalian expression vector pcDNA3.1, containing genes for ampicillin and neomycin resistance. The empty vector was used as a negative control (mock). All plasmids were grown in XL-10 Z-competent cells and prepped (Maxi Prep, Qiagen). The sequences were confirmed by sequence analysis at the Leiden Genome Technology Centre.

Cell culture and membrane preparation. HEK293T cells were grown in DMEM with stable glutamine and phenolred (PAA or Sigma) with 10% New Born Calf serum, penicillin and streptomycin. Cells were passaged every 2-3 days by resuspension in medium and seeding to the appropriate confluence. Membranes were prepared from transiently transfected HEK293T cells. One day prior to transfection 10^7 cells were seeded in a 15 cm petri dish. Cells were transfected by the addition of a 3:1 mixture of polyethyleneimine (60μg) and plasmid DNA (20μg) in 2 mL serum free medium. The medium was refreshed after 24 hours, and after 72 h the cells were harvested by suspending them in 20 mL medium. The suspension was centrifuged for 10 min at 1000 rpm, and the supernatant was removed. The cell pellet was stored at -80 ^{o}C until use.

Cell pellets were thawed on ice and suspended in lysis buffer A (20 mM HEPES, pH 7.2, 2 mM DTT, 0.25 M sucrose, 1 mM $MgCl_2$, 1x protease inhibitor cocktail (Roche cOmplete EDTA free), 25U/mL Benzonase). For hABHD6 membrane preparations, the protease inhibitor cocktail was not added. The suspension was homogenized by polytrone (3 × 7 sec) and incubated for 30 min on ice. The suspension was subjected to ultracentrifugation (93.000 × g, 30 min, 4 ^{o}C, Beckman Coulter, Type Ti70 rotor) to yield the cytosolic fraction in the supernatant and the membrane fraction as a pellet. The pellet was resuspended in lysis buffer B (20 mM HEPES, pH 7.2, 2 mM DTT, 1x protease inhibitor cocktail). The protein concentration was determined with Quick Start Bradford assay (Biorad). The protein fractions were diluted to a total protein concentration of 1 mg/mL and stored in small aliquots at -80 ^{o}C until use.

Biochemical DAGLα activity assay. The biochemical hDAGLα activity assay was performed as previously reported.[11]

Biochemical ABHD6 activity assay. The biochemical hABHD6 activity assay is based on the production of glycerol by 2-arachidonoyl glycerol (2-AG) hydrolysis by membrane preparations from HEK293T cells transiently transfected with hABHD6, as previously reported.[27] The produced glycerol is coupled to the oxidation of commercially available Amplifu™Red via a multi-enzyme cascade, resulting in a fluorescent signal from the dye resorufin. Assay reagents and enzymes (glycerol kinase from *Cellulomonas sp.*, glycerol-1-phosphate oxidase from *Streptococcus thermophilus*, horse radish peroxidase from *Horseradish*) were purchased from Sigma Aldrich.

The assay was performed in HEMNB buffer (50 mM HEPES pH 7.4, 1 mM EDTA, 5 mM $MgCl_2$, 100 mM NaCl, 0.5% (w/v) BSA) in black, flat bottom Greiner 96-wells plates. Final protein concentration of membrane preparations of HEK293T cells overexpressing hABHD6 was 0.04 μg/μL. Inhibitors were added from 40x concentrated DMSO stocks. After 30 min. incubation, assay mix containing glycerol kinase (GK), glycerol-1-phosphate oxidase (GPO), horse radish peroxidase (HRP), adenosine triphosphate (ATP), Amplifu™Red and 2-

arachidonoyl glycerol (2-AG) was added and fluorescence was measured in 5 min. intervals for 75 min. (λ_{ex} = 535 nm, λ_{em} = 595 nm) at 21°C on a plate reader (TECAN GENios microplate reader). Final assay concentrations: 0.2 U/mL GK, GPO and HRP, 0.125 mM ATP, 10 µM Amplifu™Red, 25 µM 2-AG, 5% DMSO, 1% ACN in a final volume of 200 µL. Slopes were determined in the linear interval of t = 10 to t = 35 min. All experiments were performed at N = 2, n = 2 for experimental measurements and N = 2, n = 4 for controls.

The Z'-factor for each measurement was calculated as previously reported,[11] but with ABHD6 and DMSO as a positive control and with slope values determined in the interval of t = 10 to t = 35 min. Plates with Z'≥ 0.6 were accepted for further analysis. Fluorescence values were corrected for the average fluorescence of the negative control. The average, standard deviation (SD) and standard error of mean (SEM) were calculated and normalized to the corrected positive control. Data was exported to Graphpad Prism 5.0 for the calculation of the IC_{50} using a non-linear dose-response analysis.

For K_M and V_{max} determination, the concentration of 2-AG was varied and slopes of corrected fluorescence in time were exported to GraphPad Prism 5.0 (Michaelis-Menten analysis). The calculated V_{max} value in RFU/min was then converted to a value in nmol converted glycerol/min/mg protein according to a standard curve with the rate of increase in fluorescence as a function of converted glycerol.

Preparation of mouse brain membrane proteome. Mouse brains were isolated according to guidelines approved by the ethical committee of Leiden University (DEC#13191). Mouse brains were thawed on ice and homogenized by polytrone (3 × 7 sec.) in pH 7.2 lysis buffer A (20 mM HEPES, 2 mM DTT, 1 mM $MgCl_2$, 25 U/mL Benzonase) and incubated for 15 minutes on ice, followed by low speed spin (2500 × g, 3 min. at 4 ^{o}C) to remove debris. The supernatant was subjected to ultracentrifugation (100.000 × g, 45 min. 4 ^{o}C, Beckman Coulter, Type Ti70 rotor) to yield the cytosolic fraction in the supernatant and the membrane fraction as a pellet. The pellet was resuspended in lysis buffer B (20 mM HEPES, 2 mM DTT). The total protein concentration was determined with Quick Start Bradford assay (Biorad). Membranes were stored in small aliquots at -80 ^{o}C until use.

Activity-based protein profiling activity assay. The IC_{50} of inhibitors was determined against endogenously expressed DAGLα in the mouse brain membrane proteome. Inhibitors were incubated at the indicated concentrations (total volume 20 µL) for 30 min at rt, prior to incubation with MB064 for 10 min at rt. The reaction was quenched with 10 µL standard 3 × SDS page sample buffer, and resolved on 10 % SDS-page. The gels were scanned with a ChemiDoc™ MP sytem (Cy3 settings; 605/50 filter). The percentage activity remaining was determined by measuring the integrated optical intensity of the bands using Image Lab 4.1. software. IC_{50} values were determined from a dose-response curve generated using Prism software (GraphPad).

Activity-based protein profiling selectivity assay. For gel based ABPP experiments mouse brain proteome (2.0 mg/mL, 20 µL) was preincubated for 30 min with vehicle (0.5 µL DMSO) or inhibitor in 0.5 µL DMSO at rt and subsequently treated with 250 nM (final concentration) ABP **1** or 500 nM (final concentration) TAMRA-FP (from Thermo Fischer Scientific) for 15 minutes at rt. The reactions were quenched with 10 µL standard 3 × SDS page sample buffer. The samples were directly loaded and resolved on SDS page gel (10 % acrylamide). The gels were scanned with a ChemiDoc™ MP sytem (Cy 3 settings; 605/50 filter) and analyzed using Image Lab 4.1.

Quantification of protein bands for the determination of selectivity of 14, 15 and 17 The percentage activity remaining was determined by measuring the integrated optical intensity of the bands using Image Lab 4.1 software. This activity was corrected for the total protein loading per lane as determined by Coomassie stain and imaging with a ChemiDoc™ MP sytem, followed by determination of the integrated optical intensity per lane by using Image Lab 4.1. The intensity of the protein bands from the protein samples treated with vehicle was set to 100%.

Experimental procedures chemistry

General remarks

All reactions were performed using oven or flame-dried glassware and dry solvents. Reagents were purchased from Sigma Aldrich, Acros and Merck and used without further purification unless noted otherwise. All moisture sensitive reactions were performed under an argon atmosphere. Traces of water were removed from starting compounds by co-evaporation with toluene.

^{1}H- and ^{13}C-NMR spectra were recorded on a Bruker AV 400 MHz spectrometer at 400.2 (^{1}H) and 100.6 (^{13}C) MHz using $CDCl_3$ or CD_3OD as solvent, unless stated otherwise. Chemical shift values are reported in ppm with tetramethylsilane or solvent resonance as the internal standard ($CDCl_3$: δ 7.26 for ^{1}H, δ 77.16 for ^{13}C, CD_3OD: δ 3.31 for ^{1}H, δ 49.00 for ^{13}C). Data are reported as follows: chemical shifts (δ), multiplicity (s = singlet, d = doublet, dd = double doublet, td = triple doublet, t = triplet, q = quartet, quintet = quint, br = broad, m = multiplet), coupling constants *J* (Hz), and integration. HPLC purification was performed on a preparative LC-MS system (Agilent 1200 series) with an Agilent 6130 Quadruple MS detector. High-resolution mass spectra (HRMS) were recorded on a Thermo Scientific LTQ Orbitrap XL. Liquid chromatography was performed on a Finnigan Surveyor LC-MS system, equipped with a C18 column. Melting points were measured on a Stuart SMP30 melting point apparatus. Flash chromatography was performed using SiliCycle silica gel type SiliaFlash P60 (230 – 400 mesh). TLC analysis was performed on Merck silica gel 60/Kieselguhr F254, 0.25 mm. Compounds were visualized using either Seebach's reagent (a mixture of phosphomolybdic acid (25 g), cerium (IV) sulfate (7.5 g), H_2O (500 mL) and H_2SO_4 (25 mL)) or a $KMnO_4$ stain (K_2CO_3 (40 g), $KMnO_4$ (6 g) and H_2O (600 mL)).

Methyl (2-phenoxybenzyl)glycinate (8)

To a stirred solution of 2-phenoxybenzaldehyde (**3**, 150 µL, 0.87 mmol) in MeOH (50 mL) with 3 Å MS was added methyl glycinate (377.6 mg, 3.01 mmol) and AcOH (260 µL, 4.54 mmol) at rt, the reaction mixture was stirred for 15 minutes. Lastly was added $NaCNBH_3$ (151.4 mg, 2.41 mmol) and the reaction mixture was stirred for 2 hours at rt. After completion the reaction was diluted with EtOAc and washed with $NaHCO_3$, water and brine, dried, concentrated *in vacuo* and purified by flash chromatography to yield methyl (2-phenoxybenzyl)glycinate (141.9 mg, 0.52 mmol, 60 %) as a white solid. ^{1}H NMR ($CDCl_3$, 400 MHz): δ 7.41 (d, *J* = 7.3 Hz, 1H), 7.32 (t, *J* = 7.6 Hz, 2H), 7.22 (t, *J* = 7.7 Hz, 1H), 7.16 – 7.05 (m, 2H), 6.96 (d, *J* = 8.0 Hz, 2H), 6.88 (d, *J* = 8.0 Hz, 1H), 3.88 (s, 2H), 3.68 (s, 3H), 3.45 (s, 2H), 1.92 (bs, 1H). ^{13}C NMR ($CDCl_3$, 101 MHz): δ 170.51, 157.54, 155.07, 130.54, 129.89(2C), 128.76, 125.85, 123.91, 123.12, 119.17, 118.24(2C), 54.19, 51.97, 49.87.

Methyl (3-phenoxybenzyl)glycinate (9)

The title compound was synthesized from 3-phenoxybenzaldehyde (**4**, 100 µl, 0.58 mmol) according to the procedure described for compound **8**. This yielded methyl (3-phenoxybenzyl)glycinate (125.7 mg, 0.46 mmol, 80 %) as a white solid. ^{1}H NMR ($CDCl_3$, 400 MHz): δ 7.39 – 7.27 (m, 3H), 7.13 – 7.04 (m, 2H), 7.04 – 6.97 (m, 3H), 6.90 (ddd, *J* = 8.2, 2.5, 1.0 Hz, 1H), 3.79 (s, 2H), 3.73 (s, 3H), 3.42 (s, 2H). ^{13}C NMR ($CDCl_3$, 101 MHz): δ 170.73, 157.76, 157.16, 133.93, 129.88(2C), 129.84, 123.36, 123.14, 119.04(2C), 118.73, 117.71, 99.91, 53.09, 51.74, 50.02. Spectroscopic data are in agreement with those reported in literature.[30]

Methyl (4-phenoxybenzyl)glycinate (10)

The title compound was synthesized from 4-phenoxybenzaldehyde (**5**, 100 mg, 0.50 mmol) according to the procedure described for compound **8**. This yielded methyl (4-phenoxybenzyl)glycinate (240 mg, 0.88 mmol, 44 %) as a white solid. ^{1}H NMR (400 MHz, $CDCl_3$): δ 7.38 – 7.22 (m, 4H), 7.08 (t, *J* = 7.4 Hz, 1H), 6.98 (ddd, *J* = 10.1, 7.2, 1.5 Hz, 4H), 3.77 (s, 2H), 3.72 (s, 3H), 3.42 (s, 2H), 2.18 (s, 1H); ^{13}C NMR (101 MHz, $CDCl_3$): δ 172.87, 157.37, 156.38, 134.38, 129.75(2C), 129.72(2C), 123.18, 118.97(2C), 118.76(2C), 52.68, 51.82, 49.85.

3-((5-(Trifluoromethyl)pyridin-2-yl)oxy)benzaldehyde (11a)

The title compound was synthesized from 3-hydroxybenzaldehyde (366 mg, 3 mmol) and 2-chloro-5-(trifluoromethyl)pyridine (363 mg, 2 mmol) according to the procedure described for compound **12a**. This yielded 3-((5-(trifluoromethyl)pyridin-2-yl)oxy)benzaldehyde (135 mg, 0.5 mmol, 30%) after flash chromatography as a white solid. ^{1}H NMR ($CDCl_3$, 400 MHz): δ 10.02 (s, 1H), 8.45 – 8.40 (m, 1H), 7.96 (dd, *J* = 8.6, 2.3 Hz, 2H), 7.77-7.79 (m, 1H), 7.71 – 7.67 (m, 1H), 7.62 (t, *J* = 7.8 Hz, 1H), 7.43-7.46 (m, 1H), 7.10 (d, 1H, *J* = 8.8 Hz). Spectroscopic data are in agreement with those reported in literature.[31]

Methyl (3-((5-(trifluoromethyl)pyridin-2-yl)oxy)benzyl)glycinate (11)

The title compound was synthesized from 3-((5-(trifluoromethyl)pyridin-2-yl)oxy)benzaldehyde (**6**, 183mg, 0.68mmol) according to the procedure described for compound **8**. This yielded methyl (3-((5-(trifluoromethyl)pyridin-2-yl)oxy)benzyl)glycinate (84 mg, 0.25 mmol, 37 %) as a colorless oil. ^{1}H NMR ($CDCl_3$, 400 MHz): δ 8.43 (s, 1H), 7.86 – 7.89 (m, 1H), 7.36 – 7.39 (m, 1H), 7.14 – 7.23 (m, 2H), 6.98 – 7.01 (m, 2H), 3.86 (s, 2H), 3.72 (s, 3H), 3.45 (s, 2H).

4-((5-(Trifluoromethyl)pyridin-2-yl)oxy)benzaldehyde (12a)

To a stirred solution of 4-hydroxybenzaldehyde (366 mg, 3 mmol) in DMSO (30 mL) was added K_2CO_3 (360 mg, 6 mmol) at room temperature. After 30 minutes of stirring was added dropwise a solution of 2-fluoro-5-(trifluoromethyl)pyridine (0.241 mL, 2 mmol) in DMSO (2 mL). After full completion (24 h) HCl (1 M) was added. The mixture was poured into water, and the product was extracted with EtOAc, washed with water and brine, dried, concentrated *in vacuo* and purified by flash chromatography to yield 4-((5-(trifluoromethyl)pyridin-2-yl)oxy)benzaldehyde (366 mg, 1.37 mmol, 70 %) as a white solid. ^{1}H NMR ($CDCl_3$, 400 MHz): δ 10.01 (s, 1H), 8.45 (s, 1H), 7.95 – 7.99 (m, 3H), 7.31 – 7.35 (m, 2H), 7.11 – 7.13 (m, 1H). ^{13}C NMR (101 MHz, $CDCl_3$): δ 190.94, 164.87, 158.25, 145.49 (q, *J* = 4.3 Hz), 137.24 (q, *J* = 3.2 Hz), 133.58, 131.69(2C), 123.68 (q, *J* = 272.6 Hz), 122.50 (q, *J* = 33.5 Hz), 121.92(2C), 112.24.

Methyl (4-((5-(trifluoromethyl)pyridin-2-yl)oxy)benzyl)glycinate (12)

The title compound was synthesized from 4-((5-(trifluoromethyl)pyridin-2-yl)oxy)benzaldehyde (**7**, 267 mg, 1 mmol) according to the procedure described for compound **8**. This yielded methyl (4-((5-(trifluoromethyl)pyridin-2-yl)oxy)benzyl)glycinate (215 mg, 0.63 mmol, 63 %) as a colorless oil. ^{1}H NMR ($CDCl_3$, 400 MHz): δ 8.44 (s, 1H), 7.88-7.91 (m, 1H), 7.40 (d, 2H, *J* = 8.4 Hz), 7.10-7.13(m, 2H), 7.00 (d, 1H, *J* = 8.8 Hz), 3.83 (s, 2H), 3.75 (s, 3H), 3.46 (s, 2H).

Methyl *N*-((2,2-dimethylchroman-6-yl)sulfonyl)-*N*-(2-phenoxybenzyl)glycinate (13a)

To a stirred solution of methyl (2-phenoxybenzyl)glycinate (**8**, 63.9 mg, 0.24 mmol) in CH_2Cl_2 (50 mL) was added 2,2-dimethylchromane-6-sulfonyl chloride (96 mg, 0.368 mmol), triethylamine (0.1 mL, 0.717 mmol) and 1 drop of pyridine (or 4-dimethylaminopyridine) at rt. After completion (2 h), the reaction mixture was diluted with EtOAc, washed with sat. $NaHCO_3$, brine and purified using column chromatography to yield methyl *N*-((2,2-dimethylchroman-6-yl)sulfonyl)-*N*-(2-phenoxybenzyl)glycinate (96.0 mg, 0.19 mmol, 82 %) as an oil. ^{1}H NMR ($CDCl_3$, 400 MHz): δ 7.57 – 7.46 (m, 3H), 7.33 – 7.27 (m, 2H), 7.25 – 7.19 (m, 1H), 7.14 – 7.04 (m, 2H), 6.87 – 6.74 (m, 4H), 4.55 (s, 2H), 4.02 (s, 2H), 3.52 (s, 3H), 2.74 (t, *J* = 6.7 Hz, 2H), 1.80 (t, *J* = 6.7 Hz, 2H), 1.34 (s, 6H).^{13}C NMR ($CDCl_3$, 101 MHz): δ 169.68, 157.96, 156.85, 155.46, 131.49, 130.43(2C), 129.95, 129.57, 129.51, 127.15, 126.53, 123.89, 123.52, 121.31, 118.57(2C), 118.26, 117.79, 75.73, 52.06, 48.00, 46.26, 32.38, 27.01(2C), 22.45.

_N_-((2,2-Dimethylchroman-6-yl)sulfonyl)-_N_-(2-phenoxybenzyl)glycine (13)

To a stirred solution of methyl _N_-((2,2-dimethylchroman-6-yl)sulfonyl)-_N_-(2-phenoxybenzyl)glycinate (**13a**, 60 mg, 0.121 mmol) in THF (1 mL): methanol (1 mL) was added aqueous NaOH (2 mL, 4.00 mmol) at rt. After completion (30 mins), to the reaction was added Amberlight 150 H resin until neutral, the mixture was filtered, concentrated *in vacuo,* coevaporated with toluene and purified by flash chromatography to yield _N_-((2,2-dimethylchroman-6-yl)sulfonyl)-_N_-(2-phenoxybenzyl)glycine (25.3 mg, 0.053 mmol, 43% yield) as a white solid. mp 155-157 °C. HRMS (ESI+) m/z: calculated for $C_{26}H_{28}NO_6S$ ([M + H]), 482.1632, found: 482.1631.^{1}H NMR ($CDCl_3$, 400 MHz): δ 7.72 – 7.35 (m, 3H), 7.33 – 7.27 (m, 2H), 7.23 (t, _J_ = 7.5 Hz, 1H), 7.17 – 6.98 (m, 2H), 6.94 – 6.65 (m, 4H), 4.54 (s, 2H), 4.08 (s, 2H), 2.71 (t, _J_ = 6.6 Hz, 2H), 1.78 (t, _J_ = 6.4 Hz, 2H), 1.33 (s, 6H). ^{13}C NMR ($CDCl_3$, 101 MHz): δ 173.82, 158.16, 156.62, 155.63, 131.64, 130.46, 130.02(2C), 129.76, 129.62, 127.20, 126.06, 123.88, 123.71, 121.49, 118.71(2C), 118.18, 117.85, 75.83, 48.15, 46.90, 32.31, 27.00(2C), 22.42. Purity >95% as determined by LC-MS.

Methyl _N_-((2,2-dimethylchroman-6-yl)sulfonyl)-_N_-(3-phenoxybenzyl)glycinate (14a)

The title compound was synthesized from methyl (3-phenoxybenzyl)glycinate (**9**, 37.5 mg, 0.14 mmol) according to the procedure described for compound **13a**. This yielded methyl _N_-((2,2-dimethylchroman-6-yl)sulfonyl)-_N_-(3-phenoxybenzyl)glycinate (64.5 mg, 0.13 mmol, 94 %) as an oil. ^{1}H NMR ($CDCl_3$, 400 MHz) δ 7.62 – 7.51 (m, 2H), 7.33 (t, _J_ = 8.4, 7.5 Hz, 2H), 7.29 – 7.23 (m, 1H), 7.11 (t, _J_ = 7.4 Hz, 1H), 7.03 – 6.94 (m, 3H), 6.94 – 6.80 (m, 3H), 4.44 (s, 2H), 3.92 (s, 2H), 3.57 (s, 3H), 2.80 (t, _J_ = 6.7 Hz, 2H), 1.83 (t, _J_ = 6.7 Hz, 2H), 1.35 (s, 6H). ^{13}C NMR ($CDCl_3$, 101 MHz) δ 169.45, 158.14, 157.67, 156.99, 137.43, 130.15, 129.96, 129.92(2C), 129.64, 127.15, 123.58, 123.44, 121.45, 119.06, 119.02(2C), 118.39, 117.95, 75.82, 52.13, 51.25, 46.95, 32.36, 26.99(2C), 22.48.

_N_-((2,2-Dimethylchroman-6-yl)sulfonyl)-_N_-(3-phenoxybenzyl)glycine (14)

The title compound was synthesized from methyl _N_-((2,2-dimethylchroman-6-yl)sulfonyl)-_N_-(3-phenoxybenzyl)glycinate (**14a**, 52.4 mg, 0.11 mmol) according to the procedure described for compound **13**. This yielded _N_-((2,2-dimethylchroman-6-yl)sulfonyl)-_N_-(3-phenoxybenzyl)glycine (27.9 mg, 0.06 mmol, 55 %) as a white solid after lyophilization. mp 171-173 °C. HRMS (ESI+) m/z: calculated for $C_{26}H_{28}NO_6S$ ([M + H]), 482.1632, found: 482.1630. ^{1}H NMR ($CDCl_3$, 400 MHz): δ 7.70 – 7.52 (m, 2H), 7.33 (t, _J_ = 7.9 Hz, 2H), 7.25 – 7.29 (m, 1H), 7.15 – 7.06 (m, 1H), 7.05 – 6.87 (m, 4H), 6.87 – 6.77 (m, 2H), 4.42 (s, 2H), 3.94 (s, 2H), 2.78 (t, _J_ = 6.6 Hz, 2H), 1.82 (t, _J_ = 6.7 Hz, 2H), 1.34 (s, 6H). ^{13}C NMR ($CDCl_3$, 101 MHz): δ 173.84, 158.34, 157.82, 156.91, 137.14, 130.28, 129.95(2C), 129.67, 129.56, 127.18, 123.66, 123.39, 121.63, 119.08(2C), 118.97, 118.51, 118.02, 75.93, 51.40, 46.87, 32.32, 27.00(2C), 22.47. Purity >95% as determined by LC-MS.

Methyl _N_-((2,2-dimethylchroman-6-yl)sulfonyl)-_N_-(4-phenoxybenzyl)glycinate (15a)

See compound **26**.

_N_-((2,2-Dimethylchroman-6-yl)sulfonyl)-_N_-(4-phenoxybenzyl)glycine (15)

The title compound was synthesized from methyl _N_-((2,2-dimethylchroman-6-yl)sulfonyl)-_N_-(4-phenoxybenzyl)glycinate (**15a**, 62 mg, 0.125 mmol) according to the procedure described for compound **13**. This yielded _N_-((2,2-dimethylchroman-6-yl)sulfonyl)-_N_-(4-phenoxybenzyl)glycine (54 mg, 0.11 mmol, 90%) as a white solid. mp 192-194 °C. HRMS (ESI+) m/z: calculated for $C_{26}H_{28}NO_6S$ ([M + H]) 482.1632, found 482.1631. ^{1}H NMR (400 MHz, DMSO): δ 7.58 (d, _J_ = 2.2 Hz, 1H), 7.52 (dd, _J_ = 8.6, 2.3 Hz, 1H), 7.40 (dd, _J_ = 8.5, 7.5 Hz, 2H), 7.23 (d, _J_ = 8.6 Hz, 2H), 7.15 (t, _J_ = 7.4 Hz, 1H), 7.04 – 6.97 (m, 2H), 6.93 (d, _J_ = 8.6 Hz, 2H), 6.85 (d, _J_ = 8.6 Hz, 1H), 4.37 (s, 2H), 3.84 (s, 2H), 2.80 (t, _J_ = 6.6 Hz, 2H), 1.81 (t, _J_ = 6.7 Hz, 2H), 1.31 (s, 6H); ^{13}C NMR (101 MHz, DMSO): δ 170.47, 157.70, 157.04, 156.54, 131.36, 130.66, 130.61(2C), 130.51(2C), 129.63, 127.05, 123.94,

122.03, 119.02(2C), 118.89(2C), 117.66, 76.13, 51.14, 48.15, 32.00, 27.02(2C), 22.11. Purity >95% as determined by LC-MS.

Methyl *N*-((2,2-dimethylchroman-6-yl)sulfonyl)-*N*-(3-((5-(trifluoromethyl)pyridin-2-yl)oxy)benzyl)glycinate (16a)

The title compound was synthesized from methyl (3-((5-(trifluoromethyl)pyridin-2-yl)oxy)benzyl)glycinate (**11**, 34 mg, 0.1 mmol) according to the procedure described for compound **13a**. This yielded methyl *N*-((2,2-dimethylchroman-6-yl)sulfonyl)-*N*-(3-((5-(trifluoromethyl)pyridin-2-yl)oxy)benzyl)glycinate (19 mg, 0.03 mmol, 35 %) as a white solid. ^{1}H NMR ($CDCl_3$, 400 MHz): δ 8.34 (s, 1H), 7.82-7.85 (m, 1H), 7.50-7.52 (m, 2H), 7.28-7.32(m, 1H), 7.07-7.09 (m, 1H), 7.00 (d, 2H, *J* = 8.0 Hz), 6.94 (d, 1H, *J* = 8.8 Hz), 6.76 (d, 1H, *J* = 8.4 Hz), 4.43 (s, 2H), 3.89 (s, 2H), 3.62 (s, 3H), 2.73 (t, 2H, *J* = 6.4 Hz), 1.75 (t, 2H, *J* = 6.8 Hz), 1.26 (s, 6H).

***N*-((2,2-Dimethylchroman-6-yl)sulfonyl)-*N*-(3-((5-(trifluoromethyl)pyridin-2-yl)oxy)benzyl)glycine (16)**

The title compound was synthesized from methyl *N*-((2,2-dimethylchroman-6-yl)sulfonyl)-*N*-(3-((5-(trifluoromethyl)pyridin-2-yl)oxy)benzyl)glycinate (**16a**, 9.0 mg, 0.016 mmol) according to the procedure described for compound **13**. This yielded *N*-((2,2-dimethylchroman-6-yl)sulfonyl)-*N*-(3-((5-(trifluoromethyl)pyridin-2-yl)oxy)benzyl)glycine (5.6 mg, 0.010 mmol, 63% yield) as a white solid after lyophilization. mp 149-151 °C. HRMS (ESI+) calculated for $C_{26}H_{25}F_3N_2O_6S$ ([M + H]). 551.1458, found: 551.1456. ^{1}H NMR ($CDCl_3$, 400 MHz): δ 8.47 (s, 1H), 7.92 (d, *J* = 7.2 Hz, 1H), 7.58 – 7.62 (m, 2H), 7.30 – 7.32 (m, 1H), 7.03 – 7.11 (m, 4H), 6.85 (d, *J* = 8.4 Hz, 1H), 4.47 (s, 2H), 3.96 (s, 2H), 2.82 (t, *J* = 6.4 Hz, 2H), 1.85 (t, *J* = 6.8 Hz, 2H), 1.28 (s, 6H). ^{13}C NMR (151 MHz, $CDCl_3$): δ 171.96, 165.66, 158.33, 153.54, 145.43(q, *J* = 4.1 Hz), 137.51, 137.11 (q, *J* = 3.2 Hz), 130.29, 129.72, 129.60, 127.22, 125.87, 123.73 (q, *J* = 271.5 Hz), 121.83, 121.65 (q, *J* = 33.4 Hz), 121.60, 121.46, 118.01, 111.83, 75.91, 51.27, 46.83, 32.32, 26.99(2C), 22.47. Purity >95% as determined by LC-MS.

Methyl *N*-((2,2-dimethylchroman-6-yl)sulfonyl)-*N*-(4-((5-(trifluoromethyl)pyridin-2-yl)oxy)benzyl)glycinate (17a)

The title compound was synthesized from methyl (4-((5-(trifluoromethyl)pyridin-2-yl)oxy)benzyl)glycinate (**12**, 34 mg, 0.1 mmol) and 2,2-dimethylchroman-6-sulfonyl chloride (65 mg, 0.25 mmol) according to the procedure described for compound **13a**. This yielded methyl *N*-((2,2-dimethylchroman-6-yl)sulfonyl)-*N*-(4-((5-(trifluoromethyl)pyridin-2-yl)oxy)benzyl)glycinate (45 mg, 0.080 mmol, 80 %) as a white solid. ^{1}H NMR ($CDCl_3$, 400 MHz): δ 8.45 (s, 1H), 7.92-7.95 (m, 1H), 7.62-7.65 (m, 2H), 7.34-7.36 (m, 2H), 7.11-7.14 (m, 2H), 7.02 (d, 1H, *J* = 8.8 Hz), 6.90 (d, 1H, *J* = 8.4 Hz), 4.52 (s, 2H), 3.98 (s, 2H), 3.61 (s, 3H), 2.28 (t, 2H, *J* = 6.4 Hz), 1.87 (t, 2H, *J* = 6.8Hz), 1.30 (s, 6H).

***N*-((2,2-Dimethylchroman-6-yl)sulfonyl)-*N*-(4-((5-(trifluoromethyl)pyridin-2-yl)oxy)benzyl)glycine (17)**

The title compound was synthesized from methyl *N*-((2,2-dimethylchroman-6-yl)sulfonyl)-*N*-(4-((5-(trifluoromethyl)pyridin-2-yl)oxy)benzyl)glycinate (**17a**, 42 mg, 0.075 mmol) according to the procedure described for compound **13**. This yielded *N*-((2,2-dimethylchroman-6-yl)sulfonyl)-*N*-(4-((5-(trifluoromethyl)pyridin-2-yl)oxy)benzyl)glycine (35 mg, 0.064 mmol, 85 %) as a white solid after lyophilization. mp 193-195 °C. HRMS (ESI+) calculated for $C_{26}H_{26}F_3N_2O_6S$ ([M + H]). 551.1458, found: 551.1456. ^{1}H NMR ($CDCl_3$, 400 MHz): δ 8.44 (s, 1H), 7.91 – 7.94 (m, 1H), 7.59 – 7.62 (m, 2H), 7.30 – 7.33 (m, 2H), 7.04 – 7.11 (m, 2H), 7.03 (d, *J* = 8.4 Hz, 1H), 6.86 (d, *J* = 8.4 Hz, 1H), 4.47 (s, 2H), 3.97 (s, 2H), 2.82 (t, *J* = 6.4 Hz, 2H), 1.85 (t, *J* = 6.8 Hz, 2H), 1.36 (s, 6H). ^{13}C NMR ($CDCl_3$, 101 MHz): δ 173.12, 165.66, 158.34, 153.08, 145.49 (q, *J* = 4.3 Hz), 137.08 (q, *J* = 3.1 Hz), 132.38, 130.32(2C), 129.72, 127.21, 123.72 (q, *J* = 272.5 Hz), 121.90 (q, *J* = 33.3 Hz), 121.89(2C), 121.62, 118.03, 111.81, 75.94, 51.06, 46.76, 32.34, 27.00(2C), 22.50. One quaternary carbon signal overlaps and is not reported. Purity >95% as determined by LC-MS.

Methyl *N*-((4-chlorophenyl)sulfonyl)-*N*-(3-phenoxybenzyl)glycinate (18a)

The title compound was synthesized from (3-phenoxybenzyl)glycinate (**9**, 116.5 mg, 0.429 mmol) according to the procedure described for compound **13a**. This yielded methyl *N*-((4-chlorophenyl)sulfonyl)-*N*-(3-phenoxybenzyl)glycinate (83.0 mg, 0.186 mmol, 43 % yield) as an oil. ^{1}H NMR ($CDCl_3$, 400 MHz): δ 7.84 – 7.76 (m, 2H), 7.51 – 7.43 (m, 2H), 7.38 – 7.24 (m, 3H), 7.13 (tt, *J* = 7.6, 1.2 Hz, 1H), 7.02 – 6.95 (m, 3H), 6.93 (ddd, *J* = 8.2, 2.5, 1.0 Hz, 1H), 6.85 (t, *J* = 2.0 Hz, 1H), 4.46 (s, 2H), 3.96 (s, 2H), 3.57 (s, 3H). ^{13}C NMR ($CDCl_3$, 101 MHz): δ 169.08, 157.86, 156.83, 139.41, 138.37, 136.76, 130.33, 129.96(2C), 129.36(2C), 128.98(2C), 123.71, 123.27, 119.12(2C), 118.81, 118.56, 52.28, 51.14, 46.68.

***N*-((4-Chlorophenyl)sulfonyl)-*N*-(3-phenoxybenzyl)glycine (18)**

The title compound was synthesized from methyl *N*-((4-chlorophenyl)sulfonyl)-*N*-(3-phenoxybenzyl)glycinate (**18a**, 32.2 mg, 0.07 mmol) according to the procedure described for compound **13**. This yielded *N*-((4-chlorophenyl)sulfonyl)-*N*-(3-phenoxybenzyl)glycine (11.7 mg, 0.03 mmol, 38 %) after crystallization from EtoAc/pentane as a white solid. mp 147-149 °C. HRMS (ESI+) m/z: calculated for $C_{21}H_{19}ClNO_5S$ ([M + H]), 432.0667, found: 432.0669. ^{1}H NMR ($CDCl_3$, 400 MHz): δ 7.82 – 7.74 (m, 2H), 7.48 – 7.41 (m, 2H), 7.39 – 7.31 (m, 2H), 7.30 – 7.27 (m, 1H), 7.13 (tt, *J* = 7.2, 1.2 Hz, 1H), 7.01 – 6.94 (m, 3H), 6.92 (dd, *J* = 8.3, 2.5, 1H), 6.81 (t, *J* = 2.0 Hz, 1H), 5.44 (bs, 1H), 4.45 (s, 2H), 3.98 (s, 2H). ^{13}C NMR ($CDCl_3$, 101 MHz): δ 173.48, 157.97, 156.76, 139.57, 138.17, 136.55, 130.43, 130.00(2C), 129.45(2C), 128.95(2C), 123.80, 123.24, 119.18(2C), 118.70, 118.65, 51.27, 46.59. Purity >95% as determined by LC-MS.

Methyl *N*-((2,6-dichlorophenyl)sulfonyl)-*N*-(3-phenoxybenzyl)glycinate (19a)

The title compound was synthesized from methyl (3-phenoxybenzyl)glycinate (**9**, 126.1 mg, 0.47 mmol) and 2,6-dichlorobenzenesulfonyl chloride (202.8 mg, 0.83 mmol) according to the procedure described for compound **13a.** This yielded *N*-((2,6-dichlorophenyl)sulfonyl)-*N*-(3-phenoxybenzyl)glycinate (57.7 mg, 0.12 mmol, 26 %) as an oil. ^{1}H NMR ($CDCl_3$, 400 MHz) δ 7.36 – 7.30 (m, 4H), 7.29 – 7.26 (m, 2H), 7.17 – 7.12 (m, 1H), 6.97 (d, *J* = 11.2 Hz, 4H), 6.88 (t, *J* = 2.0 Hz, 1H), 4.45 (s, 2H), 4.18 (s, 2H), 3.74 (s, 3H).

***N*-((2,6-Dichlorophenyl)sulfonyl)-*N*-(3-phenoxybenzyl)glycine (19)**

The title compound was synthesized from methyl *N*-((2,6-dichlorophenyl)sulfonyl)-*N*-(3-phenoxybenzyl)glycinate (**19a**, 23.9 mg, 0.05 mmol) according to the procedure described for compound **13**. This yielded *N*-((2,6-dichlorophenyl)sulfonyl)-*N*-(3-phenoxybenzyl)glycine (14.2 mg, 0.03 mmol, 61 %) as an oil. HRMS (ESI+) m/z: calculated for $C_{21}H_{17}Cl_2NO_5SNa$ ([M + Na]), 488.0097, found: 488.0095. ^{1}H NMR ($CDCl_3$, 400 MHz): δ 7.43 – 7.37 (m, 2H), 7.37 – 7.31 (m, 2H), 7.30 – 7.22 (m, 2H), 7.18 (tt, *J* = 7.6, 1.6 Hz, 1H), 6.99 – 6.86 (m, 4H), 6.70 (t, *J* = 2.0 Hz, 1H), 5.07 (bs, 1H), 4.62 (s, 2H), 4.15 (s, 2H). ^{13}C NMR ($CDCl_3$, 101 MHz): δ 173.49, 157.91, 156.83, 140.60, 136.56, 135.90(2C), 135.52, 132.79, 131.75(2C), 130.36, 129.99(2C), 123.70, 123.35, 119.16(2C), 118.62, 51.41, 47.47. Purity >95% as determined by LC-MS.

Methyl *N*-((4-chlorophenyl)sulfonyl)-*N*-(4-phenoxybenzyl)glycinate (20a)

The title compound was synthesized from methyl (4-phenoxybenzyl)glycinate (**10**, 41 mg, 0.15 mmol) and 4-chlorobenzene-1-sulfonyl chloride (80 mg, 0.38 mmol) according to the procedure described for compound **13a**. This yielded methyl *N*-((4-chlorophenyl)sulfonyl)-*N*-(4-phenoxybenzyl)glycinate (62 mg, 0.14 mmol, 93 %) as a white solid. ^{1}H NMR (400 MHz, $CDCl_3$) δ 7.83 (d, *J* = 8.7 Hz, 2H), 7.50 (d, *J* = 8.7 Hz, 2H), 7.38 – 7.31 (m, 2H), 7.21 (d, *J* = 8.6 Hz, 2H), 7.17 – 7.08 (m, 1H), 7.03 – 6.91 (m, 4H), 4.45 (s, 2H), 3.96 (s, 2H), 3.58 (s, 3H). ^{13}C NMR (101 MHz, $CDCl_3$) δ 169.16, 157.64, 156.80, 139.37, 138.48, 130.30(2C), 129.96(2C), 129.35(2C), 129.13, 129.01(2C), 123.77, 119.27(2C), 118.94(2C), 52.26, 50.87, 46.52.

***N*-((4-Chlorophenyl)sulfonyl)-*N*-(4-phenoxybenzyl)glycine (20)**

The title compound was synthesized from methyl *N*-((4-chlorophenyl)sulfonyl)-*N*-(4-phenoxybenzyl)glycinate (**20a**, 62.1 mg, 0.13 mmol) according to the procedure described for compound **13**. This yielded *N*-((4-chlorophenyl)sulfonyl)-*N*-(4-phenoxybenzyl)glycine (38 mg, 0.09 mmol, 70 %) as a white solid after lyophilization. mp 188-190 °C. HRMS (ESI+) calculated for $C_{21}H_{18}ClNO_5S$ ([M + H]). 432.0667, found: 432.0662. ^{1}H NMR ($CDCl_3$, 400 MHz): δ 7.75 (d, *J* = 8.0 Hz, 2H), 7.42 (d, *J* = 8.4 Hz, 2H), 7.28 – 7.30 (m, 2H), 7.12 (d, *J* = 8.4 Hz, 1H), 7.04 – 7.08 (m, 2H), 6.93 (d, *J* = 7.6 Hz, 2H), 6.88 (d, *J* = 8.0 Hz, 2H), 4.38 (s, 2H), 3.93 (s, 2H). ^{13}C NMR ($CDCl_3$, 101 MHz): δ 170.52, 157.30, 156.20, 139.20, 139.16, 130.17(2C), 129.83(2C), 129.19(2C), 128.88(2C), 123.62, 119.11, 118.83(2C), 118.79(2C), 50.60, 46.28. Purity >95% as determined by LC-MS.

Methyl *N*-((2,6-dichlorophenyl)sulfonyl)-*N*-(4-phenoxybenzyl)glycinate (21a)

The title compound was synthesized from methyl (4-phenoxybenzyl)glycinate (**10**, 41 mg, 0.15 mmol) and 2,6-dichlorobenzene-1-sulfonyl chloride (93 mg, 0.37 mmol) according to the procedure described for compound **13a**. This yielded methyl *N*-((2,6-dichlorophenyl)sulfonyl)-*N*-(4-phenoxybenzyl)glycinate (17 mg, 0.036 mmol, 25 %) as a white solid. ^{1}H NMR ($CDCl_3$, 400 MHz): δ 7.46 (d, *J* = 8.0 Hz, 2H), 7.32 – 7.38 (m, 3H), 7.10 – 7.18 (m, 3H), 6.99 (d, *J* = 7.6 Hz, 2H), 6.92 (d, *J* = 8.4 Hz, 2H), 4.67 (s, 2H), 4.12 (s, 2H), 3.63 (s, 3H). ^{13}C NMR ($CDCl_3$, 101 MHz): δ 174.93, 169.19, 157.57, 156.84, 135.96, 135.89, 132.65, 131.72(2C), 130.32(2C), 129.96(2C), 129.25, 123.75, 119.27(2C), 118.95(2C), 52.38, 51.34, 47.17.

***N*-((2,6-Dichlorophenyl)sulfonyl)-*N*-(4-phenoxybenzyl)glycine (21)**

The title compound was synthesized from methyl *N*-((2,6-dichlorophenyl)sulfonyl)-*N*-(4-phenoxybenzyl)glycinate (**21a**, 17.1 mg, 0.036 mmol) according to the procedure described for compound **13**. This yielded *N*-((2,6-dichlorophenyl)sulfonyl)-*N*-(4-phenoxybenzyl)glycine (15 mg, 0.033 mmol, 92 %) as a white solid after lyophilization. mp 140-142 °C. HRMS (ESI+) calculated for $C_{21}H_{18}Cl_2NO_5S$ ([M + H]). 466.0277, found: 466.0274. ^{1}H NMR ($CDCl_3$, 400 MHz): δ 7.50 (d, *J* = 8.0 Hz, 2H), 7.35 – 7.39 (m, 3H), 7.15 – 7.17 (m, 3H), 7.02 (d, *J* = 7.6 Hz, 2H), 6.94 (d, *J* = 8.4 Hz, 2H), 4.67 (s, 2H), 4.20 (s, 2H). ^{13}C NMR ($CDCl_3$, 101 MHz): δ 175.08, 157.61, 156.64, 135.81, 135.61, 132.71, 131.69(2C), 130.21(2C), 129.87(2C), 128.76(2C), 123.72, 119.23(2C), 118.84(2C), 51.12, 46.20. Purity >95% as determined by LC-MS.

Methyl *N*-(4-chlorobenzoyl)-*N*-(4-phenoxybenzyl)glycinate (22a)

The title compound was synthesized from methyl (4-phenoxybenzyl)glycinate (**10**, 33 mg, 0.12 mmol) and 4-chlorobenzoyl chloride (53 mg, 0.30 mmol) according to the procedure described for compound **13a**. This yielded methyl *N*-(4-chlorobenzoyl)-*N*-(4-phenoxybenzyl)glycinate (18 mg, 0.04 mmol, 33 %) as a white solid. ^{1}H NMR ($CDCl_3$, 400 MHz): δ 7.27-7.48 (m, 7H), 7.12-7.14 (m, 2H), 6.97-7.02 (m, 4H), 4.75 (s, 0.7H), 4.57 (s, 1.3H), 4.15 (s, 1.3H), 3.86 (s, 0.7H), 3.77 (s, 2.1H), 3.71 (s, 0.9H). Signals split (7:3) due to rotamers.

***N*-(4-Chlorobenzoyl)-*N*-(4-phenoxybenzyl)glycine (22)**

The title compound was synthesized from methyl *N*-(4-chlorobenzoyl)-*N*-(4-phenoxybenzyl)glycinate (**22a**, 15.8 mg, 0.039 mmol) according to the procedure described for compound **13**. This yielded *N*-(4-chlorobenzoyl)-*N*-(4-phenoxybenzyl)glycine (12 mg, 0.031 mmol, 80 % yield) as a white solid after lyophilization. mp 225-227 °C. HRMS (ESI+) calculated for $C_{22}H_{19}ClNO_4$ ([M + H]). 396.0997, found: 396.0991. ^{1}H NMR ($CDCl_3$, 400 MHz): δ 7.28 – 7.33 (m, 7H), 7.06 – 7.08 (m, 2H), 6.92 – 6.95 (m, 4H), 4.69 (s, 0.6H), 4.52 (s, 1.4H), 4.12 (s, 1.4H), 3.83 (s, 0.6H). ^{13}C NMR ($CDCl_3$, 101 MHz): δ 172.11, 157.59, 157.32, 156.76, 136.72, 133.16, 131.71, 130.35(2C), 129.87(2C), 128.86(2C), 128.30(2C), 124.93(2C), 119.35, 116.03(2C), 53.63, 46.64. Signals split (7:3) due to rotamers. Purity >95% as determined by LC-MS.

Methyl *N*-(2,6-dichlorobenzoyl)-*N*-(4-phenoxybenzyl)glycinate (23a)

The title compound was synthesized from methyl (4-phenoxybenzyl)glycinate (**10**, 33 mg, 0.12 mmol) and 2,6-dichlorobenzoyl chloride (63 mg, 0.30 mmol) according to the procedure described for compound **13a**. This yielded methyl *N*-(2,6-dichlorobenzoyl)-*N*-(4-phenoxybenzyl)glycinate (50 mg, 0.11 mmol, 92 %) as a white solid, which was directly converted to the corresponding acid **17**. ^{1}H NMR ($CDCl_3$, 400 MHz): δ 7.13-7.25 (m, 7H), 7.05-7.07 (m, 1H), 6.86-6.95 (m, 4H), 4.97 (s, 0.5H), 4.46 (s 1.5H), 4.19 (s, 1.5H), 3.76 (s, 0.5H), 3.75 (s, 2.1H), 3.68 (s, 0.9H). Signals split (3:1) due to rotamers.

***N*-(2,6-Dichlorobenzoyl)-*N*-(4-phenoxybenzyl)glycine (23)**

The title compound was synthesized from methyl *N*-(2,6-dichlorobenzoyl)-*N*-(4-phenoxybenzyl)glycinate (**23a**, 57.4 mg, 0.129 mmol) according to the procedure described for compound **13**. This yielded *N*-(2,6-dichlorobenzoyl)-*N*-(4-phenoxybenzyl)glycine (25 mg, 0.058 mmol, 45%) as an oily white solid after lyophilization. mp not determined. HRMS (ESI+) calculated for $C_{22}H_{18}Cl_2NO_4$ ([M + H]). 430.0607, found: 430.0607. ^{1}H NMR ($CDCl_3$, 400 MHz) δ 7.42 – 7.30 (m, 5H), 7.30 – 7.19 (m, 2H), 7.16 – 7.09 (m, 1H), 7.09 – 6.92 (m, 4H), 4.98 (s, 0.5H), 4.46 (s, 1.5H), 4.23 (s, 1.5H), 3.80 (s, 0.5H). ^{13}C NMR (101 MHz, $CDCl_3$) δ 175.11, 166.03, 157.77, 156.69, 134.28, 132.36(1.5C), 132.19(0.5C), 131.00(0.7C), 130.70(0.3C), 130.22(2C), 130.00(1.5C), 129.96(0.5C), 128.65, 128.54(0.5C), 128.44(1.5C), 123.88(0.7C), 123.67(0.3C), 119.42(1.5C), 119.27(0.5C), 118.99(2C), 52.48, 47.72(0.7C), 44.93(0.3C). Signals split (3:1) due to rotamers. Purity >95% as determined by LC-MS.

Methyl *N*-((4-chlorophenyl)sulfonyl)-*N*-(4-((5-(trifluoromethyl)pyridin-2-yl)oxy)benzyl)glycinate (24a)

The title compound was synthesized from methyl (4-((5-(trifluoromethyl)pyridin-2-yl)oxy)benzyl)glycinate (**12**, 41 mg, 0.12 mmol) and 4-chlorobenzene-1-sulfonyl chloride (63 mg, 0.3 mmol) according to the procedure described for compound **13a**. This yielded methyl *N*-((4-chlorophenyl)sulfonyl)-*N*-(4-((5-(trifluoromethyl)pyridin-2-yl)oxy)benzyl)glycinate (22 mg, 0.04 mmol, 36 %) as a white solid. ^{1}H NMR ($CDCl_3$, 400 MHz): δ 8.41-8.44 (m, 1H), 7.90-7.93 (m, 1H), 7.82-7.85 (m, 2H), 7.50-7.52 (m, 2H), 7.33 (d, 2H, *J* = 8.4 Hz), 7.11-7.14 (m, 2H), 7.03 (d, 1H, *J* = 8.4 Hz), 4.53 (s, 2H), 4.14(s, 2H), 3.62 (s, 3H).

***N*-((4-Chlorophenyl)sulfonyl)-*N*-(4-((5-(trifluoromethyl)pyridin-2-yl)oxy)benzyl)glycine (24)**

The title compound was synthesized from methyl *N*-((4-chlorophenyl)sulfonyl)-*N*-(4-((5-(trifluoromethyl)pyridin-2-yl)oxy)benzyl)glycinate (**24a**, 16 mg, 0.031 mmol) according to the procedure described for compound **13**. This yielded *N*-((4-chlorophenyl)sulfonyl)-*N*-(4-((5-(trifluoromethyl)pyridin-2-yl)oxy)benzyl)glycine (14 mg, 0.027 mmol, 88 %) as a white solid after lyophilization. mp 150-152 °C. HRMS (ESI+) calculated for $C_{21}H_{17}ClF_3N_2O_5S$ ([M + H]). 501.0493, found: 501.0491. ^{1}H NMR ($CDCl_3$, 850 MHz) δ 8.46 (s, 1H), 7.93 (dd, *J* = 8.7, 2.5 Hz, 1H), 7.86 – 7.77 (m, 2H), 7.54 – 7.48 (m, 2H), 7.37 – 7.31 (m, 2H), 7.15 – 7.10 (m, 2H), 7.06 (d, *J* = 8.7 Hz, 1H), 4.51 (s, 2H), 4.00 (s, 2H). ^{13}C NMR ($CDCl_3$, 214 MHz,) δ 171.55, 165.60, 153.18, 145.44 (q, *J* = 4.3 Hz), 139.51, 138.37, 137.16 (q, *J* = 3.0 Hz), 131.92, 130.31(2C), 129.41(2C), 129.04(2C), 123.71 (q, *J* = 271.4 Hz), 122.02(2C), 121.97 (q, *J* = 33.5 Hz), 111.93, 50.84, 46.21. Purity >95% as determined by LC-MS.

Methyl *N*-(4-chlorobenzoyl)-*N*-(4-((5-(trifluoromethyl)pyridin-2-yl)oxy)benzyl)glycinate (25a)

The title compound was synthesized from methyl (4-((5-(trifluoromethyl)pyridin-2-yl)oxy)benzyl)glycinate (**12**, 41 mg, 0.12 mmol) and 4-chlorobenzoyl chloride (53 mg, 0.3 mmol) according to the procedure described for compound **13a**. This yielded methyl *N*-(4-chlorobenzoyl)-*N*-(4-((5-(trifluoromethyl)pyridin-2-yl)oxy)benzyl)glycinate (48 mg, 0.10 mmol, 83 %) as a white solid. ^{1}H NMR ($CDCl_3$, 400 MHz): δ 8.36 (s, 1H), 7.84-7.86 (m, 1H), 7.38-7.46 (m, 5H), 7.20 (d, 2H, *J* = 8.4 Hz), 7.10 (d, 2H, *J* = 8.0 Hz), 6.98 (d, 1H, *J* = 8.8 Hz), 4.73 (s, 0.7H), 4.57 (s, 1.3H), 4.12 (s, 1.3H), 3.84 (s, 0.7H), 3.71 (s, 2.1H), 3.65 (s, 0.9H). Signals split (7:3) due to rotamers.

_N_-(4-Chlorobenzoyl)-_N_-(4-((5-(trifluoromethyl)pyridin-2-yl)oxy)benzyl)glycine (25)

The title compound was synthesized from methyl _N_-(4-chlorobenzoyl)-_N_-(4-((5-(trifluoromethyl)pyridin-2-yl)oxy)benzyl)glycinate (**25a**, 47.8mg, 0.1mmol) according to the procedure described for compound **13**. This yielded _N_-(4-chlorobenzoyl)-_N_-(4-((5-(trifluoromethyl)pyridin-2-yl)oxy)benzyl)glycine (13 mg, 0.03 mmol, 33 %) as a white solid after lyophilization. mp 202-204 °C. HRMS (ESI+) calculated for $C_{22}H_{17}ClF_3N_2O_4$ ([M + H]). 465.0824, found: 465.0821. ^{1}H NMR (MeOD, 850 MHz) δ 8.42 (s, 1H), 8.13 – 8.05 (m, 1H), 7.56 – 7.42 (m, 5H), 7.32 (d, _J_ = 8.3 Hz, 1H), 7.20 – 7.16 (m, 2H), 7.14 (t, _J_ = 8.5 Hz, 1H), 4.82 (s, 1H), 4.64 (s, 1H), 4.16 (s, 1H), 3.86 (s, 1H). ^{13}C NMR (MeOD, 214 MHz) δ 173.62(0.5C), 173.56(0.5C), 167.33(0.5C), 167.22(0.5C), 154.26(0.5C), 154.17(0.5C), 146.28 – 146.05 (m, 1C), 138.40 – 138.64 (m, 1C), 137.25(0.5C), 137.07(0.5C), 135.68, 135.28(0.5C), 135.18(0.5C), 134.63, 131.00(2C), 129.95, 129.92, 129.59, 129.46, 125.19 (q, 0.5C, _J_ = 271.8 Hz), 125.00 (q, 0.5C, _J_ = 269.6 Hz), 123.10, 122.84, 122.93 (q, 0.5C, _J_ = 34.2 Hz), 122.77 (q, 0.5C, _J_ = 32.1 Hz), 112.88(0.5C), 112.77(0.5C), 54.51, 50.10. Signals split (1:1) due to rotamers. Purity >95% as determined by LC-MS.

Methyl _N_-((2,2-dimethylchroman-6-yl)sulfonyl)-_N_-(4-phenoxybenzyl)glycinate (26)

The title compound was synthesized from methyl (4-phenoxybenzyl)glycinate (**10**, 50 mg, 0.18 mmol) according to the procedure described for compound **13a**. This yielded methyl _N_-((2,2-dimethylchroman-6-yl)sulfonyl)-_N_-(4-phenoxybenzyl)glycinate (84 mg, 17 mmol, 92%) as a white solid. mp 86-88 °C. HRMS (ESI+) calculated for $C_{27}H_{30}NO_6S$ ([M + H]), 496.1788, found: 496.1788. ^{1}H NMR (400 MHz, $CDCl_3$): δ 7.59 (d, _J_ = 9.3 Hz, 2H), 7.33 (t, _J_ = 7.9 Hz, 2H), 7.20 (d, _J_ = 8.4 Hz, 2H), 7.11 (t, _J_ = 7.4 Hz, 1H), 6.99 (d, _J_ = 8.0 Hz, 2H), 6.93 (d, _J_ = 8.4 Hz, 2H), 6.86 (d, _J_ = 8.4 Hz, 1H), 4.44 (s, 2H), 3.92 (s, 2H), 3.57 (s, 3H), 2.82 (t, _J_ = 6.6 Hz, 2H), 1.84 (t, _J_ = 6.7 Hz, 2H), 1.36 (s, 6H); ^{13}C NMR (101 MHz, $CDCl_3$): δ 169.46, 158.08, 157.32, 156.92, 130.28(2C), 130.08, 129.88(2C), 129.84, 129.58, 127.10, 123.60, 121.42, 119.12(2C), 118.84(2C), 117.89, 75.78, 52.04, 50.95, 46.78, 32.33, 26.95(2C), 22.46.

_N_-(2-Hydroxyethyl)-2,2-dimethyl-_N_-(3-phenoxybenzyl)chromane-6-sulfonamide (27)

To a stirred solution of methyl _N_-((2,2-dimethylchroman-6-yl)sulfonyl)-_N_-(3-phenoxybenzyl)glycinate (**14a**, 34.4 mg, 0.07 mmol) in THF (2 mL) at -5 °C was added $LiBH_4$ (0.1 mL, 2M in THF). After completion (4 h), saturated $KHCO_3$ was carefully added at -5 °C to quench the reaction. The mixture was slowly warmed up to rt, diluted with EtOAc, washed with brine, dried, concentrated _in vacuo_ and purified by flash chromatography to yield _N_-(2-hydroxyethyl)-2,2-dimethyl-_N_-(3-phenoxybenzyl)chromane-6-sulfonamide (21.1 mg, 0.05 mmol, 65 %) as a white solid. mp 148-150 °C. HRMS (ESI+) m/z: calculated for $C_{26}H_{30}NO_5S$ ([M + H]), 468.1839, found: 468.1839. ^{1}H NMR ($CDCl_3$, 400 MHz): δ 7.58 – 7.50 (m, 2H), 7.38 – 7.27 (m, 3H), 7.14 – 7.03 (m, 2H), 6.99 – 6.94 (m, 2H), 6.93 – 6.88 (m, 2H), 6.84 (d, _J_ = 8.5 Hz, 1H), 4.32 (s, 2H), 3.53 (t, _J_ = 5.4 Hz, 2H), 3.23 (t, _J_ = 5.4 Hz, 2H), 2.79 (t, _J_ = 6.7 Hz, 2H), 2.18 (bs, 1H), 1.83 (t, _J_ = 6.7 Hz, 2H), 1.35 (s, 6H). ^{13}C NMR ($CDCl_3$, 101 MHz): δ 158.25, 157.75, 157.01, 138.74, 130.25, 129.94(2C), 129.50, 129.12, 126.97, 123.62, 123.15, 121.77, 119.05(2C), 118.72, 118.33, 118.17, 75.93, 61.26, 53.45, 51.07, 32.31, 27.03(2C), 22.50. Purity >95% as determined by LC-MS.

2-((2,2-Dimethyl-_N_-(3-phenoxybenzyl)chromane)-6-sulfonamido)ethyl piperidine-1-carboxylate (28)

To a stirred solution of _N_-(2-hydroxyethyl)-2,2-dimethyl-_N_-(3-phenoxybenzyl)chromane-6-sulfonamide (**27**, 8.1 mg, 0.02 mmol) in CH_2Cl_2 (2 mL) at 0 °C was added DIPEA (3 µl, 0.017 mmol) and di(1H-imidazol-1-yl)methanone (6.6 mg, 0.04 mmol). After 10 minutes was added piperidine (6 µL, 0.06 mmol) and the mixture was stirred for 30 mins and allowed to warm up to rt. After completion (1 h), the mixture was diluted with EtOAc, washed with brine, dried, concentrated _in vacuo_ to yield 2-((2,2-dimethyl-_N_-(3-phenoxybenzyl)chromane)-6-sulfonamido)ethyl piperidine-1-carboxylate (10.0 mg, 0.02 mmol, 100 %) as a white solid after lyophilization. mp not determined. HRMS (ESI+) m/z: calculated for $C_{32}H_{39}N_2O_6S$ ([M + H]),

579.2523, found: 579.2523. ^{1}H NMR ($CDCl_3$, 400 MHz): δ 7.56 – 7.49 (m, 2H), 7.37 – 7.30 (m, 2H), 7.25 – 7.15 (m, 1H), 7.10 (tt, *J* = 7.2, 1.2 Hz, 1H), 7.04 – 6.94 (m, 3H), 6.91 – 6.85 (m, 2H), 6.82 (d, *J* = 8.5 Hz, 1H), 4.34 (s, 2H), 4.04 (t, *J* = 5.9 Hz, 2H), 3.41 (t, *J* = 5.9 Hz, 2H), 3.33 (bs, 4H), 2.79 (t, *J* = 6.7 Hz, 2H), 1.82 (t, *J* = 6.7 Hz, 2H), 1.55 – 1.44 (bs, 6H), 1.35 (s, 6H).^{13}C NMR ($CDCl_3$, 101 MHz): δ 157.53, 157.14, 156.52, 154.42, 138.73, 130.19, 130.02, 129.90(2C), 129.33, 126.82, 123.46, 123.02, 121.65, 118.94(2C), 118.71, 118.17, 118.08, 75.83, 62.77, 60.56, 52.35, 47.24, 44.90, 32.35, 27.02(2C), 24.46(2C), 22.49, 21.23. Purity >95% as determined by LC-MS.

Tert-butyl (2-(2-(2-((2,2-dimethyl-*N*-(4-phenoxybenzyl)chromane)-6 sulfonamido)acetamido)ethoxy)ethyl) carbamate (29a)

To a stirred solution of *N*-((2,2-dimethylchroman-6-yl)sulfonyl)-*N*-(4-phenoxybenzyl)glycine (**15**, 27.2 mg, 0.056 mmol) and DIPEA (30 µl, 0.172 mmol) in MeCN (20 mL) was added EDC (12.0 mg, 0.063 mmol) at rt. After 30 min tert-butyl (2-(2-aminoethoxy)ethyl)carbamate (13.6 mg, 0.067 mmol) was added and the reaction mixture was stirred for 10 h. After full completion the mixture was concentrated *in vacuo* and purified by flash chromatography to yield tert-butyl (2-(2-(2-((2,2-dimethyl-*N*-(4-phenoxybenzyl)chromane)-6-sulfonamido)acetamido)ethoxy)ethyl)carbamate (8.0 mg, 0.012 mmol, 21% yield) as an oil. ^{1}H NMR ($CDCl_3$, 400 MHz) δ 7.60 – 7.52 (m, 2H), 7.39 – 7.29 (m, 2H), 7.25 – 7.17 (m, 2H), 7.17 – 7.05 (m, 1H), 7.02 – 6.95 (m, 2H), 6.95 – 6.86 (m, 3H), 6.77 (t, *J* = 5.7 Hz, 1H), 5.25 (bs, 1H), 4.28 (s, 2H), 3.66 (s, 2H), 3.50 (t, *J* = 5.1 Hz, 2H), 3.39 (t, *J* = 5.3 Hz, 2H), 3.36 – 3.25 (m, 4H), 2.82 (t, *J* = 6.7 Hz, 2H), 1.85 (t, *J* = 6.7 Hz, 2H), 1.41 (s, 9H), 1.37 (s, 6H).

***N*-(2-(2-Aminoethoxy)ethyl)-2-((2,2-dimethyl-*N*-(4-phenoxybenzyl)chromane)-6-sulfonamido)acetamide (29)**

To a stirred solution of tert-butyl (2-(2-(2-((2,2-dimethyl-*N*-(4-phenoxybenzyl)chromane)-6-sulfonamido)acetamido)ethoxy)ethyl)carbamate (**29a**, 6.0 mg, 8.98 µmol) in CH_2Cl_2 (2.0 mL) was added TFA (1 mL) at rt. After full completion (30 min) the mixture was concentrated *in vacuo* and purified by flash chromatography to yield *N*-(2-(2-aminoethoxy)ethyl)-2-((2,2-dimethyl-*N*-(4-phenoxybenzyl)chromane)-6-sulfonamido)acetamide (4.9 mg, 8.63 µmol, 96 % yield) as white solid needles. mp 265-267 °C. HRMS (ESI+) m/z: calculated for $C_{30}H_{38}N_3O_6S$ ([M + H]), 568.2476, found: 568.2475. ^{1}H NMR (MeOD, 400 MHz): δ 7.66 – 7.54 (m, 2H), 7.40 – 7.31 (m, 2H), 7.29 – 7.21 (m, 2H), 7.16 – 7.09 (m, 1H), 7.01 – 6.93 (m, 2H), 6.93 – 6.82 (m, 3H), 4.35 (s, 2H), 3.73 (s, 2H), 3.66 (t, *J* = 4.8 Hz, 2H), 3.48 (t, *J* = 5.4 Hz, 2H), 3,29 (t, *J* = 5.6, 2H), 3.12 (t, *J* = 4.8 Hz, 2H), 2.87 (t, *J* = 6.9 Hz, 2H), 1.87 (t, *J* = 6.7 Hz, 2H), 1.36 (s, 6H). ^{13}C NMR (MeOD, 101 MHz): δ171.40, 163.07, 159.74, 158.81, 131.96(2C), 131.44, 130.97(2C), 130.76, 130.00, 128.23, 124.72, 123.40, 120.05(2C), 119.66(2C), 118.95, 77.06, 70.71, 67.56, 54.00, 51.43, 40.62, 39.91, 33.16, 27.09(2C), 23.27. Purity 93% as determined by LC-MS.

2-((3-Phenoxybenzyl)amino)acetamide (30a)

The title compound was synthesized from 3-phenoxybenzaldehyde (**4**, 250 µl, 1.45 mmol) and 2-aminoacetamide (243 mg, 2.20 mmol) according to the procedure described for compound **8**. This yielded 2-((3-phenoxybenzyl)amino)acetamide (184.7 mg, 0.72 mmol, 50 %) as a white solid. ^{1}H NMR (MeOD, 400 MHz): δ 7.42 – 7.25 (m, 3H), 7.17 – 7.07 (m, 2H), 7.08 – 7.02 (m, 1H), 7.02 – 6.95 (m, 2H), 6.92 (dd, *J* = 8.2, 1.9 Hz, 1H), 3.85 (s, 2H), 3.37 (s, 1.4H), 3.35 (s, 0.6H).^{13}C NMR (MeOD, 101 MHz): δ 174.67, 159.10, 158.50, 140.69, 131.14, 130.93(2C), 124.68, 124.54, 120.02, 119.97(2C), 119.11, 53.29, 50.65. Signals split (7:3) due to rotamers.

2-((2,2-Dimethyl-*N*-(3-phenoxybenzyl)chromane)-6-sulfonamido)acetamide (30)

The title compound was synthesized from 2-((3-phenoxybenzyl)amino)acetamide (**30a**, 184 mg, 0.72 mmol) according to the procedure described for compound **13a**. This yielded 2-((2,2-dimethyl-*N*-(3-phenoxybenzyl)chromane)-6-sulfonamido)acetamide (144 mg, 0.30 mmol, 42 %) as a white solid. mp 122-124 °C. HRMS (ESI+) m/z: calculated for $C_{26}H_{29}N_2O_5S$ ([M + H]), 481.1792, found: 481.1785. ^{1}H NMR ($CDCl_3$, 400 MHz): δ 7.60 – 7.48 (m, 2H), 7.41 – 7.20 (m, 3H), 7.15 – 7.08 (m, 1H), 7.04 – 6.91 (m, 4H), 6.90 – 6.82 (m, 2H), 6.37 (s, 1H), 5.50 (s, 1H), 4.29 (s, 2H), 3.63 (s, 2H), 2.81 (t, *J* = 6.7 Hz, 2H), 1.84 (t, *J* = 6.7 Hz, 2H), 1.36 (s, 6H).^{13}C

NMR ($CDCl_3$, 101 MHz): δ 171.07, 158.72, 157.83, 156.91, 136.92, 130.37, 129.93(2C), 129.72, 127.58, 127.17, 123.82, 123.67, 122.01, 119.30, 119.09(2C), 118.85, 118.35, 76.10, 54.04, 51.43, 32.19, 27.00(2C), 22.46. Purity >95% as determined by LC-MS.

2-((4-Phenoxybenzyl)amino)acetamide (31a)

The title compound was synthesized from 4-phenoxybenzaldehyde (**5**, 300 µL, 1.71 mmol) and 2-aminoacetamide (226 mg, 2.06 mmol) according to the procedure described for compound **8**. This yielded 2-((4-phenoxybenzyl)amino)acetamide (300 mg, 1.17 mmol, 68 %) as a white solid. ^{1}H NMR (MeOD, 400 MHz): δ 7.35 – 7.24 (m, 4H), 7.04 (t, *J* = 7.4 Hz, 1H), 6.94 – 6.85 (m, 4H), 3.68 (s, 1.2H), 3.58 (0.8H), 3.20 (s, 2H). ^{13}C NMR (MeOD, 101 MHz): δ 176.70, 158.70, 158.08(0.6C), 157.92(0.4C), 135.41(0.6C), 134.27(0.4C), 131.72, 131.09(2C), 130.88(0.6C), 130.86(0.4C), 124.42(0.6C), 124.37(0.4C), 119.86, 119.80, 119.75, 119.69, 59.22(0.6C), 57.57(0.4C), 53.47(0.6C), 51.39(0.4C). Signals split (3:2) due to rotamers.

2-((2,2-Dimethyl-*N*-(4-phenoxybenzyl)chromane)-6-sulfonamido)acetamide (31)

The title compound was synthesized from 2-((4-phenoxybenzyl)amino)acetamide (**31a**, 200 mg, 0.780 mmol) according to the procedure described for compound **13a**. This yielded 2-((2,2-dimethyl-N-(4-phenoxybenzyl)chromane)-6-sulfonamido)acetamide (237.0 mg, 0.493 mmol, 63 % yield) as a white solid. ^{1}H NMR ($CDCl_3$, 400 MHz) δ 7.59 (d, *J* = 1.6 Hz, 1H), 7.52 (dd, *J* = 8.6, 2.1 Hz, 1H), 7.45 – 7.29 (m, 3H), 7.25 – 7.22 (m, 1H), 7.20 (s, 1H), 7.17 – 7.09 (m, 1H), 7.05 (s, 1H), 7.02 – 6.96 (m, 2H), 6.95 – 6.90 (m, 2H), 6.84 (d, *J* = 8.6 Hz, 1H), 4.34 (s, 2H), 3.66 (s, 2H), 2.78 (t, *J* = 6.7 Hz, 2H), 1.79 (t, *J* = 6.7 Hz, 2H), 1.30 (s, 6H).

***N*-(Cyanomethyl)-2,2-dimethyl-*N*-(3-phenoxybenzyl)chromane-6-sulfonamide (32)**

To a stirred solution of 2-((2,2-dimethyl-*N*-(3-phenoxybenzyl)chromane)-6-sulfonamido)acetamide (**30**, 46.4 mg, 0.10 mmol) in THF (5 mL) at 0 °C was added pyridine (0.05 mL, 0.62 mmol) and then TFAA (0.04 mL, 0.28 mmol). The reaction was warmed up to rt and stirred for 2h until completion. The mixture was then diluted with EtOAc, washed with water and brine, dried, concentrated *in vacuo* and purified by flash chromatography to yield *N*-(cyanomethyl)-2,2-dimethyl-*N*-(3-phenoxybenzyl)chromane-6-sulfonamide (30.4 mg, 0.07 mmol, 69 %) as a white solid after lyophilization. mp 90-92 °C. HRMS (ESI+) m/z: calculated for $C_{26}H_{26}N_2O_4SNa$ ([M + Na]), 485.1505, found: 485.1504. ^{1}H NMR ($CDCl_3$, 400 MHz): δ 7.66 – 7.52 (m, 2H), 7.42 – 7.28 (m, 3H), 7.20 – 7.16 (m, 1H), 7.14 (tt, J = 7.2, 1.2 Hz, 1H), 7.10 – 7.06 (m, 1H), 7.02 – 6.93 (m, 3H), 6.91 (d, *J* = 8.6 Hz, 1H), 4.28 (s, 2H), 4.06 (s, 2H), 2.85 (t, *J* = 6.8 Hz 2H), 1.85 (t, *J* = 6.7 Hz, 2H), 1.36 (s, 6H).^{13}C NMR ($CDCl_3$, 101 MHz): δ 159.10, 158.16, 156.69, 135.74, 130.56, 130.02(2C), 129.91, 127.37, 127.02, 123.87, 123.39, 122.22, 119.25(2C), 118.93, 118.85, 118.51, 113.47, 76.17, 50.94, 34.62, 32.23, 27.00(2C), 22.49. Purity >95% as determined by LC-MS.

***N*-(Cyanomethyl)-2,2-dimethyl-*N*-(4-phenoxybenzyl)chromane-6-sulfonamide (33a)**

The title compound was synthesized from 2-((2,2-dimethyl-*N*-(4-phenoxybenzyl)chromane)-6-sulfonamido)acetamide (**31**, 86.2 mg, 0.179 mmol) according to the procedure described for compound **32**. This yielded *N*-(cyanomethyl)-2,2-dimethyl-*N*-(4-phenoxybenzyl)chromane-6-sulfonamide (51.3 mg, 0.111 mmol, 62 %) as an oil. ^{1}H NMR ($CDCl_3$, 400 MHz): δ 7.63 (d, *J* = 2.3 Hz, 1H), 7.61 (dd, *J* = 8.6, 2.4 Hz, 1H), 7.40 – 7.32 (m, 2H), 7.32 – 7.27 (m, 2H), 7.18 – 7.10 (m, 1H), 7.06 – 6.95 (m, 4H), 6.93 (d, J = 8.5 Hz, 1H), 4.28 (s, 2H), 4.05 (s, 2H), 2.86 (t, *J* = 6.7 Hz, 2H), 1.86 (t, J = 6.7 Hz, 2H), 1.37 (s, 6H).^{13}C NMR ($CDCl_3$, 101 MHz): δ 159.08, 158.08, 156.64, 130.52(2C), 130.02(2C), 129.91, 128.02, 127.37, 127.15, 123.94, 122.23, 119.45(2C), 119.04(2C), 118.51, 113.54, 76.17, 50.61, 34.46, 32.27, 27.01(2C), 22.51.

***N*-(2-Aminoethyl)-2,2-dimethyl-*N*-(4-phenoxybenzyl)chromane-6-sulfonamide (33)**

To a stirred solution of *N*-(cyanomethyl)-2,2-dimethyl-*N*-(4-phenoxybenzyl)chromane-6-sulfonamide (**33a**, 21.3 mg, 0.046 mmol) in THF (5 mL) was added borane THF complex (0.092 ml, 0.092 mmol) at 0 °C. The reaction mixture was heated for 10 h. at reflux. After full completion the mixture was quenched with 5 mL MeOH followed by 1M HCl (10 mL) and the reaction was refluxed for 2h, diluted with EtOAc, washed with $NaHCO_3$, brine, dried, concentrated *in vacuo* and purified by flash chromatography to yield *N*-(2-aminoethyl)-2,2-dimethyl-*N*-(4-phenoxybenzyl)chromane-6-sulfonamide (11.6 mg, 0.025 mmol, 54 %) as a white solid after lyophilization. mp not determined. HRMS (ESI+) m/z: calculated for $C_{26}H_{31}N_2O_4S$ ([M + H]), 467.1999, found: 467.1998. ^{1}H NMR ($CDCl_3$, 400 MHz): δ 7.58 (s, 1H), 7.56 – 7.47 (m, 1H), 7.36 – 7.28 (m, 2H), 7.18 (d, *J* = 8.2 Hz, 2H), 7.09 (t, *J* = 7.4 Hz, 1H), 7.03 – 6.94 (m, 2H), 6.87 (d, *J* = 8.1 Hz, 2H), 6.82 (d, *J* = 8.6 Hz, 1H), 4.27 (s, 2H), 3.41 (m, 2H), 2.96 (m, 2H), 2.79 (t, *J* = 6.3 Hz, 3H), 1.79 (t, *J* = 6.6 Hz, 3H), 1.33 (s, 6H). ^{13}C NMR ($CDCl_3$, 101 MHz): δ 159.75, 159.00, 158.17, 132.12, 131.63(2C), 131.00(2C), 130.62, 129.86, 128.06, 124.84, 123.51, 120.17(2C), 119.74(2C), 119.06, 77.07, 54.39, 47.81, 40.11, 33.14, 27.09(2C), 23.28. Purity >95% as determined by LC-MS.

***N*-((1*H*-Tetrazol-5-yl)methyl)-2,2-dimethyl-*N*-(3-phenoxybenzyl)chromane-6-sulfonamide (34)**

To a stirred solution of *N*-(cyanomethyl)-2,2-dimethyl-*N*-(3-phenoxybenzyl)chromane-6-sulfonamide (**32**, 57.4 mg, 0.12 mmol) in toluene (10 mL) was added Et_3N.HCl (51.4 mg, 0.37 mmol) and sodium azide (22.4 mg, 0.35 mmol). The reaction mixture was stirred for 120 h. at reflux. After full completion, the organic layer was washed with brine, dried, concentrated *in vacuo* and purified by flash chromatography to yield *N*-((1*H*-tetrazol-5-yl)methyl)-2,2-dimethyl-*N*-(3-phenoxybenzyl)chromane-6-sulfonamide (10.2 mg, 0.02 mmol, 16 %) as a white solid after lyophilization. mp 53-55 °C. HRMS (ESI+) m/z: calculated for $C_{26}H_{28}N_5O_4S$ ([M + H]), 506.1857, found: 506.1855. ^{1}H NMR ($CDCl_3$, 400 MHz): δ 8.01 (bs, 1H), 7.59 – 7.48 (m, 2H), 7.34 (t, *J* = 7.8 Hz, 2H), 7.20 (t, *J* = 7.9 Hz, 1H), 7.12 (t, *J* = 7.3 Hz, 1H), 6.97 – 6.82 (m, 5H), 6.82 – 6.74 (m, 1H), 4.52 (s, 2H), 4.35 (s, 2H), 2.80 (t, *J* = 5.9 Hz, 2H), 1.84 (t, *J* = 6.0 Hz, 2H), 1.36 (s, 6H).^{13}C NMR ($CDCl_3$, 101 MHz): δ 159.08, 157.96, 156.72, 152.89, 136.51, 130.41, 130.01(2C), 129.66, 127.34, 127.12, 123.76, 123.29, 122.28, 119.20(2C), 118.76, 118.66, 118.60, 76.31, 52.79, 40.82, 32.16, 27.03(2C), 22.48. Purity >95% as determined by LC-MS.

References

1. Katona, I.; Freund, T. F. Multiple functions of endocannabinoid signaling in the brain. *Annu. Rev. Neurosci.* **2012,** *35*, 529-558.
2. Gao, Y.; Vasilyev, D. V.; Goncalves, M. B.; Howell, F. V.; Hobbs, C.; Reisenberg, M.; Shen, R.; Zhang, M. Y.; Strassle, B. W.; Lu, P.; Mark, L.; Piesla, M. J.; Deng, K.; Kouranova, E. V.; Ring, R. H.; Whiteside, G. T.; Bates, B.; Walsh, F. S.; Williams, G.; Pangalos, M. N.; Samad, T. A.; Doherty, P. Loss of retrograde endocannabinoid signaling and reduced adult neurogenesis in diacylglycerol lipase knock-out mice. *J. Neurosci.* **2010,** *30*, 2017-2024.
3. Tanimura, A.; Yamazaki, M.; Hashimotodani, Y.; Uchigashima, M.; Kawata, S.; Abe, M.; Kita, Y.; Hashimoto, K.; Shimizu, T.; Watanabe, M.; Sakimura, K.; Kano, M. The endocannabinoid 2-arachidonoylglycerol produced by diacylglycerol lipase alpha mediates retrograde suppression of synaptic transmission. *Neuron* **2010,** *65*, 320-327.
4. Mackie, K. Cannabinoid receptors as therapeutic targets. *Annu. Rev. Pharmacol. Toxicol.* **2006,** *46*, 101-122.
5. Nomura, D. K.; Morrison, B. E.; Blankman, J. L.; Long, J. Z.; Kinsey, S. G.; Marcondes, M. C.; Ward, A. M.; Hahn, Y. K.; Lichtman, A. H.; Conti, B.; Cravatt, B. F. Endocannabinoid hydrolysis generates brain prostaglandins that promote neuroinflammation. *Science* **2011,** *334*, 809-813.
6. Valdeolivas, S.; Pazos, M. R.; Bisogno, T.; Piscitelli, F.; Iannotti, F. A.; Allara, M.; Sagredo, O.; Di Marzo, V.; Fernandez-Ruiz, J. The inhibition of 2-arachidonoyl-glycerol (2-AG) biosynthesis, rather than enhancing striatal damage, protects striatal neurons from malonate-induced death: a potential role of cyclooxygenase-2-dependent metabolism of 2-AG. *Cell. Death. Dis.* **2013,** *4*, 862.
7. Alhouayek, M.; Masquelier, J.; Cani, P. D.; Lambert, D. M.; Muccioli, G. G. Implication of the anti-inflammatory bioactive lipid prostaglandin D2-glycerol ester in the control of macrophage activation and inflammation by ABHD6. *Proc. Natl. Acad. Sci. USA* **2013,** *110*, 17558-17563.
8. Di Marzo, V. Targeting the endocannabinoid system: to enhance or reduce? *Nat. Rev. Drug. Discov.* **2008,** *7*, 438-455.
9. Kohnz, R. A.; Nomura, D. K. Chemical approaches to therapeutically target the metabolism and signaling of the endocannabinoid 2-AG and eicosanoids. *Chem. Soc. Rev.* **2014**.
10. Bisogno, T.; Howell, F.; Williams, G.; Minassi, A.; Cascio, M. G.; Ligresti, A.; Matias, I.; Schiano-Moriello, A.; Paul, P.; Williams, E. J.; Gangadharan, U.; Hobbs, C.; Di Marzo, V.; Doherty, P. Cloning of the first sn1-DAG lipases points to the spatial and temporal regulation of endocannabinoid signaling in the brain. *J. Cell. Biol.* **2003,** *163*, 463-468.
11. Baggelaar, M. P.; Janssen, F. J.; van Esbroeck, A. C.; den Dulk, H.; Allara, M.; Hoogendoorn, S.; McGuire, R.; Florea, B. I.; Meeuwenoord, N.; van den Elst, H.; van der Marel, G. A.; Brouwer, J.; Di Marzo, V.; Overkleeft, H. S.; van der Stelt, M. Development of an activity-based probe and in silico design reveal highly selective inhibitors for diacylglycerol lipase-alpha in brain. *Angew. Chem. Int. Ed.* **2013,** *52*, 12081–12085.
12. Bisogno T., C. M. G., Saha B., Mahadevan A., Urbani P., Minassi A., Appendino G., Saturnino C., Martin B., Razdan R., Di Marzo V. Development of the first potent and specific inhibitors of endocannabinoid biosynthesis. *Biochim. Biophys. Acta.* **2006,** *1761*, 205–212.
13. Bisogno, T.; Burston, J. J.; Rai, R.; Allara, M.; Saha, B.; Mahadevan, A.; Razdan, R. K.; Wiley, J. L.; Di Marzo, V. Synthesis and pharmacological activity of a potent inhibitor of the biosynthesis of the endocannabinoid 2-arachidonoylglycerol. *ChemMedChem* **2009,** *4*, 946-950.
14. Bisogno, T.; Mahadevan, A.; Coccurello, R.; Chang, J. W.; Allara, M.; Chen, Y.; Giacovazzo, G.; Lichtman, A.; Cravatt, B.; Moles, A.; Di Marzo, V. A novel fluorophosphonate inhibitor of the biosynthesis of the endocannabinoid 2-arachidonoylglycerol with potential anti-obesity effects. *Br. J. Pharmacol.* **2013,** *169*, 784-793.
15. Ortar, G.; Bisogno, T.; Ligresti, A.; Morera, E.; Nalli, M.; Di Marzo, V. Tetrahydrolipstatin analogues as modulators of endocannabinoid 2-arachidonoylglycerol metabolism. *J. Med. Chem.* **2008,** *51*, 6970-6979.
16. Hsu, K. L.; Tsuboi, K.; Adibekian, A.; Pugh, H.; Masuda, K.; Cravatt, B. F. DAGLbeta inhibition perturbs a lipid network involved in macrophage inflammatory responses. *Nat. Chem. Biol.* **2012,** *8*, 999-1007.

17. Thomas, G.; Betters, J. L.; Lord, C. C.; Brown, A. L.; Marshall, S.; Ferguson, D.; Sawyer, J.; Davis, M. A.; Melchior, J. T.; Blume, L. C.; Howlett, A. C.; Ivanova, P. T.; Milne, S. B.; Myers, D. S.; Mrak, I.; Leber, V.; Heier, C.; Taschler, U.; Blankman, J. L.; Cravatt, B. F.; Lee, R. G.; Crooke, R. M.; Graham, M. J.; Zimmermann, R.; Brown, H. A.; Brown, J. M. The serine hydrolase ABHD6 Is a critical regulator of the metabolic syndrome. *Cell. Rep.* **2013,** *5*, 508-520.
18. Long, J. Z.; Cravatt, B. F. The metabolic serine hydrolases and their functions in mammalian physiology and disease. *Chem. Rev.* **2011,** *111*, 6022-6063.
19. Simon, G. M.; Cravatt, B. F. Activity-based proteomics of enzyme superfamilies: serine hydrolases as a case study. *J. Biol. Chem.* **2010,** *285*, 11051-11055.
20. Appiah, K. K.; Blat, Y.; Robertson, B. J.; Pearce, B. C.; Pedicord, D. L.; Gentles, R. G.; Yu, X. C.; Mseeh, F.; Nguyen, N.; Swaffield, J. C.; Harden, D. G.; Westphal, R. S.; Banks, M. N.; O'Connell, J. C. Identification of small molecules that selectively inhibit diacylglycerol lipase-alpha activity. *J. Biomol. Screen.* **2014,** *19*, 595-605. .
21. Chupak, L. S., Zheng, X. Ding, M., Hu, S., Huang, Y., Gentles, R.G. Glycine chroman-6-sulfonamides for use as inhibitors of diacylglycerol lipase. US2011.0207749 A1. **2011**.
22. Johnson, D. S.; Stiff, C.; Lazerwith, S. E.; Kesten, S. R.; Fay, L. K.; Morris, M.; Beidler, D.; Liimatta, M. B.; Smith, S. E.; Dudley, D. T.; Sadagopan, N.; Bhattachar, S. N.; Kesten, S. J.; Nomanbhoy, T. K.; Cravatt, B. F.; Ahn, K. Discovery of PF-04457845: a highly potent, orally bioavailable, and selective urea FAAH Inhibitor. *ACS Med. Chem. Lett.* **2011,** *2*, 91-96.
23. Pedicord, D. L.; Flynn, M. J.; Fanslau, C.; Miranda, M.; Hunihan, L.; Robertson, B. J.; Pearce, B. C.; Yu, X. C.; Westphal, R. S.; Blat, Y. Molecular characterization and identification of surrogate substrates for diacylglycerol lipase alpha. *Biochem. Biophys. Res. Commun.* **2011,** *411*, 809-814.
24. Chang, J. W.; Cognetta, A. B., 3rd; Niphakis, M. J.; Cravatt, B. F. Proteome-wide reactivity profiling identifies diverse carbamate chemotypes tuned for serine hydrolase inhibition. *ACS Chem. Biol.* **2013,** *8*, 1590-1599.
25. Krieger, E.; Koraimann, G.; Vriend, G. Increasing the precision of comparative models with YASARA NOVA a self-parameterizing force field. *Proteins* **2002,** *47*, 393-402.
26. Trott, O.; Olson, A. J. AutoDock Vina: improving the speed and accuracy of docking with a new scoring function, efficient optimization, and multithreading. *J. Comput. Chem.* **2010,** *31*, 455-461.
27. Navia-Paldanius, D.; Savinainen, J. R.; Laitinen, J. T. Biochemical and pharmacological characterization of human alpha/beta-hydrolase domain containing 6 (ABHD6) and 12 (ABHD12). *J. Lipid. Res.* **2012,** *53*, 2413-2424.
28. Matias, I.; Di Marzo, V. Endocannabinoids and the control of energy balance. *Trends Endocrinol. Metab.* **2007,** *18*, 27-37.
29. Kirkham, T. C. Endocannabinoids and the non-homeostatic control of appetite. *Curr. Top. Behav. Neurosci.* **2009,** *1*, 231-253.
30. Dou, D.; Mandadapu, S. R.; Alliston, K. R.; Kim, Y.; Chang, K. O.; Groutas, W. C. Design and synthesis of inhibitors of noroviruses by scaffold hopping. *Bioorg. Med. Chem.* **2011,** *19*, 5749-5755.
31. Kharul, R., Bhuniya, D., Mookhtiar, K.A., Singu, U., Hazare, A., Patil, S., Datrange, L., Thakkar, M. Amide compounds, compositions and applications thereof. *WO2013.42139 A1* **2013**.

CHAPTER 6

Discovery of sulfonyl-1,2,4-triazole ureas as *sn*-1 diacylglycerol lipase α inhibitors by HTS-ABPP*

Introduction

The European Lead Factory (ELF), part of the Innovative Medicines Initiative (IMI), is a collaborative European drug discovery platform, aiming at facilitating European drug discovery projects.[1] The ELF provides high throughput screening facilities, expertise and access to the Joint European Compound Library (JECL), a diverse 300.000+ compound library from proprietary collections of seven pharmaceutical companies.[2] Collaborations with ten academic groups and six small and medium enterprises, all part of the ELF Chemistry Consortium, have contributed an additional 100.000 novel compounds so far. This Public Compound Collection (PCC) is developed to occupy novel explored chemical space using newly developed synthetic routes, and is expected to rise to a total of ~200.000 compounds in the future.[3] The combined JECL/ PCC can be screened in the ELF program by European academic and private parties, provided that the assay target is innovative and has relevance for disease. Furthermore, feasibility of the assay in 384-well plate format has to be demonstrated. Importantly, a milestone payment system has been created in case drug-like hits, leads or drug candidates will be identified and commercialized.[3,4]

Diacylglycerol lipases (DAGLs) are serine hydrolases responsible for the formation of the endocannabinoid 2-arachidonoylglycerol (2-AG). 2-AG is a full agonist of the cannabinoid CB1 and CB2 receptors (CB1R/CB2R) and functions as the main precursor for arachidonic acid and pro-inflammatory eicosanoids in the brain.[5] The dual role of 2-AG signifies that DAGLs could be important targets for therapeutic intervention for diseases

* Janssen, F.J, van Esbroeck, A.C.M.; Baggelaar, M.P.; den Dulk, H.; van Doornmalen, E.; Smits, N.; Morrison, A.; Russell, E.; Schulz, J.; Brown, L.; Hewitt, J.; MacLeod, F.; Robinson, J.; Geurink, P.P.; Ovaa, H.; Overkleeft, H.S.; McElroy, S.P.I.; van Boeckel, C.A.A., Rutjes, H.; Jones, P.S.; van der Stelt, M. This research has received support from the Innovative Medicines Initiative Joint Undertaking under grant agreement n' 115489, resources of which are composed of financial contribution from the European Union's Seventh Framework Programme (FP7 / 2007-2013) and EFPIA companies in-kind contribution.

where excessive 2-AG signaling (or metabolites) contributes to the specific pathophysiology (*e.g.* metabolic and neurodegenerative diseases, see Chapter 8).[6] Several DAGL inhibitors have been reported in the literature,[6] but most of these compounds do not possess the activity, selectivity or pharmacokinetic properties to act as drug candidates, or as tools to study the role of 2-AG in health and disease. Thus, there is an unmet need to identify novel chemotypes to modulate DAGLα activity.

In principle, there are two general strategies to identify new chemical matter to modulate targets: structure-based drug design (SBDD) and ligand-based drug design (LBDD). The discovery of selective DAGLα inhibitors through a SBDD-approach is, however, hampered by a lack of structural knowledge of the target, as no crystal structures are available for DAGLα. Since several biochemical assays to identify DAGL inhibitors have been reported in the literature, a LBDD-approach using high throughput screening (HTS) has been shown to be viable option. For instance, researchers from Bristol-Myers-Squibb (BMS) reported on the development of two types of surrogate substrate assays using the hydrolysis of *para*-nitrophenyl (PNP) butyrate and 6,8-difluoro-4-methylumbelliferyl (DiMFU) octanoate by membrane fractions of HEK293 cells that express recombinant human DAGLα.[7] Subsequently, BMS performed a HTS on DAGLα, using the DiMFU-octanoate as a fluorogenic surrogate substrate.[7,8] The assay was of high quality and provided signal to background (S/B) ratios of 5-8 and Z` values of ~0.7 for the most optimal conditions in 384-well format. Approximately one million compounds were screened and 314 actives were identified. During the hit triage, two deselection assays were performed to assess selectivity over monoacylglycerol lipase (MAGL) and pancreatic lipase (PL). From the DAGLα lead chemotype series that was selective over the two off-targets tested, three compounds were ultimately reported (**1**-**3**, Figure 1). Glycine sulfonamide **2** was selected for lead optimization.[8]

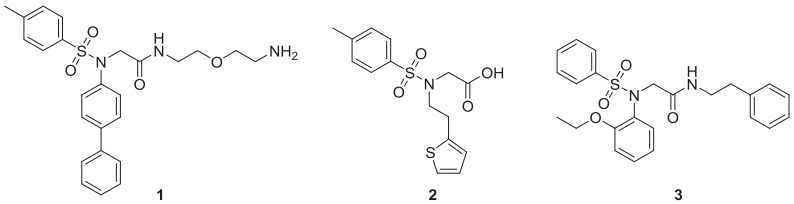

Figure 1. Three reported compounds from the lead chemotype series discovered by researchers of Bristol-Myers-Squibb (BMS).[8] Glycine sulfonamide **2** was selected for lead optimization.

DAGL, MAGL and PL all belong to the serine hydrolases, a 200+ membered family of enzymes that use an active site serine for substrate hydrolysis. Therefore, family-wide selectivity screening over many serine hydrolases is important to identify potential DAGL inhibitor off-targets, especially over targets within the endocannabinoid system. Activity-based protein profiling (ABPP) is a highly useful method to assess potency and selectivity of serine hydrolase inhibitors in complex samples, such as tissue or cell homogenates.[9] Surprisingly, very few examples in literature use ABPP in combination with HTS assays to test inhibitor

selectivity in the earliest possible stage of inhibitor discovery.[10] Baggelaar *et al*. reported on the first DAGLα targeting activity-based probe (ABP). Here, HTS-ABPP is employed to identify several novel chemotypes for DAGLα, within a lead discovery program executed in the framework of a public-private partnership with the ELF.

Results & Discussion

Optimization to 384-well-plate format and proof of principle screen

Previously, the colorimetric 96-well plate *para*-nitrophenyl (PNP) butyrate activity assay, utilizing membrane fractions of HEK293T cells overexpressing DAGLα (Figure 2A), successfully confirmed α-ketoheterocyles as DAGL inhibitors, which were identified by virtual screening of a pharmacophore model (Chapter 2).[11] To apply this assay for HTS-screening by the ELF, miniaturization to 384-wells format was required.[7,11] To this end, the assay volume (V) was reduced to highest volume possible (30 µL), to ensure optimal cross-section in 384-well plate. The enzyme concentration was varied and found to be optimal at 0.05 µg/µL.[7,11] These conditions provided optimal S/B and Z' values (Figure 2 B,C). Endpoint measurements instead of rate determination was applied to increase HTS efficiency (60 minutes as single endpoint, S/B = 2.8). Using this protocol, a proof-of-principle screen was conducted on the commercially available Library of Pharmacologically Active Compounds 1280 (LOPAC®, Sigma Aldrich). All 1280 compounds were screened at 10 µM (N = 2, n = 2) with high Z' (0.73 ± 0.08) and S/B values (3.4 ± 0.5). The screen delivered 26 actives with > 50% effect (Table S1). Eight hits were selected for full determination of dose-response curves based on their chemical structure and/or activity on their original target (Table S1, **bold**). cRaf1 kinase inhibitor **4,** containing a highly acidic phenol (carboxylic acid mimetic), was the only compound demonstrating dose-dependent reduction in DAGLα activity, but its activity could not be confirmed in detergent-containing assay buffer (Tween 0.05% m/m). This indicated that compound **4** is a false positive hit that possibly forms aggregates (Figure 2D). Nevertheless, the colorimetric 384-well assay fulfilled the assay requirements (Z' ~ 0.7 and S/B ~ 3) of the ELF for target acceptance and an application was submitted. After the target was approved by the ELF, the 384-well assay was optimized to 1536-well plate within the ELF consortium.

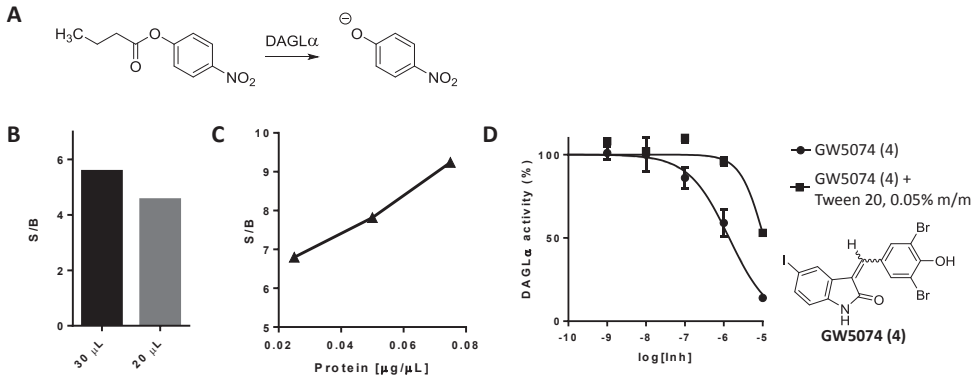

Figure 2. Development of a high throughput 384-well plate hDAGLα activity assay **A)** The assay is based on the conversion of *p*-nitrophenyl (PNP)-butyrate by HEK293T membrane fractions overexpressing hDAGLα. OD_{405} is measured over time. S/B is determined from the slope over 5-30 min. **B)** Optimization of assay volume per well; 30 µL volume provides better S/B values, N = 1 **C)** Optimization of protein concentration. Corresponding Z' values are: 0.26, 0.63 and 0.25 for a protein concentration of 0.025, 0.05 and 0.075 µg/µL respectively. Plate variance is optimal with 0.05 µg/µL DAGLα, N = 4. S/B and Z' are determined from the slope over 5-30 min. **D)** Profiling of hit compound **4** in dose response analysis with and without detergent Tween® 20 (0.05% m/m). Final screening conditions are: Clear 384-well plate, 30 µL volume, 5% DMSO, 10 µM inhibitor, 0.05 µg/µL membrane protein, 50 mM HEPES pH = 7.0, 20 minutes pre-incubation, then 300 µM PNP-butyrate. S/B is determined from the slope over 5-30 min. Endpoint at 60 minutes (OD_{405}) provides S/B values of ~2.8 (30 µL volume). Dose response analysis of hit **4** is performed in 96-well plate (as previously reported[7,11,12]). pIC_{50} for GW5074 = 5.86 ± 0.09 (normal conditions) and a ten-fold drop in potency, pIC_{50} = 4.96 ± 0.04 with Tween®20, N = 2, n = 2. This indicates **4** is a false positive. Reported concentrations are final concentrations.

Optimization to 1536-well-plate format

Substrate stability and plate edge effects: The stability of the substrate (PNP-butyrate) in assay buffer was investigated to prevent degradation, due to long storage times (up to several days) during the screening campaign. Two 0.9 mM PNP-butyrate solutions in assay buffer were stored at either room temperature or 0°C and absorption over time at 405 nm was measured over a consecutive period of 6 hours (Figure 3A). The background signal increased over time, indicating spontaneous hydrolysis of the substrate at room temperature. Substrate storage at 0°C is, therefore, essential to prevent spontaneous hydrolysis over time, especially if storage times in buffer exceed 2 h. Plate edge effect in 1536-well plates was significantly less in black clear-bottom plates compared to general clear plates as determined by a tartrazine absorption analysis (data not shown).

Substrate and protein concentration: For assay optimization to 1536-well plate, the total volume was kept at a maximum of 8.0 µL per well using the same protein and substrate concentration as in the 384-well plate assay. As expected, lower Z' and S/B values were obtained (0.64 and 2.73 respectively), presumably due to a smaller well cross section. Subsequent assay optimization focused on increasing the S/B ratios and Z' values by varying the substrate and enzyme concentrations (Figure 3B,C). First, the substrate concentration was screened in 0.3 – 1.2 mM final concentration range. Low substrate concentrations (0.3

mM) were associated with low S/B values due to lower turnover, whereas concentrations over 0.6 mM did not significantly improve S/B ratios (Figure 3B). Consequently, 0.6 mM PNP-butyrate was chosen as the optimal substrate concentration. Next, the enzyme concentration was varied and determined best at 0.025 µg/µL, which is two-fold lower than in the 384-well protocol (Figure 3C). Several validation runs using automated robotic handling and liquid dispensing demonstrated that the assay protocol was reproducible and robust. The final protocol was accepted for ultra-HTS on the Joint European Compound Library.

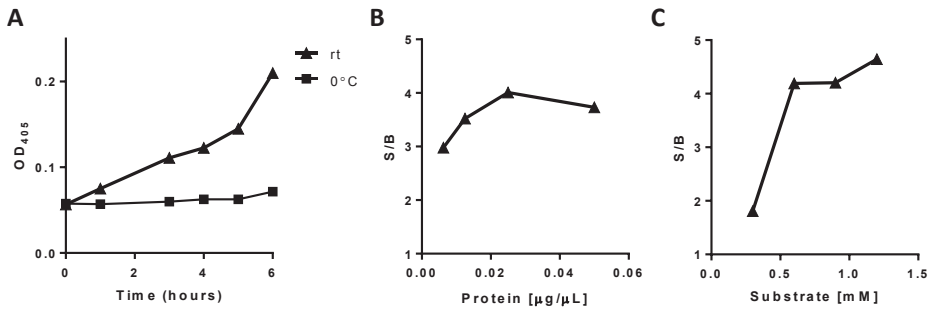

Figure 3. Development of the 1536-well plate hDAGLα activity assay. **A)** Stability test of the PNP-butyrate in assay buffer at rt and 0°C (ice). Optimal substrate storage is at 0°C. **B)** Optimization of PNP-butyrate substrate concentration. 0.6 mM was chosen as optimal since increasing the substrate concentration (1.5 or 2 fold) did not significantly improve S/B values. **C)** Optimization of protein concentration. 0.025 µg/µL was chosen as optimal. Final screening conditions are: Black Corning clear bottom 1536-well plates, 8.0 µL volume, 0.25% DMSO, 10 µM inhibitor, 0.025 µg/µL DAGLα protein, 50 mM HEPES pH = 7.0, 20 minutes pre-incubation, then 600 µM PNP-butyrate, endpoint at 90 minutes (OD_{405}). Reported concentrations are final concentrations.

High throughput screening and orthogonal ABPP assay

302.655 Compounds were screened in three days using the optimized 1536-well protocol. The primary assay resulted in 1932 hits with ≥50% effect at 10 µM inhibitor (Figure 4A, for exact values see Table S2), which corresponds to a 0.64% hit rate. The low hit rate suggested that the ELF library consists of high quality compounds with good physicochemical properties[2] and few pan-assay interference compounds (PAINS).[13] The course of the Z' and S/B values over the primary assay was monitored and is depicted in Figure 4B-C, showing the assay is robust and of good quality (S/B ~6, Z' ~0.8). Active conformation was performed at two inhibitor concentrations (10 and 1.25 µM, Table S2), resulting in a total of 263 confirmed actives (>70% eff. at 10 µM or >50% eff. at 1.25 µM)

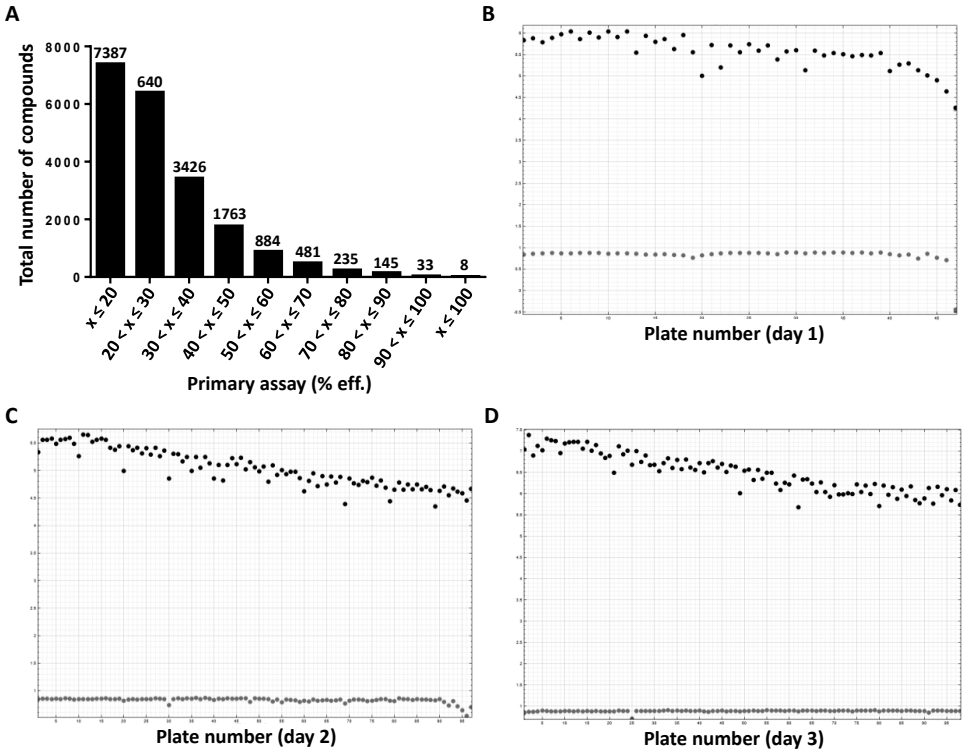

Figure 4: Overview of the HTS and assessment of screening quality over all 242 screened 1536-well plates. **A)** Total number of actives grouped per % effect. **B**-**D**) Assessment of assay quality of the primary assay over days 1-3 (B-D, respectively). A total of 47, 97 and 98 plates were measured on days 1-3. As shown, S/B (—●—) values are ~6, Z' (—●—) values are ~0.8.

To determine the activity and selectivity of the confirmed actives on endogenous DAGLα, the 263 confirmed actives were screened in an orthogonal ABPP assay on mouse brain proteome. A low throughput gel-based ABPP assay was developed based on previously reported protocols (see Experimental).[8] Using this protocol, the confirmed actives were screened at a single concentration (10 μM) for inhibition of DAGLα labeling by activity-based probe MB064 (**1**). The percentage inhibitory effect on DAGLα was calculated and normalized to control and corrected for protein loading using Coomassie staining (DMSO, N = 1).[8] Many of the compounds were less active in the ABPP assay than in the primary assay (Figure 5A, exemplary gel see 5B). However, several compounds demonstrated high activity also in the orthogonal assay, thereby confirming their cross-species DAGLα inhibitory activity. Importantly, the orthogonal ABPP assay also revealed the selectivity profile of the compounds over several other serine hydrolases, such as DDHD2, ABHD16, ABHD12, ABHD6 and LypLA2. The information of the orthogonal assay was taken into account and the hits were triaged by potency, selectivity and chemical eye (Table 1). The purity and correct m/z

of the compounds was analyzed by LC-MS. After clustering and legal clearance, the qualified hit list (QHL) contained 46 compounds (Table 2).

Table 1. Ultra-HTS assay triage overview. 46 Compounds form the Qualified Hit List (QHL).

	Compounds	Cut-off	% Total
Total screened	302.655	-	100
Primary assay hits	1932	>50% eff. (10 µM)	0.64
Active conformation hits	263	>70% eff. (10 µM) >50% eff. (1.25 µM)	0.09
Triaging and orthogonal assay[a]	46	Chemical eye, clustering, legal, purity	0.02

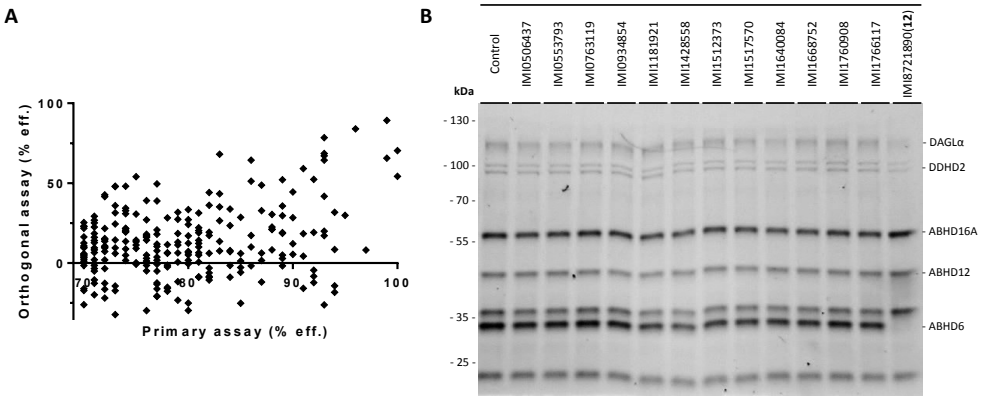

Figure 5. A) Analysis of the orthogonal assay versus primary assay (% eff. at 10 µM inhibitor). **B)** Exemplary gel of the orthogonal ABPP assay, consisting of a total of 21 analysed gels. Final ABPP screening conditions are: Incubation in 384-well plate, 20 µL Mouse brain membrane, 10 µM inhibitor (50 nL in DMSO), 30 minutes pre-incubation, then 250 nM MB064, 15 min, 2.8% DMSO, quench with 10 uL 3x Sample Buffer. All 21 gels were analysed according to the screening conditions reported. Percentage effect ABPP for DAGLα is calculated from the obtained gels, normalized for control and corrected for protein loading by Coomassie staining (N = 1). Reported concentrations are final concentrations.

Qualified hit list

The QHL contained 10 clusters of various chemotypes and 10 singletons (see Table 2) with IC_{50}-values in the range of 100-10000 nM. Actives from four distinct series were selected for resynthesis and retesting; glycine sulfonamides, α-keto amides, β-keto-α,α-difluoro amides and sulfonyl-1,2,4-triazole ureas. The two most potent compounds, IMI4906626 (**5**) and IMI4749305 (**6**) belong to the glycine sulfonamides series (Table 2, page 119), a series previously published as potent DAGLα inhibitors[8,14–16] that cross-react with ABHD6.[16] Noteworthy, compound **6** has a remarkable similarity to the previously reported LEI106 (Chapter 5) and has excellent ligand efficiency (LE = 0.36) and lipophilic efficiency (LipE = 4.3).[16] The European Screening Centre resynthesized compound **5** and confirmed its structure and activity in the PNP-assay (see experimental section). The potency of **5** is 32 nM (IC_{50}), LE is 0.29 and LipE is 3.6. Compound **5** possesses a free carboxylic acid and has

intrinsically high polar surface area (tPSA > 80 Å^2), which makes it interesting for the development of peripherally restricted inhibitors.[15] After resynthesis, compound **5** was retested on ABPP using broad-spectrum serine hydrolase probe TAMRA-FP and also MB064. This selectivity assessment showed that **5** was selective over all off-targets tested on ABPP, including ABHD6 (Figure 6B,C) which makes **5** the first known reported glycine sulfonamide inhibitor with this selectivity profile. Consequently, **5** could provide an excellent starting point for a hit optimization program.

Two additional clusters consist of α-keto amides **7**-**9** and β-keto-α,α-difluoro amides **10**, **11** (Table 2). Compounds **7-11** were resynthesized by the European Screening Centre (see experimental methods) and their structure and activity was confirmed (Table 2). Compound **7**-**9** had an IC_{50} of 1.0, 1.0 and 2.5 μM respectively, thereby making them interesting starting points for a hit optimization program with LE of 0.37 - 0.31 and LipE of 2.0 - 1.1 (Table 2). α-Keto amides are reported as peptidomimetic inhibitors of serine or cysteine proteases, such as Hepatitis C Virus serine proteases, thrombin, trypsin and cathepsin K (see [17] for a recent review). α-Keto amide motifs are incorporated in many natural products (*e.g.* Rapamycin,[18] a T-cell proliferation inhibitor) and FDA approved drugs (e.g. Boceprevir[19] and Telaprevir[20]). Moreover, this chemotype has also been used as substrate mimetic to obtain insight in anandamide hydrolysis.[21] α-Keto amides act by mechanism-based inhibition, using the activated ketone as covalent site of attachment (*i.e.* electrophilic trap) for nucleophilic residues in the catalytic site. The amide functionality can provide a template for key hydrogen bonding interactions with the target enzyme. β-Keto-α,α-difluoro amides are previously reported as porcine pancreatic elastase inhibitors[22] and are very similar to the α-keto amides in structural features. The presence of the α-keto-fluorines increases ketone reactivity. Compounds **10** and **11** have LE of 0.36 and 0.35 and LipE of 2.6 and 2.4, respectively. Both keto-amide classes show high similarity with previously published trifluoromethylketones and α-keto heterocycles, which are known chemotypes for DAGLα,[23] FAAH[24] (Chapter 2 and 3) and serine proteases.[25] Compound **7** and **10** were the most active in both the PNP- and orthogonal ABPP-assay (Table 2). After resynthesis, compound **7**-**10** were retested on ABPP using broad-spectrum serine hydrolase probe TAMRA-FP and also MB064. This ABPP analysis showed that the β-keto-α,α-difluoro amides **10** and **11** targeted ABHD6, whereas α-keto amides **7** and **8** did not (Figure 6B). Importantly, compounds **7**-**11** show excellent physicochemical properties, such as MW < 350, cLogD < 5, tPSA < 50, and HBA/HBD < 5. The α-keto amides **7**-**9** and β-keto-α,α-difluoro amides **10**, **11,** and derivatives, may provide valuable starting points for inhibitor discovery (within the serine or cysteine hydrolase/protease families).

Sulfonyl-1,2,4-triazole ureas **12**-**14** were discovered as the third novel chemotype for DAGLα. Compounds **12** and **13** were resynthesized by the European Screening Centre (see experimental) and their structure and activity was confirmed (Table 2). Compound **12** and **13** had an IC_{50} of 1.3 μM and 3.2 μM, LE of 0.35 and 0.31, respectively, and LipE of 4.2. This makes compound **12** the most optimal active among the newly discovered chemotypes (*i.e.*

best LE and LipE). The sulfonyl-1,2,4-triazole ureas are expected to be covalent irreversible inhibitors and provide a structural template bearing a reactive urea with tunable reactivity. The sulfonyl-1,2,4-triazole ureas resemble the 1,2,3-triazole ureas which were previously reported as potent DAGLα and DAGLβ inhibitors.[26,27] The sulfonyl-1,2,4-triazoles have an additional interesting feature, since their reactivity can be tuned by the sulfur oxidation state, which potentially influences the triazole pKa and, thereby, leaving group capacity. After resynthesis, compound **12** and **13** were retested on ABPP using broad-spectrum serine hydrolase probe TAMRA-FP and also MB064. Similar to the 1,2,3-triazole ureas, the sulfonyl-1,2,4-triazole ureas target ABHD6, DDHD2 and FAAH as determined by ABPP (Figure 6A,B). Compounds **12**-**14** have very good physicochemical properties (*e.g.* low MW and low cLogD), although their tPSA is relatively high (>96 $Å^2$, Table 2). Altogether, the high potency, LipE and LE of sulfonyl-1,2,4-triazole ureas **12**-**14** makes this cluster a highly interesting starting point for a hit optimization program.

Clusters 5-10 contain (fused) five-ring heterocycles such as phenyl thiazoles **15**-**19**, benzoxazoles **20**,**21** and benzimidazoles **22**,**23**. These inhibitors are expected to be non-covalent reversible inhibitors that derive their potency from specific interactions with DAGLα. Other clusters contain generally very lipophilic and linear-shaped compounds, interestingly often with multiple basic amines, including phenyl acetylene amines **24**-**26**, 4-amino piperidines **27**,**28**, pyrrolo-quinazolines **29**,**30**. Finally, a total of 10 singletons (**31**-**50**) were identified. Noteworthy, singleton **50** seems to selectively compete for labeling with a ~20 kD band on ABPP (possibly LyPLA2, Figure 6C). For DAGLα however, these compounds show a weak effect in the active conformation (Table S2), orthogonal assay (Table 2) and in retest in ABPP (Figure 6A-C). Of note, almost all of these compounds have not been resynthesized and their activity has not been confirmed.

Conclusions

The Joint European Compound Collection containing > 300.000 compounds was successfully screened using a 1536-wells high throughput assay with recombinant human DAGLα. Activity-based protein profiling (ABPP) with mouse brain proteomes was employed as an orthogonal assay to select the most interesting confirmed actives. ABPP provided highly valuable insight in activity and selectivity over many endogenously expressed brain serine hydrolases in an early hit discovery phase. This resulted in a qualified hit list of 46 compounds. Four major compound clusters were discovered, including previously published glycine sulfonamides, and three novel DAGL inhibitor chemotypes: α-keto amides, β-keto-α,α-difluoro amides and sulfonyl-1,2,4-triazole ureas. In addition, 6 minor clusters were identified together with 10 singletons. The sulfonyl-1,2,4-triazole ureas **12**-**14** were prioritized for subsequent lead optimization due to their high LE and LipE. A focused library of approximately 100 compounds of sulfonyl-1,2,4-triazoles was developed based on **12**-**14** within the European Lead Factory consortium (unpublished results). This focused library can be used for lead optimization of the sulfonyl-1,2,4-triazole as DAGL inhibitors. It is

anticipated that sulfonyl-1,2,4-triazole ureas can also serve as a novel versatile chemotype for inhibitor discovery on other unexplored serine hydrolases and related enzyme families (*e.g* cysteine proteases). In this aspect, the QHL and the focused library may serve as important screening sets. For example, compounds derived from the sulfonyl-1,2,4-triazole urea focused library were recently discovered as potent *in vivo* active compounds for α/β hydrolase domain 16A (ABHD16A, also known as BAT5), as described in Chapter 8.[28]

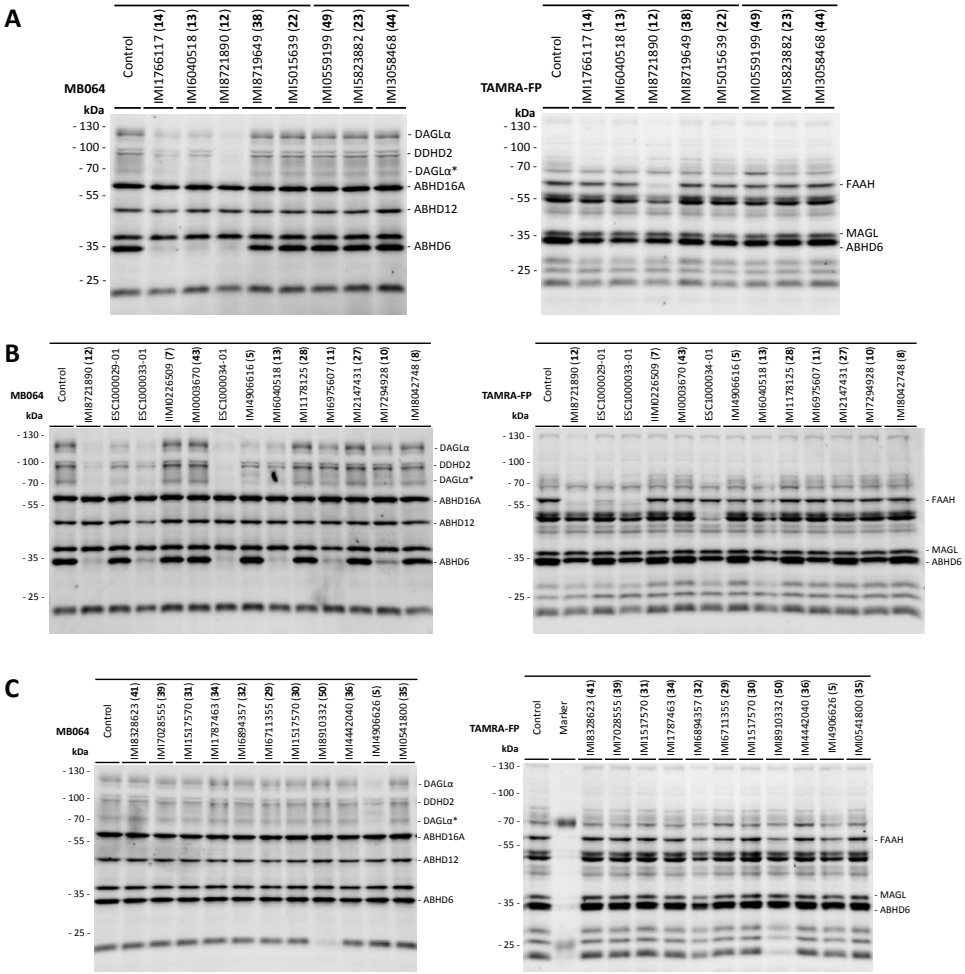

Figure 6. Overview of a select set of compounds retested on ABPP using two probes MB064 and TAMRA-FP using the standard previously reported procedures.[11] Compounds include: Glycine sulfonamide **5** (B,C), α-keto amides **7** and **8** (B), β-Keto difluoro amides **10** and **11** (B), Sulfonyl 1,2,4-triazole ureas **12-14** (A,B), Benzimidazoles **22** and **23** (A), 4-Amino piperidines **27** and **28** (B), Pyrrolo-quinazolines **29** and **30** (C) and singletons **31**, **32**, **35**, **36**, **38**, **39**, **41**, **43**, **44**, **49** and **50** (A-C). ESC1000029-01, 32-01 and 34-01 in (B) are part of the sulfonyl 1,2,4-triazole urea focused library (structures are not depicted).

Table 2. Qualified hit list compounds **5**-**50** categorized per cluster (chemotype). pIC_{50} values originate from the colorimetric PNP assay (N = 2, n = 2). Percentage effect ABPP is calculated, normalized for control and corrected for protein loading by Coomassie staining (N = 1). IMI coded compounds are actives obtained from the HTS. IMI coded compounds that have an additional ESC code are resynthesized by the European Screening Centre (ESC) and are reconfirmed actives (*i.e.* **5**, **7**, **8**, **10**, **11**, **12**, **13**, **27**, **28**, **34** and **46**, see experimental). Lipophilic efficiency, LipE = pIC_{50} - cLogD. Ligand efficiency, LE = (1.37/HA)pIC_{50}. For % effect of the primary assay and active conformation, see Table S2 (SI).

Cluster/ Chemotype	Entry	Code	Structure	pIC_{50} DAGLα (PNP)	% Eff. DAGLα (ABPP)	MW	cLogD	tPSA	HBD	HBA	LipE	LE
Glycine sulfonamide	**5**	IMI4906626 ESC1000043-01	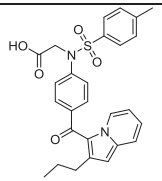	7.5	79	491	3.91	104.5	1	7	3.6	0.29
	6	IMI4749305	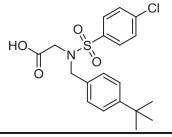	6.9	69	396	2.61	83.1	1	5	4.3	0.36
α-Keto amide	**7**	IMI0226509 ESC1000025-01	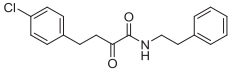	6.0	42	316	3.97	46.2	1	3	2.0	0.37
	8	IMI8042748 ESC1000026-01	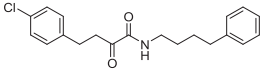	6.0	17	344	4.89	46.2	1	3	1.1	0.36
	9	IMI4961592	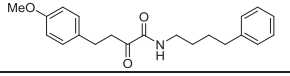	5.6	15	339	4.21	55.4	1	4	1.4	0.31
β-Keto difluoro amide	**10**	IMI7294928 ESC1000042-01	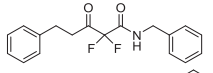	6.1	49	317	3.48	46.2	3	1	2.6	0.36
	11	IMI6975607 ESC1000044-01	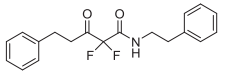	6.2	21	331	3.80	46.2	3	1	2.4	0.35

Cluster/ Chemotype	Entry	Code	Structure	pIC_{50} DAGLα (PNP)	% Eff. DAGLα (ABPP)	MW	cLogD	tPSA	HBD	HBA	LipE	LE
Sulfonyl-1,2,4-triazole urea	**12**	IMI8721890 ESC1000032-01	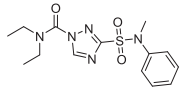	5.9	66	337	1.69	96.8	0	8	4.2	0.35
	13	IMI6040518 ESC1000048-01	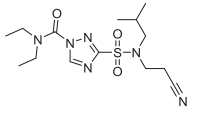	5.5	54	356	1.29	120.6	0	9	4.2	0.31
	14	IMI1766117	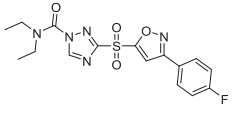	5.6	64	395	2.36	115.1	0	9	3.2	0.28
Phenyl thiazole	**15**	IMI1947191	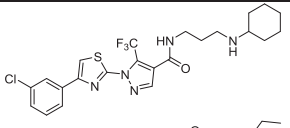	5.0	35	512	4.41	100.1	2	6	0.6	0.20
	16	IMI8258632	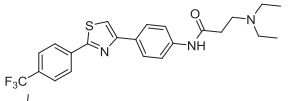	5.1	32	448	4.07	73.5	1	4	1.0	0.23
	17	IMI4843646	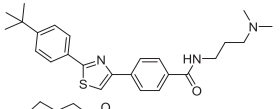	5.0	28	422	3.56	73.5	1	4	1.4	0.23
	18	IMI0512143	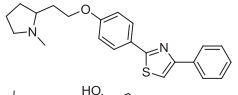	4.9	16	365	3.33	53.6	0	3	1.3	0.26
	19	IMI2088196	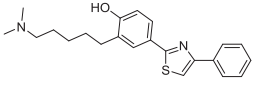	5.0	14	367	4.27	64.6	1	3	0.7	0.26

Cluster/ Chemotype	Entry	Code	Structure	pIC_{50} DAGLα (PNP)	% Eff. DAGLα (ABPP)	MW	cLogD	tPSA	HBD	HBA	LipE	LE
Benzoxazole	**20**	IMI1909578	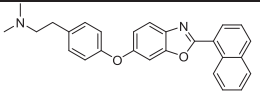	4.9	33	408	5.00	38.5	0	4	-0.1	0.22
	21	IMI7964529	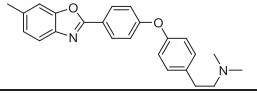	4.9	-3	372	4.58	38.5	0	4	0.3	0.24
Benzimi-dazole	**22**	IMI5015639	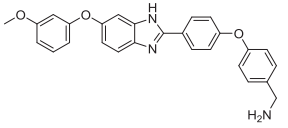	5.5	48	437	5.44	82.4	3	6	0.1	0.23
	23	IMI3058468	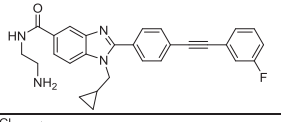	< 4.7	48	453	4.05	72.9	3	5	-	-
Phenyl acetylene-amine	**24**	IMI8077796	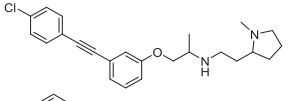	5.2	42	397	2.54	24.5	1	3	2.7	0.25
	25	IMI4618041	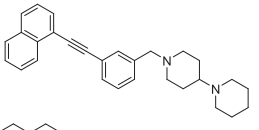	5.1	33	409	4.52	6.5	0	2	0.6	0.23
	26	IMI4545816	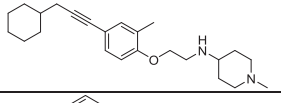	4.9	22	369	4.07	24.5	1	3	0.8	0.25
4-Amino piperidine	**27**	IMI2147431 ESC1000046-01	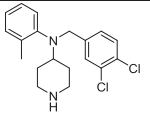	5.0	31	349	4.96	15.3	1	2	0.0	0.30

Cluster/ Chemotype	Entry	Code	Structure	pIC_{50} DAGLα (PNP)	% Eff. DAGLα (ABPP)	MW	cLogD	tPSA	HBD	HBA	LipE	LE
4-Amino piperidine	**28**	IMI1178125 ESC1000054-01	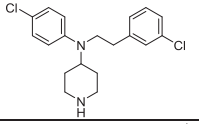	4.8	23	349	4.69	15.3	1	2	0.1	0.29
Pyrrolo-quinazoline	**29**	IMI6711355	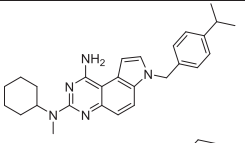	5.6	50	428	6.36	60.0	2	5	-0.8	0.24
	30	IMI2341674	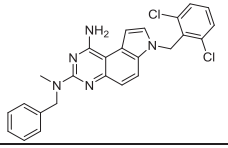	5.5	33	462	6.74	60.0	2	5	0.5	0.24
Singleton	**31**	IMI1517570	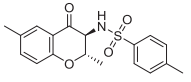	5.9	54	345	3.39	80.8	1	5	2.5	0.34
	32	IMI6894357	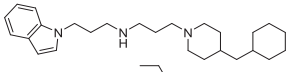	5.4	45	396	2.98	20.2	1	3	2.4	0.26
	33	IMI1371614	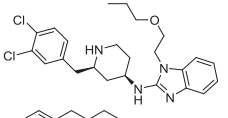	N.D.	41	461	4.14	51.1	2	5	-	-
	34	IMI1787463 ESC1000055-01	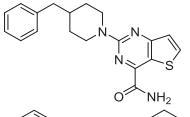	5.9	36	352	4.11	100.3	2	5	1.8	0.32
	35	IMI0541800	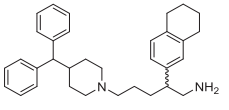	5.7	33	467	4.92	29.3	2	2	0.8	0.22

Cluster/ Chemotype	Entry	Code	Structure	pIC_{50} DAGLα (PNP)	% Eff. DAGLα (ABPP)	MW	cLogD	tPSA	HBD	HBA	LipE	LE
	36	IMI4442040	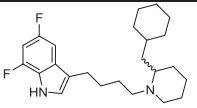	5.4	31	389	5.81	19.0	1	2	0.4	0.26
	37	IMI2233474	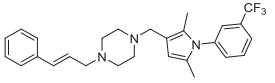	5.2	30	454	4.46	11.4	0	3	0.7	0.22
	38	IMI8719649	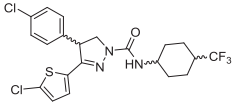	5.6	30	490	6.17	72.9	1	4	-0.6	0.25
	39	IMI7028555	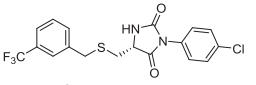	6.0	23	415	4.56	74.7	1	4	1.4	0.30
Singleton	**40**	IMI9488216	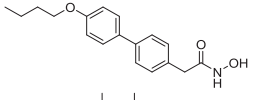	5.8	22	299	3.70	58.6	2	4	2.1	0.36
	41	IMI8328623	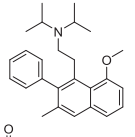	5.3	21	376	5.01	12.5	0	2	0.3	0.26
	42	IMI2499282	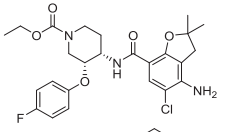	5.7	21	506	3.76	103.1	3	8	1.9	0.22
	43	IMI0003670	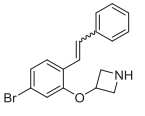	5.4	20	330	3.99	21.3	1	2	1.4	0.37

Cluster/ Chemotype	Entry	Code	Structure	pIC_{50} DAGLα (PNP)	% Eff. DAGLα (ABPP)	MW	cLogD	tPSA	HBD	HBA	LipE	LE
Singleton	**44**	IMI0559199	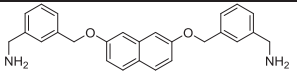	5.7	19	399	2.28	70.5	4	4	3.4	0.26
	45	IMI3277364	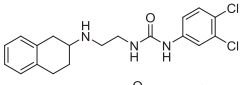	4.9	18	378	4.34	53.2	3	4	0.6	0.27
	46	IMI9906175 ESC100100	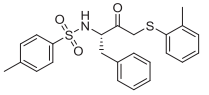	5.5	16	440	5.39	96.9	1	4	0.1	0.25
	47	IMI1224131	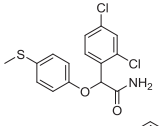	5.1	16	342	4.26	77.6	2	3	0.8	0.33
	48	IMI2003088	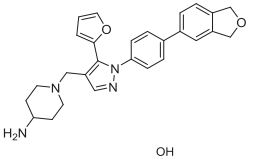	5.2	15	443	2.64	78.7	2	7	2.6	0.22
	49	IMI5823882	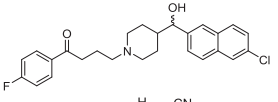	5.6	6	440	4.74	40.5	1	3	0.9	0.25
	50	IMI8910332	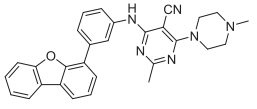	5.4	2	475	5.14	81.2	1	7	0.3	0.21

Experimental

General procedures biology

Cloning procedures

Cloning procedures were performed as previously reported.[11,12] In brief, full-length human DAGLα cDNA was purchased from Source Bioscience and cloned into mammalian expression vector pcDNA3.1, containing genes for ampicillin and neomycin resistance. The empty vector was used as a negative control (mock). All plasmids were grown in XL-10 Z competent cells and prepped (Maxi Prep, Qiagen). The sequences were confirmed by sequence analysis at the Leiden Genome Technology Centre.

Preperation of membrane fractions

Cell culture and membrane preparations were performed as previously reported.[11,12] In brief, HEK293T cells were grown in DMEM with stable glutamine and phenol red (PAA) with 10% new born calf serum, penicillin, and streptomycin. Cells were passaged every 2−3 days by resuspension in medium and seeding to the appropriate confluence. Membranes were prepared from transiently transfected HEK293T cells. 24 Hours prior to transfection, cells were seeded in Petri dishes (40 x 15 cm for HTS). Cells were transfected by the addition of a 3:1 mixture of polyethyleneimine (60 μg) and plasmid DNA (20 μg) in 2 mL of serum free medium. The medium was refreshed after 24 h, and after 72 h the cells were harvested by suspending them in 20 mL of medium. The supernatant was removed by centrifugation for 10 min at 1000 rpm. The cell pellet was flash frozen in liquid nitrogen and stored at −80 °C until use. Cell pellets were thawed on ice and suspended in lysis buffer A (20 mM HEPES, pH 7.2, 2 mM DTT, 0.25 M sucrose, 1 mM $MgCl_2$, 1× cocktail (Roche cOmplete EDTA free), 25 U/mL Benzonase). The suspension was homogenized by polytrone (3 × 7 s) and incubated for 30 min on ice. The membrane fraction was separated by ultracentrifuge (100.000g, 30 min, 4 °C, Beckman Coulter, type Ti70 rotor) and the pellet was resuspended in lysis buffer B (20 mM HEPES, pH 7.2, 2 mM DTT, 1× cocktail (Roche cOmplete EDTA free)). The protein concentration was determined with Qubit protein assay (Invitrogen). The total protein concentration was diluted to 1.0 mg/mL (~200 mL for HTS) and the samples were quickly frozen in liquid nitrogen and stored in 10 mL tubes at −80 °C until use.

Biochemical hDAGLα activity assay (96-well format)

The biochemical hDAGLα activity assay was performed as previously reported.[7,11] In brief, the biochemical hDAGLα activity assay is based on the hydrolysis of paranitrophenylbutyrate (PNP-butyrate) by membrane preparations from HEK293T cells transiently transfected with hDAGLα. Reactions (200 μL) were performed in flat bottom Greiner 96-wells plates. Final assay conditions; 200 μL total volume, 50 mM HEPES pH 7.2 buffer with 0.05 μg/μL hDAGLα transfected HEK293T membrane fractions, 300 μM PNP-butyrate, 5% DMSO. Controls were measured at N = 2, n = 4, inhibitors were measured at N = 2, n = 2. Slope is determined in 5-15 min.

Biochemical hDAGLα activity assay (384-well format)

The 384-well plate format assay is based on the above protocol. 30 μL reactions were performed in a 384-well plate (flat bottom, polypropylene). To each well was added 10 μL inhibitor solution (3x concentrated in 50 mM HEPES pH 7.2 assay buffer, 7.5% DMSO) and 10 μL membrane fraction solution (3x concentrated in assay buffer) after which the plates were centrifuged (5 s, 1000 rpm) and incubated at room temperature for 20 minutes. Lastly 10 μL substrate solution (3x concentrated in assay buffer, 7.5 % DMSO) was added to each well and the plate was centrifuged again (5 s, 1000 rpm). Enzymatic activity was followed by measuring the absorption at 405 nm on a PHERAstar microplate reader every 60-90 seconds, for up to 80 minutes at room temperature. Controls were measured at N = 2, n = 4. Final assay conditions; 30 μL total volume, 50 mM HEPES pH 7.2 buffer with 0.05 μg/μL hDAGLα transfected HEK293T membrane fractions, 300 μM PNP-butyrate, 5%

DMSO. Controls were measured at N = 2, n = 4, inhibitors were measured at N = 2, n = 2. Slope is determined in 5-30 min. End point determination is feasible at 60 minutes (S/B = 2.8).

Proof of principle LOPAC® 1280 library screen

Membrane fraction solution (10 µL 2 µg/µL), then 9.4 µl assay buffer and 0.6 µl inhibitor (50x concentrated DMSO stock, 500 µM) were added in a 384-well plate (flat bottom, polypropylene). The plate was centrifuged (5 s, 1000 rpm) and incubated at room temperature for 30 minutes. Subsequently 10 µL substrate mix (3x concentrated in assay buffer with DMSO) was added to each well and the plate was centrifuged again (5 s, 1000 rpm). Enzymatic activity was determined by measuring the absorption at 405 nm on a PHERAstar microplate reader after 60 minutes incubation at room temperature. Controls were measured at N = 2, n = 8, inhibitors at N = 2, n = 1.

Biochemical hDAGLα activity assay (1536-well format)

Using acoustic dispensing (Labcyte 555 Echo Liquid Handler), 20 nL of inhibitor solution (400x concentrated in DMSO) was added to a Black Corning clear bottom 1536-well plate, after which was added 2.5 uL of 50 mM HEPES pH 7.0 assay buffer (BioRAPTR FRD Microfluidic Workstation, Beckman Coulter) and 3 µL of membrane solution (2.67x concentrated in assay buffer, ThermoFisher Multidrop Combi). The plate was centrifuged (5 s, 1000 rpm) and incubated at room temperature for 20 minutes. Subsequently 2.5 µL of substrate solution (3.2x concentrated in assay buffer, 8.8% DMSO, BioRAPTR) was added to each well and the plate was centrifuged again (5 s, 1000 rpm). Enzymatic activity was determined by measuring the absorption at 405 nm on an Envision microplate reader after 90 minutes incubation at room temperature. Inhibitors were measured at N = 2, n = 1. Final assay conditions; 8.0 µL total volume, 50 mM HEPES pH 7.0 buffer with 0.025 µg/µL hDAGLα transfected membrane fractions, 600 µM PNP-butyrate, 0.25% DMSO. Primary assay; inhibitor 10 µM, Active conformation; inhibitor 10 and 1.25 µM final concentrations.

Preparation of mouse brain proteome

Mouse brains were isolated according to guidelines approved by the ethical committee of Leiden University (DEC No. 10095). Brain lysis was performed as previously reported.[9] In brief, mouse brains were thawed on ice and homogenized by Polytrone (3 × 7 s) in pH 7.2 lysis buffer A (20 mM HEPES, 2 mM DTT, 1 mM $MgCl_2$, 25 U/mL Benzonase) and incubated for 15 min on ice, followed by low speed spin (2500g, 3 min at 4 °C) to remove debris. The supernatant was subjected to ultracentrifugation (100.000g, 45 min, 4 °C, Beckman Coulter, type Ti70 rotor) to yield the cytosolic fraction in the supernatant and the membrane fraction as a pellet. The pellet was resuspended in lysis buffer B (20 mM HEPES, 2 mM DTT). The total protein concentration was determined with Quick Start Bradford assay (Biorad). Membranes were stored in small aliquots at −80 °C until use.

Orthogonal cABPP mDAGLα activity assay

The orthogonal cABPP protocol is based on the previously reported ABPP protocol.[8, 11] Using acoustic dispensing, 50 nL of inhibitor solution (400x concentrated, 4 mM) was added to a 384-well plate, after which was added 20 µL of mouse brain membrane proteome (2 mg/ mL). The mouse brain was incubated for 30 minutes with vehicle (0.5 µL of DMSO) or inhibitor and for 15 minutes with 0.5 µL of ABP MB064 (40x stock, 10 µM). Lastly was added 10 µL of standard 3 × SDS-PAGE sample buffer. The samples were loaded and resolved on commercially available SDS−PAGE gel (10% acrylamide). Final DMSO concentration: 2.8%. The gels were scanned with a ChemiDoc MP sytem (Cy3 settings, 605/50 filter) and analyzed using Image Lab 4.1. All 263 samples were measured at n = 1, N = 1.

ABPP selectivity assay (retest)

The cABPP selectivity assay was performed as previously reported.[11] In brief, mouse brain proteome (2.0 mg/mL, 20 µL) was preincubated for 30 min with vehicle (0.5 µL of DMSO) or inhibitor (0.5 µL of 400 µM inhibitor in DMSO) and subsequently treated with ABP (MB064 or TAMRA-FP, 250 nM and 500 nM final conc.). The reactions were quenched with 10 µL of standard 3x SDS−PAGE sample buffer. The samples were directly loaded and resolved on SDS−PAGE gel (10% acrylamide). Final DMSO concentration: 5.0%. The gels were scanned with a ChemiDoc MP sytem (Cy3 settings, 605/50 filter) and analyzed using Image Lab 4.1. All samples were measured at n = 1, N = 1.

General procedures chemistry

Synthesis of ESC compounds

Synthesis, characterization and retesting of the compounds in the colorimetric DAGLα activity assay is performed by the European Screening Centre.

2-Propylindolizine (51)

To a mixture of 1-bromopentan-2-one and 3-bromopentan-2-one (1.1 g, 3.34 mmol), was added 2-methylpyridine (0.66 ml, 6.67 mmol), $NaHCO_3$ (0.56 g, 6.67 mmol) and acetonitrile (6 mL) and it was heated in a microwave to 150°C for 1 hour. After full conversion, the reaction mixture was concentrated *in vacuo*, extracted with EtOAc/ H_2O, washed with H_2O and brine, dried over Na_2SO_4 and evaporated yielding 2-propylindolizine (377 mg, 71%) without additional purification. The crude product was used immediately in the next reaction.

(4-Nitrophenyl)(2-propylindolizin-3-yl)methanone (52)

2-Propylindolizine (**51**, 377 mg, 2.37 mmol) and triethylamine (0.4 ml, 2.84 mmol) were combined in DCM (15 mL). A solution of 4-nitrobenzoyl chloride (483.29 mg, 2.6 mmol) in DCM (5 mL) was added dropwise and the reaction stirred at rt for 18 hours. Sat. $NaHCO_3$ (20 mL) was added to the reaction mixture which was extracted with DCM (2 x 25 mL), washed with brine and dried over Na_2SO_4. Solvent was removed to afford crude product (743 mg) which was purified by flash chromatography to yield (4-nitrophenyl)(2-propylindolizin-3-yl)methanone (525mg, 72%) as a yellow solid. ^{1}H NMR (400 MHz, $CDCl_3$) δ 9.83 (d, *J* = 7.03 Hz, 1H), 8.23 - 8.44 (d, 2H), 7.77 (d, *J* = 8.53 Hz, 2H), 7.50 (d, *J* = 8.78 Hz, 1H), 7.28 (s, 2H), 7.24 (s, 1H), 6.92 (t, *J* = 7.03 Hz, 1H), 6.43 (s, 1H), 2.14 (t, *J* = 7.65 Hz, 2H), 1.40 - 1.52 (m, 2H), 0.70 (t, *J* = 7.40 Hz, 3H).

(4-Aminophenyl)(2-propylindolizin-3-yl)methanone (53)

To a suspension of (4-nitrophenyl)-(2-propylindolizin-3-yl)methanone (**52**, 525 mg, 1.7 mmol) in ethanol (12 mL) and H_2O (16 mL) was added Zinc (400.82 mg, 6.13 mmol) and AcOH (1.46 ml, 25.54 mmol). The reaction was heated to reflux for 4 hours. The reaction mixture was allowed to cool to room temperature and then filtered. Solid residues were washed with EtOAc and the resulting filtrate extracted with EtOAc. Organics were washed with sat. NaHCO and then brine, dried over Na_2SO_4 and concentrated *in vacuo*. Purification by flash chromatography yielded (4-aminophenyl)(2-propylindolizin-3-yl)methanone (492 mg, 85%). The sample was further dried and then used in subsequent reaction without additional analysis. ^{1}H NMR (400 MHz, $CDCl_3$) δ 9.41 (d, *J* = 7.28 Hz, 1H), 7.56 - 7.68 (m, 2H), 7.42 (d, *J* = 8.78 Hz, 1H), 6.93 - 7.10 (m, 3H), 6.74 (dt, *J* = 1.25, 6.90 Hz, 1H), 6.32 - 6.44 (m, 1H), 2.37 (t, *J* = 7.65 Hz, 2H), 1.42 - 1.58 (m, 2H), 0.68 - 0.81 (m, 3H).

4-Methyl-*N*-(4-(2-propylindolizine-3-carbonyl)phenyl)benzenesulfonamide (54)

(4-Aminophenyl)-(2-propylindolizin-3-yl)methanone (**53**, 403 mg, 1.45 mmol) was dissolved in DCM (5 mL) and tosyl chloride (289.82 mg, 1.52 mmol) added followed by pyridine (0.14 mL, 1.74 mmol). The reaction was stirred at room temperature for 4 hours. LC-MS indicated a small quantity of starting material remained unreacted so additional tosyl chloride (0.1eq.) and pyridine (0.1 eq.) were added and stirring continued for 16 hours, overnight. The reaction mixture was diluted with DCM (20 mL) and washed with HCl (0.5M aq., 20 mL) and brine. Organics were dried over Na_2SO_4 and concentrated *in vacuo*. Purification by flash chromatography yielded 4-methyl-N-(4-(2-propylindolizine-3-carbonyl)phenyl)benzenesulfonamide (681 mg, quant.). ^{1}H NMR (400 MHz, $CDCl_3$) δ 9.57 (d, *J* = 7.28 Hz, 1H), 7.74 (d, *J* = 8.28 Hz, 2H), 7.55 (d, *J* = 8.53 Hz, 2H), 7.44 (d, *J* = 8.78 Hz, 1H), 7.24 - 7.32 (m, 2H), 7.18 (d, *J* = 8.53 Hz, 2H), 7.06 - 7.14 (m, 1H), 6.93 (br. s., 1H), 6.80 (dt, *J* = 1.25, 6.90 Hz, 1H), 6.38 (br. s., 1H), 2.36 - 2.45 (m, 3H), 2.12 - 2.24 (m, 2H), 1.35 - 1.50 (m, 2H), 0.65 (t, *J* = 7.28 Hz, 3H).

Tert-butyl *N*-(4-(2-propylindolizine-3-carbonyl)phenyl)-*N*-tosylglycinate (55)

4-Methyl-*N*-[4-(2-propylindolizine-3-carbonyl)phenyl]benzenesulfonamide (**54**, 92%, 681 mg, 1.45 mmol) was dissolved in THF (5 mL) and cooled to 0°C in an ice-water bath. Sodium hydride (60% dispersion in mineral oil, 69.52 mg, 1.74 mmol) was added and the reaction stirred at 0°C for 20 minutes. Tert-butyl 2-bromoacetate (0.32 ml, 2.17 mmol) was added and the reaction stirred at room temperature for 1 hour. Additional tert-butyl 2-bromoacetate (0.32 ml, 2.17 mmol), NaH (60% dispersion in mineral oil, 69.52 mg, 1.74 mmol) and THF (10 mL) were added and stirring continued for 30 minutes. The reaction was subsequently heated to reflux for 2 hours. The reaction mixture was allowed to cool to rt and split between EtOAc and H_2O. Organics were washed with H_2O and brine and dried over Na_2SO_4 Solvent was evaporated *in vacuo* and purified by flash chromatography yielding tert-butyl *N*-(4-(2-propylindolizine-3-carbonyl)phenyl)-*N*-tosylglycinate (959 mg quant.). ^{1}H NMR (400 MHz, $CDCl_3$) δ 9.67 (d, *J* = 7.28 Hz, 1H), 7.59 (dd, *J* = 8.41, 14.43 Hz, 4H), 7.46 (d, *J* = 8.78 Hz, 1H), 7.22 - 7.38 (m, 4H), 7.09 - 7.19 (m, 1H), 6.83 (dt, *J* = 1.25, 6.90 Hz, 1H), 6.39 (s, 1H), 4.37 (s, 2H), 2.43 (s, 3H), 2.15 - 2.26 (m, 2H), 1.38 - 1.52 (m, 11H), 0.72 (t, *J* = 7.28 Hz, 3H).

***N*-(4-(2-propylindolizine-3-carbonyl)phenyl)-*N*-tosylglycine (5, ESC1000043)**

Tert-butyl *N*-(4-(2-propylindolizine-3-carbonyl)phenyl)-*N*-tosylglycinate (**55**, 83%, 959 mg, 1.46 mmol) was dissolved in 4M HCl (4M in dioxane) (5 ml) and the reaction stirred at room temperature for 1 hour and heated to 40°C for 1 hour. Solvent was evaporated from the reaction mixture under reduced pressure and the resulting residue dissolved in EtOAc and washed with HCl (1M, aq.). Organics were dried over Na_2SO_4 and solvent evaporated under reduced pressure to afford crude product, 822 mg. Purification by reverse phase flash chromatography (C18 column, water 5% to 95% MeCN gradient, 0.1% TFA modifier) followed by evaporation of solvent from the appropriate fractions afforded a dark green solid. The solid was suspended in MeOH, sonicated and filtered. The resulting solid was heated in EtOH for 2 hours and then filtered, washed with diethyl ether and dried to yield *N*-(4-(2-propylindolizine-3-carbonyl)phenyl)-*N*-tosylglycine (240 mg, 34%) as a pale green solid. ^{1}H NMR (400 MHz, DMSO-d6) δ 12.95 (br. s., 1H), 9.54 (d, *J* = 7.03 Hz, 1H), 7.64 (d, *J* = 8.78 Hz, 1H), 7.59 (d, *J* = 8.03 Hz, 2H), 7.51 (d, *J* = 8.53 Hz, 2H), 7.38 (d, *J* = 8.03 Hz, 2H), 7.31 (d, *J* = 8.53 Hz, 2H), 7.20 - 7.28 (m, 1H), 6.96 (dt, *J* = 1.25, 6.90 Hz, 1H), 6.51 (s, 1H), 4.50 (s, 2H), 2.39 (s, 3H), 1.98 - 2.16 (m, 2H), 1.23 - 1.46 (m, 2H), 0.61 (t, *J* = 7.28 Hz, 3H). LC-MS Purity = 100%, rt = 2.13 min, m/z [M+H] = 491.3.

Tert-butyl 2-[methoxy(methyl)amino]-2-oxo-acetate (56)

To a solution of oxalyl chloride (2.2 mL, 25.7 mmol) in dry THF (40 mL) at 0°C was added t-butanol (2.4 mL, 25.1 mmol). Stirring was continued for 1h, followed by addition of *N*-methoxymethanamine HCl (2.51 g, 25.7 mmol) with TEA (10.7 mL, 77.1 mmol) with stirring at 0°C. A rich precipitate formed quickly and stirring was continued at 0°C for 2h. The reaction was quenched with H_2O (20 mL) and the volatiles were removed *in vacuo*. The

product was extracted into EtOAc (2x) and the combined organic layers were washed with brine, dried with $MgSO_4$ and concentrated to dryness. The residual yellow oil was purified by flash chromatography yielding tert-butyl 2-[methoxy(methyl)amino]-2-oxo-acetate (2.2 g, 43%). ^{1}H NMR (400 MHz, $CDCl_3$) δ 7.18 – 7.38 (m, 2H), 3.77 (s, 3H), 3.23 (s, 3H), 1.49 – 1.70 (m, 14H). Literature protocol.[29]

Tert-butyl 4-(4-chlorophenyl)-2-oxobutanoate (57)

To a mixture of Mg turnings (0.068 g, 2.80 mmol) in dry diethylether (1 mL) was added a small piece of iodine. Then 1-(2-bromoethyl)-4-chloro-benzene was added and the mixture was subjected to ultrasound radiation for 20 minutes during which a clear yellow solution forms. The solution was stirred for an hour at rt. Then, the solution was added dropwise to a -78°C cold solution of tert-butyl 2-[methoxy(methyl)amino]-2-oxo-acetate (**56**, 0.76 g, 4.0 mmol) in 5 mL of dry diethylether. After stirring for 2h at -78°C the reaction was quenched with aq. NH_4Cl and the product was extracted into DCM (2x). The combined org extracts were dried with $MgSO_4$, concentrated *in vacuo* and purified by flash chromatography to yield tert-butyl 4-(4-chlorophenyl)-2-oxobutanoate (0.32 g, 28%). ^{1}H NMR (400 MHz, $CDCl_3$) δ 7.22 – 7.35 (m, 3H), 7.16 (d, J = 8.28 Hz, 2H, 3.73 – 3.83 (m, 1H), 3.11 (s, 2H), 2.93 (s, 2H), 1.45 – 1.66 (m, 12H). Literature protocol.[29]

4-(4-Chlorophenyl)-2-oxobutanoic acid (58)

To a solution tert-butyl 4-(4-chlorophenyl)-2-oxobutanoate (**57**, 0.32 g, 1.19 mmol) in DCM (5 mL) was added TFA (0.44 mL, 5.95 mmol) with stirring at rt. Stirring was continued overnight. The reaction mixture was concentrated *in vacuo* and purified by flash chromatography to yield 4-(4-chlorophenyl)-2-oxobutanoic acid (0.22 g, 78%). ^{1}H NMR (400 MHz, $CDCl_3$) δ 7.24 – 7.40 (m, 2H), 7.16 (d, *J* = 8.28 Hz, 2H), 3.30 (t, *J* = 7.40 Hz, 2H), 2.99 (t, *J* = 7.28 Hz, 2H). Literature protocol.[29]

4-(4-Chlorophenyl)-2-oxo-N-phenethylbutanamide (7, ESC1000025)

To a solution of 4-(4-chlorophenyl)-2-oxobutanoic acid (**58**, 100 mg, 0.47 mmol) in DMF (5.0 mL) was added DIEA (0.09 mL, 0.52 mmol) and phenethylamine (0.065 mL, 62 mg, 0.517 mmol) followed by HATU (178 mg, 0.47 mmol) while stirring. After 1h, water was added and the product was extracted into EtOAc (2x) and the combined org extracts were dried with Na_2SO_4, concentrated *in vacuo* and purified by flash chromatography to yield 4-(4-chlorophenyl)-2-oxo-N-phenethylbutanamide (75 mg, 45%). ^{1}H NMR (400 MHz, $CDCl_3$) δ 7.05 – 7.47 (m, 11H), 6.75 – 7.04 (m, 1H), 3.58 (d, *J* = 6.53, 2H), 3.26 (t, *J* = 7.40 Hz, 2H), 2.89 (td, *J* =7.25, 19.89 Hz, 4H). LC-MS Purity = 94%, rt = 3.02 min, m/z [M+H] = 315. Literature protocol.[29]

4-(4-Chlorophenyl)-2-oxo-N-(4-phenylbutyl)butanamide (8, ESC1000026)

To a solution of 4-(4-chlorophenyl)-2-oxobutanoic acid (**58**, 100 mg, 0.47 mmol) in DMF (5.0 mL) was added DIEA (0.09 mL, 0.52 mmol) and phenbutylamine (77 mg, 0.517 mmol) followed by HATU (178 mg, 0.47 mmol) while stirring. After 1h, water was added and the product was extracted into EtOAc (2x) and the combined org extracts were dried with Na_2SO_4, concentrated *in vacuo* and purified by flash chromatography to yield 4-(4-chlorophenyl)-2-oxo-N-(4-phenylbutyl)butanamide (82 mg, 46%). ^{1}H NMR (400 MHz, $CDCl_3$) δ 7.06 – 7.40 (m, 10H), 6.83 – 7.02 (m, 1H), 3.18 – 3.47 (m, 4H), 2.93 (t, *J* = 7.40 Hz, 2H), 2.66 (t, *J* = 7.40 Hz, 2H), 1.47 – 1.85 (m, 5H). LC-MS Purity = 100%, rt = 3.16 min, m/z [M+H] = 343. Literature protocol.[29]

Ethyl 2,2-difluoro-3-hydroxy-5-phenyl-pentanoate (59)

TMS-Cl (31 µL, 0.25 mmol) was added to a stirred suspension of Zn (165.91 mg, 2.54 mmol) in THF (5 mL), followed by 1,2-dibromoethane (4 µL, 0.05 mmol) and heated to 40°C under argon for 15 minutes. The temperature was increased to 60°C. A solution of ethyl 2-bromo-2,2-difluoro-acetate (500 mg, 2.46 mmol) and

3-phenylpropanal (330.52 mg, 2.46 mmol) in THF (1 mL) was added to the reaction and heating continued for 30 minutes. The reaction was allowed to cool to rt. Water, DCM and 1N HCl was added to the reaction mixture and stirred for 15 minutes. The layers were separated, the organic dried over Na_2SO_4, the solvent removed *in vacuo* and purified by flash chromatography yielding ethyl 2,2-difluoro-3-hydroxy-5-phenyl-pentanoate (239 mg, 38%) as a colourless oil. ^{1}H NMR (400 MHz, $CDCl_3$) δ 7.16 - 7.38 (m, 5H), 4.37 (d, *J* = 7.03 Hz, 2H), 3.97 - 4.12 (m, 1H), 2.89 - 3.03 (m, 1H), 2.70 - 2.82 (m, 1H), 1.80 - 2.11 (m, 3H), 1.37 (t, *J* = 7.15 Hz, 3H).

***N*-Benzyl-2,2-difluoro-3-hydroxy-5-phenyl-pentanamide (60)**

Ethyl 2,2-difluoro-3-hydroxy-5-phenyl-pentanoate (**59**, 115 mg, 0.45 mmol) and benzylamine (145.9 µl, 1.34 mmol) were combined in THF (2 mL) and heated to 120°C in the microwave for 1.5 hours. The solvent was removed at *in vacuo* and purified by flash chromatography yielding *N*-benzyl-2,2-difluoro-3-hydroxy-5-phenyl-pentanamide (85 mg, 60%). ^{1}H NMR (400 MHz, $CDCl_3$) δ 7.28 (s, 10H), 6.59 - 6.83 (m, 1H), 4.45 - 4.61 (m, 2H), 4.05 - 4.25 (m, 1H), 2.89 - 3.05 (m, 1H), 2.66 - 2.81 (m, 2H), 1.84 - 2.09 (m, 2H).

***N*-Benzyl-2,2-difluoro-3-oxo-5-phenylpentanamide (10, ESC1000042)**

DMP (318 mg, 0.76 mmol) was added to a stirred solution of *N*-benzyl-2,2-difluoro-3-hydroxy-5-phenyl-pentanamide (**60**, 80 mg, 0.25 mmol) and the reaction stirred at room temperature overnight. The reaction mixture was diluted with DCM. The reaction mixture was washed with sat. $NaHCO_3$ solution and water. The organic was dried over Na_2SO_4 and the solvent removed *in vacuo* and purified by flash chromatography to yield *N*-benzyl-2,2-difluoro-3-oxo-5-phenylpentanamide (79 mg, 31%). ^{1}H NMR (400 MHz, $CDCl_3$) δ 7.19 - 7.44 (m, 11H), 6.69 (br. s., 1H), 4.55 - 4.58 (m, 1H), 4.52 (d, *J* = 5.77 Hz, 2H), 3.15 - 3.23 (m, 2H), 2.95 - 3.03 (m, 2H). The compound has a weak UV chromophore and does not ionise well.

2,2-Difluoro-3-hydroxy-5-phenyl-N-(2-phenylethyl)pentanamide (61)

Ethyl 2,2-difluoro-3-hydroxy-5-phenyl-pentanoate (**59**, 151 mg, 0.58 mmol) and 2-phenylethanamine (220.95 µl, 1.75 mmol) were combined in THF (2 mL) and heated to 130°C in the microwave for 60 minutes. The solvent was removed *in vacuo* and purified by flash chromatography to yield 2,2-difluoro-3-hydroxy-5-phenyl-N-(2-phenylethyl)pentanamide (166 mg, 85%). ^{1}H NMR (400 MHz, $CDCl_3$) δ 7.08 - 7.45 (m, 10H), 6.30 - 6.57 (m, 1H), 3.96 - 4.17 (m, 1H), 3.62 (d, *J* = 6.78 Hz, 2H), 2.88 (t, *J* = 7.03 Hz, 3H), 2.58 - 2.80 (m, 2H), 1.76 - 2.05 (m, 2H). LC-MS Purity = 100%, rt = 1.92 min, m/z [M+H] 334.20.

2,2-Difluoro-3-oxo-N-phenethyl-5-phenylpentanamide (11, ESC1000044)

DMP (572 mg, 1.34 mmol) was added to a stirred solution of 2,2-difluoro-3-hydroxy-5-phenyl-N-(2-phenylethyl)pentanamide (**61**, 150 mg, 0.45 mmol) in DCM (10 mL) at rt and stirring continued for 4 hours. The reaction mixture was diluted with DCM. The reaction mixture was washed with sat. $NaHCO_3$ solution and water. The organic was dried over Na_2SO_4 and the solvent removed *in vacuo* and purified by flash chromatography to yield 2,2-difluoro-3-oxo-N-phenethyl-5-phenylpentanamide (24.5 mg, 31%). ^{1}H NMR (400 MHz, $CDCl_3$) δ 7.15 - 7.38 (m, 10H), 6.40 (br. s., 1H), 3.60 (q, *J* = 6.78 Hz, 2H), 3.08 - 3.18 (m, 2H), 2.93 - 3.01 (m, 2H), 2.87 (t, *J* = 7.03 Hz, 2H). The compound has a weak UV chromophore and does not ionise well.

3-(Benzylthio)-1H-1,2,4-triazole (62)

A solution of 1,2-dihydro-1,2,4-triazole-3-thione (1.0 g, 9.89 mmol) and benzyl bromide (1.76 mL, 9.89 mmol) in dry DMF (15 mL) was stirred at rt for 24h. Then, the mixture was diluted with EtOAc followed by saturated $NaHCO_3$. The org phase was separated, the aq. phase was extracted with EtOAc the combined org phases were

washed with water followed by brine. Concentration in vacuo yields crude 3-(benzylthio)-1H-1,2,4-triazole (1.80 g, 86%), which was used as is.

3-(Benzylthio)-*N*,*N*-diethyl-1*H*-1,2,4-triazole-1-carboxamide (**63**)

A solution of 3-(benzylthio)-1H-1,2,4-triazole (**62**, 1.72 g, 9.0 mmol) in dry DMF (20 mL) was added diethylcarbamoyl chloride (2.28 mL, 18.0 mmol) followed by K_2CO_3 (6.22 g, 45 mmol) while stirring at rt, overnight. The reaction was quenched with water and the product was extracted into EtOAc. The org phase was washed with water followed by brine, concentrated *in vacuo* and purified by flash chromatography, yielding 3-(benzylthio)-*N*,*N*-diethyl-1*H*-1,2,4-triazole-1-carboxamide (2.50 g, 86%). ^{1}H NMR (400 MHz, $CDCl_3$) δ 8.77 (s, 1H), 7.19 – 7.51 (m, 6H), 4.40 (s, 2H), 3.42 – 3.76 (m, 3H), 1.52 – 1.67 (m, 1H), 1.27 (t, J = 7.03 Hz, 6H). Literature protocol.[30]

1-(Diethylcarbamoyl)-1*H*-1,2,4-triazole-3-sulfonyl chloride (64)

A stirred mixture of 2M HCl (3.8 mL) and DCM (5 mL) was cooled to -5°C (internal temperature). To this mixture was added a cold 10% NaOCl solution (1.55 M, 3.25 mL, 5 mmol) at such a rate that the temp. was maintained below 0°C. Then, 3-(benzylthio)-*N*,*N*-diethyl-1*H*-1,2,4-triazole-1-carboxamide (**63**, 0.44 g, 1.50 mmol) was added in small batches while maintaining the internal temperature between -5 to -10°C. Stirring at that temp was continued for a further 15-20 minutes and the reaction mixture was used immediately in the next reaction as crude. Literature protocol.[31]

***N*,*N*-Diethyl-3-(*N*-methyl-*N*-phenylsulfamoyl)-1*H*-1,2,4-triazole-1-carboxamide (12, ESC1000032)**

To the crude reaction mixture of 1-(diethylcarbamoyl)-1*H*-1,2,4-triazole-3-sulfonyl chloride (**64**) was added N-methylaniline (401.8 mg, 3.75 mmol) while stirring at -5°C. The mixture was allowed to warm to rt and after 1h, the reaction was quenched with $NaHCO_3$. The mixture was diluted with DCM and the org phase was separated, washed with 1M HCl, then dried over $MgSO_4$ and evaporated to dryness. Normal phase flash chromatography followed by two reverse phase preparative HPLC purifications yielded *N*,*N*-diethyl-3-(*N*-methyl-*N*-phenylsulfamoyl)-1*H*-1,2,4-triazole-1-carboxamide (33 mg, 11.7%). ^{1}H NMR (400 MHz, $CDCl_3$) δ 8.90 (s, 1H), 7.15 – 7.44 (m, 7H), 4.65 (s, 2H), 3.49 (br. S., 4H), 1.01 – 1.42 (m, 6H). LC-MS Purity = 100%, rt = 1.96 min, m/z [M+H] 337.

3-(N-(2-Cyanoethyl)-N-isobutylsulfamoyl)-N,N-diethyl-1H-1,2,4-triazole-1-carboxamide (13, ESC1000048-01)

To the crude reaction mixture of 1-(diethylcarbamoyl)-1*H*-1,2,4-triazole-3-sulfonyl chloride (**64**, second batch) was added 3-aminopropanenitrile (0.56 g, 8.0 mmol) while stirring at -10°C. After stirring for 1h, the mixture was diluted with DCM and the org phase was separated, washed with 1M HCl (2x) followed by water and then dried with $MgSO_4$. The solution was concentrated *in vacuo* and purified by flash chromatography. Then, 1-bromo-2-methyl-propane (1.0 mmol) was added followed by Cs_2CO_3 (97.6 mg, 0.30 mmol) while stirring at rt over the weekend. The mixture was diluted with water and the product was extracted into EtOAc. The organic phase was washed with water twice more, followed by brine and after drying with Na_2SO_4 the volatiles are evaporated *in vacuo*. The residual material was purified on preperative HPLC yielding 3-(N-(2-cyanoethyl)-N-isobutylsulfamoyl)-N,N-diethyl-1H-1,2,4-triazole-1-carboxamide. ^{1}H NMR (400 MHz, $CDCl_3$) δ 8.89 (s, 1H), 3.48 – 3.79 (m, 3H), 3.15 (d, *J* = 7.53 Hz, 2H), 2.84 (t, *J* = 7.0 Hz, 2H), 1.87 – 2.12 (m, 1H), 1.61 (br. s., 11H), 1.34 (t, *J* = 7.03 Hz, 7H), 0.98 (d, *J* = 6.78 Jz, 7H). LC-MS Purity = 100%, rt = 1.99 min, m/z [M+H] 311.20.

Tert-butyl 4-(2-methylanilino)piperidine-1-carboxylate (65)

To a solution of tert-butyl 4-oxopiperidine-1-carboxylate (250 mg, 1.25 mmol) in DCM (2 mL) was added CH_3CO_2H (0.08 ml, 1.48 mmol) followed by 2-methylaniline (150.58 mg, 1.41 mmol). The mixture was stirred at

room temperature for 5 minutes before addition of sodium triacetoxyborohydride (276.56 mg, 1.3 mmol) as one portion. The resulting mixture was stirred at rt for 20 h then the pH was adjusted to >10 by addition of NaOH (2 M, ca. 3 mL). The mixture was extracted with DCM and the organic extracts dried over Na_2SO_4, filtered and concentrated *in vacuo*. The residue was purified by flash chromatography yielding tert-butyl 4-(2-methylanilino)piperidine-1-carboxylate (340 mg, 93%). ^{1}H NMR (400 MHz, $CDCl_3$) δ 6.99 - 7.18 (2 H, m), 6.61 - 6.79 (2 H, m), 3.97 - 4.16 (2 H, m), 3.46 - 3.56 (1 H, m), 3.33 - 3.46 (1 H, m), 2.91 - 3.07 (2 H, m), 2.15 (5 H, s), 1.50 (9 H, s), 1.23 - 1.46 (3 H, m).

Tert-butyl-4-[*N*-[(3,4-dichlorophenyl)methyl]-2-methyl-anilino]piperidine-1-carboxylate (66)

To a mixture of tert-butyl 4-(2-methylanilino)piperidine-1-carboxylate (**65**, 100 mg, 0.34 mmol) and K_2CO_3 (95.18 mg, 0.69 mmol) in DMF (2.6 mL) was added 4-(bromomethyl)-1,2-dichloro-benzene (0.06 mL, 0.41 mmol). The resulting mixture was heated at 100 °C for 32 h then partitioned between EtOAc and NaOH (2 M, aq.). The organic extracts were further washed with $NaHCO_3$, then brine, dried over Na_2SO_4, filtered and concentrated under reduced pressure. The residue was purified by flash chromatography yielding tert-butyl-4-[*N*-[(3,4 dichlorophenyl)methyl]-2-methyl-anilino]piperidine-1-carboxylate (70 mg, 45%). ^{1}H NMR (400 MHz, $CDCl_3$) δ 7.34 (1 H, d, *J* = 1.76 Hz), 7.26 (1 H, d, *J* = 8.28 Hz), 7.17 (3 H, d, *J* = 7.53 Hz), 7.09 - 7.14 (2 H, m), 7.06 (1 H, dd, *J* = 8.28, 1.76 Hz), 6.95 - 7.02 (1 H, m), 4.06 - 4.25 (4 H, m), 2.89 - 3.01 (1 H, m), 2.66 (5 H, t, *J* = 11.92 Hz), 2.31 (3 H, s), 1.86 (6 H, d, *J* = 12.30 Hz), 1.53 - 1.68 (4 H, m), 1.47 (9 H, s).

***N*-(3,4-Dichlorobenzyl)-*N*-(*o*-tolyl)piperidin-4-amine (27, ESC1000046)**

To a solution of tert-butyl 4-[*N*-[(3,4-dichlorophenyl)methyl]-2-methyl-anilino]piperidine-1-carboxylate (**66**, 70 mg, 0.16 mmol) in DCM (3 mL) was added TFA (1.2 mL). LC-MS analysis after 2 h indicated consumption of the starting material with formation of the desired product (Rt = 1.37 min, *m/z* 349.20). The mixture was concentrated under reduced pressure and purified by flash chromatography. The resulting oil was treated with HCl in MeOH (prepared from dropwise addition of 1 mmol acetyl chloride to MeOH) and concentrated under reduced pressure. As the salt ratio could not be determined, the mixture was concentrated under reduced pressure and purified by flash chromatography yielding *N*-(3,4-dichlorobenzyl)-*N*-(*o*-tolyl)piperidin-4-amine (40.9 mg, 75%) as an orange gum. ^{1}H NMR (400 MHz, $CDCl_3$) δ 7.35 (1 H, d, *J* = 1.51 Hz), 7.24 (1 H, d, *J* = 8.03 Hz), 7.15 (1 H, d, *J* = 7.28 Hz), 7.08 (3 H, s), 6.91 - 6.99 (1 H, m), 4.21 (2 H, s), 3.13 (2 H, d, *J* = 12.05 Hz), 2.81 - 2.92 (1 H, m), 2.55 (2 H, td, *J* = 12.17, 2.01 Hz), 2.31 (3 H, s), 1.88 (2 H, d, *J* = 11.80 Hz), 1.61 (2 H, qd, *J* = 12.00, 3.89 Hz), LC-MS rt = 1.71 min, m/z [M+H] 349.20.

4-Chloro-*N*-[2-(3-chlorophenyl)ethyl]aniline (67)

A mixture of 4-chloroaniline (250 mg, 1.96 mmol), 1-(2-bromoethyl)-3-chloro-benzene (0.4 ml, 1.96 mmol), KI (32.53 mg, 0.2 mmol) and DIEA (0.34 ml, 1.96 mmol) in MeCN (4 mL) was subjected to microwave irradiation at 170 °C for 2.5 h. The resulting mixture was partitioned between DCM and $NaHCO_3$ (sat. aq.). The organics were washed with brine, dried over Na_2SO_4, filtered and concentrated under reduced pressure. The material was purified by flash chromatography yielding 4-chloro-*N*-[2-(3-chlorophenyl)ethyl]aniline (414 mg, 79%) with an additional impurity and residual solvent. The material was carried into the next step without any further purification.

Tert-butyl 4-[4-chloro-*N*-[2-(3-chlorophenyl)ethyl]anilino]piperidine-1-carboxylate (68)

To a solution of tert-butyl 4-oxopiperidine-1-carboxylate (274.96 mg, 1.38 mmol) and CH_3CO_2H (0.09 ml, 1.63 mmol) in DCM (1.5 mL) was added a solution of 4-chloro-N-[2-(3-chlorophenyl)ethyl]aniline (**67**, 411.39 mg, 1.55 mmol) in DCM (2 mL). The resulting mixture was stirred at room temperature for 7 h then sodium triacetoxyborohydride (304.18 mg, 1.44 mmol) added in one portion. The mixture was stirred at room

temperature for 66 h then quenched with 2 M NaOH (adjusting pH to >10). The mixture was extracted with DCM and the organic extracts washed with brine, dried over Na_2SO_4, filtered and concentrated under reduced pressure. The material was subjected to flash chromatography yielding tert-butyl 4-[4-chloro-*N*-[2-(3-chlorophenyl)ethyl]anilino]piperidine-1-carboxylate (110 mg, 18%). ^{1}H NMR (400 MHz, $CDCl_3$) δ 7.13 - 7.26 (5 H, m), 7.03 - 7.11 (1 H, m), 6.77 (2 H, d, J = 9.03 Hz), 4.09 - 4.35 (2 H, m), 3.53 - 3.67 (1 H, m), 3.27 - 3.41 (2 H, m), 2.65 - 2.84 (4 H, m), 1.66 - 1.77 (2 H, m), 1.48 (11 H, s). LC-MS tR = 2.64 min, m/z 449.25 [M+H]+, 393.15 [M-tBu+H]+, 349.20 [M-CO_2^{t}Bu+H]+

_N_-(3-Chlorophenethyl)-_N_-(4-chlorophenyl)piperidin-4-amine (28, ESC1000054)

To a solution of tert-butyl 4-[4-chloro-N-[2-(3-chlorophenyl)ethyl]anilino]piperidine-1-carboxylate (**68**, 110 mg, 0.24 mmol) in DCM (3 mL) was added TFA (1.5 mL). The resulting solution was stirred at room temperature for 18 h then concentrated under reduced pressure. The material was subjected to flash chromatography yielding *N*-(3-chlorophenethyl)-*N*-(4-chlorophenyl)piperidin-4-amine (82.1 mg, 96%). ^{1}H NMR (400 MHz, $CDCl_3$) δ 7.05 - 7.23 (5 H, m), 7.00 (1 H, d, J = 7.03 Hz), 6.71 (2 H, d, J = 9.03 Hz), 3.49 - 3.67 (2 H, m), 3.31 (2 H, m, J = 7.50, 7.50 Hz), 3.22 (2 H, d, J = 12.30 Hz), 2.62 - 2.81 (4 H, m), 1.58 - 1.82 (4 H, m). LC-MS tR = 2.62 min, m/z 349.00.

Ethyl 2-chlorothieno[3,2-*d*]pyrimidine-4-carboxylate (69)

To a stirred solution of 2-chloro-4-(1-ethoxyvinyl)thieno[3,2-*d*]pyrimidine (318 mg, 1.32 mmol) in dioxane (21 mL) was added a solution of 0.38M $NaIO_4$ in water (6.95 ml). $KMnO_4$ (20.88 mg, 0.13 mmol) was then added, resulting in a bright pink solution. After stirring for a couple of minutes, this mixture had become a pink-brown suspension. TLC analysis after 1.5 h indicated formation of a new spot but starting material still remaining. Additional $KMnO_4$ (20.88 mg, 0.13 mmol) was then added and stirring continued for a further 2.5 h. TLC analysis indicated further conversion but starting material still remaining so additional $KMnO_4$ (20.88 mg, 0.13 mmol) was added and stirring continued for a further 1.5 h. Although starting material still remained, the mixture was quenched by addition of sat. aq. K_2CO_3 to achieve a pH of 7-8. The resulting mixture was filtered to remove a brown precipitate, washing with DCM (x4). The filtrate was diluted with water and the organic extracts washed with brine, dried over Na_2SO_4, filtered and concentrated under reduced pressure. The material was subjected to flash chromatography yielding ethyl 2-chlorothieno[3,2-*d*]pyrimidine-4-carboxylate (175 mg, 55%) as a pale yellow solid. ^{1}H NMR (400 MHz, $CDCl_3$) δ 8.26 (8 H, d, J = 5.52 Hz), 7.58 (8 H, d, J = 5.52 Hz), 4.61 (17 H, q, J = 7.03 Hz), 1.52 (25 H, t, J = 7.15 Hz).

Ethyl 2-(4-benzyl-1-piperidyl)thieno[3,2-*d*]pyrimidine-4-carboxylate (70)

A solution of ethyl 2-chlorothieno[3,2-d]pyrimidine-4-carboxylate (**69**, 175 mg, 0.72 mmol) and 4-benzylpiperidine (0.38 ml, 2.16 mmol) in N-methylpyrrolidinone (3.6 mL) was subjected to microwave irradiation at 130 °C for 3 h. The mixture was partitioned between EtOAc and water. The aqueous phase was further extracted with EtOAc (x2) and the combined organic extracts washed with water (x2), brine (x2), dried over Na_2SO_4, filtered and concentrated under reduced pressure. The material was subjected to flash chromatography yielding ethyl 2-(4-benzyl-1-piperidyl)thieno[3,2-*d*]pyrimidine-4-carboxylate (171 mg, 62%). ^{1}H NMR (400 MHz, $CDCl_3$) δ 7.90 (1 H, d, J = 5.52 Hz), 7.28 - 7.35 (2 H, m), 7.13 - 7.25 (4 H, m), 4.90 (2 H, d, J = 13.05 Hz), 4.48 - 4.58 (2 H, m), 2.92 (2 H, td, J = 12.80, 2.26 Hz), 2.54 - 2.64 (2 H, m), 1.74 - 1.92 (3 H, m), 1.45 - 1.55 (3 H, m), 1.19 - 1.39 (2 H, m).

2-(4-Benzylpiperidin-1-yl)thieno[3,2-*d*]pyrimidine-4-carboxamide (34, ESC1000055)

A mixture of ethyl 2-(4-benzyl-1-piperidyl)thieno[3,2-d]pyrimidine-4-carboxylate (**70**, 171 mg, 0.45 mmol) and 7M NH_3 in methanol (0.64 mL) in MeOH (4.5 mL) was sealed in a 20 mL microwave vial and heated at 40 °C in a sand bath for 22 h. The mixture was concentrated under reduced pressure and purified by flash

chromatography yielding 2-(4-benzylpiperidin-1-yl)thieno[3,2-*d*]pyrimidine-4-carboxamide (182 mg, 115%). ^{1}H NMR (400 MHz, $CDCl_3$) δ 7.94 - 7.99 (1 H, m), 7.73 (1 H, br. s.), 7.28 - 7.35 (2 H, m), 7.13 - 7.25 (4 H, m), 5.77 (1 H, br. s.), 4.82 (2 H, d, J = 13.30 Hz), 2.92 (2 H, td, J = 12.80, 2.51 Hz), 2.59 (2 H, d, J = 7.03 Hz), 1.73 - 1.93 (3 H, m), 1.20 - 1.37 (4 H, m). LC-MS tR = 3.04 min, m/z 353.05.

Tert-butyl *N*-[(1*S*)-1-benzyl-3-(o-tolylsulfanyl)-2-oxo-propyl]carbamate (71)

Tert-butyl *N*-[(1*S*)-1-benzyl-3-bromo-2-oxo-propyl]carbamate (310 mg, 0.91 mmol), 2-methylbenzenethiol (106.74 µL, 0.91 mmol), 2,6-lutidine (105.5 µL, 0.91 mmol) and TBAI (3.35 mg, 0.01 mmol) were combined and stirred in acetonitrile (15 mL) at rt for 1 hour. The reaction mixture was diluted with ethyl acetate and washed sequentially with 0.5M HCl, water and brine. The organic was dried over Na_2SO_4, concentrated at reduced pressure and purified by flash chromatography yielding tert-butyl *N*-[(1*S*)-1-benzyl-3-(o-tolylsulfanyl)-2-oxo-propyl]carbamate (176 mg, 50%).

(3S)-3-Amino-1-(o-tolylsulfanyl)-4-phenyl-butan-2-one hydrochloride (72)

Tert-butyl N-[(*1S*)-1-benzyl-3-(o-tolylsulfanyl)-2-oxo-propyl]carbamate (**71**, 176 mg, 0.46 mmol) was stirred in 4M HCl in dioxane (3 ml) at room temperature for 2 hours. The solvent was removed at reduced pressure to afford (3S)-3-amino-1-(o-tolylsulfanyl)-4-phenyl-butan-2-one hydrochloride (150 mg, quant.).

***N*-[(1*S*)-1-Benzyl-3-(o-tolylsulfanyl)-2-oxo-propyl]-4-methylbenzenesulfonamide (46, ESC100100)**

(*3S*)-3-Amino-1-(o-tolylsulfanyl)-4-phenyl-butan-2-one hydrochloride (**72**, 150 mg, 0.47 mmol) and tosyl chloride (88.85 mg, 0.47 mmol) were stirred at room temperature in DCM (5 mL). DIEA (162.35 µl, 0.93 mmol) was added and the reaction stirred at room temperature overnight. The reaction mixture was diluted with DCM and washed with water. The organic was dried over Na_2SO_4 and concentrated at reduced pressure. The resulting residue was purified by flash chromatography followed by acidic reverse phase preperative HPLC yielding *N*-[(1*S*)-1-benzyl-3-(o-tolylsulfanyl)-2-oxo-propyl]-4-methylbenzenesulfonamide (54 mg, 26%). ^{1}H NMR (400 MHz, $CDCl_3$) δ 7.51 - 7.59 (m, 2H), 7.06 - 7.25 (m, 8H), 6.95 - 7.05 (m, 3H), 5.16 (d, *J* = 7.78 Hz, 1H), 4.37 - 4.47 (m, 1H), 3.58 - 3.69 (m, 2H), 2.88 - 3.02 (m, 2H), 2.26 - 2.47 (m, 6H). LC-MS: RT = 1.92, m/z 440.25 [M+H]+.

Supplementary information

Proof-of-principle LOPAC screen

Table S1. All 26 hits of the LOPAC library proof-of-principle screen, ranked on % effect (> 50% at 10 µM, 2.03% hit rate). Class and function are derived from the Sigma Aldrich library descriptions. Bold are selected for subsequent dose response analysis on DAGLα.

% Eff.	Compound	MW	Class	Function
92	Tetradecylthioacetic acid	365,9	Transcription	Peroxisome proliferator-activated receptor (PPAR)-alpha agonist
88	**GW5074 (Compound 4)**	425,1	Phosphorylation	cRaf1 kinase inhibitor
86	Cortisone 21-acetate	341,8	Hormone	Anti-inflammatory cortisol
81	Palmitoyl-DL-Carnitine chloride	606,1	Phosphorylation	Long-chain acylcarnitine; modulator of PKC activation; intermediate in mitochondrial fatty acid oxidation
77	(R,R)-cis-Diethyl tetrahydro-2,8-chrysenediol	471,7	Hormone	Potent estrogen receptor beta antagonist; potent partial agonist at estrogen receptor alpha
76	**NNC 55-0396**	464,1	Ca^{2+} Channel	Selective T-type calcium channel inhibitor
75	**SB 224289 hydrochloride**	510,1	Serotonin	Selective 5-HT1B serotonin receptor antagonist
73	Bromoacetyl alprenolol menthane	786,4	Adrenoceptor	Alkylating beta adrenoceptor antagonist
73	DL-erythro-Dihydrosphingosine	502,8	Phosphorylation	Protein kinase C, phospholipase A2, and phospholipase D inhibitor
73	Phorbol 12-myristate 13-acetate	356,3	Phosphorylation	Activates protein kinase C; strong NO promoter; lymphocyte activator
72	Tamoxifen citrate	376,6	Phosphorylation	Anti-estrogen; relatively selective protein kinase C inhibitor
68	GR 127935 hydrochloride hydrate	365,9	Serotonin	Selective 5-HT1B/1D serotonin receptor antagonist.
67	Protoporphyrin IX	425,1	Cyclic Nucleotides	Activates soluble guanylyl cyclase
66	**Amiodarone hydrochloride**	341,8	Adrenoceptor	Adrenoceptor agonist; inhibits binding of 1,4-dihydropyridine to L-type Ca^{2+} channels; coronary vasodilator
65	1,3,5-tris(4-hydroxyphenyl)-4-propyl-1H-pyrazole	606,1	Hormone	Specific estrogen receptor alpha (ERalpha) agonist
64	A-77636 hydrochloride	471,7	Dopamine	Potent, orally active D1 dopamine receptor agonist
64	3',4'-Dichlorobenzamil hydrochloride	464,1	Ion Pump	Na^{+}/Ca^{2+} exchanger inhibitor
58	**PQ401**	510,1	Somatostatin	Peroxisome proliferator-activated receptor (PPAR)-alpha agonist
57	Prochlorperazine dimaleate	786,2	Dopamine	cRaf1 kinase inhibitor
57	Terfenadine	502,8	Histamine	Anti-inflammatory cortisol
55	DL-Stearoylcarnitine chloride	356,3	Phosphorylation	Long-chain acylcarnitine; modulator of PKC activation; intermediate in mitochondrial fatty acid oxidation
52	**Raloxifene hydrochloride**	376,6	Hormone	Potent estrogen receptor beta antagonist; potent partial agonist at estrogen receptor alpha
52	Ruthenium red	365,9	Ion Pump	Selective T-type calcium channel inhibitor
51	**GW7647**	425,1	Transcription	Selective 5-HT1B serotonin receptor antagonist
51	DL-Homatropine hydrobromide	341,8	Cholinergic	Alkylating beta adrenoceptor antagonist
50	**CP55940**	606,1	Cannabinoid	Protein kinase C, phospholipase A2, and phospholipase D inhibitor

Primary assay and active conformation JECL screen

Table S2. All 46 QHL hits from the ELF and their corresponding % effect in the primary screen at 10 µM inhibitor and the active conformation at 10 µM and 1.25 µM inhibitor. Concentrations are final concentrations.

Entry	Primary assay (% Eff.)	Active conformation (% Eff. 10 µM and 1.25 µM)		Entry	Primary assay (% Eff.)	Active conformation (% Eff. 10 µM and 1.25 µM)	
5	91	93	89	**28**	63	70	7
6	89	93	77	**29**	76	77	-7
7	88	72	55	**30**	67	74	9
8	78	82	36	**31**	76	58	50
9	79	80	26	**32**	86	90	29
10	86	87	54	**33**	96	93	91
11	86	77	58	**34**	72	73	17
12	99	99	81	**35**	85	80	11
13	87	86	34	**36**	64	74	19
14	76	75	22	**37**	89	89	30
15	82	83	-3	**38**	96	88	15
16	93	94	18	**39**	84	84	23
17	72	78	6	**40**	79	70	33
18	75	76	11	**41**	53	74	28
19	73	71	8	**42**	94	88	25
20	85	87	8	**43**	80	81	23
21	87	82	10	**44**	78	92	52
22	70	73	17	**45**	88	91	39
23	84	73	1	**46**	75	71	18
24	91	93	16	**47**	65	70	26
25	86	89	15	**48**	64	72	25
26	86	88	10	**49**	81	82	17
27	54	73	31	**50**	93	87	43

References

1. Mullard, A. European Lead Factory opens for business. *Nat. Rev. Drug Discov.* **12,** 173–175 (2013).
2. Besnard, J., Jones, P. S., Hopkins, A. L. & Pannifer, A. D. The Joint European Compound Library: Boosting precompetitive research. *Drug Discov. Today* **20,** 181–186 (2015).
3. Karawajczyk, A. *et al.* Expansion of chemical space for collaborative lead generation and drug discovery: The European Lead Factory Perspective. *Drug Discov. Today* **20,** 1310–1316 (2015).
4. Kingwell, K. European Lead Factory hits its stride. *Nat. Rev. Drug Discov.* **15,** 221–222 (2016).
5. Nomura, D. K. *et al.* Endocannabinoid hydrolysis generates brain prostaglandins that promote neuroinflammation. *Science* **334,** 809–813 (2011).
6. Janssen, F. J. & van der Stelt, M. Inhibitors of diacylglycerol lipases in neurodegenerative and metabolic disorders. *Bioorg. Med. Chem. Lett.* **26,** 3831–3837 (2016).
7. Pedicord, D. L. *et al.* Molecular characterization and identification of surrogate substrates for diacylglycerol lipase a. *Biochem. Biophys. Res. Commun.* **411,** 809–814 (2011).
8. Appiah, K. K. *et al.* Identification of small molecules that selectively inhibit diacylglycerol lipase-alpha activity. *J Biomol Screen* **19,** 595–605 (2014).
9. Kidd, D., Liu, Y. & Cravatt, B. F. Profiling serine hydrolase activities in complex proteomes. *Biochemistry* **40,** 4005–4015 (2001).
10. Bachovchin, D. A., Brown, S. J., Rosen, H. & Cravatt, B. F. Substrate-Free High-Throughput Screening Identifies Selective Inhibitors for Uncharacterized Enzymes. *Nat. Biotechnol.* **27,** 387–394 (2009).
11. Baggelaar, M. P. *et al.* Development of an activity-based probe and in silico design reveal highly selective inhibitors for diacylglycerol lipase-a in brain. *Angew. Chem. Int. Ed.* **52,** 12081–12085 (2013).
12. Janssen, F. J. *et al.* Discovery of glycine sulfonamides as dual inhibitors of sn-1-diacylglycerol lipase a and a/b-hydrolase domain 6. *J. Med. Chem.* **57,** 6610–6622 (2014).
13. Baell, J. & Walters, M. A. Chemical con artists foil drug discovery. *Nature* **513,** 481–483 (2014).
14. Chupak, L. S.; Zheng, X.; Ding, M.; Hu, S.; Huang, Y.; Gentles, R. & G. U.S. Patent 20110207749 A1. (2011).
15. Chupak, L. S. *et al.* Structure-activity relationship studies on chemically non-reactive glycine sulfonamide inhibitors of diacylglycerol lipase. *Bioorg. Med. Chem.* **24,** 1455–1468 (2016).
16. Janssen, F. J. *et al.* Discovery of glycine sulfonamides as dual inhibitors of sn-1-diacylglycerol lipase α and α/β hydrolase domain 6. *J. Med. Chem.* **57,** 6610–6622 (2014).
17. De Risi, C., Pollini, G. P. & Zanirato, V. Recent Developments in General Methodologies for the Synthesis of α-Ketoamides. *Chem. Rev.* **116,** 3241–3305 (2016).
18. Sehgal, S. N., Baker, H. & Vézina, C. Rapamycin (AY-22,989), a new antifungal antibiotic. II. Fermentation, isolation and characterization. *J. Antibiot. (Tokyo).* **28,** 727–732 (1975).
19. Malcolm, B. A. *et al.* SCH 503034, a mechanism-based inhibitor of hepatitis C virus NS3 protease, suppresses polyprotein maturation and enhances the antiviral activity of alpha interferon in replicon cells. *Antimicrob. Agents Chemother.* **50,** 1013–1020 (2006).
20. Perni, R. B. *et al.* Preclinical Profile of VX-950 , a Potent , Selective , and Orally Bioavailable Inhibitor of Hepatitis C Virus NS3-4A Serine Protease. *Antimicrob. Agents Chemother.* **50,** 899–909 (2006).
21. Koutek, B. *et al.* Inhibitors of arachidonoyl ethanolamide hydrolysis. *J. Biol. Chem.* **269,** 22937–22940 (1994).
22. Takahashi, L. Crystal structure of the covalent complex formed by a peptidyl. alpha.,. alpha.-difluoro-. beta.-keto amide with porcine pancreatic elastase at 1.78. ANG. resolution. *J. Am. Chem. Soc.* **32,** 3368–3374 (1989).
23. Baggelaar, M. P. *et al.* Highly Selective, Reversible Inhibitor Identified by Comparative Chemoproteomics Modulates Diacylglycerol Lipase Activity in Neurons. *J. Am. Chem. Soc.* **137,** 8851–8857 (2015).
24. Boger, D. L. *et al.* Exceptionally potent inhibitors of fatty acid amide hydrolase: the enzyme responsible for degradation of endogenous oleamide and anandamide. *Proc. Natl. Acad. Sci. U.S.A.* **97,** 5044–5049 (2000).
25. Imperiali, B. & Abeles, R. H. Inhibition of serine proteases by peptidyl fluoromethyl ketones. *Biochemistry* **25,** 3760–3767 (1986).
26. Hsu, K. L. *et al.* DAGLβ inhibition perturbs a lipid network involved in macrophage inflammatory responses. *Nat. Chem. Biol.* **8,** 999–1007 (2012).
27. Ogasawara, D. *et al.* Rapid and profound rewiring of brain lipid signaling networks by acute diacylglycerol lipase inhibition. *Proc. Natl. Acad. Sci. U.S.A.* **113,** (2015).

28. Kamat, S. S. *et al.* Immunomodulatory lysophosphatidylserines are regulated by ABHD16A and ABHD12 interplay. *Nat. Chem. Biol.* **11,** 164–71 (2015).
29. Nakamura, A., Lectard, S., Hashizume, D., Hamashima, Y. & Sodeoka, M. Diastereo- and enantioselective conjugate addition of alpha-ketoesters to nitroalkenes catalyzed by a chiral Ni(OAc)(2) complex under mild conditions. *J. Am. Chem. Soc.* **132,** 4036–4037 (2010).
30. Nobuyuki, Y. *et al.* Pharmaceutical use of N-Carbamoylazole derivatives. European Patent EP1258480 B1 (2002).
31. Bornholdt, J., Fjære, K. W., Felding, J. & Kristensen, J. L. Heterocyclic pentafluorophenyl sulfonate esters as shelf stable alternatives to sulfonyl chlorides. *Tetrahedron* **65,** 9280–9284 (2009).

CHAPTER 7

Discovery of 1,2,4-triazole sulfonamide ureas as *in vivo* active α/β hydrolase domain type 16A inhibitors*

Introduction

Phospholipids constitute a class of small-molecules, which are located in and impart structural integrity to membranes of mammalian cells. They may also serve as important signaling molecules. Phosphatidylcholine (PC) and phosphatidylethanolamine (PE) are the most abundant phospholipids, whereas phosphatidylserine (PS), phosphatidic acid (PA) and phosphatidylinositol (PI) constitute quantitatively minor classes.[1] PS is located primarily in the inner leaflet of the cell membrane and its externalization (loss of symmetry) is considered a common signal for apoptosis and macrophage phagocytosis.[2] Moreover PS is known to activate intracellular enzymes, including protein kinase C[3] and is involved in blood coagulation.[4]

PS is ubiquitously present in all mammalian cell types, although it is most abundant in brain tissue.[1] Here, PS formation occurs by *L*-serine base exchange from membrane PC and PE by PS synthase-1 and 2 (PSS1 and PSS2), respectively, within the endoplasmic reticulum.[1] Several phospholipases are involved in the degradation of PS. Different phospholipases can either hydrolyse fatty acid esters at the *sn*-1 or *sn*-2 position, cleave the glycerol-phosphate or serine-phosphate bond. In addition, PS can be converted to PE by the mitochondrial enzyme PS decarboxylase. The exact contribution of each of these enzymes to the physiological role of PS remains poorly understood. Recently, a novel enzyme has been

* This research has received support from the Innovative Medicines Initiative Joint Undertaking under grant agreement n' 115489, resources of which are composed of financial contribution from the European Union's Seventh Framework Programme (FP7 / 2007-2013) and EFPIA companies in-kind contribution. Alex van der Ham is kindly acknowledged for all inhibitor optimization and characterization and for help with the biological evaluation of the compounds reported in this chapter. Hui Deng, Juan Zhou and Bobby Florea are kindly acknowledged for their help with the *in vivo* studies in mice.

identified in regulating PS levels; the serine hydrolase α/β hydrolase domain type 16A (ABHD16A also known as BAT5).[5] The development of ABHD16A knockout mice in combination with a small molecule ABHD16A inhibitor, have characterized ABHD16A as a principal PS lipase. ABHD16A cleaves the fatty acyl chain specifically at the *sn*-1 position (Figure 1A), forming *lyso*-PS as a main product.[5] *Lyso*-PS is an important signaling phospholipid involved in T-cell growth,[6] mast cell activation[7,8] and neurite outgrowth.[9] Although ABHD16A is ubiquitously expressed throughout the body, it has a relatively high expression in the brain, consistant with the levels of its PS substrate.[10] Within the brain, mRNA studies show high expression of ABHD16A in the cerebellum, a region mostly involved in fine motor movement and in some cognitive skills.[11] In addition, site specific mutations in the ABHD16A gene are associated with Kawasaki's disease,[12] an autoimmune disease characterized by inflammation of the blood vessels, known as vasculitis. Interestingly, *in vitro* studies have shown that ABHD16A exhibits monoacylglycerol lipase activity.[13] Savinainen *et al.* showed that catalytically active ABHD16A overexpressed in HEK293T cells hydrolysed several medium and long chain monoacylglycerols, as assessed by a multi-enzyme cascade fluorescent glycerol assay.[13] The exact role of this dual ABHD16A function *in vivo* is not known to date.

Lyso-PS is a toll like receptor 2 (TLR2) agonist,[14] and is involved in immune responses. α/β Hydrolase domain type 12 (ABHD12) hydrolyses *lyso*-PS, as reported by Blankman *et al.*[15] ABHD12$^{-/-}$ mice accumulated several distinct long chain *lyso*-PS lipids in the brain. Human genetic studies identified null-mutations of ABHD12 as the cause for the onset of a rare neurological disease that causes polyneuropathy, hearing loss, ataxia, retinitis pigmentosa and cataract (PHARC).[16,17] ABHD12 knockout studies confirmed that mice devoid of ABHD12 activity suffered from neuroinflammation and displayed multiple symptoms of PHARC.[15] ABHD12$^{-/-}$ mice may, therefore, serve as an excellent mouse model to investigate this neurological disease.[15] The exact molecular mechanism of the development of PHARC is currently unknown, but the accumulation of *lyso*-PS and subsequent excessive signaling via TLR2 are hypothesized to be involved in the neuroinflammatory response. To test this hypothesis, selective and *in vivo* potent inhibitors for ABHD16A, which are predicted to reduce the formation of *lyso*-PS, are required. If this hypothesis can be validated, then substrate reduction therapy by lowering *lyso*-PS levels through ABHD16A inhibition may serve as a potential treatment for PHARC patients.

Currently, three different chemotypes of ABHD16A inhibitors have been reported. Profiling of serine hydrolase inhibitors by Hoover *et al.* identified methylarachidonoyl-fluorophosphonate (**1**, MAFP, Figure 1B) and β-lactone tetrahydrolipstatin (**2**, THL, Figure 1B) as potent ABHD16A inhibitors.[18] The β-lactone activity-based probe (ABP) MB064, efficiently labelled ABHD16A in mouse brain proteomes.[19] Using this ABP, 1,3,4-oxadiazolone LEI103 (**3**, Figure 1B) was discovered as a non-selective ABHD16A inhibitor by Baggelaar *et al*., 2013. Savinainen *et al.* further explored 1,3,4-oxadiazolones as ABHD16A inhibitors and their hit optimization efforts resulted in the discovery of C7600 (**4**, Figure 1B).[13] Neutral cholesterol

ester hydrolase 1 (KIAA1363) was observed as an important off-target of C7600 (**4**). Camara *et al.* reported on the development of α-methylene-β-lactone derivatives as serine hydrolase inhibitors.[20] Activity-based protein profiling (ABPP) using broad-spectrum probe carboxytetramethylrhodamine fluorophosphonate (TAMRA-FP) led to the discovery of KC01 (**5**), a highly potent ABHD16A inhibitor and its corresponding paired control compound KC02 (**6**, Z/E: 4:1, Figure 1B), that did not inhibit ABHD16A.[5,20] All three ABHD16A inhibitor chemotypes presumably act as irreversible inhibitors, reacting with the catalytic Ser355, using their warhead (*i.e.* electrophilic trap) as site of covalent attachment. These three chemotypes are not selective and lack bioavailability, thus there is a need for selective and *in vivo* active ABHD16A inhibitors.

A high throughput screening campaign was initiated to discover *sn*-1 diacylglycerol lipase α (DAGLα) inhibitors, in collaboration with the European Lead Factory (Chapter 6). Using a primary surrogate substrate assay in combination with an orthogonal competitive ABPP assay, several novel serine hydrolase inhibitors were discovered. The 1,2,4-triazole sulfonamide ureas were selected for subsequent hit-to-lead optimization, resulting in a ~100 membered focused library. Assessment of the selectivity of this library with ABPP using probe MB064 identified several ABHD16A inhibitors. As aforementioned, MB064 efficiently visualizes ABHD16A activity, but also several additional serine hydrolases in mouse brain proteome, including DDHD domain containing 2 (DDHD2), ABHD6, ABHD12, and DAGLα.[21] Hence MB064 was used to simultaneously assess activity on ABHD16A and selectivity over this panel of off-targets. Here the identification and optimization of potent 1,2,4-triazole sulfonamide urea ABHD16A inhibitors is described followed by *in vivo* characterization in mice.

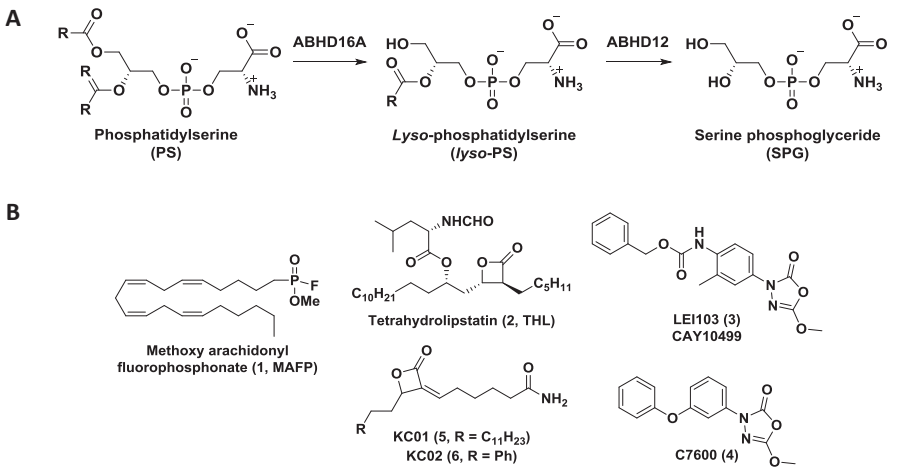

Figure 1. A) Phosphatidylserine (PS) and lyso-phosphatidylserine (lyso-PS) levels are regulated by α/β hydrolase domain type 12 and 16A (ABHD12 and ABHD16A). ABHD16A cleaves specifically at the PS *sn*-1 fatty ester, whereas ABHD12 cleaves the remaining *sn*-2 fatty ester of lyso-PS. **B)** Current inhibitors of ABHD16A are: *i)* Fluorophosphonates, such as methoxy arachidonoyl fluorophosphonate (**1**, MAFP), *ii)* β-Lactones (THL **2** and

KC01 **5**) and *iii)* 1,3,4-Oxadiazolones (LEI103, CAY10499 **3**) and C7600 (**4**). KC02 (**6**) has been reported as a paired inactive control compound of KC01 (**5**). Two activity-based probes (ABPs) have been reported for ABHD16A; TAMRA-fluorophosphonate (TAMRA-FP) and THL based β-lactone MB064.[5,13,18,21]

Results

Competitive ABPP on the focused library of 100 triazole sulfonamides (Chapter 6) revealed several 1,2,4-triazole sulfonamide ureas as ABHD16A inhibitors. All inhibitors, which have over 50% inhibitory effect on ABHD16A, are depicted in Table 1. Potency and selectivity of the inhibitors is influenced by the nature of the staying group (R_1, compare **10** and **11**) as well as the leaving group (R_2, compare **11**-**16**). ABHD16A seems to prefer small cyclic amine staying groups, since secondary and non-cyclic amines are not active (data not shown). The most potent ABHD16A inhibitors have, for example, a piperidine, morpholine or pyrolidine as preferred staying group (entries **7**, **8** and **10**, Table 1). Of note, 3-phenyl substituted pyrolidine is also allowed, indicating that a lipophilic pocket is present near the active site (entries **11-16**, Table 1). Compounds **14-16** show that triazole ureas sulfoxides are also allowed, albeit they appear to inhibit ABHD16A to a lesser extent. The leaving group can be enlarged, thereby increasing inhibitor potency (entries **14-16**, Table 1). This could indicate that the leaving group is located in a larger ABHD16A pocket.

All triazole ureas are non-selective and inhibit multiple off-targets (Table 1), which suggested that on one hand the triazole sulfonamide functions as a reactive warhead and on the other hand that the enzymes share similar active sites in which the current substituents are not able to make selective interactions. Increasing potency and selectivity are, therefore, the two main priorities for the hit-to-lead optimization process. Compound **8** appeared the most selective inhibitor based on a single concentration (Table 1). Therefore compound **8** was profiled in a full dose response using competitive ABPP with MB064 on mouse membrane proteome (Figure 2). Compound **8** had an IC_{50} of ~400 nM on ABHD16A and did not inhibit DAGLα. ABHD6 and ABHD12 were identified as important off-target activities. To study *lyso*-PS formation, it will be important to have inhibitors which are selective over ABHD12. Compound **10**, a methyl substituted sulfonamide, does not exhibit any ABHD12 activity, therefore it was decided to investigate the effect of methylation of the sulfonamide in compound **8**. To this end, a synthetic route was developed as depicted in Scheme 1A. In brief, sulfenamide **17a** was obtained from *in situ* prepared *N*-chloro-*N*-methylbenzylamine and subsequently treated with morpholine carbamoyl chloride. Lastly sulfonamide **17** was synthesized from the corresponding sulfenamide by oxidation with $NaIO_4$ and $RuCl_3$.

Table 1. Initial hit compounds for ABHD16A, sulfonamides **7**-**13** and sulfoxides **14**-**16**. R^1 is staying group, R^2 is leaving group. Values are % inhibition in ABPP for ABHD6, 12, 16, DDHD2 and FAAH, at 10 µM inhibitor concentration (N = 1). DAGLα values are pIC_{50} PNP assay in dose response analysis (N = 2, n = 2). See experimental section for assay procedures.

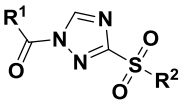

#	R^1	R^2	ABHD16A (% eff.)	ABHD12 (% eff.)	DDHD2 (% eff.)	ABHD6 (% eff.)	FAAH (% eff.)	DAGLα PNP (pIC_{50})
7			100	56	99	96	84	6.1
8			100	83	0	94	73	< 4.7
9	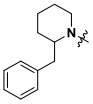		74	86	70	99	51	7.2
10			91	0	73	98	98	6.3
11	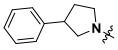		76	50	100	99	100	7.2
12	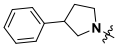		72	38	87	95	100	8.0
13	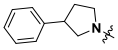		59	53	96	99	98	7.1
14	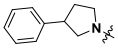		52	0	94	94	90	7.0
15	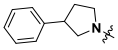		64	57	84	99	98	7.9
16	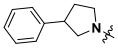		78	73	100	92	100	8.0

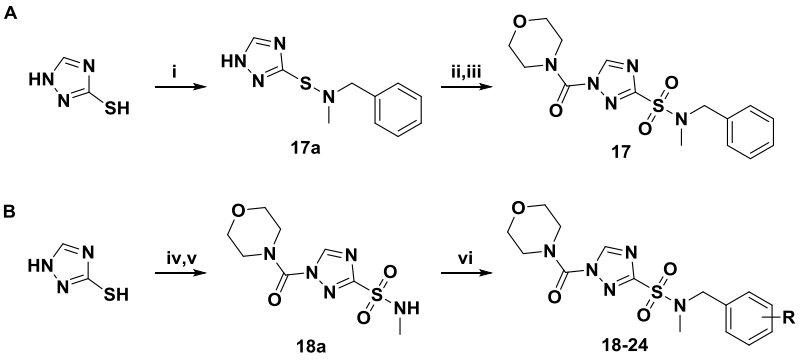

Scheme 1. Synthesis of 1,2,4-triazole sulfonamides **17**-**24**. A) Initial synthesis of compound **17:** *i)* NCS, NHMeBn 0°C, CH_2Cl_2, 30 min, then 1,2,4-triazole-3-thiol (sol. in THF), rt, 3h. *ii)* Morpholine carbamoyl chloride, DIPEA, DMAP, rt, 10 h. 16% (2 steps). *iii)* NaI_4, $RuCl_3$, $MeCN/H_2O$ 3:1, rt, 14 h., 43% (**17**). **B)** Synthesis of compounds **18**-

24, with last step derivatization of R-group: *iv)* NaOCl, HCl, H_2O, Dioxane, DCM, then NHMe (aq), rt. 2 hr. *v)* Morpholine carbamoyl chloride, DIPEA, DMAP, rt, ON. 28% yield over 2 steps. *vi)* Derivatization; corresponding benzyl/ phenoxybenzyl halide, NaH, rt, ON, 3-50% yield. R = H, 4-Me, 4-Cl, 4-OMe, 4-OPh, 3-OPh, 3(2-oxy-5-(trifluoromethyl)pyridine) (**18**-**24**).

Dose response analysis of **17** on ABPP indicated that it was a potent ABHD16A inhibitor with an IC_{50} of 616 nM and 100-fold selectivity over ABHD12 (Figure 2). However, off-target ABHD6 activity was significantly increased.

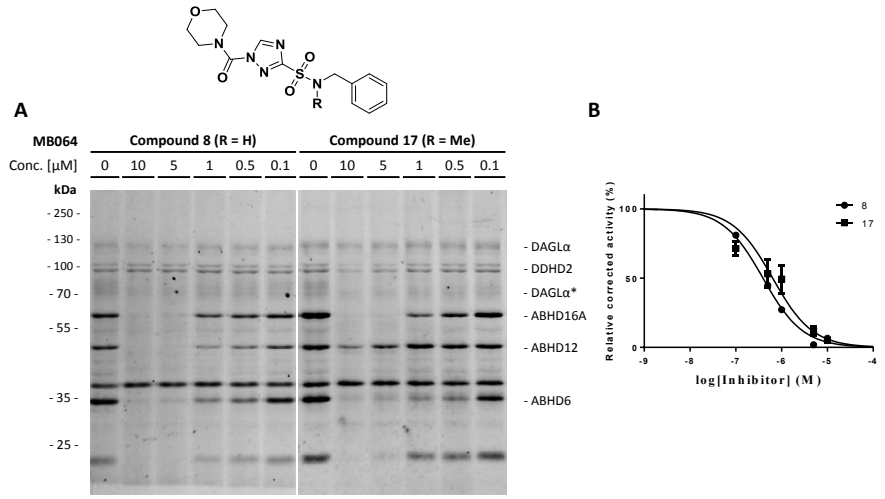

Figure 2. A) On-gel dose response analysis of hit compound **8** (R = H) and optimized compound **17** (R = Me) on ABPP with MB064 on mouse brain proteome. Compound **8** competes with probe labeling on ABHD16A, as well as ABHD6 and ABHD12. Compound **17** competes with probe labeling on ABHD16A with equal potency compared to **8**, but displays some ~100 fold more selectivity over ABHD12. B) Dose response curve of compounds **8** (N = 1) and **17** (N = 3). pIC_{50} values: 6.41 and 6.18 ± 0.18 (for compounds **8** and **17** respectively).

An optimization strategy, analogous to a Topliss scheme, was conducted on the benzylamine group of compound **17,** in which a *p*-methyl group (**18**), an electron withdrawing (*p*-Cl, **19**) or donating substituent (*p*-OMe, **20**) were introduced to investigate the electronic and lipophilic properties of the phenyl ring (see Scheme 1B for the synthetic route). Compound **19** showed increased inhibitor potency, whereas **20** was equally active and **18** was less active (4-Cl > 4-OMe > H > 4-Me, Table 2, entries **17-20**). Of note, preference for electron withdrawing and lipophilic substituents has also been observed during optimization of 1,3,4-oxadiazol-2(3*H*)-ones C7600 as ABHD16A inhibitors.[13] To probe the size of the binding pocket, a 4-phenoxy moiety was introduced (**21**). This increased inhibitor potency almost 33-fold compared to **17** (Table 2). Similar to the development of C7600 (Figure 1),[13] changing the phenoxy substituent from *para*- to *meta*-position (**22**) increased inhibitor potency, almost 100-fold compared to compound **17** (Table 2). This suggests that the aryl ether substituent is located in a lipophilic pocket that normally accommodates an acyl chain of PS. Lastly, compound **23** was designed, in which the biphenyl ether was replaced by a 3-(2-

pyridinyl)-4-CF_3 phenoxy ether. This group has been previously applied in PF-04457845, a clinical trial drug candidate for another serine hydrolase FAAH, to increase metabolic stability.[22] The activity of compound **23** was, however, slightly decreased (Table 2), which could perhaps be explained by its reduced lipophilicity.

Table 2. Structure-activity relationships of 1,2,4-triazole sulfonamides **17**-**23** as ABHD16A inhibitors. Activity assay is ABPP on mouse brain. Values are ABHD16A pIC_{50} ± SEM, N = 3. pIC_{50} values were determined using Graphpad Prism after normalization to control and correction for protein loading via Coomassie staining. The activity-based probe is MB064 (250 nM final concentration).

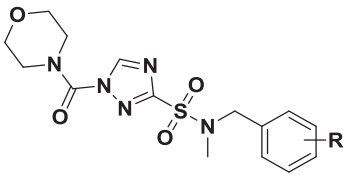

Entry	R group	R position	pIC_{50} ± SEM
17	H	-	6.18 ± 0.18
18	Me	4	5.02 ± 0.16
19	Cl	4	7.48 ± 0.04
20	OMe	4	6.84 ± 0.13
21	OPh	4	7.70 ± 0.20
22	OPh	3	8.10 ± 0.13
23	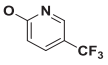	3	7.44 ± 0.27

To obtain a more comprehensive selectivity profile of compounds **22** and **23**, a comparative ABPP assay was performed using two ABPs, *i.e.* MB064 and TAMRA-FP (Figure 3). Both compounds were not selective and did inhibit several serine hydrolases. ABHD6 was identified as an important off-target. Moreover, inhibition of DDHD2, ABHD12 and FAAH is observed at the highest inhibitor concentrations for both **22** and **23**. Compound **22** appeared more fold-selective due to its higher potency on ABHD16A in the ABPP setting (Table 3).

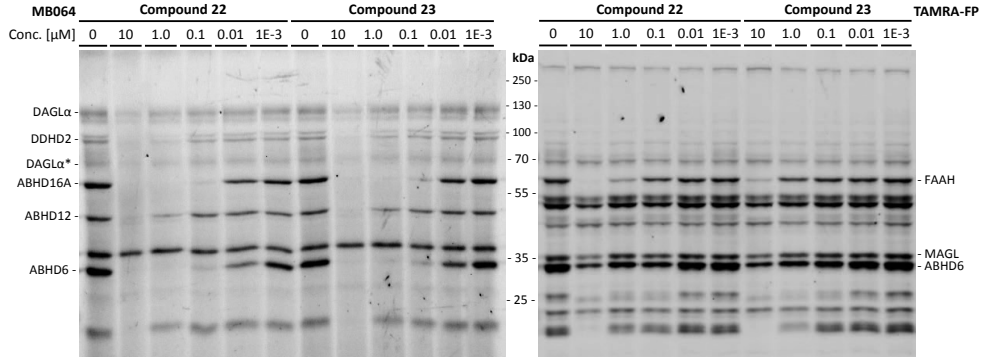

Figure 3. Representative gels of the selectivity profile of compounds **22** and **23** on mouse brain proteome using ABPs MB064 and TAMRA-FP. Both compounds were measured at N = 3.

Table 3. All identified and quantified off-targets of **22** and **23** in mouse brain proteome. N = 3. pIC_{50} values were determined using Graphpad Prism after normalization to control and correction for protein loading via Coomassie staining. All values are N = 3. The activity-based probe is MB064 (250 nM final concentration) and TAMRA-FP (500 nM final concentration). Apparent selectivity is determined as $IC_{50}/IC_{50\ (ABHD16A)}$.

	pIC_{50} ± SEM 22	**Apparent fold selectivity**	**pIC_{50} ± SEM 23**	**Apparent fold selectivity**
ABHD16a	**8.10 ± 0.13**	-	**7.44 ± 0.27**	-
DAGLα	5.46 ± 0.11	437	5.15 ± 0.20	195
DDHD2	6.75 ± 0.30	22	6.52 ± 0.20	8
ABHD12	6.29 ± 0.20	65	6.07 ± 0.12	23
ABHD6	**8.18 ± 0.08**	**1**	**7.70 ± 0.10**	**1**
LyPLA1/2	5.86 ± 0.10	174	5.62 ± 0.16	66
FAAH	6.14 ± 0.10	91	5.68 ± 0.10	58
PLA2G7	4.64 ± 0.18	>1000	4.62 ± 0.14	661
MAGL	4.97 ± 0.07	>1000	4.88 ± 0.08	363

Next, the activity of both compounds was measured on recombinant human ABHD16A overexpressed in HEK293T cell membrane fractions. Active hABHD16A was labelled by MB064 and dose dependently competed by **22** and **23.** The pIC_{50}s were 7.67 ± 0.13 and 7.54 ± 0.11 for **22** and **23**, respectively (N = 3, Figure 4A). To assess whether **22** and **23** were active in a cellular setting, an *in situ* ABHD16A cellular assay was developed using Neuro 2A cells (N2A) that endogenously express ABHD16A. Compound **22** was highly active on ABHD16A, as 5 minutes pre-incubation of living N2A cells with 100 nM of **22** completely

blocked ABHD16A labeling by MB064 (Figure 4B, panel 1). Surprisingly, ABHD6 was not significantly inhibited, even at the highest incubation time tested (60 min with 100 nM of **16,** Figure 4B, panel 1). ABHD16A has an extracellular localization whereas ABHD6 has not, indicating that **22** and **23** cannot cross the cell membrane effectively. Upon further investigation, both compounds dose-dependently blocked ABHD16A labeling by ABP MB064 (Figure 4B). Similar cellular activity was observed for both compounds (pIC_{50} = 7.8 ± 0.1 and 7.9 ± 0.1 for **22** and **23**, respectively). Of note, an unidentified off-target (Figure 4B, * in panels 1-3) was observed in N2A cells.

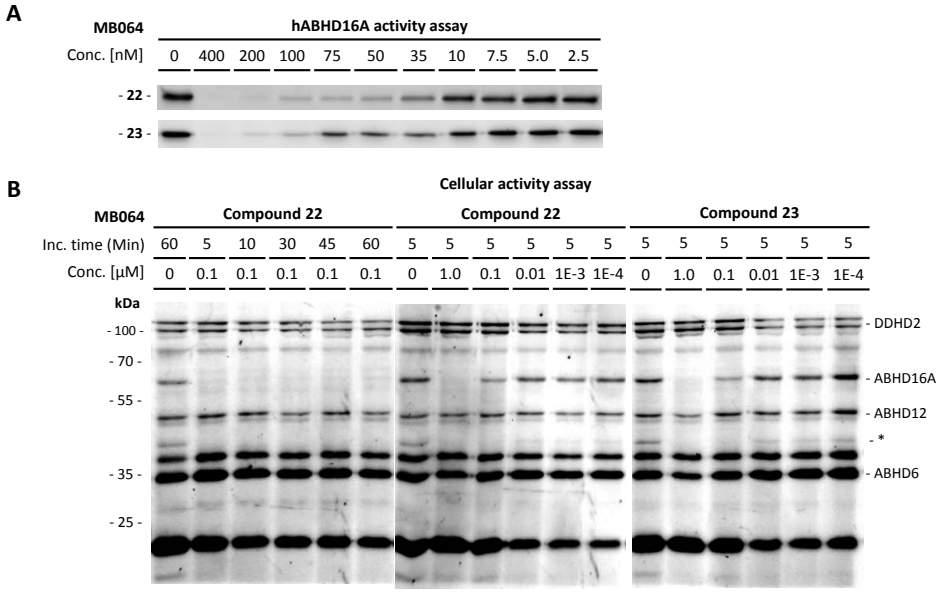

Figure 4. A) Dose response analysis of **22** and **23** on human ABHD16A overexpressed HEK293T cell membrane fractions. pIC_{50} values are 7.67 ± 0.13 and 7.54 ± 0.11 for **22** and **23**, respectively. **B)** Cellular Neuro 2A assay. Panel 1; Time dependent incubation of compound **22** at 100 nM concentration. Labeling of cellular ABHD16A is completely prevented at 5 minutes incubation with compound **22**. Panel 2; *In situ* dose response analysis of compound **22** on cellular ABHD16A with 5 minutes pre-incubation. Panel 3; *In situ* dose response analysis of compound **23** on cellular ABHD16A. pIC_{50} = 7.8 ± 0.1 and 7.9 ± 0.1 for **22** and **23** respectively. * is an off-target of **22** and **23** which remains to be indentified. pIC_{50} values were determined using Graphpad Prism after normalization to control and correction for protein loading via Coomassie staining. All values are N = 3. The activity-based probe is MB064 (250 nM final concentration).

Finally, it was investigated if both compounds would be able to inhibit ABHD16A activity *in vivo*. 12 Male C57 black-6 mice were divided into 4 groups, 3 mice served as control, and the remaining mice received either 45 mg/kg or 15 mg/kg of compound **22**, or 45 mg/kg of compound **23** by *i.p.* injection. The mice appeared to exhibit normal behaviour after administration of the compounds. After two hours, the mice were sacrificed by cervical dislocation. Brain and spleen tissues were harvested, lysed and subjected to ABPP analysis using ABPs MB064 and TAMRA-FP. Both compounds significantly reduced ABHD16A labeling

by MB064 in brain (Figure 5), albeit not fully at the highest dose tested. This indicates that the compounds are active *in vivo*, but may have difficulties crossing the blood brain barrier (BBB). This hypothesis is strengthened by analysis of mouse spleen, here multiple proteins are fully inhibited (see supporting information). Interestingly, both compounds did not seem to inhibit brain ABHD6 to a large extent (Figure 5A, panel 1), which is in line with the results obtained from the cellular experiments and indicates restricted cell permeability. ABHD12 and ABHD6 do appear to be inhibited to a minor extent. The reduced DAGLα labeling is probably an artefact, as this enzyme is very sensitive towards degradation due to freeze-thaw cycles. Labeling by broad-spectrum probe TAMRA-FP displays some minor inhibition on FAAH and MAGL (Figure 5A, panel 2) at the highest dose tested.

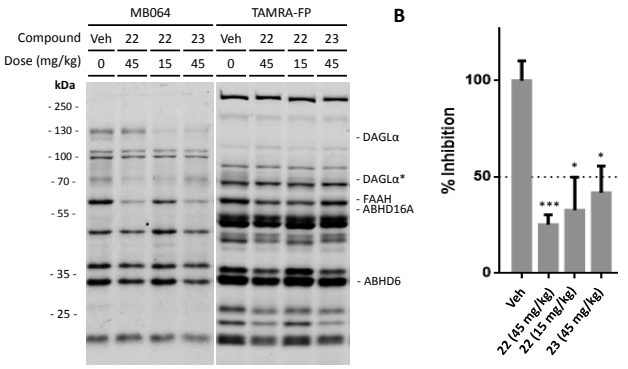

Figure 5. A) Representative gels of the *in vivo* characterization of compounds **22** and **23** with ABP MB064 and TAMRA-FP on mouse brain. Significant reduction of ABHD16A labeling is observed. Some reduced DAGLα labeling is also observed, which is due to instability of this enzyme. **B)** Average inhibition of ABHD16A MB064 labeling in brain by compounds **22** and **23** (N = 3). Significance, T-Test: *P < 0.05; **P < 0.01; ***P < 0.001.

Conclusions

To conclude, 1,2,4-triazole sulfonamides were discovered as potent ABHD16A inhibitors. Original hit compound **8**, was rapidly optimized to **22** and **23** using a rational design approach. Both compounds were active on murine as well as human ABHD16A and were active in a cellular context . Cellular experiments strongly indicate that both compounds do not penetrate cells efficiently, but do potently inhibit extracellular ABHD16A. 1,2,4 Triazole sulfonamides **22** and **23** partially, but significantly, inhibit ABHD16A *in vivo*, after *i.p.* administration. This makes compounds **22** and **23**, the first *in vivo* active ABHD16A inhibitors in current literature. As brain ABHD16A was not completely inhibited at high doses of both compounds, future work could focus on optimization of brain penetration by decreasing the polar surface area and increasing metabolic stability. This optimization, however, is highly likely to increase off-target activity *in vivo*. Hence the development of a paired inactive control compound is advised, to exclude potential off-targets effect during studies on animal

models. The structure-activity relationships from this study provide an excellent starting point for further optimization of the next generation of *in vivo* active ABHD16A inhibitors. Ultimately it is shown that 1,2,4-triazole sulfonamides may provide excellent tool compounds to investigate the role of ABHD16A inhibition as a potential treatment of the debilitating disease PHARC.

Experimental

Procedures chemical biology

Cell Culture and Membrane Preparation

Cell culture and membrane preparations were performed as earlier reported.[19] In brief, HEK293T and N2A cells were grown in DMEM with stable glutamine and phenol red (PAA or Sigma) with 10% new born calf serum, penicillin, and streptomycin. Cells were passaged every 2−3 days by resuspension in medium and seeding to the appropriate confluence.

Membranes were prepared from transiently transfected HEK293T. One day prior to transfection, 10^7 cells were seeded in a 15 cm Petri dish. Cells were transfected by the addition of a 3:1 mixture of polyethyleneimine (60 μg) and plasmid DNA (20 μg) in 2 mL of serum free medium. The medium was refreshed after 24 h, and after 72 h the cells were harvested by suspending them in 20 mL of medium. The suspension was centrifuged for 10 min at 1000 rpm, and the supernatant was removed. The cell pellet was stored at −80 °C until use.

Cell pellets were thawed on ice and suspended in lysis buffer A (20mM HEPES, pH 7.2, 2 mM DTT, 0.25 M sucrose, 1 mM $MgCl_2$, 25 U/mL Benzonase). For hABHD16a HEK293T membrane preparations, protease inhibitor cocktail was not added. The suspension was homogenized by polytrone (3 × 7 s) and incubated for 30 min on ice. The suspension was subjected to ultracentrifugation (93.000g, 30 min, 4 °C, Beckman Coulter, type Ti70 rotor) to yield the cytosolic fraction in the supernatant and the membrane fraction as a pellet. The pellet was suspended in lysis buffer B (20 mM HEPES, pH 7.2, 2 mM DTT). The protein concentration was determined with a Quick Start Bradford assay (Biorad). The protein fractions were diluted to a total protein concentration of 5 and 9 mg/mL and stored in aliquots at −80 °C until use.

Colorimetric DAGLα assay (PNP-butyrate assay)

The colorimetric DAGα activity assay was performed as previously reported.[19,21,23,24]

Tissue sample preparation

Tissue sample preparations was performed as earlier reported.[19] In brief, mouse brains were isolated according to guidelines approved by the ethical committee of Leiden University (DEC#14137). Mouse brains were thawed on ice and dounce-homogenized in lysis buffer A (20 mM HEPES, 2 mM DTT, 1 mM $MgCl_2$, 25 U/mL Benzonase) and incubated for 15 minutes on ice, followed by low speed spin (2500 × g, 3 min. at 4 ^{o}C) to remove debris. The supernatant was subjected to ultracentrifugation (37,000 rpm, 45 min. 4 ^{o}C, Beckman Coulter, Type Ti70 rotor) to yield the cytosolic fraction in the supernatant and the membrane fraction as a pellet. The pellet was resuspended in lysis buffer B (20 mM HEPES, 2 mM DTT). The total protein concentration was determined with Quick Start Bradford assay (Biorad). Membranes were stored in small aliquots at -80 ^{o}C until use.

Cellular ABPP experiment

Neuro2A (N2A) cells were grown according to the cell culture protocol above. Cells were harvested, homogenized by pipetting and washed 3x with serum free DMEM medium. The cells were divided equally over 6-well cell culture plates and stabilized for 30 min at 37°C. Inhibitors were added from the corresponding DMSO stock (1:1000 final DMSO conc.) to the appropriate inhibitor conc. (1.0 μM – 0.1 nM). Cells were incubated for the appropriate time (5-60 min.) with inhibitor and after washed 3 x with PBS and harvested in

PBS. The samples were centrifuged in eps for 10 min at 8000 rpm, the supernatant was removed and the samples were flash frozen in liquid nitrogen.

The cell pellets were thawed on ice, lysis buffer A (20 mM HEPES, 2 mM DTT, 1 mM $MgCl_2$, 25 U/mL Benzonase) was added, whereafter the samples were mixed with a pipet and incubated for 15 minutes on ice. Protein concentration of all the samples was determined with a Bradford assay. Samples were diluted to 2 mg/ mL with lysis buffer B (20 mM HEPES, 2 mM DTT) and analysed using the ABPP protocol as previously reported and described below.[19]

ABPP for murine and human ABHD16A

ABPP was performed as earlier reported.[19] In brief, IC_{50} determination of inhibitors against endogenously expressed ABHD16A in the mouse brain membrane proteome. Inhibitors were incubated at the indicated concentrations (total volume 20 µL) for 30 min at rt, prior to incubation with probe MB064 or TAMRA-FP for 15 min at rt. The reaction was quenched with 7.5 µL standard 4 × SDS page sample buffer, and resolved on 10 % SDS-page. The gels were scanned and the percentage activity remaining was determined by measuring the integrated optical intensity of the bands using Image Lab 5.2. software. IC_{50} values were determined from a dose-response curve generated using Prism software (GraphPad).

ABPP of *in vivo* samples

ABPP was performed as earlier reported.[19] In brief, proteomes were diluted to the same concentration (Brain = 2 mg/ mL, Testis = 1mg/ mL, Spleen = 0.5 mg/mL) and 20 µL of proteome incubated with either MB064 (final concentration: 250 nM) or TAMRA-FP (Thermo Fischer Scientific, final concentration: 500nM) at rt for 15 minutes. The reactions were quenched using 7.5 µL of standard SDS-PAGE sample buffer. The samples were then directly loaded and resolved on SDS-PAGE gels (10% acrylamide). The gels were scanned using a ChemiDoc MP system and analysed using ImageLab v.4.1. IC_{50} values were determined by integration of the fluorescent proteins bands, corrected for protein loading using Coomassie staining, and expression of the band intensity relative to control (DMSO). The resultant data were then exported to Graphpad Prism v.5 and analysed using non-linear fitting. All values are based on N = 3, and SEMs are given for each data point.

***In vivo* dosing experiments**

Compounds **22** and **23** were prepared as a solution or emulsion in carrier, consisting of 18:1:1 PBS:PEG-40:EtOH. The final concentrations of the solution were 1.5 mg/µL and 4.5 mg/µL. Twelve C57 Black-6 (C57BL/6) mice, 10-weeks of age, were weighted prior to intraperitoneal (i.p) injection of the compounds at 15 mg/kg and 45 mg/kg dosing respectively (1 µL/ kg). Mice receiving only carrier served as the control group (3 mice per group). After 2 hours the mice were sacrificed by cervical dislocation, the tissues harvested and immediately flash frozen in liquid nitrogen (DEC#14137, Date of experiment: 08-12-'15).

Procedures chemistry

General Remarks.

All reactions were performed using oven- or flame-dried glassware and dry solvents. Reagents were purchased from Sigma-Aldrich, Acros, and Merck and used without further purification unless noted otherwise. All moisture sensitive reactions were performed under an argon atmosphere. Traces of water were removed from starting compounds by coevaporation with toluene. ^{1}H and ^{13}C NMR spectra were recorded on a Bruker AV 400 MHz spectrometer at 400.2 (^{1}H) and 100.6 (^{13}C) MHz using the reported deuterated solvent. Chemical shift values are reported in ppm with tetramethylsilane or solvent resonance as the internal standard ($CDCl_3$: δ 7.26 for ^{1}H, δ 77.16 for ^{13}C; CD_3OD: δ 3.31 for ^{1}H, δ 49.00 for ^{13}C; CD_3CN: δ 1.94 for ^{1}H, δ 118.32 and 1.32 for ^{13}C). Data are reported as follows: chemical shifts (δ), multiplicity (s = singlet, d = doublet, dd = double doublet, td =

triple doublet, t = triplet, q = quartet, quintet = quint, b = broad, m = multiplet, appd = apparent doublet), coupling constants *J* (Hz), and integration. High resolution mass spectra were recorded on a Thermo Scientific LTQ Orbitrap XL. Compound purity was measured by liquid chromatography on a Finnigan Surveyor LC-MS system equipped with a C18 column. Flash chromatography was performed using SiliCycle silica gel type SiliaFlash P60 (230–400 mesh). TLC analysis was performed on Merck silica gel 60/Kieselguhr F254, 0.25 mm. Compounds were visualized using either a $KMnO_4$-stain (K_2CO_3 (40 g), $KMnO_4$ (6 g), and H_2O (600 mL)) or Ninhydrin-stain (Ninhydrin (200mg), *n*-butanol (95ml) and AcOH (10%, 5ml)).

_N_-Methyl-_N_-phenyl-1-(piperidine-1-carbonyl)-_1H_-1,2,4-triazole-3-sulfonamide (7)

Verified screening hit. HRMS (ESI+) m/z: calculated for $C_{15}H_{20}N_5O_4S$ ([M + H]), 350.1281; found, 350.1283. Purity of >95% as determined by LC-MS.

_N_-Benzyl-1-(morpholine-4-carbonyl)-_1H_-1,2,4-triazole-3-sulfonamide (8)

Verified screening hit. HRMS (ESI+) m/z: calculated for $C_{14}H_{18}N_5O_4S$ ([M + H]), 352.1074; found, 352.1068. Purity of >95% as determined by LC-MS.

_N_-Benzyl-N-methyl-1-(pyrrolidine-1-carbonyl)-_1H_-1,2,4-triazole-3-sulfonamide (10)

Verified screening hit. HRMS (ESI+) m/z: calculated for $C_{15}H_{20}N_5O_3S$ ([M + H]), 350.1281; found, 350.1283. Purity of >95% as determined by LC-MS.

_N_-Benzyl-_N_-methyl-1-(3-phenylpyrrolidine-1-carbonyl)-_1H_-1,2,4-triazole-3-sulfonamide (11)

Verified screening hit. HRMS (ESI+) m/z: calculated for $C_{21}H_{24}N_5O_3S$ ([M + H]), 426.1594; found, 426.1592. Purity of >95% as determined by LC-MS.

(3-((Benzyl(methyl)amino)thio)-1_H_-1,2,4-triazol-1-yl)(morpholino)methanone (17a)

To a stirred solution of *N*-chlorosuccinimide (3.3 g, 25 mmol) in CH_2Cl_2 (80 mL) was slowly added methylbenzylamine (9.6 mL, 75 mmol) at 0°C. After 30 minutes a solution of commercially available 1,2,4-triazole-3-thiol (2.5 g, 25 mmol) in dry THF (60 mL) was added slowly and the solution was gradually warmed up to rt and was stirred for an additional 3 h. The reaction mixture was poured into acetone, filtered, concentrated *in vacuo* and purified by flash chromatography. The sulfenamide was dissolved in dry THF (10 mL) and cooled to 0°C, after which was added DIPEA (262 µL, 1.5 mmol) and DMAP (12.2 mg, 0.1 mmol) and finally morpholinecarbamoyl chloride (133.5 µL, 1.1 mmol). The mixture was stirred for 4h until completion, after which the reaction mixture was diluted with EtOAc, washed with water, brine, dried, concentrated *in vacuo* and purified by flash chromatography to obtain (3-((benzyl(methyl)amino)thio)-1*H*-1,2,4-triazol-1-yl)(morpholino)methanone (53 mg, 0.16 mmol, 16%). ^{1}H NMR (CD_3CN, 400 MHz): δ 8.77 (s, 1H), 7.35-7.27 (m, 5H), 4.27 (s, 2H), 3.78 (brs, 4H), 3.74 (s, 4H), 2.93 (s, 3H). ^{13}C NMR (CD_3CN, 101 MHz): δ 163.99, 149.30, 148.38, 139.43, 129.86(2C), 129.28(2C), 128.47, 67.09(2C), 64.94, 47.52(2C), 46.40.

_N_-benzyl-_N_-methyl-1-(morpholine-4-carbonyl)-1_H_-1,2,4-triazole-3-sulfonamide (17)

To a stirred solution of (3-((benzyl(methyl)amino)thio)-*1H*-1,2,4-triazol-1-yl)(morpholino)methanone (**17a**, 10 mg, 30 nmol) in MeCN/ H_2O (3:1) was added $NaIO_4$ (19.3 mg, 90 nmol, 3 eq) and $RuCl_3$ (0.5 mg, 2.4nmol, 0.08 eq). The solution was stirred at rt for 14 h. until completion, after which the reaction mixture was diluted with EtOAc, washed with water, brine, dried, concentrated *in vacuo* and purified by flash chromatography to obtain *N*-benzyl-N-methyl-1-(morpholine-4-carbonyl)-1*H*-1,2,4-triazole-3-sulfonamide (4.3 mg, 13 nmol, 43%). HRMS (ESI+) m/z: calculated for $C_{15}H_{20}N_5O_4S$ ([M + H]), 366.1231; found, 366.1229. ^{1}H NMR (400 MHz, $CDCl_3$) δ 8.88 (s, 1H), 7.41 – 7.29 (m, 5H), 4.45 (s, 2H), 3.81 (s, 8H), 2.87 (s, 3H). ^{13}C NMR (101 MHz, $CDCl_3$) δ 148.19, 147.48,

141.90, 135.15, 129.13, 128.89, 128.53(2C), 128.31(2C), 66.62, 54.74, 47.92, 34.97. Purity of 93% as determined by LC-MS.

_N_-methyl-1-(morpholine-4-carbonyl)-1_H_-1,2,4-triazole-3-sulfonamide (18a)

To a cooled (-10°C) stirred solution of HCl in dioxane (4 M, 16 mL, 120 mmol) was added dry CH_2Cl_2 (80 mL) and subsequently aq. NaOCl solution (10%, 25 mL, 120 mmol) was added dropwise. After 15 minutes of stirring, 1,2,4-triazole-3-thiol (0.5 g, 5 mmol) was added and the solution was stirred for an additional 30 minutes and quenched with aqueous methylamine (11 M, 5 mL, 55 mmol). The solution was allowed to gradually warm up to rt, stirred for an additional 2 hours and subsequently concentrated *in vacuo*. The residue was taken up dry THF (80 mL) after which was added DIPEA (1.3 mL, 75 mmol), DMAP (60 mg, 0.5 mmol) and morpholine carbamoyl chloride (0.88 mL, 7.5 mmol). The solution was stirred at rt for 14 h. until completion, after which the reaction mixture was concentrated *in vacuo* and purified by flash chromatography to obtain *N*-methyl-1-(morpholine-4-carbonyl)-1*H*-1,2,4-triazole-3-sulfonamide (385 mg, 1.4 mmol, 28%). ^{1}H NMR (400 MHz, CD_3CN) 8.87 (s, 1H), 5.95 (d, J = 3.60Hz, 1H), 3.72 (s, 8H), 2.73 (d, *J* = 5.2Hz, 3H). ^{13}C NMR (101 MHz, CD_3CN) δ 162.33, 149.22, 148.60, 66.94 (2C), 47.51 (brs, 2C), 29.90.

_N_-methyl-_N_-(4-methylbenzyl)-1-(morpholine-4-carbonyl)-1_H_-1,2,4-triazole-3- sulfonamide (18)

To a stirred solution of NaH (11 mg, 0.27 mmol, 60% in mineral oil) in dry DMF was added *N*-methyl-1-(morpholine-4-carbonyl)-1*H*-1,2,4-triazole-3-sulfonamide (**18a**, 74 mg, 0.27 mmol) and commercially available 4-methylbenzyl bromide (50 mg, 0.27 mmol). The solution was stirred for 14 hours until completion, after which the reaction mixture was diluted with EtOAc, washed with brine 3x, dried, concentrated *in vacuo* and purified by flash chromatography to obtain *N*-methyl-*N*-(4-methylbenzyl)-1-(morpholine-4-carbonyl)-1*H*-1,2,4-triazole-3-sulfonamide (52 mg, 0.14 mmol, 50%). LC-MS (ESI+) m/z: calculated for $C_{16}H_{22}N_5O_4S$ ([M + H]), 380.14; found, 379.73. ^{1}H NMR (400 MHz, CD_3CN) δ 8.89 (s, 1H), 7.24 - 7.16 (m, 4H), 4.34 (s, 2H), 3.72 (bs, 8H), 2.81 (s, 3H), 2.32 (s, 3H). ^{13}C NMR (101 MHz, CD_3CN) δ 161.78, 149.22, 148.59, 138.77, 133.68, 130.23(2C), 129.32(2C), 66.96(2C), 54.86, 47.70(bs, 2C), 35.54, 21.15. Purity of 90% as determined by LC-MS.

_N_-(4-chlorobenzyl)-_N_-methyl-1-(morpholine-4-carbonyl)-1_H_-1,2,4-triazole-3-sulfonamide (19)

The title compound was synthesized from *N*-methyl-1-(morpholine-4-carbonyl)-1*H*-1,2,4-triazole-3-sulfonamide (**18a**, 100 mg, 0.36 mmol) and commercially available 4-chlorobenzyl chloride (58 mg, 0.36 mmol) according to procedure described for compound **12**. This yielded *N*-(4-chlorobenzyl)-*N*-methyl-1-(morpholine-4-carbonyl)-1*H*-1,2,4-triazole-3-sulfonamide (12 mg, 0.03 mmol, 9%) after preperative HPLC purification. HRMS (ESI+) m/z: calculated for $C_{15}H_{19}ClN_5O_4S$ ([M + H]), 400.0841; found, 400.0837. ^{1}H NMR (400 MHz, $CDCl_3$) δ 8.89 (s, 1H), 7.36 – 7.28 (m, 4H), 4.42 (s, 2H), 4.12 – 3.68 (m, 8H), 2.86 (s, 3H). ^{13}C NMR (101 MHz, $CDCl_3$) δ 161.65, 148.22, 147.40, 134.21, 133.75, 129.82(2C), 129.08(2C), 66.56(2C), 54.11, 48.1(bs), 45.94(bs), 35.00. Purity of 97% as determined by LC-MS.

_N_-(4-methoxybenzyl)-_N_-methyl-1-(morpholine-4-carbonyl)-1_H_-1,2,4-triazole-3-sulfonamide (20)

The title compound was synthesized from *N*-methyl-1-(morpholine-4-carbonyl)-1*H*-1,2,4-triazole-3-sulfonamide (**18a**, 68 mg, 0.25 mmol) and commercially available 4-methoxybenzyl chloride (37 µL, 0.25 mmol) according to procedure described for compound **12**. This yielded *N*-(4-methoxybenzyl)-*N*-methyl-1-(morpholine-4-carbonyl)-1*H*-1,2,4-triazole-3-sulfonamide (26 mg, 0.1 mmol, 40%). HRMS (ESI+) m/z: calculated for $C_{16}H_{22}N_5O_5S$ ([M + H]), 396.1336; found, 396.1334. ^{1}H NMR (400 MHz, CD_3CN) δ 8.89 (s, 1H), 7.25 (d, *J* = 8.8 Hz, 2H), 6.90 (d, *J* = 8.8 Hz, 2H), 4.32 (s, 2H), 3.77 (s, 3H), 3.71 (brs, 8H), 2.80 (s, 3H). ^{13}C NMR (101 MHz, CD_3CN) δ 161.84, 160.48, 149.21, 148.60, 130.80(2C), 128.53, 114.93(2C), 66.96(2C), 55.92, 54.57, 47.52 (brs, 2C), 35.43. Purity of 90% as determined by LC-MS.

4-Phenoxybenzyl alcohol (24)

To a stirred solution of commercially available 4-phenoxybenzaldehyde (1.0 g, 5.0 mmol) in dry THF (40 mL) was added borane in THF (6.0 mL, 1 M, 6 mmol) at 0°C. The reaction was stirred for 10 minutes and was then allowed to warm up to rt. The solution was stirred for 1 h. until completion, after which was added 10 mL of sat. NH_4Cl (aq.). The mixture was diluted with EtOAc (40 mL), washed with brine, dried, filtered, concentrated *in vacuo* to obtain 4-phenoxybenzyl alcohol (0.99 g, 4.9 mmol, 99%). ^{1}H NMR (400 MHz, $CDCl_3$) δ 7.35-7.31 (m, H), 7.10 (t, *J* = 7.4 Hz, H), 7.01-6.99 (m, H), 4.67 (s, 2H), 1.78 (brs, 1H). ^{13}C NMR (101 MHz, $CDCl_3$) δ 157.31, 156.94, 135.85, 129.89(2C), 128.83(2C), 123.43, 119.08(2C), 118.99(2C), 65.04.

4-Phenoxybenzyl bromide (25)

To a stirred solution of 4-phenoxybenzyl alcohol (**24**, 0.99 g, 4.94 mmol) in dry CH_2Cl_2 (40 mL) was added 33% HBr in HOAc (10 mL) at 0°C. The reaction was stirred for 10 minutes and was then allowed to warm up to rt. The solution was stirred for 14 h. until completion, after which was added 20 mL of sat. $NaHCO_3$ (aq.). The mixture was extracted with CH_2Cl_2 (3 x 40 mL), washed with brine, dried, filtered, concentrated *in vacuo* to obtain 4-phenoxybenzyl bromide (821 mg, 4.10 mmol, 83%). ^{1}H NMR (400 MHz, $CDCl_3$) δ 7.34-7.30 (m, 4H), 7.10 (t, *J* = 7.2 Hz, 1H), 7.00 (d, *J* = 8.2 Hz, 2H), 6.93 (d, *J* = 8.8Hz, 2H), 4.46 (s, 2H).

***N*-methyl-1-(morpholine-4-carbonyl)-*N*-(4-phenoxybenzyl)-1*H*-1,2,4-triazole-3-sulfonamide (21)**

The title compound was synthesized from *N*-methyl-1-(morpholine-4-carbonyl)-1*H*-1,2,4-triazole-3-sulfonamide (**18a**, 281 mg, 1.02 mmol) and 4-phenoxybenzyl bromide (**25**, 253 mg, 0.96 mmol) according to procedure described for compound **18**. This yielded *N*-methyl-1-(morpholine-4-carbonyl)-*N*-(4-phenoxybenzyl)-1*H*-1,2,4-triazole-3-sulfonamide (24 mg, 0.05 mmol, 5%). HRMS (ESI+) m/z: calculated for $C_{21}H_{24}N_5O_5S$ ([M + H]), 458.1493; found, 458.1492. ^{1}H NMR (400 MHz, CD_3CN) δ 8.90 (s, 1H), 7.41-7.32 (m, 4H), 7.16 (t, *J* = 7.2 Hz, 1H), 7.03- 6.97 (m, 4H), 4.37 (s, 2H), 3.72 (brs, 8H), 2.84 (s, 3H). ^{13}C NMR (101 MHz, CD_3CN) δ 161.74, 158.12, 157.93, 149.26, 148.58, 131.61(2C), 131.06, 130.98(2C), 124.64, 119.92(2C), 119.60(2C), 66.96(2C), 54.52, 48.06(2C), 35.57. Purity of 90% as determined by LC-MS.

***N*-methyl-1-(morpholine-4-carbonyl)-*N*-(3-phenoxybenzyl)-1*H*-1,2,4-triazole-3-sulfonamide (22)**

The title compound was synthesized from *N*-methyl-1-(morpholine-4-carbonyl)-1*H*-1,2,4-triazole-3-sulfonamide (**18a**, 240 mg, 0.87 mmol) and commercially available 3-phenoxybenzyl chloride (161 µL, 0.87 mmol) according to procedure described for compound **18**. This yielded *N*-methyl-1-(morpholine-4-carbonyl)-*N*-(3-phenoxybenzyl)-1*H*-1,2,4-triazole-3-sulfonamide (67 mg, 1.46 mmol, 17%). HRMS (ESI+) m/z: calculated for $C_{21}H_{24}N_5O_5S$ ([M + H]), 458.1493; found, 458.1491. ^{1}H NMR (400 MHz, CD_3CN) δ 8.88 (s, 1H), 7.40-7.34 (m, 3H), 7.17-7.10 (m, 2H), 7.03-6.92 (m, 4H), 4.37 (s, 2H), 3.71 (brs, 8H), 2.30 (s, 3H). ^{13}C NMR (101 MHz, CD_3CN) δ 161.60, 149.21, 148.50, 158.79, 157.86, 139.06, 131.14(2C), 130.92, 124.56, 124.04, 119.72(2C), 119.25, 118.95, 66.90(2C), 54.72, 47.39(brs, 2C), 35.71. Purity of 95% as determined by LC-MS.

2-(3-Formylphenoxy)-5-(trifluoromethyl)pyridine (26)

The title compound was synthesized from commercially available 3-hydroxybenzaldehyde (671 mg, 5.5 mmol), 2-chloro-5-trifluoromethylpyridine (1.0 g, 5.5 mmol) and K_2CO_3 (1.54 g, 8.5 mmol) according to previously published procedures[23] to obtain 2-(3-formylphenoxy)-5-(trifluoromethyl)pyridine (1.47 g, 5.5 mmol, 100%). ^{1}H NMR (400 MHz, $CDCl_3$) δ 10.03 (s, 1H), 8.42 (t, *J* = 0.8 Hz, 1H), 7.96 (dd, *J* = 8.8, 2.4 Hz, 1H), 7.78 (dt, *J* = 7.6, 1.2 Hz, 1H) 7.69-7.68 (m, 1H), 7.62 (t, *J* = 8.0 Hz, 1H), 7.45 (dq, *J* = 8.0, 1.2 Hz, 1H), 7.11 (d, *J* = 8.8 Hz, 1H). Spectroscopic data are in agreement with those reported in literature.[23]

3-(5-Trifluoromethyl-2-pyridyloxy)benzyl alcohol (27)

The title compound was synthesized from 2-(3-formylphenoxy)-5-(trifluoromethyl)pyridine (**26**, 1.47 g, 5.5 mmol) according to procedures discribed for compound **24**. This yielded 3-(5-trifluoromethyl-2-pyridyloxy)benzyl alcohol (1.16 g, 4.3 mmol, 78%). ^{1}H NMR (400 MHz, $CDCl_3$) δ 8.40 (q, *J* = 0.8 Hz, 1H), 7.90 (dd, *J* = 8.8, 2.4 Hz, 1H), 7.40 (t, *J* = 8.0 Hz, 1H), 7.23 (dd, *J* = 12.0, 0.4 Hz, 1H), 7.16 (s, 1H), 7.05 (dd, *J* = 8.0, 2.0Hz, 1H), 7.00 (d, *J* = 8.8Hz, 1H), 4.68 (s, 2H). ^{13}C NMR (101 MHz, $CDCl_3$) δ 165.87, 153.46, 145.51 (q, *J* = 4 Hz), 143.38, 136.90 (q, *J* = 3.0 Hz), 130.01, 132.92, 123.85 (q, *J* = 271.5 Hz), 122.50, 121.67 (q, *J* = 33.5 Hz), 119.84, 111.55, 64.66.

2-(3-(Bromomethyl)phenoxy)-5-(trifluoromethyl)pyridine (28)

The title compound was synthesized from 3-(5-trifluoromethyl-2-pyridyloxy)benzyl alcohol (**27**, 1.16 g, 4.3 mmol) according to procedure described for compound **25**. This yielded 2-(3-(bromomethyl)phenoxy)-5-(trifluoromethyl)pyridine (1.25 g, 3.8 mmol, 88%). ^{1}H NMR (400 MHz, CD_3CN) δ 8.45 (d, *J* = 0.8 Hz, 1H), 7.91 (dd, *J* = 8.8, 2.4 Hz, 1H), 7.40 (t, *J* = 8.0 Hz, 1H), 7.29-7.27 (m, 1H), 7.21 (t, *J* = 2.0 Hz, 1H), 7.10 (dd, *J* = 2.4, 0.8 Hz, 1H), 7.02 (d, *J* = 8.8 Hz, 1H), 4.49 (s, 2H). ^{13}C NMR (101 MHz, CD_3CN) δ 165.61, 153.34, 145.50 (q, *J* = 4.0 Hz), 139.81, 136.98 (q, *J* = 3.0 Hz), 130.25, 126.17, 123.71 (q, *J* = 271.5 Hz), 122.17, 121.83 (q, *J* = 33.7 Hz), 121.59, 111.59, 33.64.

N-methyl-1-(morpholine-4-carbonyl)-N-(3-((5-(trifluoromethyl)pyridin-2-yl)oxy)benzyl)-1H-1,2,4-triazole-3-sulfonamide (23)

The title compound was synthesized from *N*-methyl-1-(morpholine-4-carbonyl)-1*H*-1,2,4-triazole-3-sulfonamide (**18a**, 240 mg, 0.87 mmol) and 2-(3-(bromomethyl)phenoxy)-5-(trifluoromethyl)pyridine (**28**, 319 mg, 0.96 mmol) according to procedure described for compound **18**. This yielded N-methyl-1-(morpholine-4-carbonyl)-N-(3-((5-(trifluoromethyl)pyridin-2-yl)oxy)benzyl)-1H-1,2,4-triazole-3-sulfonamide (86 mg, 0.16 mmol, 18%). HRMS (ESI+) m/z: calculated for $C_{21}H_{22}F_3N_6O_5S$ ([M + H]), 527.1315; found, 527.1319. ^{1}H NMR (400 MHz, $CDCl_3$) δ 8.88 (s, 1H), 8.43 (s, 1H), 7.93 (dd, *J* = 8.7, 2.5 Hz, 1H), 7.43 (t, *J* = 7.9 Hz, 1H), 7.30 – 7.21 (m, 1H), 7.17 (t, *J* = 1.9 Hz, 1H), 7.12 (dd, *J* = 8.2, 2.4 Hz, 1H), 7.04 (d, *J* = 8.6 Hz, 1H), 4.48 (s, 2H), 4.08 – 3.68 (m, 8H), 2.91 (s, 3H). ^{13}C NMR (101 MHz, $CDCl_3$) δ 165.62, 161.61, 153.58, 148.20, 147.39, 145.51 (q, *J* = 8.6 Hz), 137.39, 136.93, 130.21, 125.38, 123.74 (q *J* = 272.7 Hz), 121.82 (q, *J* = 33.3 Hz), 121.40, 121.38, 111.66, 66.53(2C), 54.36, 46.99 (2C, bd, *J* = 215.5 Hz), 35.15. Purity of 98% as determined by LC-MS.

Supplementary information

Representative gels of *in vitro* ABPP analysis on compounds **18**-**21** and *in vivo* ABPP analysis on spleen and testes on compounds **22** and **23**.

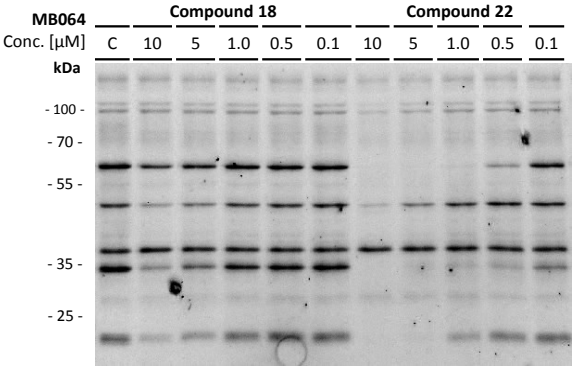

SI Figure 6. Representative gels of the ABPP analysis of compound **18** (left) and **20** (right) with ABP MB064. Conditions were used as described in the experimental section.

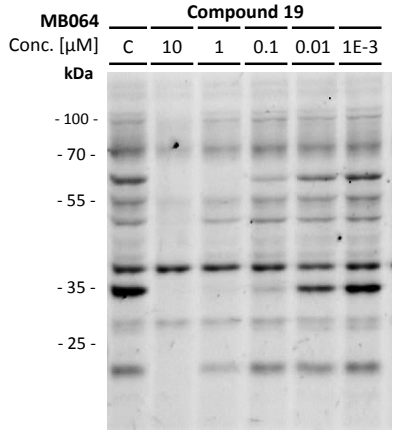

SI Figure 7. Representative gels of the ABPP analysis of compound **19** with ABP MB064. Conditions were used as described in the experimental section.

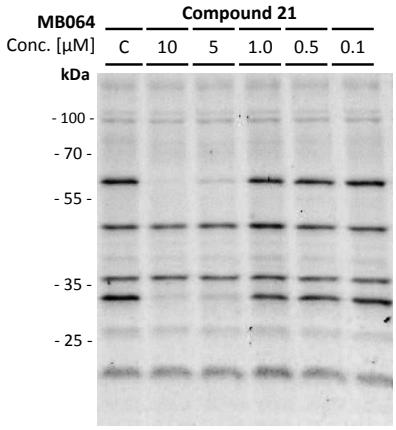

SI Figure 8. Representative gels of the ABPP analysis of compound **21** with ABP MB064. Conditions were used as described in the experimental section.

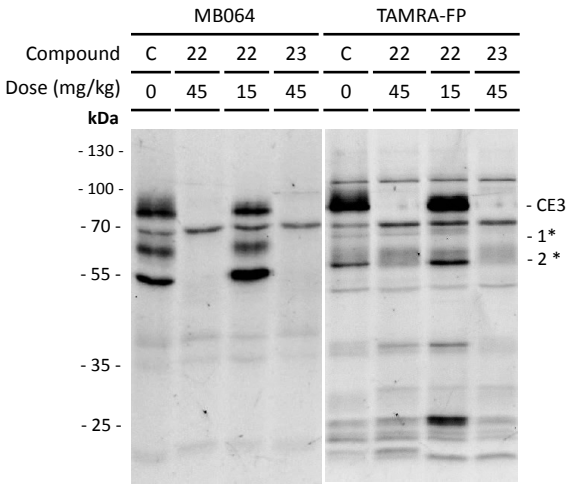

SI Figure 9: Representative gels of the *in vivo* characterization of compounds **22** and **23** with ABPs MB064 and TAMRA-FP on mouse spleen. Several off-targets were identified in the spleen using ABP MB064, including CE3 and two unknowns. Unknown 1*, however, is likely to be spleen ABHD16A as the apparent MW is in the expected kD range, although this should be further investigated by pull-down and mass spectrometry based proteomics using a biotin tagged ABP. Similar off-target effects were observed with TAMRA-FP (panel 2).

References

1. Vance, J. E. Phosphatidylserine and phosphatidylethanolamine in mammalian cells: two metabolically related aminophospholipids. *J. Lipid Res.* **49,** 1377–87 (2008).
2. Schlegel, R. a & Williamson, P. Phosphatidylserine, a death knell. *Cell Death Differ.* **8,** 551–563 (2001).
3. Newton, A. C. Protein Kinase C : Structure , Function, and Regulation. *J. Biol. Chem.* **270,** 1–52 (2003).
4. Lentz, B. R. Exposure of platelet membrane phosphatidylserine regulates blood coagulation. *Prog. Lipid Res.* **42,** 423–438 (2003).
5. Kamat, S. S. *et al.* Immunomodulatory lysophosphatidylserines are regulated by ABHD16A and ABHD12 interplay. *Nat. Chem. Biol.* **11,** 164–71 (2015).
6. Bellini, F. & Brunib, A. Role of a serum phospholipase A1 in the phosphatidylserine-induced T cell inhibition. *FEBS Lett.* **316,** 4–7 (1993).
7. Martin, T. W. & Lagunoff, D. Interactions of lysophospholipids and mast cells. *Nature* **279,** 250–252 (1979).
8. Smith, G. A., Hesketh, T. R., Plumb, R. W. & Metcalfe, J. C. The exogenous lipid requirement for histamine release from rat peritoneal mast cells stimulated by concanavalin A. *FEBS Lett.* **105,** (1979).
9. Lourenssen, S. & Blennerhassett, M. G. Lysophosphatidylserine potentiates nerve growth factor-induced differentiation of PC12 cells. *Neurosci. Lett.* **248,** 77–80 (1998).
10. Lord, C. C., Thomas, G. & Brown, J. M. Mammalian alpha beta hydrolase domain (ABHD) proteins: Lipid metabolizing enzymes at the interface of cell signaling and energy metabolism. *Biochim. Biophys. Acta - Mol. Cell Biol. Lipids* **1831,** 792–802 (2013).
11. Ramnani, N. The primate cortico-cerebellar system: anatomy and function. *Nat. Rev. Neurosci.* **7,** 511–22 (2006).
12. Hsieh, Y.-Y. *et al.* Human lymphocyte antigen B-associated transcript 2, 3, and 5 polymorphisms and haplotypes are associated with susceptibility of Kawasaki disease and coronary artery aneurysm. *J. Clin. Lab. Anal.* **24,** 262–8 (2010).
13. Savinainen, J. R. *et al.* Biochemical and pharmacological characterization of the human lymphocyte antigen B-associated transcript 5 (BAT5/ABHD16A). *PLoS One* **9,** 1–17 (2014).
14. van der Kleij, D. *et al.* A novel host-parasite lipid cross-talk. Schistosomal lyso-phosphatidylserine activates toll-like receptor 2 and affects immune polarization. *J. Biol. Chem.* **277,** 48122–48129 (2002).
15. Blankman, J. L., Long, J. Z., Trauger, S. a, Siuzdak, G. & Cravatt, B. F. ABHD12 controls brain lysophosphatidylserine pathways that are deregulated in a murine model of the neurodegenerative disease PHARC. *Proc. Natl. Acad. Sci. USA* **110,** 1500–1505 (2013).
16. Fiskerstrand, T. *et al.* A novel Refsum-like disorder that maps to chromosome 20. *Neurology* **72,** 20–27 (2009).
17. Fiskerstrand, T. *et al.* Mutations in ABHD12 cause the neurodegenerative disease PHARC: An inborn error of endocannabinoid metabolism. *Am. J. Hum. Genet.* **87,** 410–417 (2010).
18. Hoover, H. S., Blankman, J. L., Niessen, S. & Cravatt, B. F. Selectivity of inhibitors of endocannabinoid biosynthesis evaluated by activity-based protein profiling. *Bioorganic Med. Chem. Lett.* **18,** 5838–5841 (2008).
19. Baggelaar, M. P. *et al.* Development of an activity-based probe and in silico design reveal highly selective inhibitors for diacylglycerol lipase-a in brain. *Angew. Chem. Int. Ed.* **52,** 12081–12085 (2013).
20. Camara, K., Kamat, S. S., Lasota, C. C., Cravatt, B. F. & Howell, A. R. Combining cross-metathesis and activity-based protein profiling: New b-lactone motifs for targeting serine hydrolases. *Bioorganic Med. Chem. Lett.* **25,** 317–321 (2015).
21. Baggelaar, M. P. M. P. M. P. *et al.* A highly selective, reversible inhibitor identified by comparative chemoproteomics modulates diacylglycerol lipase activity in neurons. *J. Am. Chem. Soc.* **137,** (2015).
22. Johnson, D. S. *et al.* Discovery of PF-04457845: A highly potent, orally bioavailable, and selective urea FAAH inhibitor. *ACS Med. Chem. Lett.* **2,** 91–96 (2011).
23. Janssen, F. J. *et al.* Discovery of glycine sulfonamides as dual inhibitors of sn-1-diacylglycerol lipase α and α/β hydrolase domain 6. *J. Med. Chem.* **57,** 6610–6622 (2014).
24. Janssen, F. J. *et al.* Comprehensive Analysis of Structure-Activity Relationships of α-Ketoheterocycles as sn-1-Diacylglycerol Lipase α Inhibitors. *J. Med. Chem.* **58,** 9742–9753 (2015).

Inhibitors of diacylglycerol lipases in neurodegenerative and metabolic disorders*

2-Arachidonoylglycerol (2-AG) is an important endogenous signaling lipid. 2-AG activates the cannabinoid receptors type 1 and 2 (CB1R and CB2R) and is, therefore, termed an endocannabinoid.[1–3] Multiple lipid species can activate the CBRs, but 2-AG, together with anandamide, is the most well studied endocannabinoid. 2-AG contributes to CB1R mediated synaptic plasticity and acts as a retrograde messenger inhibiting GABAergic and glutamatergic neurotransmission.[4,5] The CBRs are involved in many physiological functions, including food intake,[6–8] inflammation,[9,10] memory formation,[11–13] mood,[14,15] locomotor activity,[16,17] pain sensation,[18] addiction and reward.[19] The exact contribution of 2-AG to these physiological processes remains poorly understood. The levels of 2-AG are tightly regulated in the central nervous system, because it is produced on demand and rapidly degraded by specialized enzymes.[20–22] Phospholipase C β (PLCβ) catalyses the formation of diacylglycerols from cell membrane phospholipid phosphatidylinositol-4,5-bisphosphate (PIP_2). Diacylglycerols are subsequently converted by *sn*-1 specific diacylglycerol lipases α and β (DAGLs) to monoacylglycerols, including 2-AG.[20] DAGLs belong to the large family of serine hydrolases, having a typical α/β hydrolase fold and Ser-His-Asp catalytic triad. The two DAGL isoforms (α and β) share extensive homology and differ mostly in a large C-terminal tail, which is present in DAGLα, but not in DAGLβ.[20] Genetic disruption of DAGLα in mice resulted in a strong reduction of 2-AG levels in the brain (80-90%), whereas in $DAGL\beta^{-/-}$ mice the 2-AG level was approximately 50% reduced in the brain.[4,5] 2-AG is mainly metabolized by monoacylglycerol lipase (MAGL) and to a lesser extent by α/β hydrolase domain proteins 6 and 12 (ABHD6 and ABHD12). This leads to the production of arachidonic acid (AA).[22] Both 2-AG and AA may serve as substrates for oxidative enzymes (cyclooxygenases) yielding pro-inflammatory prostaglandins and their ester derivatives, respectively (Figure 1).[23] Inhibitors of MAGL have contributed to the understanding of the

* Janssen F.J. and van der Stelt, M. Inhibitors of diacylglycerol lipases in neurodegenerative and metabolic disorders. *Bioorg. Med. Chem. Lett.*, 26, 3831–3837 (**2016**). Invited Digest Review.

physiological role of 2-AG (see for recent reviews[24–26]) and are currently tested in preclinical models and clinical trials for neurodegenerative diseases. This Digest will review the current state of the art of the diacylglycerol lipases inhibitors and discuss their potential in metabolic disorders and neurodegeneration.

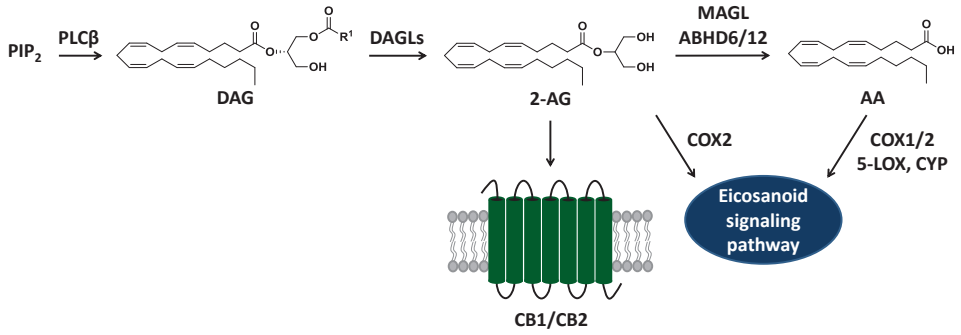

Figure 1. Overview of the biosynthetic pathway of 2-AG. Phospholipase C-β (PLCβ) converts membrane associated phosphatidylinositol-4,5-bisphosphate (PIP_2) to diacylglycerol (DAG), which in turn acts as substrate for *sn*-1 specific diacylglycerol lipases α and β (DAGLs).[20] DAGLs produce endocannabinoid 2-arachidonoylglycerol (2-AG), a ligand for the cannabinoid receptors type 1 and 2 (CB1R and CB2R). 2-AG is degraded by several enzymes including monoacylglycerol lipase (MAGL), α/β hydrolase domain 6 and 12 (ABHD6 and ABHD12) to arachidonic acid (AA), which serves as a precursor for the formation of several distinct eicosanoids, such as pro-inflammatory prostaglandin PGE_2 and thromboxane TBX_2. Other oxidative pathways involved in AA degradation include cytochrome P450 (CYP) and 5-lipoxygenase (5-LOX) to produce epoxyeicosanoids and leukotrienes, respectively, while direct oxidation of 2-AG by cyclooxygenase COX2 may result in the formation of prostaglandin-esters.[23,27]

Assays to measure DAGL activity

Several DAGL activity assays are currently available. The first class of assays employs surrogate substrates, i.e. para-nitrophenylbutyrate, 6,8-difluoro-4-methylumbelliferyl (DiMFU) octanoate and EnzChek®, and is generally used for inhibitor identification.[28–31] The main advantage is that product formation can be monitored real-time, generally by absorption or fluorescence measurement. The cost-effectiveness and easy detection of surrogate substrates/ products make these assays valuable tools for high-throughput screening applications.[28,30,32] However, surrogate substrates generally have attenuated binding affinities for the enzyme compared to DAGLs' natural substrate *sn*-1-stearoyl-2-arachidonoyl-glycerol. This may affect inhibitor potencies (IC_{50}) obtained with these assays. Consequently, the use of the natural substrate is preferred for further inhibitor profiling.

The second class of assays makes use of a natural substrate of DAGLs. Radiometric assays have been used to measure DAGLα activity *in vitro*, utilizing radiolabeled diacylglycerol, such as *sn*-1-stearoyl-2-[^{14}C]arachidonoylglycerol, as a substrate.[20] This method is highly sensitive, but requires lipid extraction, fractionation on thin layer chromatography and quantification of radiolabeled 2-[^{14}C]arachidonoylglycerol via scintillation counting, thereby

making this assay labor-intensive. Of note, the radioactive substrate is not commercially available. This restricts the widespread use of the radiometric assay. Alternatively, liquid chromatographic (LC) methods coupled to mass spectrometry (MS), have been employed to measure direct 2-AG formation.[33] Although LC-MS methods avoid the use of radiolabeled substrates and are highly accurate, it does require lipid extraction and separation of phases. Consequently, only limited number of samples can be measured. Both radiometric and LC-MS-based assays prohibit monitoring of reaction progress in real-time due to their discontinuous setup. Therefore, a third method was recently developed, in which the conversion of the natural substrate 1-stearoyl-2-arachidonoyl-*sn*-glycerol (SAG) was coupled to the formation of a fluorescent dye employing a five enzyme cascade.[34] Extraction or fractionation steps were not necessary, allowing SAG hydrolysis to be studied in real time in 96-well plate format using recombinant DAGLα or DAGLβ as well as mouse brain membrane fractions.[34,35]

Finally, the third class of assays employs activity-based protein profiling (ABPP). ABPP is a chemical biological technique that allows the rapid and efficient visualization of endogenous serine hydrolase activity in complex, native samples without the need of having substrate assays.[36,37] Typically, ABPP is used in a competitive setting, where a pool of enzymes is treated with an inhibitor, followed by a broad-spectrum or tailored activity-based probe (ABP) that labels all residual serine hydrolase activity. The ABP reporter tag allows for identification and quantification of inhibitor off-targets that are shared by the probe, using either in-gel fluorescence scanning or mass spectrometry. As such, ABPP measures activity and selectivity of irreversible and reversible inhibitors in cells and tissue lysates,[38] making it a highly valuable and complementary method next to classical substrate assays. Three different tailored ABPs have been developed for the detection of DAGL activity in proteomes: HT-01,[33] MB064[39] and DH379.[35]

DAGL inhibitor classes

To date, six different chemotypes have been reported as DAGL inhibitors, which can be classified into (a) reversible inhibitors: α-ketoheterocycles and glycine sulfonamides, and (b) irreversible inhibitors: bis-oximino-carbamates, β-lactones, fluorophosphonates and 1,2,3-triazole ureas.

α-ketoheterocycles: Using an ABPP-screen with the tailored activity-based probe MB064 and a pharmacophore model, Baggelaar *et al.* identified the α-ketoheterocycle LEI104 (Figure 2) as the first reversible inhibitor for DAGLα (Chapter 2). LEI104 was, however, weakly active in a cellular assay and not selective over FAAH, the enzyme responsible for the metabolism of the other endocannabinoid anandamide (Table 1).[39] The structure-activity relationships (SAR) of the α-ketoheterocycles were investigated by screening a focused library of 1040 compounds (Chapter 3). The α-keto group functioned as an electrophilic warhead and its reactivity could be tuned by selection of appropriate substituents on the scaffold. The 4*N*-oxazolopyridine heterocycle proved to be the most optimal scaffold and compounds with a

C6-C9 methylene phenyl acyl substituent were the most potent inhibitors.[32] Using this extensive SAR, a DAGLα homology model was validated and applied to the design of LEI105, a *p*-tolyl derivative of LEI104 (Figure 2).[40] Competitive and comparative chemoproteomics revealed that LEI105 was a highly potent and selective, covalent reversible inhibitor of DAGLα and DAGLβ, which did not target other proteins in the endocannabinoid system, including CB1R and CB2R, ABHD6, ABHD12, MAGL and FAAH (Table 1). LEI105 dose-dependently reduced 2-AG levels in neuronal cells without affecting anandamide levels. Finally, LEI105 attenuated synaptic plasticity by blocking depolarization-induced suppression of inhibition (DSI) in CA1 pyramidal neurons in mouse hippocampal slices. LEI105 has not been tested in *in vivo* models yet.

Glycine sulfonamides: The glycine sulfonamides were reported by Appiah *et al.* as the first non-covalent reversible inhibitors of DAGL.[28] Their high throughput screening campaign identified compound **1** as a DAGLα inhibitor, which was selective over MAGL and pancreatic lipase (Figure 2, Table 1). Interestingly, the glycine sulfonamides lack an obvious warhead that can covalently interact with the catalytically active serine in the enzyme. SAR studies revealed that the sulfonamide was required for proper positioning of the side groups, probably due to its characteristic perpendicular angle, and the carboxylate was essential for activity (Chapter 5).[41] Based on the initial hit compound **1**, and patent literature,[42] LEI106 (Figure 2) was identified as a DAGL inhibitor with nanomolar potency. ABPP revealed LEI106 to be selective over MAGL, but ABHD6 and two additional unknown off-targets were inhibited (Table 1). Docking of LEI106 in a DAGLα homology model suggested that the carboxylate interacted with an intricate hydrogen bonding network of the catalytic triad. Recently, Chupak *et al.* published a full account of their extensive optimization of the glycine sulfonamides, which resulted in the identification of compounds **3** and **24** (Figure 2, Table 1).[43] They found that glycine sulfonamide **3** is a cellular active and orally bio-available DAGLα/β inhibitor. Due to potential toxicity issues associated with biphenyl-amines, compound **3** was further optimized to compound **24**. The latter compound was a peripherally restricted, highly potent and dual DAGLα/β inhibitor with some minor affinity for the human ether-a-go-go channel (IC_{50} = 40 μM) and a good pharmacokinetic profile.[43] No additional functional or *in vivo* efficacy data have been reported with this series to date.

Bis-oximino-carbamates: RHC80267 (Figure 2) was one of the first DAGL inhibitors reported in the literature, but it is only weakly active on DAGLα and not selective. RHC80267 inhibited at least 7 others targets, including fatty acid amide hydrolase (FAAH) and lipoprotein lipase (LPL, see Table 1).[39,44] This activity and selectivity profile makes it less suitable to study the biological role of DAGLs .

β-*lactones:* Tetrahydrolipstatin (THL, Orlistat, Figure 2) is a peripherally restricted, FDA approved anti-obesity drug (Xenigal®, Alli®) that inhibits gastric and pancreatic lipases, which are essential for fat processing in the gastrointestinal track.[45–47] Since the discovery of THL as a potent DAGL inhibitor,[20] β-lactones have been extensively investigated as DAGL

inhibitors with a focus on changing the amino acid substituent on the chiral δ-hydroxyl moiety.[48,49] THL inhibited DAGLα and DAGLβ with nanomolar potency in natural substrate assays to a similar extent (Table 1). OMDM-188, a *N*-formyl-*L*-isoleucine derivative of THL (Figure 2), demonstrated improved selectivity over FAAH and MAGL, but micromolar antagonistic activity on the CB1R (K_i = 6 μM, Table 1). This may complicate the interpretation of results obtained with this compound, if the *in vitro* studies are carried out at high inhibitor concentration (> 10 μM).[48] OMDM-188 has been used to investigate whether 2-AG is released 'on demand' or from preformed pools during neuronal activity. While some studies with THL and OMDM-188 show that acute DAGL inhibition attenuates DSI in hippocampal CA1 pyramidal cells,[50,51] other studies with the same inhibitors found no such effect.[52] The discrepancy between the various electrophysiological studies could be potentially attributed to differences in tissue penetration of the compounds, due to their relatively high lipophilicity,[50] but off-target effects cannot be ruled out either. Recent studies using novel DAGL inhibitors, such as LEI105[40] and 1,2,3-triazole ureas,[35] have confirmed that CB1R-mediated synaptic plasticity is dependent on acute DAGL activity, which supports the hypothesis of 'on demand' production of 2-AG.

Recently, OMDM-188 has been used to study the biological role of DAGLα in gastrointestinal motility. Bashashati *et al.* showed that DAGLα is expressed throughout the enteric nervous system and its inhibition by OMDM-188 reversed slowed gastrointestinal motility, intestinal contractility and constipation through a CB1R dependent mechanism.[53] Conversely, inhibition of MAGL prolonged the whole gut transit time.[54] These studies suggest that DAGLα is a potential target for the treatment of constipation. 2-AG levels in the ileum or colon of the genetically constipated mice were, however, not significantly affected and the effect of OMDM-188 on pancreatic and gastrointestinal lipase is currently unknown. Further studies may address these questions.

Fluorophosphonates: O-3640, O-3841 and O-5596 covalently inhibit DAGL and are mimetics of the endogenous lipid 2-oleoylglycerol carrying a fluorophosphonate group as a warhead (Figure 2).[55,56] These compounds have nanomolar potency in a natural substrate assay and in particular O-3841 and O-5596 show few off-target activities (Table 1).[55,56] O-3640 and O-3841 have, however, little to no effect in a cellular assay in which ionomycin is used to stimulate the formation of 2-AG in N18TG2 cells. The lack of cellular activity is perhaps due to chemical instability of the inhibitors or low cell membrane permeability.[55,56] Remarkably, O-3841 was neuroprotective in a malonate model of Huntington's disease.[57] O-3841 prevented the formation of prostaglandin E2 glyceryl ester that exerted neurotoxicity, whereas MAGL-inhibitors exacerbated neuronal damage. Optimization of the substituent at the *sn*-3 position of O-3841 led to the identification of O-7460 (Figure 2), which was moderately active on human DAGLα (IC_{50} = 690 nM) and reduced 2-AG levels *in situ*. Neutral cholesterol ester hydrolase 1 (KIAA1363) was detected with ABPP as an important off-target. O-5596 and O-7460 decreased the amount of palatable food ingested by mice in a

dose-dependent manner and slightly reduced body weight.[56,58] These observations are in line with the results obtained with DAGLα KO mice (see below).[59]

1,2,3-Triazole ureas: DAGL inhibitors based on the 1,2,3-triazole urea scaffold have been instrumental to determine the physiological role of DAGLs in macrophages and brain. Hsu *et al.* developed the first DAGLβ inhibitors that were active in an *in vivo* model of inflammation.[33] KT109 and KT172 (Figure 2), but not KT195, a control compound, reduced the levels of 2-AG, AA and eicosanoids (thromboxane A2, leukotriene B4, prostaglandin D2 and E2) in peritoneal macrophages of lipopolysacharide (LPS)-treated mice.[33] Moreover, KT109 and KT172 significantly decreased pro-inflammatory cytokine tumor necrosis factor α (TNFα) in LPS-treated mice. This demonstrated that DAGLβ plays a pivotal role in the regulation of macrophage inflammatory response *in vivo*. Of note, KT109 does inhibit DAGLα (Table 1) and depending on its concentration and time of incubation, DAGLα may be fully inhibited. KT109 and KT172 do not act in the central nervous system, presumably, because they are not able to cross the blood-brain barrier. Wilkerson *et al.* investigated the effect of DAGLβ inhibition on inflammatory and neuropathic pain.[60] Local inhibition of DAGLβ by KT109 at the site of inflammation reduced LPS-induced allodynia in mice, whereas general *i.c.v.* or *i.t* administration was ineffective. This suggests that peripheral inhibition of DAGLβ may represent a novel avenue to treat pathological pain.[60]

To investigate the biological role of DAGLs in the brain, Ogasawara *et al.* developed the triazole ureas DH376 and DO34 (Figure 2). DH376 and DO34 were highly potent and selective DAGL inhibitors.[35] ABPP experiments demonstrated a limited off-target profile for DH376 and DO34 in the brain and designated DO53 as a paired control compound. Both DAGL inhibitors, but not DO53, fully blocked GABAergic (DSI) and glutamatergic (DSE) neurotransmission in hippocampal and cerebellar slices, respectively. Acute blockade of DAGL in mice produced a striking reorganization of bioactive lipid networks, including elevations of DAGs and reductions in endocannabinoids and eicosanoids. For example, dose- and time-dependent reductions in 2-AG, AA and PGE_2 levels were observed in the brain of mice treated *i.p.* with DO34 or DH376, but not with DO53. Importantly, the *in vivo* half-life of DAGLα was short (2-4h) and accompanied by ongoing DAGLα protein production in the brain that generated a strong, tonic flux of 2-AG. It was suggested that modulation of DAGLα half-life may thus provide neurons with a mechanism to influence the magnitude and duration of 2-AG signaling and associated physiological processes, such as learning and memory.[35] Of note, anandamide levels were also affected by DAGL inhibition by DH376 and DO34 and not by control compound DO53. The molecular mechanism underlying this *in vivo* cross-talk between the two endocannabinoids is not clear at the moment, but was also observed in DAGL KO animals.[4,5,61] DAGL inhibition by DH376 and DO34 reduced the formation of 2-AG, AA and pro-inflammatory prostaglandins as well as pro-inflammatory cytokine IL1β upon LPS-treatment in mice.[35] DAGL inhibition also attenuated LPS-induced anapyrexia (reduction of core body temperature), which is in contrast to enhanced anapyrexia mediated by acute blockade of MAGL.[62] This suggests that 2-AG has an

important role in the regulation of body temperature during neuroinflammation. Viader *et al.* demonstrated by combined genetic and pharmacological evaluation that disruption of either DAGLα or DAGLβ contributes to lower the neuroinflammatory response *in vivo*.[75] They found that DAGLβ is key in regulating 2-AG levels in microglia and that LPS treated DAGLβ$^{-/-}$ mice show attenuated microglial activation without changes in overall 2-AG and prostaglandin levels in brain.

Buczynski *et al.* showed that inhibition of DAGL by KT172 (Figure 2), but not control compound KT185, restores GABAergic signaling at dopaminergic neurons in the ventral tegmental area (VTA), which is lost during chronic nicotine exposure.[63] Accordingly, rats treated with KT172 significantly less self-administered nicotine without affecting other operant response or locomotion. This may indicate that the 2-AG signaling, mediated by DAGLα, is involved in the regulation of reward and addiction.

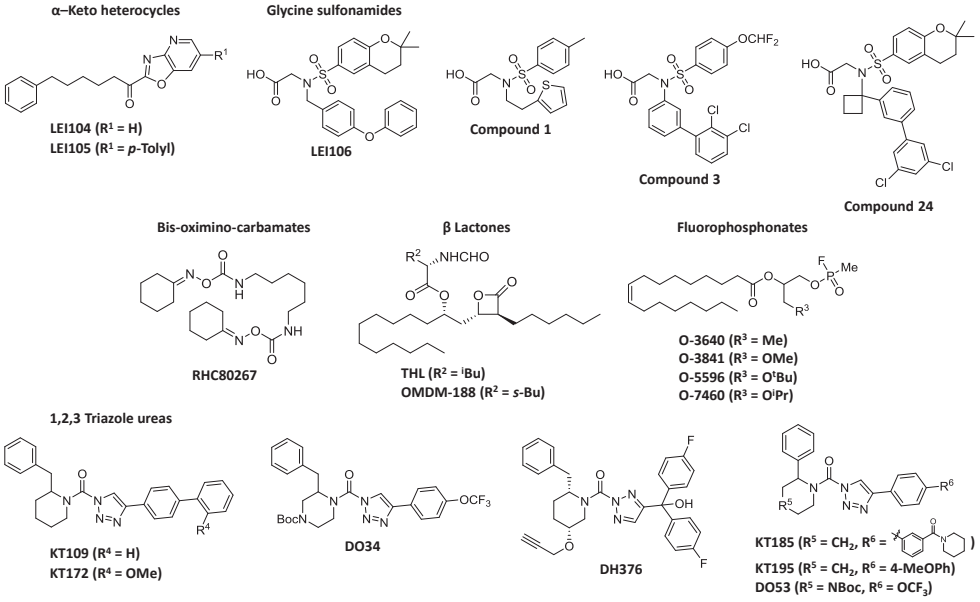

Figure 2. Current DAGL chemotypes and their corresponding inhibitors.[20,28,33,35,41,43,48,55,56,58]

Table 1. Overview of known DAGL inhibitors per assaytype and chemotype, values are pIC_{50}.

Chemotype	Compound	Surrogate substrate assay	Natural substrate assay	ABPP assay	Identified off-targets
Bis-oximino-carbamates	RHC80267	5.3 (α)[i] 4.6 (α)[ii]	-	-	ABHD6[44] FAAH LPL
β-Lactones	THL	9.6 (α)[i] 9.4 (α)[ii] 7.6 (β)[iii]	8.4 (α)[iv] 7.2 (α)[v] 7.0 (β)[v] 6.0 (α)[vi]	6.6 (α)[vii] 5.7 (β)[vii]	ABHD6[39,44,48] ABHD12 ABHD16A DDHD2 LyPLA CB1
	OMDM-188	8.2 (β)[iii]	7.8 (α)[vi]	-	CB1R (minor)[48]
Fluoro phosphonates	O-3640	-	6.3 (α)[vi]	-	TAGL[55] FAAH MAGL (minor) CB1R (minor)
	O-3841	-	6.8 (α)[vi]	-	None reported[55]
	O-5596	-	7.0 (α)[vi]	-	None reported[56]
	O-7460	-	6.2 (α)[vi]	-	KIAA1363[58]
1,2,3-Triazole ureas	KT109	-	7.6 (α)[iv] 7.1 (β)[viii]	5.6 (α)[vii] 7.4 (β)[vii]	ABHD6[33] PLA2G7
	KT172		7.1 (β)[viii]	6.9 (α)[vii] 7.2 (β)[vii]	ABHD6[33] MAGL (minor) PLA2G7 (minor)
	DH376	-	8.2 (α)[vi] 8.6 (β)[ix]	8.9 (α)[vii] 8.3 (β)[vii]	ABHD6[35] CES1C LIPE BCHE
	DO34	-	8.2 (α)[vi] 8.1 (β)[ix]	9.3 (α)[vii] 8.6 (β)[vii]	ABHD6[35] CES1C PLA2G7 PAFAH2 ABHD2
α-Keto heterocycles	LEI104	7.4 (α)[x]	6.3 (α)[vi]	6.3 (α)[xi]	FAAH[40,64]
	LEI105	8.5 (α)[x]	6.6 (α)[vi] 7.9 (α)[xi]	7.6 (α)[xi]	None reported[40] (FAAH selective)
Glycine sulfonamides	1	6.3 (α)[xii]	-	-	None reported[28]
	3	8.6 (α)[xii] 7.4 (β)[xii]	-	-	None reported[43]
	24	9.2 (α)[xii] 7.4 (β)[xii]	-	-	hERG (minor)[43]
	LEI106	7.7 (α)[x]	6.0 (α)[iv] 6.2 (α)[vi]	6.9 (α)[xi]	ABHD6[41] Two unknown

Conditions: i) Pedicord *et al.*, colorimetric surrogate substrate assay: 4.3 μg/mL hDAGLα overexpressing HEK293F membrane fractions, 250 μM PNP butyrate.[30] ii) Pedicord *et al.*, fluorogenic surrogate substrate assay: 4.0 μg/mL hDAGLα overexpressing HEK293F membrane fractions, 10 μM DiMFU-octanoate.[30] iii) Singh *et al.*, fluorogenic surrogate substrate assay: 12.5 μg/mL purified GST-DAGLβ CD, 5 minutes preincubation, then 2 μM EnzChek.[29] iv) Van der Wel *et al.*, Enzyme coupled natural substrate assay: 50 μg/mL hDAGLα overexpressing HEK293T membrane fractions, 20 min preincubation, 100 μM SAG.[34,35] v) Bisogno *et al.* 2003, Radiometric natural substrate assay: DAGL overexpressing COS-7 membrane fractions, 15 min preincubation at 37°C, ^{14}C labeled diacylglycerol 50 μM.[20] vi) Bisogno *et al.* 2006, Radiometric natural substrate assay: DAGL overexpressing COS-7 membrane fractions, 20 min preincubation at 37°C, ^{14}C labeled diacylglycerol 25 μM.[41,48,55,58] vii) Hsu *et al.*, ABPP: 2 mg/mL hDAGLα or mDAGLβ hDAGLα overexpressing HEK293T membrane fractions, 30

min preincubation at 37°C, then ABP HT01, 1 µM, 30 min incubation.[33] viii) Hsu *et al.*, LC-MS natural substrate assay: 300 µg/mL mDAGLβ overexpressing HEK293T membrane fractions, 30 min preincubation at 37°C, 500 µM SAG.[33] ix) Ogasawara *et al.*, Enzyme coupled natural substrate assay: 50 µg/mL mDAGLβ overexpressing HEK293T membrane fractions, 5 mM $CaCl_2$, 20 min preincubation, 75 µM SAG.[35] x) Baggelaar *et al.*, Colorimetric surrogate substrate assay: 50 µg/mL DAGLα overexpressing HEK293T membrane fractions, 20 minutes preincubation, 300 µM PNP butyrate.[39–41] xi) Baggelaar *et al*, Activity-based protein profiling: Mouse brain proteome 2 mg/mL, 30 min preincubation, then ABP MB064, 250 nM, 15 min incubation.[39–41] xii) Appiah *et al.*, Fluorogenic surrogate substrate assay: 12.0 µg/mL DAGLα overexpressing membranes, 10 µM DiMFU-octanoate.[28,43]

Therapeutic potential of DAGL inhibitors in anti-obesity and neuroprotection

The endocannabinoid system is a clinically proven signaling pathway controlling the energy balance in humans. In fact, the first generation CB1R antagonist/inverse agonist Rimonabant was considered one of the most promising therapeutic drugs to treat human obesity, until the appearance of central psychiatric side effects resulted in its removal from the market in 2008.[65–67] Rimonabant reduced food intake, body weight and waist circumference in obese patients and improves cardiovascular risk factors.[65,66,68] Currently, several lines of evidence suggest that 2-AG, and not anandamide (nor constitutively active CB1Rs), regulates CB1R-dependent food intake. 2-AG levels are increased in the hypothalamus of fasting mice[7] and pharmacological intervention using O-5596 and O-7460 leads to reduced food intake in mice.[58] Third, DAGLα$^{-/-}$ mice showed hypophagia and leanness similar to that of CB1R$^{-/-}$ mice, while knockout mice of DAGLβ and *N*-acyl phosphatidylethanolamine phospholipase D (NAPE-PLD, the main enzyme responsible for anandamide synthesis) did not share this phenotype.[59,61] Interestingly, DAGLα knockout mice had also low fasting insulin, triglyceride, and total cholesterol levels, and after glucose challenge had normal glucose but very low insulin levels.[59] Taken together, these data suggest that selective interference with DAGLα signaling may represent a novel therapeutic avenue to treat obesity and the metabolic syndrome.

Inflammatory processes are associated with obesity and with many neurodegenerative diseases, including stroke, Parkinson's and Alzheimer's disease.[69] Prostaglandins produced by cyclooxygenases from arachidonic acid (AA) are important pro-inflammatory stimuli. Cyclooxygenase inhibitors show neuroprotection in animal models of Parkinson's and Alzheimer's disease, but their gastrointestinal and cardiovascular actions have limited their use in humans.[70] Nomura *et al.* discovered that MAGL regulates AA levels in specific tissues, which is required for prostaglandin synthesis by cyclooxygenases type 1 and 2 (COX1 and COX2).[71] For instance, MAGL is the predominant enzyme producing AA in the brain, liver and lung, whereas phospholipase A2 (PLA_2) regulates AA levels in the gut and spleen. Inhibition of MAGL activity in LPS-treated mice resulted in an attenuated neuroinflammatory response as witnessed by a marked decrease in pro-inflammatory prostaglandins and cytokine formation in the brain. MAGL inhibitors improved neurological outcome in animal models of Multiple Sclerosis,[72] Parkinson's[71,73] and Alzheimer disease,[24] thereby providing proof-of-principle for therapeutic intervention using this biochemical pathway in various models of neuroinflammation and neurodegeneration. Of note, CB1R activation by elevated 2-AG levels did not seem to be involved in the protective response.

Concomitant chronic activation of the CB1R by elevated 2-AG levels has previously been shown to lead to adaptations of the endocannabinoid system (*e.g.,* down regulation of CB1R and physical dependence).[74] It is currently unknown how elevated 2-AG levels will impact CB1R-mediated signaling under chronic neurodegenerative conditions. Therefore, DAGL inhibition may provide an alternative approach to reduce AA formation in the brain without accumulation of 2-AG and (chronic) CB1R activation. The first studies with 1,2,3-triazole ureas DH376 and DO34 have demonstrated that DAGLs regulate the formation of proinflammatory prostaglandins and cytokines under neuroinflammatory conditions.[35] The efficacy of DAGL inhibitors in mouse models of Multiple Sclerosis, Parkinson's and Alzheimer's diseases have, however, not been reported yet. Of note, in a malonate model of Huntington's disease DAGL inhibitors conferred neuroprotection, whereas MAGL inhibitors exacerbated neuronal damage.[27,57] Oxidative metabolism of 2-AG was suggested to result in the formation of toxic metabolites.[57] In conclusion, it will be important to determine the efficacy and therapeutic window of both MAGL and DAGL inhibitors in parallel with respect to CB1R mediated adverse effects and activation of alternative metabolic pathways.

Potential adverse side effects of DAGL inhibitors

Suppression of CB1R signaling with antagonists such as Rimonabant, is linked to neuropsychiatric side effects, including anxiety and depression.[75] The exact contribution of DAGLs in the regulation of emotion has been studied with DAGLα knockout mice. These studies indicate that 2-AG signaling is also important for the regulation of neuropsychiatric behavior.[61,59,76] For example, Jenniches *et al*. reported that DAGLα$^{-/-}$ mice display significantly reduced maternal care, increased anxiety in light/dark box and open field tests, reduced fear extinction and increased behavioral despair.[61] Powell *et al.* noted similarities in behavioral phenotypes of CB1R$^{-/-}$ mice and DAGLα$^{-/-}$ in the hot plate, marble burying, open-field rearing, forced swim and open-field distance traveled tests, which were different from their wild-type counterparts. Importantly, there were some phenotypic differences between the CB1R and DAGLα knockout mice. In particular, DAGLα knockout mice demonstrated anxiolytic responses in platform tests and in the open field test, which were not observed with CB1R$^{-/-}$ mice.[59] Shoneshy *et al*. noted increased anxiety in both male and female DAGLα$^{-/-}$ mice, while only female mice displayed increased anhedonia.[76] Several studies indicate that perturbation of DAGLα activity, surprisingly, also decreased anandamide levels.[4,5,35,61] The consequences of this *in vivo* cross-talk between the two biosynthetic pathways in relation to potential neuropsychiatric behavior is not known to date. Interestingly, partial restoration of 2-AG levels in DAGL$^{-/-}$ mice by treatment of a MAGL inhibitor normalized the anxiety-related behavior.[76] DAGL inhibitors that produce a graded, dose-dependent blockade of 2-AG production in the CNS, such as DH376 and DO34, may, therefore, provide an excellent opportunity to test whether a therapeutic window can be established. In addition, selective DAGLβ inhibitors could be of therapeutic importance since disruption of DAGLβ activity has been shown to attenuate neuroinflammatory response *in*

vivo without affecting synaptic transmission.[77]

Box 1. Important questions regarding DAGL inhibitors in metabolic and neurological disorders.

General

- Can truly subtype-selective (peripherally restricted) DAGL inhibitors be developed?
- Does chronic DAGL inhibition alter CB receptor sensitivity?
- Does pharmacological DAGL inhibition induce anxiety, stress and fear responses?
- Can a therapeutic window be established using (reversible) DAGL inhibitors?
- Can anandamide and 2-AG biosynthesis be uncoupled using DAGL inhibitors?

Metabolic disorders

- Can centrally active selective DAGLα inhibitors reduce food seeking behavior and induce weight loss, without inducing neuropsychiatric side effects?
- Can peripherally restricted DAGL inhibitors induce weight loss, improve cardiovascular risk factors and decrease insulin resistance?

Neurological disorders

- Can selective DAGL inhibitors reduce negative reward associated behavior and contribute to the treatment of drug abuse (*e.g* alcohol or opioids)?
- What is the specific role 2-AG signaling during neuroinflammation (*i.e.* DAGL versus MAGL inhibition)?
- Are DAGL inhibitors effective in models of neurodegenerative disease (Alzheimer's and Parkinson's disease, MS, etc.)?

To conclude, the development of DAGL knockout mice in combination with *in vivo* active DAGL inhibitors has greatly contributed to the understanding of the physiological role of DAGLs. Recent findings suggest that DAGL inhibition may be beneficial in the treatment of metabolic disorders, such as obesity, diabetes and metabolic syndrome, as well as neuroinflammation, addiction and pathological pain. Exciting times lie ahead as several drug discovery efforts to further optimize DAGLs inhibitors are ongoing. Several important questions still need to be addressed (see Box 1). For example, can orally, bioavailable, subtype selective and centrally active DAGL inhibitors be developed? In addition, peripheral restricted subtype selective inhibitors would also be of interest. This would complete the set of chemical tools required to elucidate the specific roles of DAGLα and β in the various tissues. From a therapeutic point of view, the establishment of a therapeutic window over the untoward neurological outcomes could perhaps best be achieved with reversible, selective DAGL inhibitors.

References

1. Sugiura, T. *et al.* 2-Arachidonoylglycerol: a possible endogenous cannabinoid receptor ligand in brain. *Biochem. Biophys. Res. Commun.* **215,** 89–97 (1995).
2. Mechoulam, R. *et al.* Identification of an endogenous 2-monoglyceride, present in canine gut, that binds to cannabinoid receptors. *Biochem. Pharmacol.* **50,** 83–90 (1995).
3. Stella, N., Schweitzer, P. & Piomelli, D. A second endogenous cannabinoid that modulates long-term potentiation. *Nature* **388,** 773–778 (1997).
4. Tanimura, A. *et al.* The endocannabinoid 2-arachidonoylglycerol produced by diacylglycerol lipase a mediates retrograde suppression of synaptic transmission. *Neuron* **65,** 320–327 (2010).
5. Gao, Y. *et al.* Loss of Retrograde Endocannabinoid Signaling and Reduced Adult Neurogenesis in Diacylglycerol Lipase Knock-out Mice. *J. Neurosci.* **30,** 2017–2024 (2010).
6. Colombo, G. *et al.* Appetite supression and weight loss after the cannabinoid antagonist SR 141716. *Life Sci.* **63,** 113–117 (1998).
7. Di Marzo, V. *et al.* Leptin-regulated endocannabinoids are involved in maintaining food intake. *Nature* **410,** 822–825 (2001).
8. Koch, M. *et al.* Hypothalamic POMC neurons promote cannabinoid-induced feeding. *Nature* **519,** 45–50 (2015).
9. Rajesh, M. *et al.* Pivotal Advance: Cannabinoid-2 receptor agonist HU-308 protects against hepatic ischemia/reperfusion injury by attenuating oxidative stress, inflammatory response, and apoptosis. *J. Leukoc. Biol.* **82,** 1382–1389 (2007).
10. Rajesh, M. *et al.* CB2-receptor stimulation attentuates TNF-a induce human endothelial cell activation, transendothelial migation of monocytes, and monocyte-endothelial adhesion. *Am. J. Physiol.* **141,** 520–529 (2007).
11. Reibaud, M. *et al.* Enhancement of memory in cannabinoid CB1 receptor knock-out mice. *Eur. J. Pharmacol.* **379,** R1–R2 (1999).
12. Hampson, R. E. & Deadwyler, S. A. Role of cannabinoid receptors in memory storage. *Neurobiol. Dis.* **5,** 474–482 (1998).
13. Marsicano, G. *et al.* The endogenous cannabinoid system controls extinction of aversive memories. *Nature* **418,** 530–534 (2002).
14. Navarro, M. *et al.* Acute administration of the CB1R cannabinoid receptor antagonist SR 141716A induces anxiety-like responses in the rat. *Neuroreport* **8,** 491–496 (1997).
15. Haller, J., Bakos, N., Szirmay, M., Ledent, C. & Freund, T. F. The effects of genetic and pharmacological blockade of the CB1R cannabinoid receptor on anxiety. *Eur. J. Neurosci.* **16,** 1395–1398 (2002).
16. Dewey, W. L. Cannabinoid pharmacology. *Pharmacol. Rev.* **38,** 151–178 (1986).
17. Zimmer, A., Zimmer, A. M., Hohmann, A. G., Herkenham, M. & Bonner, T. I. Increased mortality, hypoactivity, and hypoalgesia in cannabinoid CB1 receptor knockout mice. *Proc. Natl. Acad. Sci. U.S.A.* **96,** 5780–5 (1999).
18. Calignano, A., La Rana, G., Giuffrida, A. & Piomelli, D. Control of pain initiation by endogenous cannabinoids. *Nature* **394,** 277–281 (1998).
19. Ledent, C. *et al.* Unresponsiveness to Cannabinoids and Reduced Addictive Effects of Opiates in CB1 receptor Knockout Mice. *Science* **283,** 401–404 (1999).
20. Bisogno, T. *et al.* Cloning of the first sn1-DAG lipases points to the spatial and temporal regulation of endocannabinoid signaling in the brain. *J. Cell Biol.* **163,** 463–468 (2003).
21. Dinh, T. P. *et al.* Brain monoglyceride lipase participating in endocannabinoid inactivation. *Proc. Natl. Acad. Sci. U.S.A.* **99,** 10819–24 (2002).
22. Blankman, J. L., Simon, G. M. & Cravatt, B. F. A Comprehensive Profile of Brain Enzymes that Hydrolyze the Endocannabinoid 2-Arachidonoylglycerol. *Chem. Biol.* **14,** 1347–1356 (2007).
23. Rouzer, C. A. & Marnett, L. J. Endocannabinoid oxygenation by cyclooxygenases, lipoxygenases, and cytochromes P450: Cross-talk between the eicosanoid and endocannabinoid signaling pathways. *Chem. Rev.* **111,** 5899–5921 (2011).
24. Chen, R. *et al.* Monoacylglycerol Lipase Is a Therapeutic Target for Alzheimer's Disease. *Cell Rep.* **2,** 1329–1339 (2012).
25. Kohnz, R. A. & Nomura, D. K. Chemical approaches to therapeutically target the metabolism and signaling of the endocannabinoid 2-AG and eicosanoids. *Chem. Soc. Rev.* **43,** 6859–6869 (2014).

26. Mulvihill, M. M. & Nomura, D. K. Therapeutic Potential of Monoacylglycerol Lipase Inhibitors. *Life Sci.* **92,** 492–497 (2013).
27. Kozak, K. R., Rowlinson, S. W. & Marnett, L. J. Oxygenation of the endocannabinoid, 2-arachidonylglycerol, to glyceryl prostaglandins by cyclooxygenase-2. *J. Biol. Chem.* **275,** 33744–33749 (2000).
28. Appiah, K. K. *et al.* Identification of small molecules that selectively inhibit diacylglycerol lipase-alpha activity. *J Biomol Screen* **19,** 595–605 (2014).
29. Singh, P. K. *et al.* Assay and Inhibition of the Purified Catalytic Domain of Diacylglycerol Lipase Beta. *Biochemistry* **55,** 2713–2721 (2016).
30. Pedicord, D. L. *et al.* Molecular characterization and identification of surrogate substrates for diacylglycerol lipase a. *Biochem. Biophys. Res. Commun.* **411,** 809–814 (2011).
31. Singh, P. K., Markwick, R., Howell, F. V, Williams, G. & Doherty, P. A novel cell assay to measure diacylglycerol lipase α activity. *Biosci. Rep.* **0,** 1–8 (2016).
32. Janssen, F. J. *et al.* Comprehensive Analysis of Structure-Activity Relationships of α-Ketoheterocycles as sn-1-Diacylglycerol Lipase α Inhibitors. *J. Med. Chem.* **58,** 9742–9753 (2015).
33. Hsu, K. L. *et al.* DAGLβ inhibition perturbs a lipid network involved in macrophage inflammatory responses. *Nat. Chem. Biol.* **8,** 999–1007 (2012).
34. Van Der Wel, T. *et al.* A natural substrate-based fluorescence assay for inhibitor screening on diacylglycerol lipase α. *J. Lipid Res.* **56,** 927–935 (2015).
35. Ogasawara, D. *et al.* Rapid and profound rewiring of brain lipid signaling networks by acute diacylglycerol lipase inhibition. *Proc. Natl. Acad. Sci. U.S.A.* **113,** (2015).
36. Liu, Y., Patricelli, M. P. & Cravatt, B. F. Activity-based protein profiling: the serine hydrolases. *Proc. Natl. Acad. Sci. U.S.A.* **96,** 14694–14699 (1999).
37. Kidd, D., Liu, Y. & Cravatt, B. F. Profiling serine hydrolase activities in complex proteomes. *Biochemistry* **40,** 4005–4015 (2001).
38. Leung, D., Hardouin, C., Boger, D. L. & Cravatt, B. F. Discovering potent and selective reversible inhibitors of enzymes in complex proteomes. *Nat. Biotechnol.* **21,** 687–691 (2003).
39. Baggelaar, M. P. *et al.* Development of an activity-based probe and in silico design reveal highly selective inhibitors for diacylglycerol lipase-a in brain. *Angew. Chem. Int. Ed.* **52,** 12081–12085 (2013).
40. Baggelaar, M. P. *et al.* Highly Selective, Reversible Inhibitor Identified by Comparative Chemoproteomics Modulates Diacylglycerol Lipase Activity in Neurons. *J. Am. Chem. Soc.* **137,** 8851–8857 (2015).
41. Janssen, F. J. *et al.* Discovery of glycine sulfonamides as dual inhibitors of sn-1-diacylglycerol lipase α and α/β hydrolase domain 6. *J. Med. Chem.* **57,** 6610–6622 (2014).
42. Chupak, L. S.; Zheng, X.; Ding, M.; Hu, S.; Huang, Y.; Gentles, R. & G. Glycine chroman-6-sulfonamides for use as inhibitors of diacylglycerol lipase. U.S. Patent 20110207749 A1 (2011).
43. Chupak, L. S. *et al.* Structure-activity relationship studies on chemically non-reactive glycine sulfonamide inhibitors of diacylglycerol lipase. *Bioorg. Med. Chem.* **24,** 1455–1468 (2016).
44. Bachovchin, D. A. *et al.* A high-throughput, multiplexed assay for superfamily-wide profiling of enzyme activity. *Nat. Chem. Biol.* **10,** 656–663 (2014).
45. Borgstriim, B. Mode of action of tetrahydrolipstatin: a derivative of the naturally occurring lipase inhibitor lipstatin. *Enzyme* 308–316 (1988).
46. Hadváry, P., Lengsfeld, H. & Wolfer, H. Inhibition of pancreatic lipase in vitro by the covalent inhibitor tetrahydrolipstatin. *Biochem. J.* **256,** 357–361 (1988).
47. Zhi, J., Melia, A. T., Eggers, H., Joly, R. & Patel, I. H. Review of limited systemic absorption of orlistat, a lipase inhibitor, in healthy human volunteers. *J. Clin. Pharmacol.* **35,** 1103–1108 (1995).
48. Ortar, G. *et al.* Tetrahydrolipstatin analogues as modulators of endocannabinoid 2-arachidonoylglycerol metabolism. *J. Med. Chem.* **51,** 6970–6979 (2008).
49. Johnston, M. *et al.* Assay and inhibition of diacylglycerol lipase activity. *Bioorganic Med. Chem. Lett.* **22,** 4585–4592 (2012).
50. Hashimotodani, Y. *et al.* Acute inhibition of diacylglycerol lipase blocks endocannabinoid-mediated retrograde signaling: evidence for on-demand biosynthesis of 2-arachidonoylglycerol. *J. Physiol.* **591,** 4765–76 (2013).
51. Zhang, L., Wang, M., Bisogno, T., di Marzo, V. & Alger, B. E. Endocannabinoids generated by Ca2+ or by metabotropic glutamate receptors appear to arise from different pools of diacylglycerol lipase. *PLoS One* **6,** 0–8 (2011).
52. Min, R. *et al.* Diacylglycerol Lipase Is Not Involved in Depolarization-Induced Suppression of Inhibition

at Unitary Inhibitory Connections in Mouse Hippocampus. *J. Neurosci.* **30,** 2710–2715 (2010).
53. Bashashati, M. *et al.* Inhibiting endocannabinoid biosynthesis: A novel approach to the treatment of constipation. *Br. J. Pharmacol.* 3099–3111 (2015). doi:10.1111/bph.13114
54. Duncan, M. *et al.* Distribution and function of monoacylglycerol lipase in the gastrointestinal tract. *Am. J. Physiol. Gastrointest. Liver Physiol.* **295,** G1255–G1265 (2008).
55. Bisogno, T. *et al.* Development of the first potent and specific inhibitors of endocannabinoid biosynthesis. *Biochim. Biophys. Acta - Mol. Cell Biol. Lipids* **1761,** 205–212 (2006).
56. Bisogno, T. *et al.* Synthesis and pharmacological activity of a potent inhibitor of the biosynthesis of the endocannabinoid 2-arachidonoylglycerol. *ChemMedChem* **4,** 946–950 (2009).
57. Valdeolivas, S. *et al.* The inhibition of 2-arachidonoyl-glycerol (2-AG) biosynthesis, rather than enhancing striatal damage, protects striatal neurons from malonate-induced death: a potential role of cyclooxygenase-2-dependent metabolism of 2-AG. *Cell Death Dis.* **4,** e862 (2013).
58. Bisogno, T. *et al.* A novel fluorophosphonate inhibitor of the biosynthesis of the endocannabinoid 2-arachidonoylglycerol with potential anti-obesity effects. *Br. J. Pharmacol.* **169,** 784–793 (2013).
59. Powell, D. R. *et al.* Diacylglycerol Lipase a Knockout Mice Demonstrate Metabolic and Behavioral Phenotypes Similar to Those of Cannabinoid Receptor 1 Knockout Mice. *Front. Endocrinol.* **6,** 86 (2015).
60. Wilkerson, J. L. *et al.* Diacylglycerol lipase beta inhibition reverses nociceptive behavior in mouse models of inflammatory and neuropathic pain. *Br. J. Pharmacol.* **173,** 1678–1692 (2016).
61. Jenniches, I. *et al.* Anxiety, Stress, and Fear Response in Mice with Reduced Endocannabinoid Levels. *Biol. Psychiatry* **79,** 858–868 (2014).
62. Nass, S. R. *et al.* Endocannabinoid Catabolic Enzymes Play Differential Roles in Thermal Homeostasis in Response to Environmental or Immune Challenge. *J. Neuroimmune Pharmacol.* **10,** 364–370 (2015).
63. Buczynski, M. W. *et al.* Diacylglycerol lipase disinhibits VTA dopamine neurons during chronic nicotine exposure. *Proc. Natl. Acad. Sci. U.S.A.* **113,** 1086–1091 (2016).
64. Boger, D. L. *et al.* Exceptionally potent inhibitors of fatty acid amide hydrolase: the enzyme responsible for degradation of endogenous oleamide and anandamide. *Proc. Natl. Acad. Sci. U.S.A.* **97,** 5044–5049 (2000).
65. Despres, J. P., Golay, A., Sjostrom, L. & Rimonabant in Obesity-Lipids Study, G. Effects of rimonabant on metabolic risk factors in overweight patients with dyslipidemia. *N. Engl. J. Med.* **353,** 2121–2134 (2005).
66. Van Gaal, L. F. *et al.* Effects of the cannabinoid-1 receptor blocker rimonabant on weight reduction and cardiovascular risk factors in overweight patients: 1-year experience from the RIO- Europe study. *Lancet* **19,** 737–43. (2005).
67. Pi-Sunyer, F. *et al.* Effect of rimonabant, a cannabinoid-1 receptor blocker, on weight and cardiometabolic risk factors in overweight or obese patients: Rio-north america: a randomized controlled trial. *J. Am. Med. Assoc.* **295,** 761–775 (2006).
68. Gruden, G., Barutta, F., Kunos, G. & Pacher, P. Role of the endocannabinoid system in diabetes and diabetic complications. *Br. J. Pharmacol.* **173,** 1116–1127 (2015).
69. Glass, C. K., Saijo, K., Winner, B., Marchetto, M. C. & Gage, H. Mechanisms Underlying Inflammation in Neurodegeneration. *Cell* **140,** 918–934 (2010).
70. Simmons, D. L., Botting, R. M. & Hla, T. Cyclooxygenase isozymes: the biology of prostaglandin synthesis and inhibition. *Pharmacol. Rev.* **56,** 387–437 (2004).
71. Nomura, D. K. *et al.* Endocannabinoid hydrolysis generates brain prostaglandins that promote neuroinflammation. *Science* **334,** 809–813 (2011).
72. Hernández-Torres, G. *et al.* A reversible and selective inhibitor of monoacylglycerol lipase ameliorates multiple sclerosis. *Angew. Chem. Int. Ed.* **53,** 13765–13770 (2014).
73. Fernandez-Suarez, D. *et al.* The monoacylglycerol lipase inhibitor JZL184 is neuroprotective and alters glial cell phenotype in the chronic MPTP mouse model. *Neurobiol. Aging* **35,** 2603–2616 (2014).
74. Schlosburg, J. E. *et al.* Chronic monoacylglycerol lipase blockade causes functional antagonism of the endocannabinoid system. *Nat. Neurosci.* **13,** 1113–1119 (2010).
75. Moreira, F. A., Grieb, M. & Lutz, B. Central side-effects of therapies based on CB1R cannabinoid receptor agonists and antagonists: focus on anxiety and depression. *Best Pract. Res. Clin. Endocrinol. Metab.* **23,** 133–144 (2009).
76. Shonesy, B. C. *et al.* Genetic Disruption of 2-Arachidonoylglycerol Synthesis Reveals a Key Role for Endocannabinoid Signaling in Anxiety Modulation. *Cell Rep.* **9,** 1644–1654 (2014).
77. Viader, A. *et al.* A chemical proteomic atlas of brain serine hydrolases identifies cell type-specific pathways regulating neuroinflammation. *Elife* **5,** 1–24 (2016).

CHAPTER 9

Summary and future prospects

This Thesis reports on the discovery and optimization of potent inhibitors for the serine hydrolases *sn*-1 diacylglycerol lipase α (DAGLα) and α/β hydrolase domain 16A (ABHD16A). Several structure- and ligand-based drug discovery methodologies were employed in combination with activity-based protein profiling (ABPP).

DAGLs are multidomain membrane proteins belonging to the large family of serine hydrolases. They contain a typical α/β hydrolase fold and employ a Ser-His-Asp catalytic triad for specific hydrolysis of *sn*-1 fatty acid chains of arachidonate containing 1,2-diacylglycerols. As such, DAGLs are key proteins involved in the formation of 2-monoacylglycerols, including 2-arachidonoylglycerol (2-AG, see Figure 1). The two DAGL isoforms (α and β) share extensive homology and differ mostly in a large C-terminal tail, which is present in DAGLα, but not in DAGLβ.[1] Genetic disruption of DAGLα in mice results in a strong reduction of 2-AG levels in the brain (80-90%), whereas in DAGLβ$^{-/-}$ mice the 2-AG level is approximately 50% reduced in the brain.[2,3] As one of the two major endocannabinoids, 2-AG contributes to cannabinoid type 1 receptor (CB1R) mediated synaptic plasticity and acts as a retrograde messenger inhibiting GABAergic and glutamatergic neurotransmission.[2,3]

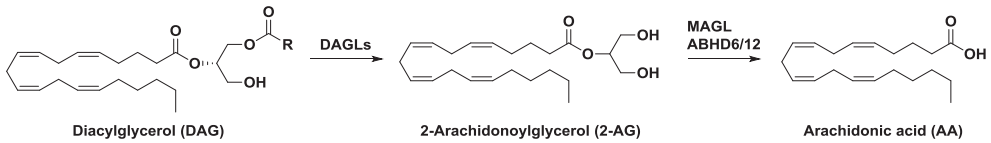

Figure 1. Diacylglycerol (DAG) is a substrate for *sn*-1 specific diacylglycerol lipases α and β (DAGLs) which produce the endocannabinoid 2-arachidonoylglycerol (2-AG), a ligand for the cannabinoid receptors type 1 and 2 (CB1R and CB2R).[1] 2-AG is degraded by several enzymes including monoacylglycerol lipase (MAGL), α/β hydrolase domain 6 and 12 (ABHD6 and ABHD12) to arachidonic acid (AA), which serves as a precursor for the formation of several distinct eicosanoids, such as proinflammatory prostaglandins.

The CBRs are involved in many physiological functions, including food intake,[4–6] inflammation,[7,8] memory formation,[9–11] mood,[12,13] locomotor acivity,[14,15] pain sensation,[16] addiction and reward.[17] In fact, the endocannabinoid system is a clinically proven signaling

pathway controlling the energy balance in humans. The first generation CB1R antagonist/inverse agonist Rimonabant was considered one of the most promising therapeutic drugs to treat human obesity, until the appearance of central psychiatric side effects resulted in its removal from the market in 2008.[18–20] Rimonabant reduces food intake, body weight and waist circumference in obese patients and improves cardiovascular risk factors.[18,19,21] Currently, several lines of evidence suggest that 2-AG, and not anandamide (nor constitutively active CB1Rs), regulates CB1R-dependent food intake. 2-AG levels are increased in the hypothalamus of fasting mice[5] and pharmacological intervention leads to reduced food intake in mice.[22] Third, DAGLα$^{-/-}$ mice showed hypophagia and leanness similar to that of CB1R$^{-/-}$ mice, while knockout mice of DAGLβ and *N*-acyl phosphatidylethanolamine phospholipase D (NAPE-PLD, the main enzyme responsible for anandamide synthesis) did not share this phenotype.[23,24] Interestingly, DAGLα knockout mice also had low fasting insulin, triglyceride, and total cholesterol levels, and after glucose challenge had normal glucose but very low insulin levels.[24] Taken together, this data suggests that selective interference with DAGLα signaling represents a novel therapeutic avenue to treat obesity and the metabolic syndrome.

Inflammatory processes are associated with obesity and with many neurodegenerative diseases, including stroke, Parkinson's and Alzheimer's disease.[25] Prostaglandins produced by cyclooxygenases from arachidonic acid (AA) are important pro-inflammatory stimuli. Cyclooxygenase inhibitors show neuroprotection in animal models of Parkinson's and Alzheimer's disease, but their gastrointestinal and cardiovascular actions have limited their use in humans.[26] Nomura *et al.* discovered that monoacylglycerol lipase (MAGL) regulates AA levels in specific tissues, which is required for prostaglandin synthesis by cyclooxygenases type 1 and 2 (COX1 and COX2).[27] For instance, MAGL is the predominant enzyme producing AA in the brain, liver and lung, whereas phospholipase A2 (PLA2) regulates AA levels in the gut and spleen. Inhibition of MAGL activity in LPS-treated mice resulted in an attenuated neuroinflammatory response as witnessed by a marked decrease in pro-inflammatory prostaglandins and cytokine formation in the brain. MAGL inhibitors improved neurological outcome in animal models of Multiple Sclerosis,[28] Parkinson's[27,29] and Alzheimer disease.[30] Of note, CB1R activation by elevated 2-AG levels did not seem to be involved in the protective response. Concomitant chronic activation of the CB1R by elevated 2-AG levels has previously been shown to lead to adaptations of the endocannabinoid system (*e.g.,* downregulation of CB1R and physical dependence).[31] It is currently unknown how elevated 2-AG levels will impact CB1R-mediated signaling under chronic neurodegenerative conditions. Therefore, DAGL inhibition may provide an alternative approach to reduce AA formation in the brain without accumulation of 2-AG and (chronic) CB1R activation. However, pharmacological characterization of DAGLs has long been hampered due to the lack of multi-well activity assays and potent and selective DAGL inhibitors. Several small molecule DAGL inhibitors have been reported, yet most lack selectivity, *in vivo* activity or pharmacokinetic properties to act as drug candidates, or to

study the role of 2-AG. Thus, there is an unmet need to identify novel chemotypes to modulate DAGL activity. Throughout this Thesis, five DAGL chemotypes are reported, the glycine sulfonamides and newly discovered α-ketoheterocycles, α-keto amides, β-keto difluoroamides and sulfonyl 1,2,4-triazole ureas.

α-Keto heterocycles were discovered as potent DAGLα inhibitors in **Chapter 2** by ligand-based pharmacophore screening. Two pharmacophore models were constructed based on a known previously published bioactive conformation of a non-selective DAGLα inhibitor, tetrahydrolipstatin (THL). *In silico* screening of a focused library of 16 lipase and endocannabinoid system associated inhibitors identified LEI103, an oxadiazolone and LEI104, an α-keto heterocycle (**1**, Table 1), as two high ranking binding poses in both models. The potency of LEI103 and LEI104 was confirmed in a DAGLα surrogate substrate activity assay using PNP-butyrate. This assay showed that, of both DAGLα inhibitors, LEI104 is most potent. To determine a potential binding mode, a homology model was constructed based on a previously reported co-crystal structure which was used as template. The DAGLα model contains an α/β hydrolase fold and well-aligned catalytic triad consisting of the previously reported residues. LEI104 was covalently docked, forming a hemiketal adduct and subsequently optimized by molecular dynamics (MD) in the presence of the model. MD simulations indicated that the formed oxyanion is stabilized by hydrogen bonding interactions with Thr400 OH, backbone NH and Leu473 backbone NH (the 'oxyanion hole'). The binding mode via the ketone is supported by the alcohol precursor of LEI104 being inactive. The pyridine and oxazole nitrogens form crucial interactions in the DAGLα homology model with His471 and His650 respectively. The importance of the pyridine nitrogen was confirmed, as its removal, leading to the corresponding benzoxazole, resulted in significantly decreased inhibitor potency. The structure-activity relationships of LEI104 (Figure 2A) were thoroughly investigated in **Chapter 3** by synthesis of several analogs and screening of a 1040 focused library of α-keto heterocycle derivatives. This Chapter shows that the heterocyclic scaffold is crucial for inhibitor potency, as many tested hetrocycles (*e.g.* benzoxazole, -imidazole, -thiazoles, imidazolopyridine, thiazolopyridine and oxadiazoles) are less potent on DAGLα compared to oxazolopyridines. By synthesis of all possible oxazolopyridine regioisomers, it was shown that the original *4N*-oxazolopyridine regioisomer is optimal. This is in line with the reported homology model, as only this specific position can form hydrogen bonding interactions with His471 and His650. Potency of oxazole inhibitors can be increased by introduction of electron withdrawing substituents at the *meta*- but not at the *para*-position. The 2-acyl substituent on the heterocyclic scaffold was also investigated. In the case of a 2-acyl phenylmethylene spacer, a C8 spacer is most potent (pIC_{50} = 8.44, lipophilic efficiency, LipE = 2.78) and a C5 spacer is most efficient (pIC_{50} = 7.43, LipE = 3.35). 2-Acyl fatty acid spacers are also allowed. Interestingly, in terms of potency oleoyl >> arachidonoyl, indicating that the 2-acyl spacer is possibly situated in the pocket normally accommodating the *sn*-1 acyl chain that is specifically cleaved by DAGLα. Most α-keto heterocycles that have previously been published are dual FAAH and DAGLα inhibitors. The structure-activity relationships in this study are fully in line with the homology model,

which was instrumental in the optimization towards LEI105, a potent dual DAGLα/DAGLβ inhibitor that is selective over FAAH and modulates DSI in hippocampal CA1 pyramidal neurons.[32] The lead optimization of LEI105 to optimize its physicochemical properties is described in **Chapter 4**, starting from optimization of the 2-acyl substituent (Figure 2B). Synthesis of shorter spacer analogs of LEI105 showed that the C5 methylenephenyl spacer in LEI105 is most potent, but a C3 spacer has optimal LipE. Introduction of aliphatic spacers containing terminal trifluoromethyl (CF_3) groups increased LipE 100-fold. In particular, a 4,4,4-trifluoromethylbutanoyl spacer was further optimized, focusing primarily on the heterocyclic scaffold. Methoxy- and cyano-groups were incorporated to assess the electronic effects on the phenyl ring, moreover *p*-chloro and *p*-fluoro groups were introduced to increase metabolic stability. All inhibitors were also tested in a DAGLα natural substrate assay. The selectivity of the highest LipE compounds were assessed over endogenous serine hydrolases in mouse brain proteome using ABPP on two broad-spectrum probes MB064 and TAMRA-FP. Ultimately, *p*-fluorophenyl derivative LEI107, an exquisitely selective DAGLα inhibitor with drug-like chemical properties was discovered. LEI107 is more potent than LEI105 and is 1000+ fold improved in lipophilic efficiency (Figure 2B and **2** in Table 1).

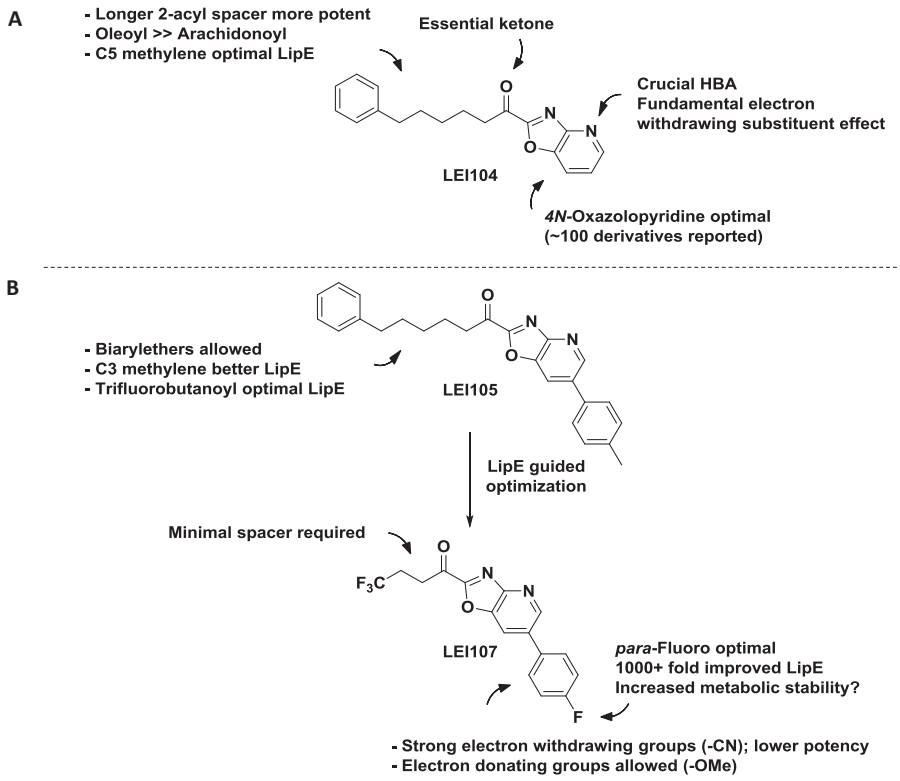

Figure 2. A) Structure-activity relationships of LEI104. **B)** Structure-activity relationships of the optimization of LEI105 to LEI107.

Glycine sulfonamides were investigated in **Chapter 5** as DAGLα inhibitors via a systematic structure-activity relationship analysis. Glycine sulfonamides were identified as DAGLα inhibitors by a high throughput screening (HTS) performed by researchers of Bristol Meyers-Squibb (BMS). Starting from these reported compounds,[33,34] the biaryl-ether scaffolds, side groups and carboxylic acid were investigated. All compounds were tested in a 96-well DAGLα surrogate substrate assay. The glycine carboxylic acid was an important focus of the investigation, as this chemotype was the only reported inhibitor without a clear warhead or mechanism of action. Hence, the carboxylic acid was investigated by synthesis of the corresponding methyl ester, alcohol, secondary and primary amide, nitrile, tetrazole and a piperidine carbamate**,** all of which were uniformly inactive (Figure 3). Activity is lost upon derivatization of the carboxylic acid moiety, which indicates that it is an essential feature for inhibiting DAGLα.[35,36] By synthesis of 13 different scaffold analogs it was discovered that DAGLα tolerates all substitution patterns on the scaffold, however *para* > *meta* > *ortho* indicating a large linear-like binding groove. Several sulfonamide side groups are tolerated, although the originally reported 2,2-dimethylchroman sulfonamide remains the most potent. Ultimately, systematic analysis of the structural requirements in this study led to the discovery of LEI106, a highly potent DAGLα inhibitor (Figure 3 and compound **3** in Table 1). Due to the presence of the essential carboxylic acid, the binding mode of LEI106 was investigated using docking in the newly developed DAGLα homology model (see Chapter 2 for model development). The modeling indicated that the carboxylic acid might interfere with the hydrogen bonding network of the catalytic triad. The activity and selectivity of LEI106 was assessed over endogenous serine hydrolases in mouse brain proteome using ABPP. The ABPP approach showed that glycine sulfonamide LEI106 is selective over several endocannabinoid system related enzymes, including monoacylglycerol lipase (MAGL) and fatty acid amide hydrolase (FAAH). However, LEI106 did inhibit α/β hydrolase domain 6 (ABHD6) in the ABPP setting used. Testing of LEI106 in a natural substrate assay based on the conversion of 2-AG by ABHD6, confirmed that LEI106 potently inhibited ABHD6 (K_i = 0.8 ± 0.1 μM). LEI106 inhibited DAGLα in a natural substrate assay based assay (K_i = 0.7 ± 0.08 μM) making LEI106 the first reported reversible dual DAGLα/ ABHD6 inhibitor.

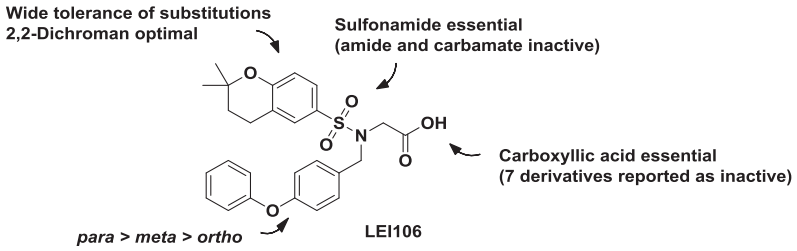

Figure 3. Structure-activity relationships of LEI106.

Chapter 6 encompassed the miniaturization of the PNP-butyrate DAGLα activity assay from 96-well plate to 1536-well plate and subsequent HTS-ABPP. The 96-well plate assay was first

optimized to 354-well plate by optimizing total volume (30 µL), enzyme concentration (0.05 µg/µL) and changing readout from kinetic readout to endpoint determination. The assay was used in a proof-of-principle screen on the commercially available 'List of pharmaceutically active compounds' (LOPAC®, Sigma-Aldrich) library. This screen showed that the assay is of high quality and robust over multiple screening days. The 384-well plate assay was subsequently optimized to 1536-well plate within the European Lead Factory (ELF). Thorough optimization of assay plates, substrate storage conditions, assay volume, enzyme and substrate concentration resulted in an optimized 1536-well plate protocol that was robust and of high quality. The protocol was used in automated HTS as primary screen (single point 10 µM inhibitor) of the Joint European Compound Library (JECL), consisting of 300.000+ compounds. The primary assay was followed up by active conformation at two inhibitor concentrations, resulting in a total of 263 confirmed actives. Orthogonal ABPP was employed to assess activity and selectivity of these actives over multiple serine hydrolases in mouse brain proteome. For high throughput purposes, an ABPP assay protocol was developed that uses incubation in 384-well plate. DAGLα activity was investigated by labeling with ABP MB064 and subsequent in-gel analysis using SDS-PAGE and fluorescence scanning. In addition to DAGLα, MB064 reports on DDHD2, ABHD6, ABHD12, ABHD16A off-target activity. After triaging based on the orthogonal assay activity and selectivity, chemical eye, purity analysis and legal clearance, 46 actives were obtained forming the Qualified Hit List (QHL). The list contains 10 clusters and 10 singletons, including previously reported glycine sulfonamides and three important novel chemotypes: α-keto amides, β-keto difluoro amides and sulfonyl 1,2,4-triazole ureas.

Glycine sulfonamides IMI4906626 and IMI4749305 were identified as the most potent DAGLα inhibitors across the entire screening campaign (**4** and **5**, Table 1). Compound **5** was resynthesized and retested by the European Screening Centre. Similar ABPP assessment (as with LEI106) on **5** indicated that it is selective over ABHD6, making this the first reported glycine sulfonamide DAGL inhibitor that seems selective over this specific off-target on ABPP. Compound **4** has not been resynthesized and retested, nevertheless **4** did significantly inhibit ABHD6 in the orthogonal ABPP assay. **α-Keto amides** and **β-keto difluoro amides** are reversible inhibitors that use an activated ketone as electrophilic trap, presumably reacting with Ser472 of DAGLα. Both chemotypes are interesting leads for inhibitor development as IMI0226509, IMI8042748, IMI7294928 and IMI6975607 (**6**-**9**, Table 1) have great physicochemical properties and good LipE (~2) and ligand efficiency, LE (~0.35). These compounds were all resynthesized and retested by the European Screening Centre. ABPP analysis revealed that α-keto amides **6** and **7** did not appear to inhibit ABHD6 to a large extent in the ABPP setting used, whereas β-keto difluoro amides **8** and **9** did inhibit ABHD6 labeling. Both chemotypes can be important for inhibitor development on future uncharacterized serine hydrolases or cysteine proteases in which the QHL can serve as important screening tool. **Sulfonyl 1,2,4-triazole ureas** IMI18721890, IMI18721890 and IMI1788117 (**10**-**12**, Table 1) were highly potent inhibitors in both the primary and orthogonal DAGLα assays. This chemotype uses an activated carbonyl as covalent

irreversible electrophilic trap. Compounds **10** and **11** were resynthesized and retested by the European Screening Centre. Selectivity assessment of **10** and **11** on ABPP reveals that ABHD6 as well as FAAH and DDHD2 are targeted. Due to their potency, sulfonyl 1,2,4-triazole ureas were selected for subsequent lead optimization and a focused library of ~100 derivatives was synthesized within the ELF consortium by the European Screening Centre. The focused library can serve as an important tool for inhibitor optimization on DAGLs and other targets, such as future uncharacterized serine hydrolases or cysteine proteases.

Chapter 8 encompassed an extensive review on the effect of several DAGL inhibitors in pre-clinical models of metabolic disorders and neurodegenerative diseases. Several parts of this Chapter have been mentioned throughout this summary.

The development of DAGL knockout mice in combination with *in vivo* active DAGL inhibitors has greatly contributed to the understanding of the physiological role of DAGLs. Studies using 1,2,3-triazole ureas DO34 and DH376 have demonstrated that DAGLs regulate the formation of proinflammatory prostaglandins and cytokines under neuroinflammatory conditions.[37] The efficacy of DO34 and DH376 in mouse models of disease has not been reported to date and could provide important insights in the contribution of 2-AG signaling and metabolites in neurodegenerative diseases. One study does show that O-3841, a fluorophosphonate DAGL inhibitor, was neuroprotective in a malonate model of Huntington's disease. Interestingly, MAGL inhibitors exacerbated neuronal damage and oxidative metabolism of 2-AG by COX2 was suggested to result in the formation of the toxic metabolites.[38,39] Considering that several studies indicate that 2-AG signaling, via DAGLα, is involved in the regulation of neuropsychiatric behavior, application of centrally active inhibitors for DAGLα necessitates caution *in vivo*.[23,24,40] Therefore, it will be highly important to determine the efficacy and therapeutic window of both MAGL and DAGL inhibitors in parallel with respect to CB1R mediated adverse effects and activation of alternative metabolic pathways during neuroinflammation.

The 1,2,3-triazole ureas provide a structural template bearing a reactive urea with tunable reactivity, which seems ideal for optimization of serine hydrolase inhibition. It is expected that the newly discovered sulfonyl 1,2,4-triazole ureas are very similar in that aspect. Moreover, their reactivity can potentially be tuned by the sulfur oxidation state, which could influence the triazole pKa, and thereby leaving group capacity. The sulfonyl 1,2,4-triazole ureas have very good physicochemical properties (*e.g.* low MW and low cLogD) although their tPSA is relatively high (>96 A^2). Potential drawbacks of the triazole ureas are their off-target activity and covalent irreversible mode of action. This makes the 1,2,3-triazole ureas and sulfonyl 1,2,4-triazole ureas less suitable as potential drug candidates. As such, triazole ureas can best be viewed as tool compounds to report on DAGL function in health and disease, and possibilities regarding DAGLα or DAGLβ subtype selectivity might be explored. To this end, development of paired control compounds is necessary. Reversible inhibitors, like the ketones reported in this Thesis, are perhaps more suitable as drug candidates.

Table 1. Overview of the all inhibitors discovered in this Thesis.

Entry	Code	Structure	DAGLα PNP (pIC_{50})	cLogD	LipE	HBA	HBD	LE	MW	tPSA	Off-targets
1	LEI104 (OL-100)	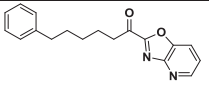	7.4	4.1	3.4	4	0	-	294	51	FAAH
2	LEI107	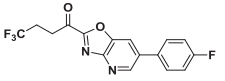	8.6	3.3	5.3	4	0	-	338	51	No off-targets identified
3	LEI106	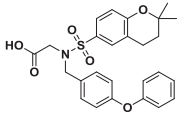	7.7	3.7	4.0	7	1	-	482	93	ABHD6 2 unknown
4	IMI4906626 ESC1000043-01	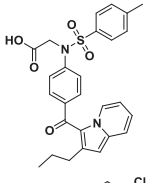	7.5	3.9	3.6	7	1	0.29	491	105	No off-targets identified
5	IMI4749305	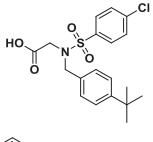	6.9	2.6	4.3	5	1	0.36	396	83	ABHD6
6	IMI0226509 ESC1000025-01	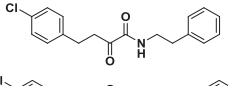	6.0	4.0	2.0	2	1	0.37	316	46	-
7	IMI8052748 ESC1000026-01	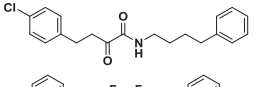	6.0	4.9	1.9	2	1	0.36	344	46	-
8	IMI7294928 ESC1000042-01	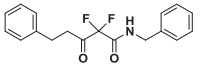	6.1	3.5	2.6	2	1	0.36	317	46	ABHD6

9	IMI6975607 ESC1000044-01	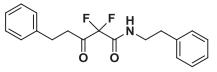	6.2	3.8	2.4	2	1	0.35	331	46	ABHD6
10	IMI18721890 ESC1000032-01	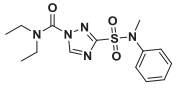	5.9	1.7	4.2	8	0	0.35	337	97	ABHD6 FAAH DDHD2
11	IMI18721890 ESC1000048-01	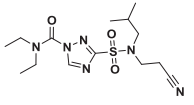	5.5	1.4	4.1	9	0	0.31	356	121	ABHD6 FAAH DDHD2
12	IMI1788117	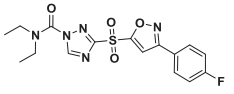	5.6	2.4	3.2	9	0	0.28	393	115	ABHD6 FAAH DDHD2

Entry	Code	Structure	ABHD16A ABPP (pIC_{50})	cLogP	LipE	HBA	HBD	LE	MW	PSA	Selectivity
13	XGN67	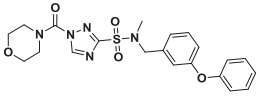	8.1	3.0	5.1	10	0	-	458	104	ABHD6 FAAH CES3 And others
14	XGN75	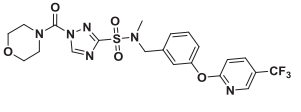	7.4	2.5	4.9	11	0	-	526	117	ABHD6 FAAH CES3 And others

In particular, the α-keto heterocycles such as LEI105 and LEI107 are highly potent and selective. LEI107 shows an ideal combination of high potency, high selectivity and drug-like physicochemical properties, making it the most suitable candidate in this Thesis for *in vivo* studies. LEI107 can be used to assess the effect of pharmacological intervention of DAGL in mouse models of obesity, Multiple Sclerosis, Alzheimer's and Parkinson's disease. Moreover, it can be used to investigate whether a therapeutic window can be established over possible CB1R-related adverse side effects. Proof of target engagement in mice is still required for the α-keto heterocycles, as well as investigation into its *in vivo* stability. Important to keep in mind is that hemiacetal formation can occur at the ketone and its consequences *in vivo* are not known to date.

Interestingly, very recently it has been demonstrated that disruption of DAGLβ alone contributes to lowering the neuroinflammatory response *in vivo*.[41] DAGLβ is key in regulating 2-AG levels in microglia and LPS treated DAGLβ$^{-/-}$ mice show attenuated microglial activation without changes in overall 2-AG and prostaglandin levels in brain. Therefore, DAGLβ can be an important target to attenuate the neuroinflammatory response *in vivo* without affecting synaptic transmission,[41] and therefore could be potentially be devoid of CNS mediated side-effects. Consequently, orally bioavailable, centrally active and selective DAGLβ inhibitors are highly desired and could play a pivotal role in the potential treatment of neurodegenerative diseases such as Multiple Sclerosis, Parkinson's, Alzheimer's and Huntington's disease (Table 2).

Table 2. Potential therapeutic areas for subtype selective DAGL inhibitors with central and peripheral activity.

	DAGLα selective	**DAGLβ selective**	**Dual DAGLα/β**
Central nervous system (CNS)	Addiction Obesity Neuroinflammation Therapeutic window? Adverse side effects?	**Neuroinflammation**	Therapeutic window? Adverse side effects?
Peripheral system	**Metabolic syndrome** **Diabetes** **Pheripheral obesity**	**Pathological pain**	**Metabolic syndrome** **Diabetes** **Pheripheral obesity** **Pathological pain**

Another important line of research is the development of peripherally restricted DAGL inhibitors (Table 2). Inhibitors that do not enter the central nervous system (CNS) are most likely devoid of adverse central side effects and may, therefore, not require full DAGLα/β subtype selectivity. The most important chemotype for this application are the glycine sulfonamides, as they are reversible and have been reported as non-brain penetrable. As a matter of fact, after the publication of LEI106, BMS published a full account of their SAR studies on glycine sulfonamides from the lead optimization program that followed after the

HTS.[33,36] As such, Compounds **3** and **24** (Chapter 8) were identified as highly potent DAGLα/β inhibitors. Reportedly, **3** is cellular active and orally bio-available and **24** is peripherally restricted, picomolar potent and shows a good pharmacokinetic profile. Unfortunately no additional functional or *in vivo* efficacy data have been reported with this series to date. Due to an improved selectivity profile, glycine sulfonamide IMI4906626 (**4**) could provide an interesting starting point for optimization. The key features of **4** that provide selectivity over ABHD6 are not known to date ans is important to address. Investigation into the effect of peripheral inhibition of DAGLα/β *in vivo* for the potential treatment of obesity and metabolic disorders is also important. The main questions are whether glycine sulfonamides can induce weight loss, decrease insulin resistance and/or improve cardiovascular risk factors via perturbation of DAGL α/β activity. The effect of ABHD6 as a peripheral off-target needs to be addressed as well and could potentially be beneficial through polypharmacology.[35] Moreover, local application of peripheral DAGLβ inhibitors, like the glycine sulfonamides, for treatment of pathological pain is another avenue to explore.[42]

Chapter 7 describes the application of ABPP for the development of *in vivo* active inhibitors for ABHD16A, a principal phosphatidyl serine (PS) lipase. ABHD16A cleaves the fatty acyl chain specifically at the *sn*-1 position (Figure 4), forming *lyso*-PS as the main product.[43] *Lyso*-PS is an important signaling phospholipid involved in T-cell growth,[44] mast cell activation[45,46] and neurite outgrowth.[47] Moreover, it is a toll-like receptor 2 (TLR2) agonist.[48] α/β Hydrolase domain type 12 (ABHD12) hydrolyses *lyso*-PS *in vitro* and indeed, ABHD12$^{-/-}$ mice have been shown to accumulate several distinct long chain *lyso*-PS lipids in the brain.[49] Human genetic studies identified null-mutations of ABHD12 as the cause for the onset of a rare neurological disease: polyneuropathy, hearing loss, ataxia, retinitis pigmentosa and cataract (PHARC).[50,51] ABHD12 knockout studies confirmed that mice devoid of ABHD12 activity suffer from multiple symptoms of PHARC.[49] Therefore, ABHD12$^{-/-}$ mice may serve as an excellent mouse model to investigate this neurological disease.[49] The exact molecular mechanism of the development of PHARC is currently unknown, but the accumulation of *lyso*-PS and subsequent excessive signaling via TLR2 are hypothesized to be involved in the neuroinflammatory response. To test this hypothesis, *in vivo* active inhibitors for ABHD16A are required. In this chapter, ABPP on a focused library of several sulfonyl 1,2,4-triazole ureas revealed that this chemotype can target ABHD16A.

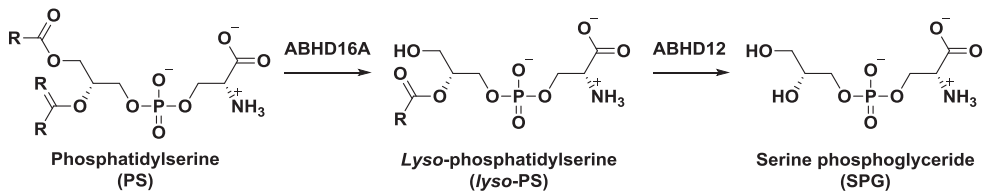

Figure 4. Phosphatidylserine (PS) and lyso-phosphatidylserine (lyso-PS) levels are regulated by α/β hydrolase domain type 12 and 16A (ABHD12 and ABHD16A). ABHD16A cleaves specifically at the PS *sn*-1 fatty ester, whereas ABHD12 cleaves the remaining *sn*-2 fatty ester of *lyso*-PS.

A particular sulfonyl 1,2,4-triazole urea was used as a starting point for further optimization. A ligand-based rational design approach led to XGN67 and XGN75 (**13** and **14**, Table 1). Cellular experiments strongly indicate that **13** and **14** do not efficiently penetrate cells, but do potently inhibit extracellular ABHD16A *in situ*. 1,2,4-Triazole urea sulfonamides **13** and **14** partially, but significantly, inhibit ABHD16A *in vivo* after *i.p.* administration. This makes compounds **13** and **14**, the first *in vivo* active ABHD16A inhibitors in the literature. As brain ABHD16A was not completely inhibited at high doses of both compounds, future work should focus on optimization of brain penetration by decreasing the polar surface area (< 100 A^2) and increasing metabolic stability. This, however, is likely to increase off-target activity *in vivo*. Hence the development of a paired inactive control compound is required, to exclude potential off-target effects in animal models. The structure-activity relationships from this chapter provide an excellent starting point for further optimization of the next generation *in vivo* active ABHD16A inhibitors. These inhibitors could provide proof-of-principle for substrate reduction therapy by lowering *lyso*-PS levels through ABHD16A inhibition as a potential treatment for the debilitating disease PHARC.

In general, drug discovery is best practiced by applying multiple methods for inhibitor discovery in parallel. In target-based drug discovery, HTS can be considered the best method to obtain novel hits if multi-well assays are available (or can be developed) for the target of interest. Provided that the screening library is of high quality, the resulting hits should be drug-like and suitable for medicinal chemistry optimization. Academic access to high quality drug-like libraries, such as the JECL, is therefore of paramount importance to boost academic research and hit discovery (in Europe). However, HTS is time-consuming, costly and good hits are not guaranteed. Therefore other (higher risk) methods should be performed as well. For serine hydrolases in particular, library screening in combination with ABPP (for 'target hopping') has proven a rewarding strategy. Its success is twofold; off-target activity is highly common among serine hydrolase inhibitors as this large protein family shares many common substrates and therefore often has similar binding pockets. In addition, all members have a highly conserved catalytic mechanism. These features, combined with readily available broad-spectrum probes, such as TAMRA-fluorophosphonate, allow rapid assessment of off-target selectivity. Recent developments of activity assays for serine hydrolases, such as Enplex, enable high-throughput superfamily-wide profiling of activity and selectivity of inhibitors over many targets.[52] This method is expected to have high impact in serine hydrolase drug discovery and should be applied as early in the pipeline as possible for counter screening and inhibitor optimization purposes. Lastly, ligand- and structure-based *in silico* strategies, such as high throughput docking and pharmacophore modeling, are powerful low-cost alternatives that can be performed in parallel as well. *In silico* strategies require thorough knowledge of the field and of the methods, algorithms and scoring functions that can be applied. Phenotypic approaches are considered very promising as well, although these are not discussed or applied in this Thesis. Phenotypic screening in combination with novel chemical biology methods (such as incorporation of bio-orthogonal handles and subsequent chemical proteomics) can provide powerful strategies to

interrogate biological systems.

Projecting forward, glycine sulfonamides, such as LEI106, are important peripherally restricted inhibitors that can be used to evaluate the contribution of perturbing DAGL activity in the potential treatment of metabolic syndrome, diabetes and pheriphiral obesity. α-Keto heterocycles, such as LEI107, could be important inhibitors to evaluate if a therapeutic window can be established for (central) DAGL inhibitors in the potential treatment of addiction, obesity and neuroinflammation. Lastly, 1,2,4-triazole urea sulfonamides can be used as novel tool compounds to evaluate DAGL and ABHD16A function in both health and disease.

References

1. Bisogno, T. *et al.* Cloning of the first sn1-DAG lipases points to the spatial and temporal regulation of endocannabinoid signaling in the brain. *J. Cell Biol.* **163,** 463–468 (2003).
2. Gao, Y. *et al.* Loss of Retrograde Endocannabinoid Signaling and Reduced Adult Neurogenesis in Diacylglycerol Lipase Knock-out Mice. *J. Neurosci.* **30,** 2017–2024 (2010).
3. Tanimura, A. *et al.* The endocannabinoid 2-arachidonoylglycerol produced by diacylglycerol lipase a mediates retrograde suppression of synaptic transmission. *Neuron* **65,** 320–327 (2010).
4. Colombo, G. *et al.* Appetite supression and weight loss after the cannabinoid antagonist SR 141716. *Life Sci.* **63,** 113–117 (1998).
5. Di Marzo, V. *et al.* Leptin-regulated endocannabinoids are involved in maintaining food intake. *Nature* **410,** 822–825 (2001).
6. Koch, M. *et al.* Hypothalamic POMC neurons promote cannabinoid-induced feeding. *Nature* **519,** 45–50 (2015).
7. Rajesh, M. *et al.* Pivotal Advance: Cannabinoid-2 receptor agonist HU-308 protects against hepatic ischemia/reperfusion injury by attenuating oxidative stress, inflammatory response, and apoptosis. *J. Leukoc. Biol.* **82,** 1382–1389 (2007).
8. Rajesh, M. *et al.* CB2-receptor stimulation attentuates TNF-a induce human endothelial cell activation, transendothelial migation of monocytes, and monocyte-endothelial adhesion. *Am. J. Physiol.* **141,** 520–529 (2007).
9. Reibaud, M. *et al.* Enhancement of memory in cannabinoid CB1 receptor knock-out mice. *Eur. J. Pharmacol.* **379,** R1–R2 (1999).
10. Hampson, R. E. & Deadwyler, S. A. Role of cannabinoid receptors in memory storage. *Neurobiol. Dis.* **5,** 474–482 (1998).
11. Marsicano, G. *et al.* The endogenous cannabinoid system controls extinction of aversive memories. *Nature* **418,** 530–534 (2002).
12. Navarro, M. *et al.* Acute administration of the CB1R cannabinoid receptor antagonist SR 141716A induces anxiety-like responses in the rat. *Neuroreport* **8,** 491–496 (1997).
13. Haller, J., Bakos, N., Szirmay, M., Ledent, C. & Freund, T. F. The effects of genetic and pharmacological blockade of the CB1R cannabinoid receptor on anxiety. *Eur. J. Neurosci.* **16,** 1395–1398 (2002).
14. Dewey, W. L. Cannabinoid pharmacology. *Pharmacol. Rev.* **38,** 151–178 (1986).
15. Zimmer, A., Zimmer, A. M., Hohmann, A. G., Herkenham, M. & Bonner, T. I. Increased mortality, hypoactivity, and hypoalgesia in cannabinoid CB1 receptor knockout mice. *Proc. Natl. Acad. Sci. U.S.A.* **96,** 5780–5 (1999).
16. Calignano, A., La Rana, G., Giuffrida, A. & Piomelli, D. Control of pain initiation by endogenous cannabinoids. *Nature* **394,** 277–281 (1998).
17. Ledent, C. *et al.* Unresponsiveness to Cannabinoids and Reduced Addictive Effects of Opiates in CB1 receptor Knockout Mice. *Science* **283,** 401–404 (1999).
18. Despres, J. P., Golay, A., Sjostrom, L. & Rimonabant in Obesity-Lipids Study, G. Effects of rimonabant on metabolic risk factors in overweight patients with dyslipidemia. *N. Engl. J. Med.* **353,** 2121–2134 (2005).
19. Van Gaal, L. F. *et al.* Effects of the cannabinoid-1 receptor blocker rimonabant on weight reduction and cardiovascular risk factors in overweight patients: 1-year experience from the RIO- Europe study. *Lancet* **19,** 737–43. (2005).
20. Pi-Sunyer, F. *et al.* Effect of rimonabant, a cannabinoid-1 receptor blocker, on weight and cardiometabolic risk factors in overweight or obese patients: Rio-north america: a randomized controlled trial. *J. Am. Med. Assoc.* **295,** 761–775 (2006).
21. Gruden, G., Barutta, F., Kunos, G. & Pacher, P. Role of the endocannabinoid system in diabetes and diabetic complications. *Br. J. Pharmacol.* **173,** 1116–1127 (2015).
22. Bisogno, T. *et al.* A novel fluorophosphonate inhibitor of the biosynthesis of the endocannabinoid 2-arachidonoylglycerol with potential anti-obesity effects. *Br. J. Pharmacol.* **169,** 784–793 (2013).
23. Powell, D. R. *et al.* Diacylglycerol Lipase a Knockout Mice Demonstrate Metabolic and Behavioral Phenotypes Similar to Those of Cannabinoid Receptor 1 Knockout Mice. *Front. Endocrinol.* **6,** 86 (2015).
24. Jenniches, I. *et al.* Anxiety, Stress, and Fear Response in Mice with Reduced Endocannabinoid Levels. *Biol. Psychiatry* **79,** 858–868 (2014).
25. Glass, C. K., Saijo, K., Winner, B., Marchetto, M. C. & Gage, H. Mechanisms Underlying Inflammation in Neurodegeneration. *Cell* **140,** 918–934 (2010).

26. Simmons, D. L., Botting, R. M. & Hla, T. Cyclooxygenase isozymes: the biology of prostaglandin synthesis and inhibition. *Pharmacol. Rev.* **56,** 387–437 (2004).
27. Nomura, D. K. *et al.* Endocannabinoid hydrolysis generates brain prostaglandins that promote neuroinflammation. *Science* **334,** 809–813 (2011).
28. Hernández-Torres, G. *et al.* A reversible and selective inhibitor of monoacylglycerol lipase ameliorates multiple sclerosis. *Angew. Chem. Int. Ed.* **53,** 13765–13770 (2014).
29. Fernandez-Suarez, D. *et al.* The monoacylglycerol lipase inhibitor JZL184 is neuroprotective and alters glial cell phenotype in the chronic MPTP mouse model. *Neurobiol. Aging* **35,** 2603–2616 (2014).
30. Chen, R. *et al.* Monoacylglycerol Lipase Is a Therapeutic Target for Alzheimer's Disease. *Cell Rep.* **2,** 1329–1339 (2012).
31. Schlosburg, J. E. *et al.* Chronic monoacylglycerol lipase blockade causes functional antagonism of the endocannabinoid system. *Nat. Neurosci.* **13,** 1113–1119 (2010).
32. Baggelaar, M. P. *et al.* Highly Selective, Reversible Inhibitor Identified by Comparative Chemoproteomics Modulates Diacylglycerol Lipase Activity in Neurons. *J. Am. Chem. Soc.* **137,** 8851–8857 (2015).
33. Appiah, K. K. *et al.* Identification of small molecules that selectively inhibit diacylglycerol lipase-alpha activity. *J Biomol Screen* **19,** 595–605 (2014).
34. Chupak, L. S.; Zheng, X.; Ding, M.; Hu, S.; Huang, Y.; Gentles, R. & G. Glycine chroman-6-sulfonamides for use as inhibitors of diacylglycerol lipase. U.S. Patent 20110207749 A1 (2011).
35. Janssen, F. J. *et al.* Discovery of glycine sulfonamides as dual inhibitors of sn-1-diacylglycerol lipase α and α/β hydrolase domain 6. *J. Med. Chem.* **57,** 6610–6622 (2014).
36. Chupak, L. S. *et al.* Structure-activity relationship studies on chemically non-reactive glycine sulfonamide inhibitors of diacylglycerol lipase. *Bioorg. Med. Chem.* **24,** 1455–1468 (2016).
37. Ogasawara, D. *et al.* Rapid and profound rewiring of brain lipid signaling networks by acute diacylglycerol lipase inhibition. *Proc. Natl. Acad. Sci. U.S.A.* **113,** (2015).
38. Kozak, K. R., Rowlinson, S. W. & Marnett, L. J. Oxygenation of the endocannabinoid, 2-arachidonylglycerol, to glyceryl prostaglandins by cyclooxygenase-2. *J. Biol. Chem.* **275,** 33744–33749 (2000).
39. Valdeolivas, S. *et al.* The inhibition of 2-arachidonoyl-glycerol (2-AG) biosynthesis, rather than enhancing striatal damage, protects striatal neurons from malonate-induced death: a potential role of cyclooxygenase-2-dependent metabolism of 2-AG. *Cell Death Dis.* **4,** e862 (2013).
40. Shonesy, B. C. *et al.* Genetic Disruption of 2-Arachidonoylglycerol Synthesis Reveals a Key Role for Endocannabinoid Signaling in Anxiety Modulation. *Cell Rep.* **9,** 1644–1654 (2014).
41. Viader, A. *et al.* A chemical proteomic atlas of brain serine hydrolases identifies cell type-specific pathways regulating neuroinflammation. *Elife* **5,** 1–24 (2016).
42. Wilkerson, J. L. *et al.* Diacylglycerol lipase beta inhibition reverses nociceptive behavior in mouse models of inflammatory and neuropathic pain. *Br. J. Pharmacol.* **173,** 1678–1692 (2016).
43. Kamat, S. S. *et al.* Immunomodulatory lysophosphatidylserines are regulated by ABHD16A and ABHD12 interplay. *Nat. Chem. Biol.* **11,** 164–71 (2015).
44. Bellini, F. & Brunib, A. Role of a serum phospholipase A1 in the phosphatidylserine-induced T cell inhibition. *FEBS Lett.* **316,** 4–7 (1993).
45. Martin, T. W. & Lagunoff, D. Interactions of lysophospholipids and mast cells. *Nature* **279,** 250–252 (1979).
46. Smith, G. A., Hesketh, T. R., Plumb, R. W. & Metcalfe, J. C. The exogenous lipid requirement for histamine release from rat peritoneal mast cells stimulated by concanavalin A. *FEBS Lett.* **105,** (1979).
47. Lourenssen, S. & Blennerhassett, M. G. Lysophosphatidylserine potentiates nerve growth factor-induced differentiation of PC12 cells. *Neurosci. Lett.* **248,** 77–80 (1998).
48. van der Kleij, D. *et al.* A novel host-parasite lipid cross-talk. Schistosomal lyso-phosphatidylserine activates toll-like receptor 2 and affects immune polarization. *J. Biol. Chem.* **277,** 48122–48129 (2002).
49. Blankman, J. L., Long, J. Z., Trauger, S. a, Siuzdak, G. & Cravatt, B. F. ABHD12 controls brain lysophosphatidylserine pathways that are deregulated in a murine model of the neurodegenerative disease PHARC. *Proc. Natl. Acad. Sci. USA* **110,** 1500–1505 (2013).
50. Fiskerstrand, T. *et al.* A novel Refsum-like disorder that maps to chromosome 20. *Neurology* **72,** 20–27 (2009).
51. Fiskerstrand, T. *et al.* Mutations in ABHD12 cause the neurodegenerative disease PHARC: An inborn error of endocannabinoid metabolism. *Am. J. Hum. Genet.* **87,** 410–417 (2010).

52. Bachovchin, D. A. *et al.* A high-throughput, multiplexed assay for superfamily-wide profiling of enzyme activity. *Nat. Chem. Biol.* **10,** 656–663 (2014).

Samenvatting

Dit proefschrift beschrijft de ontdekking van potente remmers voor de serine hydrolases *sn*-1 diacylglycerol lipase α (DAGLα) en α/β hydrolase domein 16A (ABHD16A). Verscheidene strategieën zijn toegepast voor de ontdekking van nieuwe remmers en potentiele kandidaat geneesmiddelen, in combinatie met 'activity-based protein profiling' (ABPP).

DAGLs zijn multi-domein membraanproteïnen die behoren tot de grote familie van serine-hydrolases. Ze bevatten een typische α/β hydrolase structuur en gebruiken de aminozuren serine (Ser), histidine (His) en asparaginezuur (Asp) als katalytische triade voor specifieke hydrolyse van *sn*-1 vetzuur-ketens van arachidonzuur bevattende 1,2-diglycerides. Hierdoor zijn DAGLs belangrijke enzymen betrokken bij de formatie van 2-monoglycerides, zoals 2-arachidonoylglycerol (2-AG). De twee DAGL isovormen (α en β) zijn verwant aan elkaar, maar verschillen met name in het C-terminale domein, dat langer is in DAGLα dan in DAGLβ. Genetische aanpassing van DAGLα activiteit in muizen resulteert in een sterke verlaging van 2-AG in de hersenen (80-90%), terwijl in DAGLβ$^{-/-}$ muizenhersenen 2-AG verlaagd is met 50%. 2-AG voorziet de hersenen van cannabinoïd receptoren (CBR) gerelateerde synaptische plasticiteit en werkt als signaalmolecuul dat GABAerge en glutamaterge neurotransmissie beïnvloed. DAGLs zijn onderdeel van het endocannabinoïd systeem, een klinisch bewezen systeem dat de energiebalans regelt in de mens. Rimonabant, het eerste medicijn dat werkte op de cannabinoïd receptor type 1 (CB1R), werd beschouwd als een van de meest veelbelovende therapeutische geneesmiddelen voor de behandeling van obesitas. Het verschijnen van centrale bijwerkingen leidde echter tot verwijdering van de markt. Rimonabant verminderde voedselinname, lichaamsgewicht en tailleomtrek bij obese patiënten en verbeterde cardiovasculaire risicofactoren. Tegenwoordig wijst de consensus ernaar dat 2-AG (en niet andere endogene cannabinoïden), CB1R-afhankelijke voedselinname reguleert. 2-AG niveaus zijn verhoogd in de hypothalamus van vastende muizen en farmacologische interventie leidt tot verminderde voedselinname. Ook vertonen DAGLα$^{-/-}$ muizen hypofagie en hebben ze lage vetgehaltes. Dit is vergelijkbaar met CB1R$^{-/-}$ muizen, terwijl knockout muizen van DAGLβ en *N*-acyl phosphatidylethanolamine phospholipase D (NAPE-PLD) niet dit fenotype hebben. Deze punten suggereren dat

selectieve interferentie van DAGLα activiteit een nieuwe therapeutische toepassing kan zijn in de behandeling van obesitas en het metabool syndroom.

Ontstekingsprocessen worden geassocieerd met obesitas en vele neurodegeneratieve ziekten, waaronder de ziekten van Parkinson en Alzheimer. Prostaglandines gevormd uit arachidonzuur door cyclooxygenases zijn belangrijke pro-inflammatoire stimuli. Cyclooxygenase remmers vertonen neuroprotectie in diermodellen van de ziekten van Parkinson en Alzheimer, maar het gebruik van deze remmers is beperkt door gastro-intestinale en cardiovasculaire complicaties. Recent is ontdekt dat monoacylglycerol lipase (MAGL) arachidonzuur gehaltes regelt in specifieke weefsels, die van belang zijn voor de synthese van prostaglandines door cyclooxygenases type 1 en 2 (COX1 en COX2). Vooral MAGL produceert arachidonzuur met name in de hersenen, lever en longen, terwijl fosfolipase A2 (PLA2) voornamelijk arachidonzuur in de darm en milt produceert. Remming van MAGL activiteit in lipopolysacharide (LPS) behandelde muizen resulteert in verminderde neuroinflammatie, lagere concentraties van prostaglandines en cytokines in de hersenen. Ook hebben MAGL remmers een neurobeschermende werking in diermodellen van Multiple Sclerose (MS) en de ziekten van Parkinson en Alzheimer. Het lijkt erop dat verhoging van 2-AG niet betrokken is bij neuroprotectie.

Chronische activering van CB1R, door verhoging van 2-AG leidt tot veranderingen in het endocannabinoïdensysteem (bijvoorbeeld lagere expressie van CB1R en lichamelijke afhankelijkheid). Het is nog niet bekend hoe verhoogde 2-AG niveaus CB1R signalering beïnvloeden onder chronische neurodegeneratieve aandoeningen. Desalniettemin kan remming van DAGL een alternatieve benadering zijn voor het voorkomen van arachidonzuur vorming in de hersenen zonder accumulatie van 2-AG en (chronische) CB1R activering. Therapeutische interventie op DAGLs is echter moeilijk door het gebrek aan assays en potente en selectieve remmers. Er zijn enkele remmers gerapporteerd, echter deze zijn niet selectief, *in vivo* actief of missen de farmacokinetische eigenschappen die nodig zijn voor kandidaat geneesmiddelen. Er is dus een grote behoefte aan nieuwe remmers voor DAGL. Dit proefschrift beschrijft vijf DAGL remmers; glycine sulfonamiden, α-ketoheterocyclische verbindingen, α-keto amiden, β-keto difluoroamides en sulfonyl 1,2,4-triazole ureas.

α-Keto heterocyclische verbindingen zijn ontdekt als potente DAGLα remmers in **hoofdstuk 2** door virtuele farmacofoor screening. Twee farmacofoor modellen zijn geconstrueerd op basis van een eerder gepubliceerde en bekende bioactieve conformatie van een niet-selectieve DAGLα remmer, tetrahydrolipstatine (THL). *In silico* screening van een set van 16 lipase remmers resulteerde in LEI103 en LEI104 als twee interessante hits. De inhibitie van LEI103 en LEI104 is bevestigd in een DAGLα surrogaat substraat assay met behulp van *para*-nitrofenyl (PNP)-butyraat. Uit deze assay blijkt dat LEI104, een α-keto heterocyclische verbinding, potenter was dan LEI103. Om te onderzoeken hoe LEI104 DAGLα remt is een virtueel homologie model geconstrueerd op basis van een eerder beschreven co-

kristalstructuur van een vergelijkbare lipase. Het model bevat eenzelfde α/β hydrolase structuur en een goed gepositioneerde katalytische triade bestaande uit de eerder gerapporteerde DAGLα residuen. LEI104 werd covalent gebonden aan het model via een hemiketaal adduct en vervolgens geoptimaliseerd door moleculaire dynamica (MD) simulaties. Uit deze MD-simulaties blijkt dat het gevormde anion wordt gestabiliseerd door waterstofbruggen met Thr400 OH en NH en Leu473 NH (het 'oxyanion hole'). De binding aan het keton wordt bevestigd door het feit dat de alcohol precursor van LEI104 inactief is. De pyridine en oxazool stikstoffen vormen cruciale interacties in het DAGLα homologie model met respectievelijk His471 en His650. Het belang van de pyridine wordt ondersteunt door het feit dat de corresponderende benzoxazool significant minder potent is. De structuur-activiteit relaties van LEI104 zijn uitgebreid onderzocht in **hoofdstuk 3** door middel van synthese van verschillende analoga en screening van een bibliotheek van 1040 α-keto heterocyclische derivaten. Dit hoofdstuk laat zien dat de heterocyclische kernstructuur cruciaal is voor inhibitie van DAGLα. Veel geteste hetrocycli (bijv. benzoxazool, imidazool, -thiazool, imidazolopyridines, thiazolopyridines en oxadiazolen) zijn minder potent dan oxazolopyridines. Synthese van alle mogelijke regio-isomeren van de oxazolopyridine heeft aangetoond dat *4N*-oxazolopyridine optimaal is. Dit is in oveereenstemming met het gerapporteerde homologie model, omdat alleen deze specifieke stikstof positie waterstofbindingen kan vormen met His471. De remming van α-keto-oxazolen kan worden versterkt door elektron zuigende groepen op de *meta*- maar niet op de *para*-positie. Ook 2-acyl fenylmetyleen ketens zijn onderzocht in dit hoofdstuk. Een 2-acyl C8 methyleen is het meest potent, terwijl een C5 keten efficiënter is. 2-Acyl vetzuur ketens zijn ook toegestaan, waarbij oleoyl >> arachidonoyl. Dit suggereert dat de 2-acyl keten gepositioneerd is op de plek van de *sn*-1 acyl keten van het natuurlijk substraat. De meeste α-ketoheterocyclische verbindingen in dit hoofdstuk remmen zowel FAAH als DAGLα. De structuur-activiteit relaties in deze studie komen overeen met het homologie model, dat gebruikt is voor de optimalisatie tot LEI105, een duale DAGLα/ DAGLβ remmer die selectief is over FAAH. **Hoofdstuk 4** beschrijft het optimaliseren van de fysicochemische eigenschappen van LEI105 (met name lipofiele efficiëntie; LipE). Uit synthese van kortere ketens van LEI105 bleek dat de C5 methyleenfenyl keten het meest potent is, maar de C3 keten een optimale LipE heeft. Introductie van alifatische ketens met een eindstandige trifluormethyl (CF_3) groep resulteert in een 100-voudige verbetering van LipE ten opzichte van LEI105. De α-keto-heterocyclische verbindingen zijn verder geoptimaliseerd door de substituenten op de heterocyclische kernstructuur te veranderen. De elektronische effecten op de fenylring zijn onderzocht door middel van methoxy- en cyaan-groepen. Alle remmers zijn ook getest in een DAGLα activiteit assay gebruik makend van een natuurlijk substraat. De selectiviteit van de beste verbindingen is beoordeeld met behulp van 'activity-based protein profiling' (ABPP). Deze techniek maakt gebruik van twee 'activity-based probes' (ABPs), MB064 en TAMRA-FP, chemische tools die rapporteren over activiteit van meerdere serine hydrolases. Hieruit blijkt dat LEI107 een uiterst selectieve en potente remmer is van DAGLα. LEI107 is even potent als

LEI105, maar door een LipE van > 5 heeft het betere fysicochemische eigenschappen om een potentieel kandidaat geneesmiddel te worden.

Glycine sulfonamiden zijn onderzocht in **hoofdstuk 5** als DAGLα remmers door middel van systematische structuur-activiteit relaties. Glycine sulfonamiden werden eerder geïdentificeerd als DAGLα remmers door onderzoekers van Bristol Meyers-Squibb (BMS). Uitgaande van deze verbindingen zijn diverse analoga gesynthetiseerd en onderzocht op hun activiteit in de 96-wells DAGLα surrogaat substraat assay. Het carbonzuur van de glycine is belangrijk in het onderzoek, aangezien dit chemotype geen duidelijk mechanisme heeft om DAGLα te remmen. Het carbonzuur is vervangen door een methylester, alcohol, secundaire en primaire amide, nitrile, tetrazool en piperidine carbamaat. Al deze derivaten waren inactief. Dit geeft aan dat het carbonzuur essentieel is voor het remmen van DAGLα. Door synthese van 13 verschillende kernstructuren en zijgroepen is ontdekt dat DAGLα verscheidene substitutiepatronen tolereert, waarin de substituenten op de posities *para* > *meta* > *ortho*. Verschillende sulfonamide zijgroepen worden getolereerd, hoewel de oorspronkelijk gerapporteerde 2,2-dimethylchroman sulfonamide van BMS het meest potent is. De systematische analyse in dit hoofdstuk heeft geleid tot de ontdekking van LEI106, een zeer potente DAGLα remmer. De bindingsmodus van LEI106 is onderzocht met behulp van het DAGLα homologie model. Het carbonzuur lijkt hier het netwerk van de katalytische triade te verstoren via ionische interacties. De activiteit en selectiviteit van LEI106 is beoordeeld over endogene serine hydrolases in muizenhersenen met behulp van ABPP. Hieruit blijkt dat LEI106 selectief is over meerdere enzymen binnen het endocannabinoïd systeem, inclusief monoacylglycerol lipase (MAGL) en fatty acid amide hydrolase (FAAH). LEI106 remt echter ook α/β hydrolase domein 6 (ABHD6) in ABPP. Het testen van LEI106 in een natuurlijk substraat assay, gebaseerd op de omzetting van 2-AG door ABHD6 bevestigd dat LEI106 zeer actief is op ABHD6 (K_i = 0.8 ± 0.1 μM). LEI106 remt ook DAGLα in een natuurlijk substraat assay (K_i = 0.7 ± 0.1 μM). LEI106 is de eerste reversibele duale DAGLα/ ABHD6 remmer gerapporteerd in de wetenschappelijke literatuur.

Hoofdstuk 6 beschrijft het opzetten van de PNP-butyraat DAGLα assay in een 1536-well plaat en de daaropvolgende high throughput screening. De 96-well plaat assay is geoptimaliseerd naar een 354-well plaat protocol en is veranderd van een kinetische naar een eindpunt bepaling. Het protocol werd getest in een 'proof-of-principle screen' op de commercieel verkrijgbare 'List Of Pharmaceutically Active Compounds' (LOPAC®, Sigma-Aldrich) bibliotheek. Uit deze test screen bleek dat de assay van hoge kwaliteit is en robuust over meerdere dagen. De 384-well plaat assay is vervolgens geoptimaliseerd tot 1536-well plaat assay binnen de European Lead Factory (ELF). Een uitgebreide optimalisatie van type assay platen, totaal volume, enzym en substraatconcentratie resulteerde in een nieuw protocol voor het uitvoeren van de test in een 1536-well plaat. Dit protocol is gebruikt voor de volledig automatische screening van de Joint European Compound Library (JECL), bestaande uit 300.000+ verbindingen. De primaire screening werd gevolgd door een hertest op twee concentraties, wat resulteerde in 263 bevestigde remmers. ABPP werd gebruikt om

activiteit en selectiviteit van de actieve remmers te beoordelen over meerdere serine hydrolases. DAGLα activiteit is onderzocht met ABP MB064. Naast DAGLα rapporteert MB064 ook op DDHD2, ABHD6, ABHD12 en ABHD16A activiteit. Van de 263 bevestigde verbindingen zijn er 46 geselecteerd voor de Qualified Hit List (QHL). Deze lijst bevat 10 clusters en 10 singletons, inclusief de glycine sulfonamiden en drie nieuwe chemotypes: α-keto amides, β-keto difluor amides en sulfonyl 1,2,4-triazool ureas.

Glycine sulfonamiden IMI4906626 en IMI4749305 zijn geïdentificeerd als de meest potente DAGLα remmers in de screening. IMI4906626 werd opnieuw gesynthetiseerd en getest door het European Screening Centre (ESC) en bleek na ABPP selectief te zijn over ABHD6. Dit maakt IMI4906626 de eerst gerapporteerde glycine sulfonamide die selectief lijkt over dit off-target. IMI4749305 is niet opnieuw gesynthetiseerd, maar bleek ABHD6 wel te raken tijdens de orthogonale ABPP screen. **α-Keto amides** en **β-keto difluoro amides** zijn reversibele remmers met een geactiveerd keton die vermoedelijk reageert met Ser472 van DAGLα. Beide chemotypes zijn interessante leads omdat ze goede fysicochemische eigenschappen hebben en goede activiteit. Al deze verbindingen zijn opnieuw gesynthetiseerd en getest door het ESC. Uit ABPP analyse bleek dat α-keto amides ABHD6 niet raken, in tegenstelling tot β-keto difluor amides. Beide chemotypes kunnen belangrijk zijn voor de ontwikkeling van remmers voor serine hydrolases of cysteïne proteases in de toekomst. **Sulfonyl 1,2,4-triazool ureas** IMI18721890, IMI18721890 en IMI1788117 zijn zeer potente remmers in zowel de primaire en orthogonale DAGLα assay. Dit chemotype gebruikt waarschijnlijk een geactiveerde carbonyl voor het covalent irreversibel labelen van Ser472 van DAGLα. IMI18721890 en IMI18721890 zijn opnieuw gesynthetiseerd en getest door het ESC. ABPP op deze stoffen liet zien dat ze ABHD6 ook raken, evenals FAAH en DDHD2. Sulfonyl 1,2,4-triazool ureas zijn geselecteerd, mede door hun activiteit, voor vervolgstudies en optimalisatie. Een bibliotheek van ~100 derivaten werd gesynthetiseerd in de ELF consortium door de European Screening Centre. Deze bibliotheek is belangrijk voor inhibitor ontwikkeling op DAGLs en andere targets, zoals serine hydrolases of cysteïne proteasen.

Hoofdstuk 7 beschrijft de toepassing van ABPP voor de ontwikkeling van *in vivo* actieve remmers voor ABHD16A, een fosfatidylserine (PS) lipase. ABHD16A splitst vetzuur acyl ketens specifiek op de *sn*-1 positie van PS. Het product, *lyso*-PS, is een belangrijke fosfolipide betrokken bij groei van T-cellen, mastcellen en groei van neurieten. Bovendien is het een toll-like receptor 2 (TLR2) agonist. α/β Hydrolase domain type 12 (ABHD12) breekt *lyso*-PS af *in vitro* en ABHD12$^{-/-}$ muizen accumuleren verscheidene *lyso*-PS lipiden in de hersenen. Genetische studies hebben mutaties van ABHD12 geïdentificeerd als oorzaak voor het ontstaan van een zeldzame genetische neurologische ziekte: polyneuropathie, gehoorverlies, ataxie, retinitis pigmentosa en cataract (PHARC). ABHD12 knockout studies bevestigen dat muizen zonder ABHD12 activiteit verscheidene symptomen van PHARC vertonen. Hierdoor zijn ABHD12$^{-/-}$ muizen een geschikt diermodel voor deze neurologische ziekte. Hoe PHARC precies ontstaat is op dit moment onbekend, maar ophoping van *lyso*-PS en daaropvolgende signalering via TLR2 kan betrokken zijn bij de neuro-inflammatoire reactie. Om deze

hypothese te testen zijn *in vivo* actieve remmers van ABHD16A vereist. In dit hoofdstuk zijn sulfonyl 1,2,4-triazool ureas als ABHD16A remmers geïdentificeerd door middel van ABPP. Een specifieke sulfonyl 1,2,4-triazool urea werd gebruikt als startpunt voor verdere optimalisatie. Een rationeel ontwerp heeft geleid tot de ontdekking van twee remmers (XGN67 en XGN75). Cellulaire experimenten duiden erop dat beide remmers niet efficiënt de cel in komen, maar wel extracellulair ABHD16A remmen *in situ*. Beide remmers zijn ook getest *in vivo* in muizen, waar ze gedeeltelijk, maar significant ABHD16A activiteit remmen in de hersenen. Beide stoffen zijn de eerst gerapporteerde *in vivo* actieve ABHD16A remmers in de literatuur. Gezien beide stoffen ABHD16A niet volledig remmen bij een hoge dosering (45 mg/kg) dient een tweede generatie remmers te worden ontwikkeld. Hierbij kan worden gelet op het optimaliseren van de polariteit (tPSA) en metabole stabiliteit. Ook dient een controle remmer te worden ontwikkeld om effecten van off-targets in diermodellen uit te sluiten. De structuur-activiteit relaties van dit hoofdstuk bieden een uitstekend uitgangspunt voor verdere optimalisatie van de volgende generatie *in vivo* actieve ABHD16A remmers. Deze remmers kunnen gebruikt worden om te bewijzen of substraat reductie therapie, door middel van ABHD16A inhibitie, een potentiële behandeling is voor de neuronale genetische ziekte PHARC.

Hoofdstuk 8 beschrijft een uitgebreid overzicht van het effect van verschillende DAGL remmers in pre-klinische modellen van metabole en neurodegeneratieve ziekten. Verschillende delen van dit hoofdstuk zijn in deze samenvatting vermeld.

De ontwikkeling van genetische knockout muizen in combinatie met *in vivo* actieve DAGL remmers hebben bijgedragen aan de kennis over de fysiologische rol van DAGL. Studies met 1,2,3-triazool ureas hebben aangetoond dat DAGLs de vorming van pro-inflammatoire cytokines en prostaglandines reguleren onder neuroinflammatoire condities. Het effect van DAGL remmers in muismodellen van ziekten is tot op heden nauwelijks onderzocht en zou belangrijke inzichten kunnen bieden in 2-AG signalering en metabolieten in neurodegeneratieve ziekten. Één studie heeft aangetoond dat een DAGL remmer beschermend was in een model van de ziekte van Huntington. Opmerkelijk was dat MAGL remmers de neuronale schade verergerden en het oxidatief metabolisme van 2-AG door cyclooxygenase 2 (COX2) leek te resulteren in de vorming van de toxische metabolieten. Het is daarom belangrijk om de werkzaamheid en therapeutische werking van zowel MAGL als DAGL remmers parallel te onderzoeken ten aanzien van CB1R bijwerkingen en activatie van alternatieve metabole routes tijdens neuroinflammatie.

Een reactief ureum in de 1,2,3-triazool ureas is ideaal gebleken voor optimalisatie van de remming van serine hydrolases. Verwacht wordt dat de nieuwe sulfonyl 1,2,4-triazool ureas in dit proefschrift zeer vergelijkbaar zijn. Bovendien kan de reactiviteit mogelijk worden veranderd door middel de zwavel oxidatietoestand. De sulfonyl 1,2,4-triazool ureas hebben goede fysicochemische eigenschappen, hoewel hun tPSA relatief hoog is. Potentiële nadelen van de triazool ureas zijn off-target activiteit en covalent irreversibele inhibitie. Dit maakt de

1,2,3-triazool ureas en sulfonyl 1,2,4-triazool ureas minder geschikt als potentiële kandidaat-geneesmiddelen. Daarom kunnen triazool ureas het beste worden gebruikt als chemische 'tool compounds'. De ontwikkeling van controle compounds is hiervoor nodig. Misschien zijn reversibele remmers, zoals de ketonen beschreven in dit proefschrift meer geschikt als kandidaat geneesmiddelen. Met name de α-keto heterocycli, zoals LEI105 en LEI107, zijn zeer potente en selectieve DAGL remmers. LEI107 heeft een ideale combinatie van activieit, hoge selectiviteit en goede fysicochemische eigenschappen, waardoor het een geschikte kandidaat is voor *in vivo* studies. LEI107 kan worden gebruikt om het effect te onderzoeken van farmacologische interventie van DAGL in muismodellen van obesitas en neurodegeneratie.

Zeer recent is aangetoond dat de verstoring van DAGLβ activiteit voldoende is om de neuro-inflammatoire respons *in vivo* te verminderen. DAGLβ is belangrijk bij het reguleren 2-AG gehaltes in microglia. DAGLβ$^{-/-}$ muizen behandeld met lipopolysaccharide (LPS) vertonen verminderde microgliale activering, terwijl algemene 2-AG en prostaglandine niveaus in de hersenen ongewijzigd bleven. Dit wijst erop dat DAGLβ een belangrijke target kan zijn om de neuro-inflammatoire response te onderdrukken zonder centrale bijwerkingen. Oraal bio-beschikbare, centraal actieve en selectieve remmers van DAGLβ zijn daarom zeer gewenst en kunnen een cruciale rol spelen in de behandeling van neurodegeneratieve ziekten zoals Multiple Sclerose (MS) en de ziekten van Parkinson, Alzheimer en Huntington.

List of publications

1. **Discovery of glycine sulfonamides as dual inhibitors of *sn*-1-diacylglycerol lipase α and α/β hydrolase domain 6**
   Janssen, F. J.; Deng, H.; Baggelaar, M. P.; Allarà, M.; Van Der Wel, T.; Den Dulk, H.; Ligresti, A.; Van Esbroeck, A. C. M.; McGuire, R.; Di Marzo, V.; Overkleeft, H. S.; van der Stelt, M. *J. Med. Chem.* **2014**, *57*, 6610–6622.

2. **Comprehensive analysis of structure-activity relationships of α-ketoheterocycles as *sn*-1-diacylglycerol lipase α inhibitors**
   Janssen, F. J.; Baggelaar, M. P.; Hummel, J. J. A.; Overkleeft, H. S.; Cravatt, B. F.; Boger, D. L.; van der Stelt, M. *J. Med. Chem.* **2015**, *58*, 9742–9753.

3. **Inhibitors of diacylglycerol lipases in neurodegenerative and metabolic disorders**
   Janssen, F. J. and van der Stelt, M. *Bioorg. Med. Chem. Lett.* **2016**, *26*, 3831–3837. Invited Digest Review.

4. **Pharmaceutically active compounds as DAG-lipase inhibitors**
   Janssen, F. J.; Baggelaar, M. P.; Hummel, J. J. A; van Boeckel, C. A. A.; van der Stelt, M. European Patent Number EP 15 169 052.6. Priority date 22 May **2015**. Filing date 23 May **2016**. Publication date: 22 November **2016**.

5. **Development of an activity-based probe and *in silico* design reveal highly selective inhibitors for diacylglycerol lipase-α in brain**
   Baggelaar, M. P.; Janssen, F. J.; van Esbroeck, A. C. M.; den Dulk, H.; Allara, M.; Hoogendoorn, S.; McGuire, R.; Florea, B. I.; Meeuwenoord, N.; van den Elst, H.; van der Marel, G. A.; Brouwer, J.; Di Marzo, V.; Overkleeft, H. S.; van der Stelt, M. *Angew. Chemie - Int. Ed.* **2013**, *52*, 12081–12085.

6. **A natural substrate-based fluorescence assay for inhibitor screening on diacylglycerol lipase α**

   van der Wel, T.; Janssen, F. J.; Baggelaar, M. P.; Deng, H.; den Dulk, H.; Overkleeft, H. S.; van der Stelt, M. *J. Lipid Res.* **2015**, *56*, 927–935.

7. **Highly selective, reversible inhibitor identified by comparative chemoproteomics modulates diacylglycerol lipase activity in neurons**

   Baggelaar, M. P.; Chameau, P. J.; Kantae, V.; Hummel, J.; Hsu, K. L.; Janssen, F.J; van der Wel, T.; Soethoudt, M.; Deng, H.; den Dulk, H.; Allarà, M.; Florea, B. I.; Di Marzo, V.; Wadman, W. J.; Kruse, C. G.; Overkleeft, H. S.; Hankemeier, T.; Werkman, T. R.; Cravatt, B. F.; van der Stelt, M. *J. Am. Chem. Soc.* **2015**, *137*, 8851-8857.

8. **Triazole ureas act as diacylglycerol lipase inhibitors and prevent fasting-induced refeeding**

   Deng, H.; Kooijman, S.; van den Nieuwendijk, A. M. C. H.; Ogasawara, D.; van der Wel, T.; van Dalen, F.; Baggelaar, M. P.; Janssen, F. J.; van den Berg, R. J. B. H. N.; den Dulk, H.; Cravatt, B. F.; Overkleeft, H. S; Rensen, P. C. N & van der Stelt, M.; *manuscript submitted.*

9. **Discovery of *in vivo* active and selective *sn*-1-diacylglycerol lipase α inhibitors**

   Janssen, A. P. A.; Janssen, F. J.; Baggelaar, M. P.; van Esbroeck, A. C. M.; den Dulk, H.; Deng, H.; van Doornmalen, E.; Smits, N.; Morrison, A.; Russell, E.; Schulz, J.; Brown, L.; Hewitt, J.; MacLeod, F.; Robinson, J.; Geurink, P. P.; Ovaa, H.; Florea, B. I.; Overkleeft, H. S.; McElroy, S. P. l; van Boeckel, C. A. A., Rutjes, H.; Jones, P. S.; van der Stelt, M.; *manuscript in preparation.*

10. **α-Keto heterocycles as highly selective and drug-like *sn*-1 diacylglycerol lipase inhibitors (working title)**

    Janssen, F. J.; Ming, J.; Baggelaar, M. P.; van Boeckel, C. A. A.; van der Stelt. M.; *manuscript in preparation.*

11. **Discovery of 1,2,4-triazole sulfonamides ureas as *in vivo* active α/β hydrolase domain 16A inhibitors (working title)**

    Janssen, F. J.; van der Ham, A.; Deng, H.; Florea, B.; Morrison, A.; Russell, E.; Schulz, J.; Brown, L.; Hewitt, J.; MacLeod, F.; Robinson, J.; Overkleeft, H. S.; McElroy, S. P. l; Jones, P. S.; van der Stelt M; *manuscript in preparation.*

Curriculum Vitae

Nederlands

Freek Janssen werd geboren op 25 Maart 1988 te Geldrop, Nederland. Hij behaalde in 2005 het Havo-diploma aan het Raayland College te Venray. In hetzelfde jaar startte hij zijn HBO studie Toegepaste Natuurwetenschappen aan de Fontys Hogenscholen Eindhoven met een major in organische chemie en een minor in toegepaste psychologie. Tijdens zijn studie was hij een actief lid van de opleidingscommissie. Zijn eindstage heeft hij verricht bij Schering-Plough/ Organon in Oss in 2009. Hier heeft hij onderzoek gedaan naar de toepassing van continue flow technologie in medicijn ontwikkeling. Hij heeft zijn Bachelor of Applied Science (BASc) *cum laude* behaald en kreeg een eervolle vermelding van de Koninklijke Nederlandse Chemie Vereniging (KNCV) 'Gouden Spatel' voor zijn bachelor rapport in datzelfde jaar.

In September 2009 startte hij met de master Chemistry aan de Radboud Universiteit Nijmegen. Tijdens zijn hoofd onderzoeksproject, in de groep van prof. dr. F.P.J.T. Rutjes, heeft hij zich gericht op de totaal synthese van iminosuiker natuurproducten via biokatalyse met aldolases in multi-enzym cascades. In 2012 behaalde hij zijn Masters of Science (MSc) *bene meritum* bij de Radboud Universiteit. Tijdens zijn studie was hij ook hoofddocent scheikunde bij Lyceo examentraining en entertainer bij Chemistry4Fun.

In September 2012 begon hij als promovendus aan de Universiteit van Leiden in de vakgroep bio-organische synthese. Het onderzoek vond plaats onder supervisie van prof. dr. H.S. Overkleeft en dr. M. van der Stelt. Tijdens zijn laatste twee jaar voerde hij onderzoek uit in de vakgroep Moleculaire Fysiologie, geleid door dr. M. van der Stelt. Op verschillende nationale en internationale conferenties werden delen van het onderzoek gepresenteerd. Zo werd zijn poster presentatie tijdens een chemische biologie meeting in Oxford bekroond met een posterprijs ('Mining the Chemical Proteome', 2015). Zijn mondelinge presentatie bij FIGON Dutch Medicine Days te Ede (2015) werd als beste presentatie verkozen door de KNCV sectie Pharmacochemie. Hij werd geselecteerd als delegatie van Nederland en uitgenodigd voor het Young Medicinal Chemist Symposium (EFMC-YMCS'16) in Manchester, Verenigd Koninkrijk. Zijn mondelinge presentatie over selectieve en reversibele diacylglycerol lipase remmers werd daar bekroond door de European Federation of Medicinal Chemistry (EFMC) als beste presentatie uit alle aanwezige landelijke prijswinnaars en sprekers. Hij is een uitgenodigd spreker voor het Advances in Synthetic and Medicinal Chemistry (EFMC-ASMC'17) symposium in Augustus 2017 in Wenen (Oostenrijk).

Curriculum Vitae

English

Freek Janssen was born on March 25th 1988 in Geldrop, the Netherlands. He obtained his higher general secondary education diploma (Havo) at Raayland College in Venray in 2005. He started his Bachelor Applied Science at Fontys Hogescholen in Eindhoven with a major in organic chemistry and minor in applied psychology. In addition, he was an active member of the educational committee. His final internship was conducted at Schering-Plough/ Organon in Oss, the Netherlands in 2009. Here, he focused on application of continuous flow technology in drug development. He completed his Bachelors of Applied Science (BASc) with distinction and received an honorable mention from the Dutch Chemistry Society (KNCV) 'Gouden Spatel' for his bachelor thesis in the same year.

In September 2009 he started the masters Chemistry at the Radboud University of Nijmegen. During his research project in the group of prof. dr. F.P.J.T. Rutjes, he focused on the total synthesis of natural product iminosugars, employing one-pot multi enzyme cascade biocatalysis with aldolases. In 2012 he obtained his Masters of Science (MSc) *bene meritum* from the Radboud University. During his masters he was also main teacher Chemistry at Lyceo and entertainer at Chemistry4Fun.

In September 2012, he started as a PhD candidate at Leiden University in the Bio-organic Synthesis group. His research was conducted under supervision of prof. dr. H.S. Overkleeft and dr. M. van der Stelt. During the final two years he transferred to the new department of Molecular Physiology, led by dr Mario van der Stelt. Parts of the research have been presented at various conferences. During the Chemical Biology meeting in Oxford he was awarded a poster presentation prize ('Mining the Chemical Proteome', 2015). His oral presentation during FIGON Dutch Medicine Days in Ede, the Netherlands (2015) was awarded as best oral presentation by the KNCV section Medicinal Chemistry. He was selected as delegate for the Netherlands and invited to present his work at the Young Medicinal Chemist Symposium (EFMC-YMCS'16) in Manchester, United Kingdom. Here, he presented his work on selective and reversible diacylglycerol lipase inhibitors and was awarded the best oral presentation by the European Federation of Medicinal Chemistry (EFMC) from all the national winners and speakers. He is an invited speaker at the Advances in Synthetic and Medicinal Chemistry (EFMC-ASMC'17) symposium in August 2017 in Vienna (Austria).